

HYBRID DEVICES: MORPHOLOGY CONTROL BY SELF-ASSEMBLY

DISSERTATION

zur Erlangung des akademischen Grades
eines Doktors der Naturwissenschaften (Dr. rer. nat.)
im Fach Chemie der Fakultät für
Biologie, Chemie und Geowissenschaften der Universität Bayreuth

vorgelegt von

Johannes Christopher Brendel

geboren in Pegnitz / Deutschland

Bayreuth, 2013

Die vorliegende Arbeit wurde in der Zeit von Mai 2009 bis Juli 2013 am Lehrstuhl für Angewandte Funktionspolymere/ Makromolekulare Chemie I der Universität Bayreuth unter der Betreuung von Prof. Dr. Mukundan Thelakkat angefertigt.

Dissertation eingereicht am:	04. Juli 2013
Zulassung durch die Promotionskommission:	10. Juli 2013
Wissenschaftliches Kolloquium:	27. September 2013

Prüfungsausschuss:

Prof. Dr. Mukundan Thelakkat	(Erstgutachter)
Prof. Dr. Stephan Förster	(Zweitgutachter)
Prof. Dr. Carlo Unverzagt	(Vorsitzender)
Prof. Dr. Josef Breu	

Amtierender Dekan: Prof. Dr. Rhett Kempe

Für meine Familie

“Per aspera ad astra”

Latin phrase

TABLE OF CONTENTS

SUMMARY / ZUSAMMENFASSUNG	1
1. INTRODUCTION	7
1.1 SEMICONDUCTING POLYMERS	7
1.2 SYNTHESIS OF WELL-DEFINED FUNCTIONAL POLYMERS	11
1.3 HYBRID PHOTOVOLTAIC DEVICES	14
1.4 STRUCTURE DIRECTING TEMPLATES	19
1.5 CHARACTERIZATION METHODS	26
1.6 OBJECTIVE OF THE THESIS	30
1.7 REFERENCES	31
2. OVERVIEW OF THE THESIS	39
INDIVIDUAL CONTRIBUTIONS TO JOINT PUBLICATIONS	55
3. SOLID-STATE DYE-SENSITIZED SOLAR CELLS USING RED AND NEAR-IR ABSORBING BODIPY SENSITIZERS	59
4. SOLID-STATE DYE-SENSITIZED SOLAR CELLS FABRICATED WITH NANOPOROUS TiO ₂ AND TPD DYES: ANALYSIS OF PENETRATION BEHAVIOR AND I–V CHARACTERISTICS	85
5. SEMICONDUCTOR AMPHIPHILIC BLOCK COPOLYMERS FOR HYBRID DONOR-ACCEPTOR NANOCOMPOSITES	97
6. MACROSCOPIC VERTICAL ALIGNMENT OF NANODOMAINS IN THIN FILMS OF SEMICONDUCTOR AMPHIPHILIC BLOCK COPOLYMERS	125
7. OPTICAL PROPERTIES OF WELL-DEFINED CONJUGATED POLYELECTROLYTES: INFLUENCE OF MOLECULAR WEIGHT, CONCENTRATION, SOLVENT AND ADDED SALT	155
8. CONTROLLED SYNTHESIS OF A CONJUGATED POLYELECTROLYTE LEADING TO EXCELLENT HOLE TRANSPORT MOBILITY	175
9. APPENDIX: NANOCRYSTALLINE TITANIA NETWORK FOR SOLID STATE DYE SENSITIZED SOLAR CELLS	187
LIST OF PUBLICATIONS	209
DANKSAGUNG	211
ERKLÄRUNG	213

SUMMARY

This thesis focuses on innovative concepts for hybrid photovoltaic devices. In particular, it aims at the improvement of light harvesting and the control of morphology. Hybrid devices combine the advantage of excellent electronic properties of inorganic semiconductors and the convenient processability of organic materials. However, the creation of suitable morphologies which guarantee a high interface area between donor and acceptor as well as continuous charge percolation pathways still remains a challenge. Established systems such as dye sensitized solar cells offer a good control, whereas composite blends of semiconductor polymers and inorganic nanoparticles provide only a limited control on these morphological aspects. In the wake of new developments in modern organic and polymer synthesis, we raise some interesting questions: First of all, can organic sensitizers improve light harvesting and broaden the spectral absorption range of hybrid devices? Is it possible to control the structure of the inorganic semiconductor using advanced polymer templates? And, in addition, can the polymer template fulfill all requirements for charge transport? This thesis addresses the aforementioned issues utilizing state-of-the-art synthesis and characterization methods for the development of highly functional dyes as well as well-controlled polymers and blockcopolymers.

In the first part, BODIPY (4,4-difluoro-4-bora-3a,4a-diaza-s-indacene) dyes were investigated which feature a broad absorption range up to the IR region accompanied by high extinction coefficients. These dyes were tested in solid state dye sensitized solar cells. Varying the anchor position, a distinct correlation between the electronic coupling and the electron injection efficiency was identified. In addition, triphenylamine based sensitizers were examined which feature beneficial redox potentials and excellent stability but at the expense of the broad absorption. Besides the light harvesting, a second issue concerning solid state dye sensitized solar cells is the lack of control over the morphology of the titania network such as network wall thickness and pore diameter. On basis of polymer brush particles made of a polystyrene core and a polystyrene sulfonate corona, a novel template assisted preparation of a mesoporous TiO₂ electrode was established. The sulfonated corona catalyzes the in-situ hydrolysis of TiO₂ in anatase configuration at room temperature. In contrast to established methods, our template permits the individual control of the TiO₂ network density and pore size. With variation of the TiO₂ content during the hydrolysis, a fundamental correlation between the TiO₂ density, the sensitized interface area and the resulting current generation was discovered. These results contribute to an improved knowledge toward dye sensitized hybrid solar cells.

Building up on the knowledge gained from the polymer brush templates, novel amphiphilic semiconducting block copolymers were developed which facilitate the self-assembly of hybrid composites. The semiconductor component is based on well-known triphenylamine derivatives, while the hydrophilic block comprises the polystyrene sulfonate which features unique coordination and catalytic characteristics. A crucial requirement for the preparation of these materials is the investigation of suitable synthetic protocols to maintain the control over the polymerization. The controlled reversible addition-fragmentation chain-transfer (RAFT) process was chosen for polymerization, but the complexity and reactivity of the semiconductor monomers necessitates an elaborate optimization of the reaction conditions to maintain the

control. In order to improve the versatility, the procedure was extended toward a combination of RAFT and “click” chemistry. Creating a well-defined scaffold polymer, the semiconducting moiety is conveniently introduced using a highly efficient polymer analogous reaction such as the copper catalyzed azide-alkyne cycloaddition. The resulting amphiphilic semiconductor block copolymers form micelles in polar solvents or water. I utilized the highly charged micelles to attach oppositely charged CdSe nanorods. The creation of such donor-acceptor composite particles circumvents the use of stabilizing but insulating ligands and further affords the processing from aqueous solutions. On the other hand, these block copolymer micelles were assembled on conductive substrates and annealed in saturated DMF vapor leading to microphase separation and a vertical alignment of the microdomains. This was the first time that such a favorable orientation of microdomains was achieved for semiconductor block copolymers. Altogether, these studies pave the way for a profound basis for the development of morphology controlled hybrid devices. This is possible since the presented amphiphilic semiconductor block copolymers combine the crucial requirements of capability of processing from environmental benign solvents, confinement of inorganic nanoparticles and the alignment of the domains.

In the final part of this thesis the concept of amphiphilic semiconductor polymers or conjugated polyelectrolyte was developed in order to completely avoid insulating organic blocks. In this regard, a conjugated polythiophene backbone was combined with the sulfonate groups in the side chain creating a hydrophilic, coordinative semiconductor polyelectrolyte. Although similar materials are known in literature, the presented approach significantly improves the control of the polymer synthesis permitting the modulation of the molecular weight, a narrow polymer distribution, a regioregular conformation and well-defined end groups. Starting from a controlled Kumada catalyst transfer polymerization of a precursor polymer which bears bromine side groups, the sulfonate group could be quantitatively introduced *via* nucleophilic substitution under optimized conditions. This route basically enables the formation of block copolymers due to the excellent end-group control and the living character of the polymerization. Moreover, the highly regioregular conformation induces an unprecedented aggregation phenomenon. Studying the optical properties of the conjugated polyelectrolytes, a distinct correlation between molecular weight and aggregation was observed in aqueous solutions. While short chains remain well-dissolved, the increase of molecular weight first leads to concentration dependent aggregation and finally for large polymers, permanently aggregates structures were observed. This unexpected behavior raises the question whether charge transport is affected, too. To elucidate a potential effect on the transport, the electrical properties were studied in detail. A bulk hole transport mobility of $1.3 \pm 0.5 \times 10^{-2} \text{ cm}^2/\text{Vs}$ was determined which is among the highest values reported so far. In contrast to other conjugated polyelectrolytes impedance spectroscopy revealed a pure electronic transport mechanism without ion reorganization. The presented results underline the potential of these tailor-made materials and the introduced synthesis route offers the design of further functionalized polymer architectures.

In conclusion, this thesis comprises innovative concepts to improve light harvesting and gain control over the morphology of hybrid devices. The established synthesis protocols enable the controlled preparation of well-defined functional amphiphilic polymers and block copolymers. The achieved results not only allow new approaches for the optimization of hybrid devices, but also provide the basis for a more comprehensive investigation of physical processes due to the systematic morphology control in such devices.

ZUSAMMENFASSUNG

Die vorliegende Dissertation befasst sich mit der Entwicklung innovativer Konzepte in Hybridsolarzellen. Kernziele sind eine Verbesserung der Lichtausbeute und die Morphologiekontrolle. Hybridzellen vereinen beides, die hervorragenden elektronischen Eigenschaften anorganischer Halbleiter und die einfache Verarbeitung organischer Materialien. Allerdings stellt die Erschaffung geeigneter Morphologien mit ausreichenden Donor-Akzeptor Grenzflächen und kontinuierlichen Ladungsträgerpfaden immer noch eine Herausforderung dar. Bekannte Systeme, wie farbstoffsensibilisierte Solarzellen ermöglichen bereits eine gute Kontrolle, während gemischte Komposite aus Halbleiterpolymeren und anorganischen Nanopartikeln nur bedingt Kontrolle über die Morphologie bieten. In Folge neuer Entwicklungen in der organischen Synthesen und der Polymerisationsmethoden eröffnen sich interessante Fragestellungen: Sind organische Farbstoffe in der Lage die Absorption von Hybridsolarzellen über einen breiten Spektralbereich zu verbessern? Kann die Struktur der anorganischen Halbleiter mit Hilfe fortschrittlicher Polymertemplate eingestellt werden? Können diese Template zudem alle Kriterien für den Ladungstransport erfüllen? Diese Fragestellungen werden in der Arbeit aufgegriffen und mit Hilfe modernster Synthese- und Charakterisierungsmethoden zur Entwicklung spezialisierter Farbstoffe und wohl definierter Polymere bzw. Blockcopolymere bearbeitet.

Im ersten Teil werden neuartige BODIPY-Farbstoffe (4,4-difluoro-4-bora-3a,4a-diaza-s-indacen) untersucht, die sich durch ein breites Absorptionsspektrum bis in den IR-Bereich und hohen Extinktionskoeffizienten auszeichnen. Eingesetzt in farbstoffsensibilisierten Feststoffsolarzellen, konnte durch Variation der Ankergruppenposition ein eindeutiger Zusammenhang zwischen der elektronischen Kopplung und der Elektroneninjektionseffizienz ermittelt werden. Alternativ wurden Triphenylaminderivate als Farbstoffe untersucht, die geeignete Redoxpotentiale und eine ausgezeichnete Stabilität aufweisen. Dies geht aber auf Kosten der breiten Absorption. Ein weiteres Problem farbstoffsensibilisierter Feststoffsolarzellen ist die limitierte Morphologiekontrolle bezüglich der TiO_2 -Netzwerkwandstärke und des Porendurchmessers. Ausgehend von Polymerbürstenpartikeln aus Polystyrol (Kern) und Polystyrolsulfonat (Korona) wurde eine neuartige templatgesteuerte Herstellung von porösen TiO_2 -Elektroden etabliert. Die Sulfonatgruppen der Korona katalysieren eine direkte Hydrolyse von TiO_2 in der Anatas-Konfiguration bei Raumtemperatur. Im Gegensatz zu den etablierten Verfahren ermöglicht das vorgestellte Templatverfahren eine individuelle Kontrolle der TiO_2 -Netzwerkdichte und Porengröße. Durch Variation des TiO_2 -Anteils während der Hydrolyse konnte ein grundsätzlicher Zusammenhang zwischen der TiO_2 -Dichte, der nutzbaren Grenzfläche und der resultierenden Stromdichte ermittelt werden. Diese Ergebnisse tragen zu einem generellen Verständnis von farbstoffsensibilisierten Hybridsolarzellen bei.

Aufbauend auf den Erkenntnissen, die mit den Polymerbürsten gewonnen wurden, sind neuartige amphiphile Halbleiterblockcopolymere entwickelt worden, die ein Self-Assembly der Hybridkomposite ermöglichen. Die Halbleiterkomponente basiert auf bekannten Triphenylaminderivaten, während der hydrophile Block aus Polystyrolsulfonat mit seinen einzigartigen Koordinations- und Katalyseeigenschaften besteht. Eine entscheidende

Voraussetzung für die Herstellung solcher Materialien ist die Erforschung geeigneter Syntheseverfahren zur Kontrolle der Polymerisation. Als geeignete Methode wurde die kontrollierte RAFT-Polymerisation (Addition-Fragmentation Chain-Transfer) untersucht. Jedoch erfordert die Komplexität und Reaktivität der Halbleitermonomere eine sorgfältige Optimierung der Reaktionsbedingungen. Um mehr Flexibilität zu gewährleisten, wurde das Verfahren mit Hilfe einer Kombination aus RAFT und „Klick“-Chemie erweitert. Aufbauend auf einem definierten Gerüstpolymer wird hierbei die Halbleiterkomponente mittels hocheffizienter polymeranaloger Reaktionen, wie der kupferkatalysierten Alkin-Azid Cycloaddition, eingeführt. Die in beiden Verfahren erhaltenen amphiphilen Halbleiterblockcopolymere bilden Mizellen sowohl in polaren Lösungsmitteln als auch in Wasser aus. Diese hochgeladenen Mizellen ermöglichen ein Anlagern von gegensätzlich geladenen CdSe-Nanostäbchen. Die Erschaffung solcher Donor-Akzeptor-Kompositpartikel umgeht den Einsatz von stabilisierenden Liganden, die isolierend wirken, und gestattet eine Verarbeitung aus wässrigen Dispersionen. Zum anderen wurden diese Mizellen auf leitfähigen Substraten aufgebracht und mit gesättigtem DMF-Dampf behandelt, was die Ausbildung einer Mikrophasenseparation und einer vertikalen Ausrichtung der Mikrodomänen zur Folge hatte. Solch eine vorteilhafte Orientierung der Mikrodomänen ist für Halbleiterpolymere in dieser Arbeit zum ersten Mal gezeigt. Zusammen genommen bieten diese Ergebnisse eine gute Grundlage für die Entwicklung Morphologie kontrollierter Hybridsolarzellen. Dies ist möglich, da die beschriebenen amphiphilen Halbleiterblockcopolymere sowohl die Grundvoraussetzung zur Verarbeitung aus umweltfreundlichen Lösungsmitteln mitbringen als auch die Einbindung von anorganischen Nanopartikeln und die Anordnung der Domänen ermöglichen.

Im letzten Teil dieser Arbeit entwickelten wir ein Konzept für der amphiphilen Halbleiterpolymere bzw konjugierter Polyelektrolyte, um auf isolierende organische Blöcke vollständig verzichten zu können. In diesem Zusammenhang wurde ein konjugiertes Polythiophenrückgrat mit den bereits erwähnten Sulfonatgruppen versehen, mit dem Ziel einen hydrophilen, koordinativen Halbleiterpolyelektrolyten zu erschaffen. Obwohl bereits ähnliche Materialien in der Literatur bekannt sind, bietet der vorgestellte Ansatz eine deutlich erweiterte Kontrolle der Polymersynthese, was die Einstellung des Molekulargewichts, eine enge Polymerverteilung, eine regioreguläre Konformation und definierte Endgruppen ermöglicht. Ausgehend von der Kumada-Polymerisation (KCTP, Kumada Catalyst Transfer Polymerization) eines polymeren Übergangprodukts mit bromierten Seitenketten konnten mittels nucleophiler Substitution unter optimierten Bedingungen quantitativ Sulfonatgruppen eingeführt werden. Grundsätzlich erlaubt diese Vorgehensweise die Synthese von Blockcopolymeren aufgrund der hervorragenden Endgruppenkontrolle und des lebenden Charakters der Polymerisation. Darüber hinaus induziert die regioreguläre Konformation ein für ähnliche konjugierte Polyelektrolyte unerwartetes Aggregationsverhalten. Auf Basis der optischen Eigenschaften der Materialien konnte ein eindeutiger Zusammenhang zwischen Molekulargewicht und Aggregation in wässrigen Lösungen ermittelt werden. Während kurze Ketten immer gut gelöst sind, führt die Erhöhung des Molekulargewichts zunächst zu einem konzentrationsabhängigen Aggregationsverhalten und schließlich für lange Polymere zu einer permanenten Aggregation. Dieses unerwartete Verhalten wirft die Frage auf, ob auch der Ladungstransport beeinträchtigt wird. Um einen möglichen Effekt aufzuklären, wurden die elektrischen Eigenschaften des Polymers im Detail untersucht. Hierbei ergab sich eine Lochtransportmobilität von $1.3 \pm 0.5 \times 10^{-2} \text{ cm}^2/\text{Vs}$, was als einer der höchsten bisher veröffentlichten Werte für Bulkmessungen gilt. Im

Gegensatz zu anderen konjugierten Polyelektrolyten kann aus der Impedanzspektroskopie auf einen rein elektrischen Transportmechanismus ohne Ionenbewegung geschlossen werden. Die gezeigten Ergebnisse unterstreichen das Potential solch definierter Materialien und der vorgestellte Syntheseweg eröffnet die Entwicklung weiterer funktioneller Polymerarchitekturen. Zusammenfassend beinhaltet diese Dissertation innovative Ansätze sowohl die Lichtabsorption und Umwandlung zu verbessern, als auch eine Morphologiekontrolle in Hybridzellen zu erlangen. Die erarbeiteten Syntheseverfahren erlauben zudem die kontrollierte Herstellung definierter und funktioneller amphiphiler Polymere und Blockcopolymere. Die erzielten Ergebnisse eröffnen nicht nur neue Optimierungsansätze für Hybridsolarzellen, sondern bilden aufgrund der Möglichkeit die Morphologie systematisch einstellen zu können die Grundlage für umfassendere Analysen der physikalischen Prozesse in solchen Systemen.

1. INTRODUCTION

1.1 SEMICONDUCTING POLYMERS

BACKGROUND

The development of conducting polymers in the 1970s had a tremendous impact on research in chemistry and physics, resulting in the noble prize in chemistry of 2000 for Alan J. Heeger, Alan G. MacDiarmid and Hideki Shirakawa.¹ With Introduction of permanent charges into the conjugated π -system by doping the material, they were able to convert the semiconductor polyacetylene into a conductor, wherein electrons were delocalized among the sp^2 -hybridized carbon of the polymer chain. In the ensuing years countless structural variations of conducting and semiconducting polymers were reported based on conjugated backbones or at least extended π -systems.² In contrast to inorganic semiconductor materials such as silicon, organic semiconductors possess the advantage of solution processability and improved mechanical flexibility and toughness.³ And in fact, these materials already silently influenced our daily life as they are applied in anti-static coatings,⁴ corrosion protection,⁵ electrodes for batteries,⁶ chemical sensors⁷ and, more recently, in organic light emitting diodes (OLED) for displays⁸ or lighting.⁹ Furthermore, actual research promises this material to have a great impact on flexible organic field effect transistors (OFET) and displays,¹⁰ superconductive materials¹¹ and printable photovoltaic devices (Figure 1–1).¹²

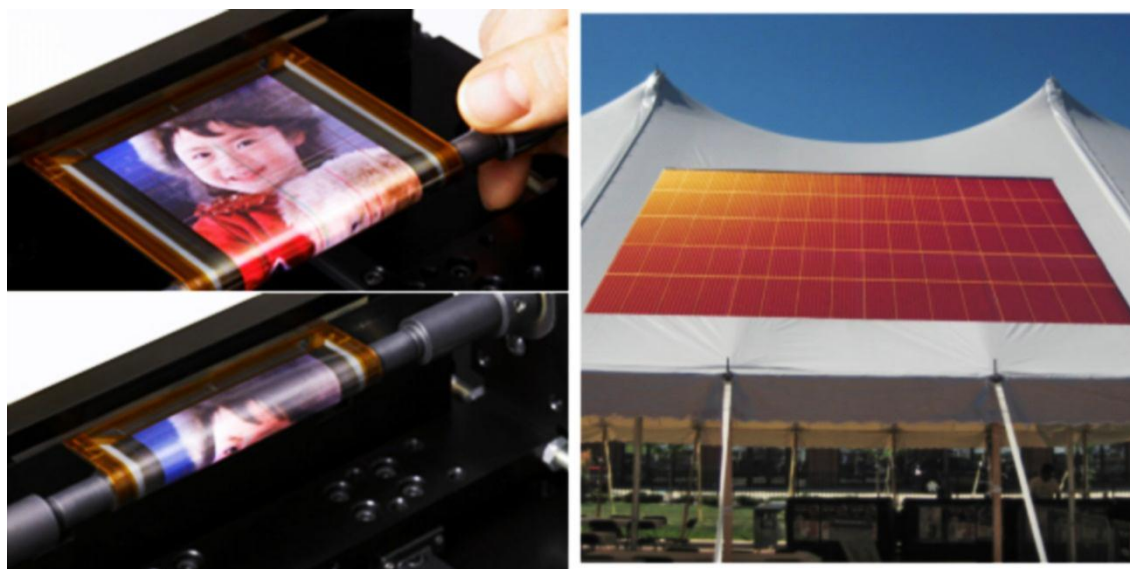


Figure 1–1. Flexible OLED display based on organic thin-film transistors (left) and tent covered with flexible plastic solar cells (right). Both are prototypes highlighting the future potential of organic electronic materials. Source: www.sony.net and www.konarka.com (22.11.2012).

Reconsidering the history of conjugated polymers some reports can already be found in the late 19th and early 20th century comprising the electropolymerization of polyaniline and the reaction

of thiophene with strong acids.^{13,14} In that time the structure was rather considered to be similar to other low molecular weight dyes than a macromolecule.¹⁵ It took almost one century to resolve the real structure.^{16,17} However, these findings led to the investigation of various new materials or conjugated polymers, such as polyaniline, polythiophene,¹⁷ polypyrrole,¹⁸ and polyacetylene (Figure 1–2). At this point the exceptional potential of these materials was recognized and gained increased attention in the scientific community.

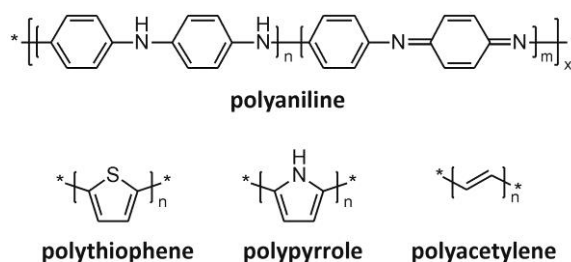


Figure 1–2. Structures of polyaniline, polythiophene, polypyrrole and polyacetylene, which were among the first conjugated polymers.

SOLUBLE SEMICONDUCTING POLYMERS AND THEIR APPLICATIONS

The development of side-chain functionalized polymers, such as polyvinyl carbazole, introduced the first processable semiconductor polymers, which were soluble in common organic solvents.¹⁹ In contrast to polymers with conjugated main chains, the flexibility of the polymer backbone reduces the aggregation of the conjugated groups, but the conductivity of the first side-chain functionalized macromolecules remained unsatisfying. Nevertheless, the research during the last decades led to various new semiconducting groups which could be attached to a polymer backbone improving the charge carrier transport and overcome this bottleneck. The most important structural units in this context have certainly become triphenyl amine derivatives which act as donors and modified perylene bisimides acting as acceptors.²⁰ But further semiconducting moieties such as fullerenes were also grafted to various polymer backbones.²¹ A milestone in the research on conductive polymers was achieved with the development of soluble conjugated polymers. While the first conjugated polymers were hardly soluble due to their rigid backbone and strong π - π interactions, this new generation enables the processing from solution and paved the way for realization of printable electronics.²² Prominent examples are poly(para-phenylene vinylene) derivatives,²³ substituted polyfluorenes²⁴ and poly(3-alkylthiophenes), including poly(3-hexylthiophene) (P3HT) (Figure 1–3).²⁵ The introduction of aliphatic side-chains mediated the solubility in common solvents and turned these materials into the most studied semiconducting polymers in research.



Figure 1–3. Selected examples of soluble conjugated polymers, which are most commonly studied in literature. The side chains (R) usually comprise linear or branched alkylchains of various lengths.

Considering the last decade of research in this field, a new generation of semiconducting polymers emerged, which feature improved charge carrier mobility and broaden the absorption from the visible up to the near infrared region.²⁶⁻²⁹ These low-band gap polymers are of particular interest for photovoltaic application, since they are able to harvest a wide spectral

range of the incident sunlight. Currently published reports highlight the potential of these materials as 8% power conversion efficiency (PCE) were reached in blends with PCBM (phenyl-C61-butyric acid methyl ester) as electron acceptor.³⁰ Recently, the Mitsubishi Chemical Corporation even announced a polymer based device with more than 10% efficiency.³¹ Nevertheless, these results were achieved in laboratory scale with systematically optimized preparation procedures and measured under inert conditions, *i.e.* oxygen and water free atmosphere. But the transfer of highly efficient systems to printed large-area modules and systems, which are stable under ambient conditions, is still a challenging issue for research.³² Therefore materials research and novel concepts have to be further developed featuring prospective stability, steady morphologies and low-cost processability from solution.

CONJUGATED POLYELECTROLYTES

The introduction of aliphatic side-chains to conjugated polymers was clearly a turning point in the history of organic electronics as the materials became soluble in organic solvents. Going one step further the question arises, how to modify these unique materials to create aqueous based systems as they are necessary for biological applications or enable an environmental benign

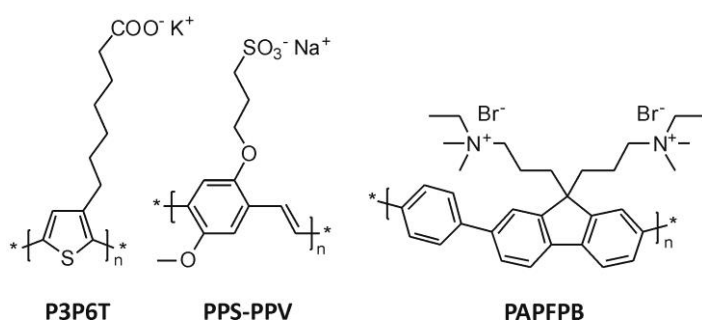


Figure 1–4. Prominent examples of conjugated polyelectrolytes including polythiophene, poly(*p*-phenylene vinylene) and polyfluorene derivatives. The utilized ionic groups vary from anionic sulfonate and carboxylic groups to cationic quaternary ammonium groups. P3P6T: poly[3-(potassium-6-hexanoate)thiophene],⁴⁰ MPS-PPV: sodium poly[5-methoxy-2-(3-sulfopropoxy)-1,4-phenylvinylene],⁴¹ PAPFPB: poly[(9,9-bis(3'-((*N,N*-dimethyl)-*N*-ethylammonium)-propyl)-2,7-fluorene)-alt-1,4-phenylene] dibromide.⁴²

processing. As often, nature itself evidences the best methods to create water soluble polymers, introducing highly polar or charged groups as they appear in DNA, polysaccharides or many proteins.³³ In consequence polyelectrolytes have been an important matter of science for almost a century and are still an attractive and extensively discussed field of research.³⁴⁻³⁷ So it is no wonder that conjugated polyelectrolytes (CPE) were demonstrated soon after the introduction of polymers soluble

in organic solvents.³⁸ In the adjacent years numerous varieties of CPEs have been reported (Figure 1–4).³⁹ The most important applications for CPEs emerged in biology or medicine, where they turned out to be particularly useful as sensor materials, actuators or more recently as soft electronic material for bio-communication.⁴³⁻⁴⁸ Therefore the photophysical properties of several compounds have been studied in detail, including aggregation phenomena and influence of counter ions.⁴⁹⁻⁵² Keeping the solubility and processability from cheap polar solvents such as water or alcohols in mind, semiconducting polyelectrolytes should furthermore enable a highly cost-effective production of photovoltaic devices. Early attempts using CPEs were started 1996 using LbL coating which is a method unique for polyelectrolytes.⁵³⁻⁵⁵ Work on simple bilayer devices using the polythiophene derivative sodium poly[2-(3-thienyl)-ethoxy-4-butylsulfonate] (PTEBS:Na⁺) and vapour deposited Fullerene demonstrated the potential of these materials as

PCEs of 0.43% were obtained.⁵⁶ However, the best devices using CPEs only reached efficiencies of 0.8% in hybrid composites, which is not competitive with systems based on organic solvents.^{57,58}

This fact is generally attributed to the low transport mobility of conjugated polyelectrolytes, which is assumed to be caused by the impeded stacking of the backbone due to the steric hindrance of the bulky ionic groups.^{57,59} Moreover, the presence of charged groups and their counter ions complicates the physical processes involved and makes a clear understanding difficult. Thus, the electric fields, occurring in the heterojunctions or applied by an external bias, may cause a reorientation of the ionic groups. These assumption bases on experiments and model simulations of Friend *et al.* that reveal an efficient screening of the external field by reorganization of ions in a blend of PEO with lithium triflate and poly(*p*-phenylene-vinylene) (PPV).⁶⁰ In consequence a strong energy band bending occurs at the interfaces to the electrodes. As a result, the electric field within the bulk becomes negligible and thus the charge transport comes to be solely diffusion limited (Figure 1–5). Comparable conclusions were drawn by Bazan *et al.* for CPEs used as electron transport layers in LEDs.⁶¹ However, the confirmation of this effect in the active layer of photovoltaic devices is so far still missing in the literature. Nevertheless, these observations raised new possible applications of CPEs in injection layers as these materials reduce the barrier impedance of electronic devices.^{62–65} While the physical processes are basically understood, only few facts are known of structure-property relationship, *e.g.* the influence of the attached charged group or the counter ion on the electron transport properties.^{59,66} The influence of chain conformation, degree of polymerization, molecular weight distribution and the related aspects of chain aggregation and crystallization is not considered yet in literature. This lack of knowledge is more or less based on the limited control on the synthesis of polyelectrolytes, which are usually prepared *via* polycondensation reactions or uncontrolled oxidative coupling reactions. In consequence new synthesis routes have to be developed to elucidate a comprehensive structure-property relationship. Furthermore controlled polymerization techniques may open new avenues for promising polymer architectures and applications.

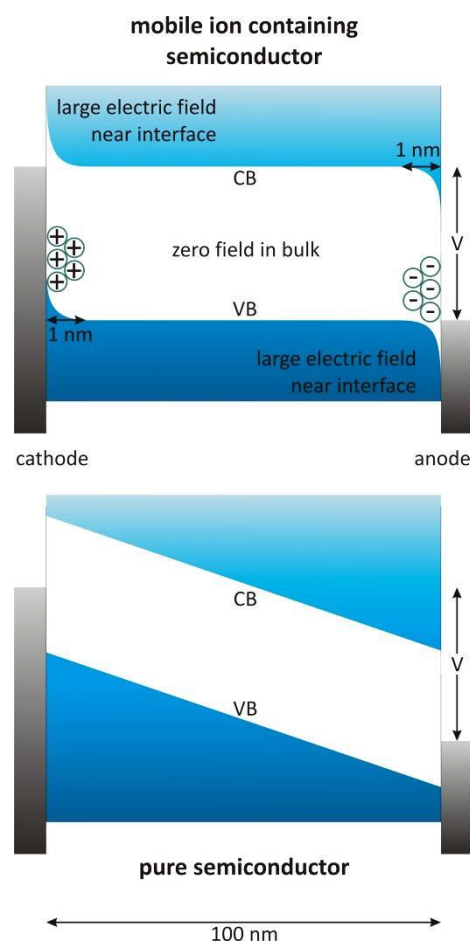


Figure 1–5. Schematic band diagrams of a semiconductor including mobile ions under an applied bias V (top). The ion accumulation at the electrodes effectively screens the electric field and leads to very thin, but steep barrier layers at the interface. Thus charges do not feel any field within the bulk material. For comparison a typical band diagram of a pure semiconductor is shown, too (bottom).

1.2 SYNTHESIS OF WELL-DEFINED FUNCTIONAL POLYMERS

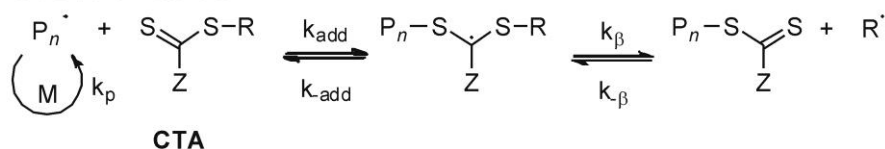
REVERSIBLE ADDITION-FRAGMENTATION CHAIN TRANSFER (RAFT) POLYMERIZATION

Classical methods to prepare well-defined polymers from vinyl-type monomers are living ionic polymerizations. The excellent control enables extreme narrow polydispersities of less than 1.05 and the construction of complex polymer architectures.⁶⁷ Nevertheless, its use for functional macromolecules such as conductive polymers is limited due to the sensitivity of the propagating ionic chain end. Therefore, alternative methods were developed which mainly comprise controlled radical polymerization techniques such as atom-transfer radical-polymerization, nitroxide mediated radical polymerization (NMR) or reversible addition-fragmentation chain transfer polymerization (RAFT).⁶⁸⁻⁷⁰ They allow the synthesis of side-chain polymers with electro-active pendant groups. All these methods are based on the process of the free radical polymerization, but introduce a particularly adjusted equilibrium of the active radical with an inactive or dormant state.⁷¹ While for ATRP the reaction of copper complexes with activated halides is utilized, NMRP takes advantage of nitroxides reversibly decomposing into free radicals upon heating. The RAFT mechanism is slightly more complicated as not only the equilibrium between an active and dormant species is involved. An overview of the RAFT process is shown in Figure 1–6, while a more detailed description of this mechanism is given in reviews of the first investigators Moad, Rizzardo and Thang.^{72,73}

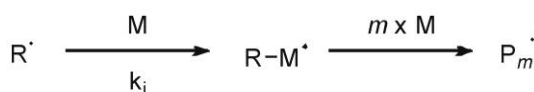
Initiation:



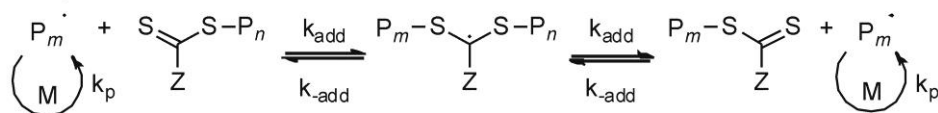
Reversible chain transfer:



Reinitiation:



Chain equilibrium:



Termination:

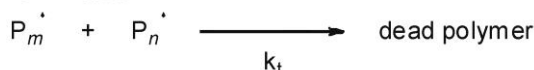


Figure 1–6. General mechanism of the RAFT polymerization. The chain transfer agents (CTA) are dithioesters with a stabilizing Z group and a leaving group R. For a controlled polymerization the transfer rate constants k_{add} and $k_{\text{-add}}$ as well as k_{β} and k_{β} must be fast in comparison to the propagation rate constant k_p (for reinitiation: k_i). M: monomer, P_n : polymer with chain length n .⁷³

In the RAFT process a specially designed dithioester reacts with the active radical releasing a new active chain end. As this process is reversible, all chain ends capped with this ester or chain transfer agent (CTA), respectively, can be reactivated, but the overall concentration of active radicals in the reaction remains constantly low. The control arise from the fast kinetics of chain transfer limiting the time of activity so that only few more monomer units were added to the propagating chain before reacting with another CTA. As all CTAs in solution are involved in this process each one starts one polymer chain growing slowly, but uniformly.

The critical point in the RAFT technique is clearly related to the lability of the CTA. Not only the reactivity with primary amines and other strong bases leads to the cleavage, but also high temperatures may cause the decomposition.⁷⁴ As a result, usually a thiol end-group is released which easily couples with another thiol under ambient conditions to form disulfides or rather coupled chains. Nevertheless, RAFT is still considered to be the most versatile tool for controlled radical polymerization. This fact is due to the excellent compatibility with a large variety of monomers, the tolerance of most functional groups and the mild reaction conditions. Furthermore, the RAFT process is applicable in almost all environments, ranging from non-polar media to highly polar solvents or even water. As a consequence of this advantages, many CTAs already become commercially available and are well adapted for the most important kinds of monomers and solvents.⁷³

KUMADA CATALYST TRANSFER POLYMERIZATION

Considering organic semiconductors, synthesis methods for main-chain conjugated polymers have to be mentioned, besides radical polymerization techniques which are limited to vinyl-type monomers. Early conjugated polymers were prepared by ionic or redox polymerization processes which are limited to a few monomers. Nowadays, the vast majority of these polymers are synthesized *via* well-established catalytic cross-coupling reactions including Suzuki-, Sonogashira-, Negishi- or Stille-coupling.⁷⁵⁻⁷⁹ However, these methods usually induce a step-growth polycondensation resulting in broad molecular weight distributions and limited control on the polymer conformation and end groups. A fortunate, but very successful exception was found in the controlled Kumada catalyst-transfer polymerization (KCTP) of 3-hexylthiophene (Figure 1–7).^{80,81} The actual active monomer is the Grignard complex 2-bromo-5-chloromagnesium-3-hexylthiophene, which is commonly generated by Grignard metathesis, which gives the prevalent nomenclature GRIM polymerization. Although the main reaction is still a catalytic condensation, the whole process becomes a controlled chain growth process, due to the coordination of the nickel catalyst at the chain end after reductive elimination. The detailed mechanism was evaluated by Yokozawa *et al.* and McCullough *et al.*^{82,83} In the ensuing years, the optimization of reaction conditions led to an excellent control of polydispersity, chain conformation and end-groups for poly(alkylthiophenes) and revealed a “quasi” living nature of the polymerization.⁸⁴⁻⁸⁸ Subsequently, also other monomers were found to be suitable for the KCTP including substituted phenylenes, pyrroles, carbazoles and fluorenes.⁸⁹⁻⁹¹ These exceptional characteristics further enabled the synthesis of various well-defined block copolymers, which were either conjugated and prepared fully *via* KCTP or they were linked at the controlled end group.⁹²⁻⁹⁶ These results on new polymer architectures comprising conjugated polymers promise new pathways towards functional materials suitable for batteries, sensors and photovoltaics.⁹⁷⁻¹⁰⁰

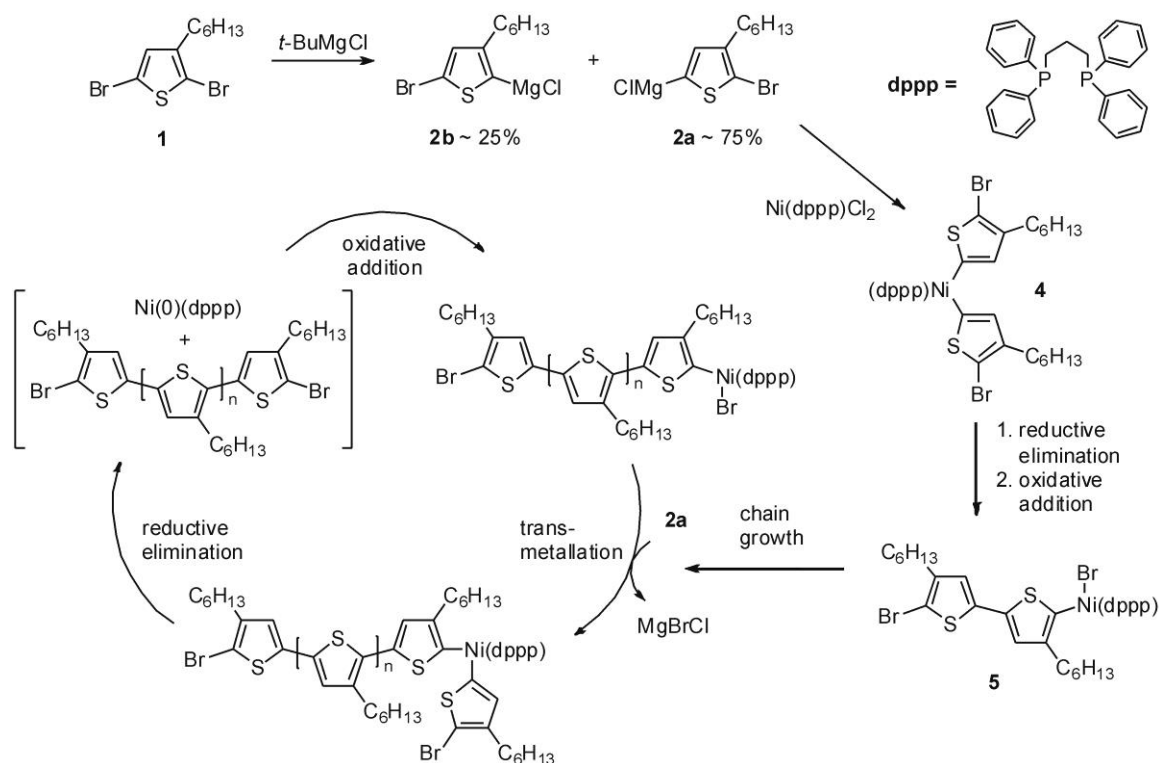


Figure 1-7. Mechanism of the Kumada catalyst-transfer polymerization (KCTP) of P3HT according to the route of McCullough.⁸¹

FUNCTIONAL POLYMERS BY “CLICK” CHEMISTRY

Other versatile tools for the design of functional polymers are so called “click”-reactions. This term, originally defined by Sharpless *et al.*, comprises reactions of high selectivity and excellent yield at mild conditions.¹⁰² The most prominent example is the azide-alkyne Huisgen cycloaddition, yielding a 1,4-triazole *via* copper(I) catalyzed 1,3-dipolar cycloaddition (Figure 1-8).¹⁰³ A crucial advantage of “click” reactions and especially the azide-alkyne cycloaddition is that they commit no side reactions and tolerate many other functional groups. Furthermore, these reactions enable quantitative yields turning them into ideal processes for polymer analogous reactions. Recently, Lang *et al.* demonstrated the potential of “click” chemistry for preparation of semiconducting polymers by the synthesis of a well-defined macromolecules comprising of bulky perylene bisimide derivatives attached to a propargyl-oxy-styrene backbone.¹⁰⁴ The versatility of this approach makes it applicable for any semiconductor moiety with a terminal azide group. Future research will certainly yield in interesting and exciting new polymer architectures and materials.

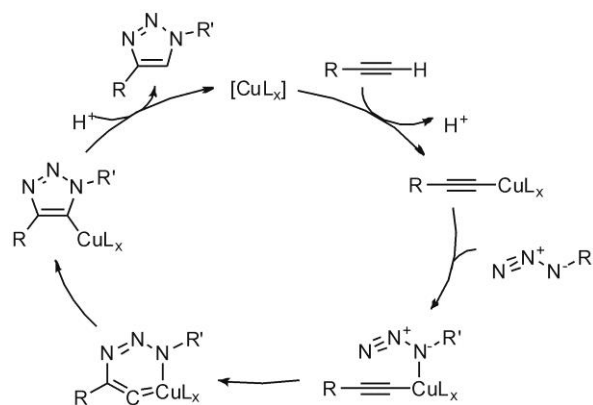


Figure 1-8. Proposed mechanism of the azide-alkyne Huisgen cycloaddition.¹⁰¹

1.3 HYBRID PHOTOVOLTAIC DEVICES

BASIC DEVICE PRINCIPLES

The first organic devices based on single layers of organic semiconductors, which were made analogous to well-known silicon devices. Brought into contact with electrodes exhibiting different work functions the Fermi levels of the materials equilibrate resulting in a band bending within the semiconductor. In consequence a charge depletion or space charge region is formed, which is the effective driving force for separation of electrons and holes. In contrast to inorganic semiconductors the excitons in organic materials are localized to few molecules (Frenkel excitons) and exhibit strong coulomb binding energies in the order of 0.1 to 1 eV, which is a result of the comparably low dielectric constants of organics.^{105,106} Thus the probability of charge separation at the depletion region of an organic single layer device is drastically reduced and the efficiencies of these devices remained low (< 1%).^{107,108}

A remarkable improvement was observed in bilayer devices of donor and acceptor materials (Figure 1–9). Tang *et al.* soon reported efficiencies of up to 1% using copper phthalocyanine and a perylene tetracarboxylic derivative.¹⁰⁹ In this device charge separation occurs at the interface of the two materials and the driving force was given by the energy offsets of the highest occupied molecular orbitals (HOMO) or the lowest unoccupied molecular orbitals (LUMO) of the two materials, respectively. Thus this energy offset can overcome the strong coulomb binding energy in contrast to the weak built-in potential of single layer devices. Nevertheless, the major limiting factor for high power conversion efficiencies in such bilayer devices is an intrinsic dilemma: In organic solar cells the exciton diffusion length is limited to approx. 10-15 nm. However, the extinction coefficients of the materials necessitate layer thicknesses in the order of 100 - 200 nm for sufficient light absorption. In consequence, both short distances to the interface and sufficient thick layers need to be prepared simultaneously.

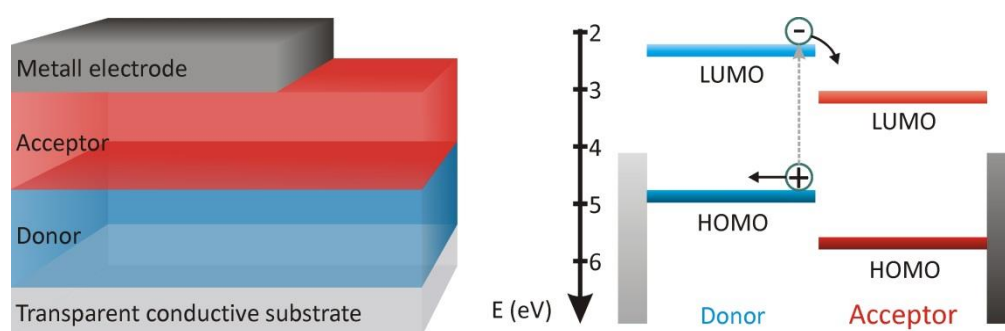


Figure 1–9. Scheme of a bilayer device (left) comprising an electron donor (p-type) and acceptor (n-type) and a representative energy diagram (right) visualizing the process of charge generation and separation at the donor/acceptor interface; HOMO: highest occupied molecular orbital, LUMO: lowest unoccupied molecular orbital.

BLEND STRUCTURES

The manipulation of the morphology is a subtle method to accomplish both, a close interface and the required layer thickness. A straightforward route for an increase of the interface area is the blending of both donor and acceptor materials in the active layer (Figure 1–10).^{110,111}

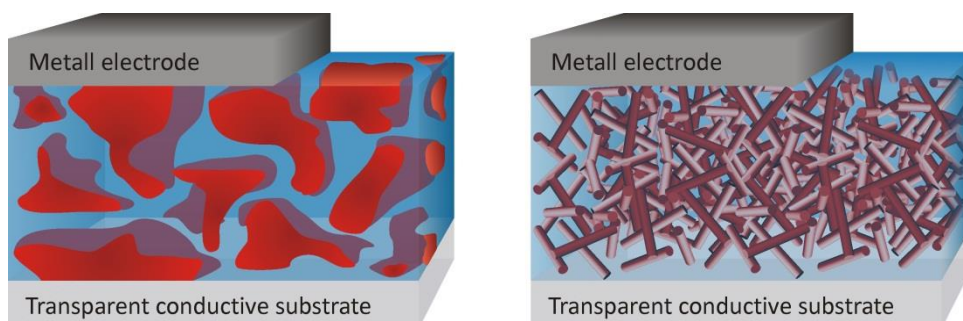


Figure 1–10. Schematic representation of an organic (left) and a hybrid (right) bulk heterojunction device consisting of a blend of donor (blue) and acceptor (red) materials.

Despite the facts that phase separation in such blends can induce the accumulation of one material at the electrodes and the formation of macroscopic and isolated domains, the fine tuning of domain sizes in such devices led to the highest efficiencies so far reported for organic photovoltaic devices. P3HT combined with the fullerene derivative ICBA (indene- C_{60} bisadduct), for example, reached power conversion efficiencies of up to 6.5% and, as already mentioned, novel low-band gap polymers exceed 10%.^{31,112} A recent physical study on charge generation and separation in such devices provided a deeper insight into the important processes and gave reasons for the excellent efficiencies.¹¹³ This report substantiate the need for high interface areas for charge separation. But it also accounts for the importance of pure domains providing the energetical driving force and transport pathways to the individual electrodes. In these blend devices, this favourable morphology is mainly accomplished by extensive optimization of composition and annealing conditions as well as using processing additives.^{12,114}

While the majority of organic semiconducting materials are electron donors, only a few organic semiconductors exhibit reasonable electron mobilities and stability (*e.g.* fullerene, naphthalene diimides or perylene diimides).^{115–117} A promising alternative is the use of inorganic semiconductors, which are well-known for their n-type character and their excellent performance even under ambient conditions.¹¹⁸ Early hybrid blend devices were reported in 2003 by Alivisatos *et al.* achieving a PCE of 1.7% by a combination of P3HT and CdSe nanorods.¹¹⁹ Further improvements were attained using CdSe tetrapods or dendritic inorganic nanocrystals.^{120,121} Replacing P3HT with a novel low-band gap polymer poly[2,6-(4,4-bis-(2-ethylhexyl)-4H-cyclopenta[2,1-*b*;3,4-*b'*]dithiophene)-*alt*-4,7-(2,1,3-benzothiadiazole)] (PCPDTBT) led to PCEs of more than 3%.¹²² Despite these promising results, polymer hybrid solar cells still cannot compete with organic devices involving PCBM. This fact is related to the insufficient control on the blend morphology in hybrid devices.¹²³ Photoluminescence quenching studies revealed that not all absorbed photons generate charges, which is crucial for efficient devices.¹²⁴ Due to dipole-dipole interactions inorganic nanoparticles tend to aggregate causing the formation large domain sizes and reduction of the interface surface for charge separation. Commonly inorganic nanoparticles are stabilized by organic ligands.¹²⁵ However, bulky ligands,

comprising long alkyl chains, negatively affect the charge separation at the donor-acceptor interface as well as the interparticle charge transport.^{126,127} One way to circumvent these isolating properties is the use of functionalized active polymers as ligands. Recent studies revealed that, this way, stable and well-dispersed composites can be established with up to 30 vol% inorganic nanoparticles.¹²⁸ Using amino end-group modified P3HT for a better dispersion of CdSe nanoparticles the beneficial influence of the modification on the device properties was demonstrated.¹²⁹ Recently, the controlled alignment of P3HT and CdS nanoparticles led to an efficiency of more than 4% and prove the importance of a well-defined morphology.¹³⁰ Another alternative is the in-situ synthesis of inorganic semiconductors from soluble precursors. This way, Janssen *et al.* created bicontinuous structures of P3HT and ZnO using diethyl zinc as soluble precursor.¹²³ Furthermore various metal sulfites are accessible *via* fragmentation of metal xanthates at elevated temperatures.¹³¹ Blends of CdS and P3HT obtained *via* the described precursor route resulted in PCEs of more than 2% and using a combination of CuInS and a low-band gap polymer efficiencies could be improved further.^{132,133} Nevertheless, the control on the resulting morphology and optimized light harvesting remain critical issues in these structures.

SOLID STATE DYE SENSITIZED SOLAR CELLS

A well-known approach, to create hybrid devices with large interface areas, is based on the preparation of porous inorganic semiconductor scaffolds, which are backfilled with a hole conductor. The most common devices in this context are dye sensitized solar cells (DSC), where sensitizers are attached to the inorganic semiconductor to harvest the sunlight. Liquid dye sensitized solar cells (Grätzel cells) comprise a solution based redox shuttle, *e.g.* I^-/I_3^- in acetonitrile, as hole transport material and PCEs of more than 12% were achieved.^{134,135} In solid state dye sensitized solar cells (SDSC) the liquid electrolyte is replaced by organic hole conductors, which circumvents the bottleneck of the intricate sealing of the device. An overview of the preparation steps involved for fabrication of a typical SDSC are depicted in Figure 1–11.

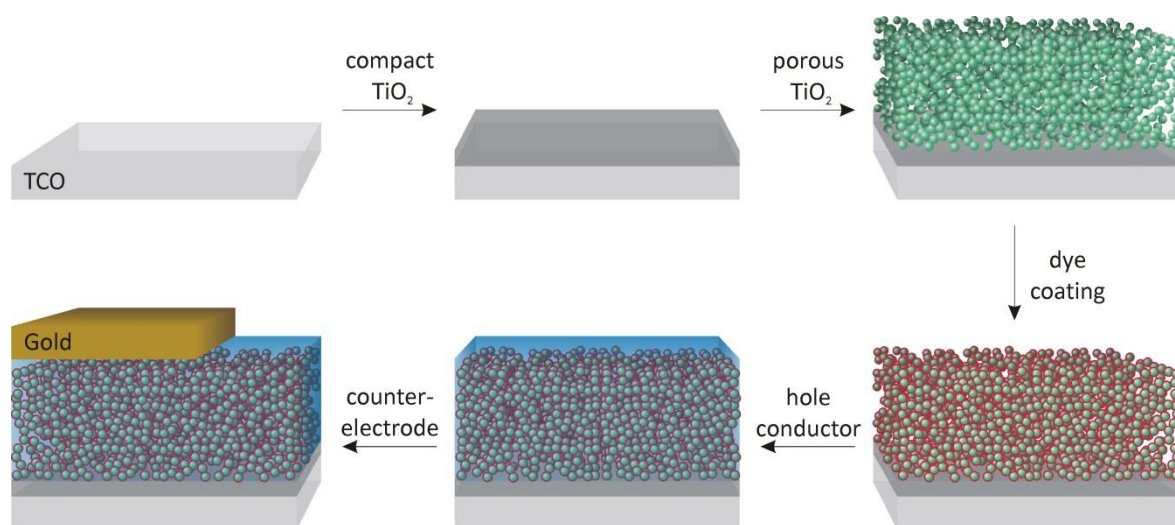


Figure 1–11. Schematic representation of the preparation steps for the fabrication of solid-state dye sensitized solar cells: First the transparent conducting oxide (TCO) is covered with a compact layer of TiO₂. On top a porous layer of TiO₂ is applied, which is subsequently coated with a monolayer of dye. Finally the hole conductor is filled into the pores and the gold counter electrode is vacuum deposited.

These devices consist of several layers, which are subsequently applied. Common substrates are glass with a thin layer of a transparent conductive oxide (TCO) such as fluorine-doped tin oxide (FTO). On top a compact blocking layer of the inorganic semiconductor, usually TiO_2 , is applied to inhibit the recombination of the separated charges at the interface of the TCO and the finally infiltrated hole conductor. To generate a large interface area, a porous layer of TiO_2 is prepared, which mainly is based on printable pastes of crystalline nanoparticles and binders. This porous layer is subsequently sensitized with a dye to absorb the incident light. Examples of applied dyes are described later in this chapter. To transport the positive charges from the interface to the cathode, an organic semiconductor is finally infiltrated into the porous layer. Top electrodes are usually fabricated by vacuum deposition of noble metals such as gold or silver. The main physical processes, which occur in the SDSC are summarized in Figure 1–12.

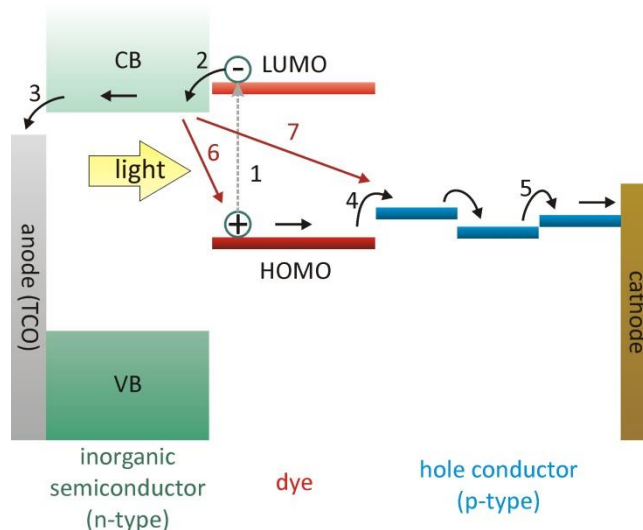


Figure 1–12. Scheme of the physical processes occurring in a solid-state dye sensitized solar cell: light is absorbed by the dye and an electron is excited to the LUMO of the dye (1). This electron is injected to the conduction band (CB) of the inorganic semiconductor (2) and finally transferred to the anode (3). On the other side the positive charge (hole) in the HOMO of the dye is regenerated by the hole conductor (4). This hole is transported to the cathode (5). Critical processes are the recombination of separated charges at the interface of n-type material and dye (6) or hole conductor (7).

The concept of solid-state DSCs was initially shown by the group of Haarer, who applied amorphous triphenyldiamine (TPD) derivatives as hole transport material.¹³⁶ A significant improvement was achieved by Bach *et al.* using the TPD based hole conductor 2,2',7,7'-tetrakis-(*N,N*-di-*p*-methoxyphenylamine)-9,9'-spirobifluorene (spiro-OMeTAD) (Figure 1–13) and incorporating dopants and additives.¹³⁷ The introduction and optimization of a compact blocking layer between the conductive substrate and the mesoporous TiO_2 further reduced the recombination considerably and the efficiency was pushed to more than 2%.¹³⁸

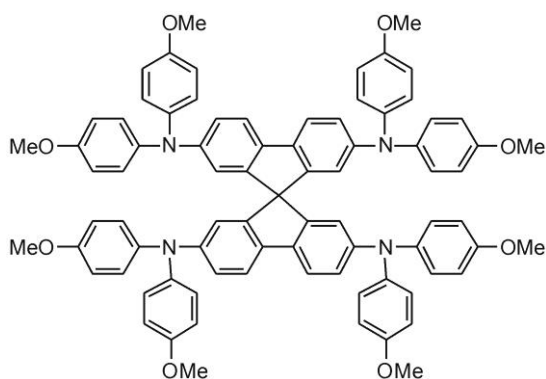


Figure 1–13. Scheme of the hole conductor 2,2',7,7'-tetrakis-(*N,N*-di-*p*-methoxyphenylamine)-9,9'-spirobifluorene (spiro-OMeTAD).

A critical part of the SDSC is certainly the interface between n-type and p-type semiconductor and the monomolecular dye layer which lacks the problem of exciton diffusion. At this boundary, the most important physical processes occur, which includes the light absorption and the charge separation, but also recombination processes. In consequence, the key for efficient SDSCs is the development of well-designed dyes, which are beneficial for charge generation. First devices mainly comprised ruthenium metal-organic sensitizers, among which the most

studied dyes are surely $\text{Ru}(2,2'\text{-bipyridyl-4,4'-dicarboxylic acid})_2(\text{NCS})_2$ complexes with variable degrees of protonation (Figure 1–14).^{139,140} These complexes are still considered as promising sensitizers for DSCs due to their reasonable stability and several modified derivatives were reported.¹⁴¹ Very recently, a complete new generation of hybrid devices were reported exhibiting very high PCEs.¹⁴² They involve the use of perovskites such as CsSnI_x or $\text{CH}_3\text{NH}_3\text{PbI}_x$.^{143,144} In combination with spiro-OMeTAD these devices reached PCEs of more than 12%.¹⁴⁵ However, organic dyes still gain considerable attention in research due to their excellent absorption properties and low production costs avoiding rare metals. Recent reports highlight the potential of these sensitizers for SDSCs as they reach efficiencies of more than 7% (Figure 1–14).¹⁴⁶ The current research focuses on the development of organic dyes with increased absorption capabilities in the red and near IR spectrum. Examples for this class are BODIPY (4,4-difluoro-4-bora-3a,4a-diaza-s-indacene) based dyes (Figure 1–14).¹⁴⁷ However, numerous other structures were examined in DSCs and SDSCs, which are summarized in comprehensive reviews.^{148,149}

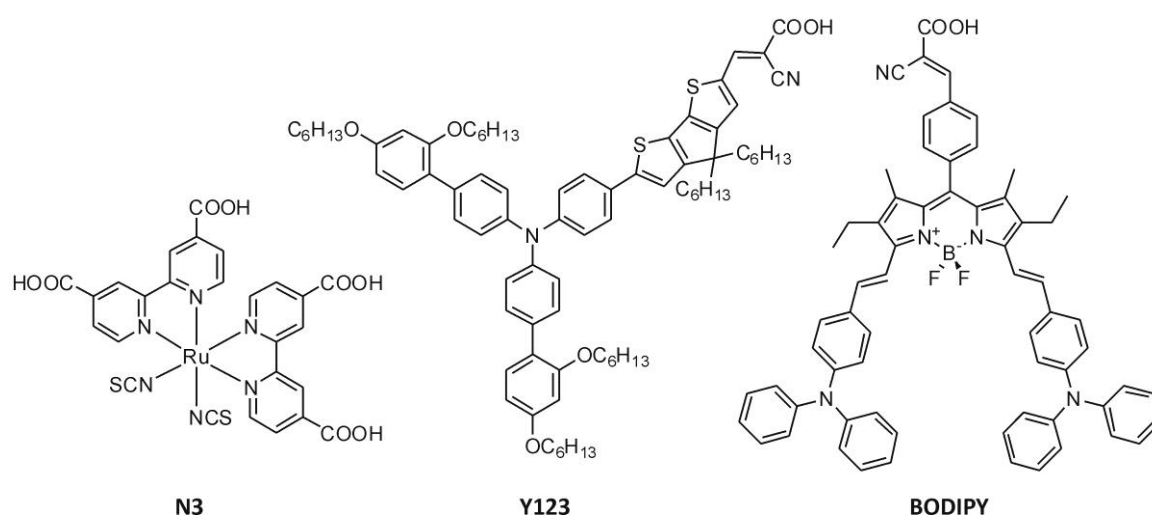


Figure 1–14. Examples for dyes used in SDSCs: a metal-organic ruthenium complex (N3);¹³⁷ an organic, triphenylamine based sensitizer (Y123);¹⁴⁰ a BODIPY dye.¹⁴¹

Keeping the good hole transport mobility and broad absorption of conjugated polymers in mind, even higher efficiencies are imaginable using these polymers instead of spiro-OMeTAD. However, a serious challenge is certainly a sufficient filling of the porous layer using polymers.¹⁵⁰ While small molecules still diffuse into the mesoporous layer even during the drying process, large macromolecules remain on the surface.¹⁵¹ Therefore alternative structures have to be developed to facilitate a better infiltration with polymeric hole conductors. One approach is based on TiO_2 nanotubes with inner diameters of 70 nm, which significantly improve the fill fraction.¹⁵² Similar improvements were obtained for ZnO nanorods grown on a conductive substrate and covered with P3HT.¹⁵³ An innovative method towards densely filled pores is the infiltration of the mesoporous structure with liquid monomer precursors and their subsequent electropolymerization to generate a conjugated polymer in-situ. Following this approach Liu *et al.* fabricated solid state devices with more than 6% PCE.¹⁵⁴ These promising results emphasize the development of tailor-made structures to integrate semiconductor polymers into hybrid composites for solar cells.

1.4 STRUCTURE DIRECTING TEMPLATES

BLOCK COPOLYMER MICROSTRUCTURES

The long-term control over the donor-acceptor morphology is still a bottleneck both in organic and hybrid bulk heterojunction devices. For hybrid systems new concepts are necessary to manage a microphase separated system which guarantees a good contact of the inorganic nanoparticles, bicontinuous structures for charge transport and a high yield in charge separation.

In literature various ways are presented creating defined microstructures in length scales ranging from micrometers down to nanometers, which are commonly considered as top-down and bottom-up approaches.¹⁵⁵ Besides well-known top-down lithographic methods, the self-assembly of block copolymers is a subtle bottom-up process, which provides tailor-made structures in the range of few nanometers, ideal for charge separation.¹⁵⁶ Block copolymers inherently form microphase separated domains on lengthscales of nanometers, if the individual blocks are not miscible.¹⁵⁷ Generally polymers tend to segregate in contrast to small molecules due to the reduced impact of entropy on the Gibbs free energy, while the enthalpy in most cases remains a factor countering the intermixing.¹⁵⁸ Based on the theory of Flory and Huggins thus the miscibility of polymers relies on the interaction parameter χ and the lengths of the polymers given by the polymerization index N .^{159,160} By covalent attachment of two or more immiscible segments, the individual polymers are confined to the interface and their domain size is limited by the block length. As a result block copolymers form well defined microstructures which vary with the block ratio and the segment length (Figure 1–15).^{161,162} With variation of the degree of polymerization of both blocks the sizes of the microdomains can be tuned. This feature of block copolymers enables domain sizes well-adapted to the exciton diffusion length improving the charge separation efficiency in photovoltaic devices. Additionally, the microphase separated domains guarantee charge percolation pathways.

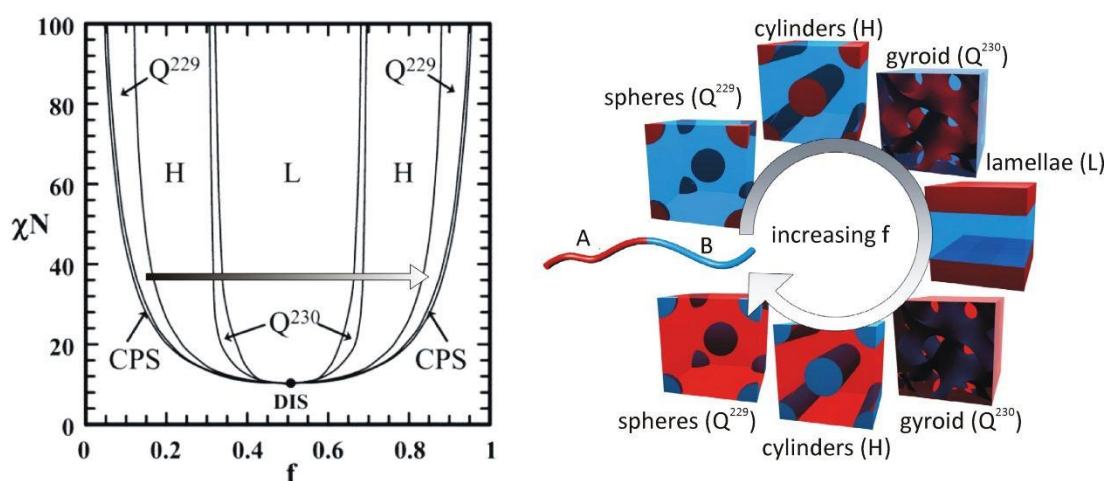


Figure 1–15. Typical phase diagram (left) and schemes of the most important morphologies (right) of a diblock copolymer, the grey arrow in the left diagram indicates the morphology transitions through the structures shown on the right side; f : volume fraction of one block, χ : Flory-Huggins interaction parameter, N : degree of polymerization, L: lamellae, H: hexagonally packed cylinders, Q^{230} : double-gyroid phase, Q^{229} : body-centered spheres, CPS: closed-packed spheres, DIS: disordered phase. (adapted from ref. 162)

SACRIFICIAL ORGANIC TEMPLATES

A common application of block copolymers is their use as structure directing agent for preparation of inorganic scaffolds.¹⁶³ In this case, the polymer maintains the control on the morphology, but it is removed afterwards either by high temperature calcination processes or chemical etching. Typical examples are binder polymers as they are used in commercial pastes for the preparation of the mesoporous TiO₂ layer for SDCs.

Considering hybrid photovoltaic devices various attempts have been undertaken to create well defined porous scaffolds of inorganic semiconductors, which can be infiltrated with an organic hole conductor.¹⁶⁴ The most prominent example of sacrificial templated nanostructures is the sol-gel preparation of mesoporous metal oxides using microemulsions of amphiphilic block copolymers.¹⁶⁵ In most cases block copolymers of poly(propylene oxide) (PPO) and poly(ethylene oxide) (PEO) were utilized as structure directing agent. These surfactants are commercially available and are synthesized in industrial scales. The metal oxides were obtained by hydrolysis of soluble precursors, such as metal alkoxides (*e.g.* TEOT: tetraethyl orthotitanate). The process of the formation of the porous morphology was well-studied by Soler-Illia and co-workers.^{166,167} A simplified scheme is shown in Figure 1–16.

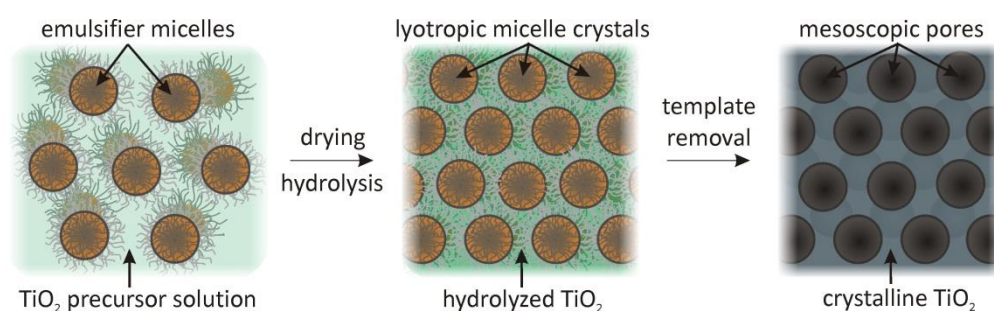


Figure 1–16. Scheme of the templated sol-gel process to form mesoporous TiO₂. Commercial emulsifiers, such as PEO-*b*-PPO, form micellar structures in solution, which condense to lyotropic crystals during the drying process. Simultaneously, the TiO₂ precursors are hydrolysed to form the inorganic framework. Finally the template is removed to reveal the mesoporous TiO₂.¹⁶⁶

In general, the block copolymers assemble into well-defined micelles, which form ordered liquid crystalline structures during the drying process. Simultaneously, the precursor is hydrolysed in the surrounding medium to create the metal oxide framework (*e.g.* TiO₂ sol). The shape is defined by the micelle structure (spherical, cylindrical, lamellar, *etc.*). To obtain well-defined porous structures, an exactly adjusted balance between hydrolysis, micelle formation and crystallization has to be established. A different approach relies on ordered thin films of block copolymers, where one block can be selectively removed to give the template.¹⁶⁸ The resulting cavities were filled with the inorganic semiconductor. Finally, the template is removed to give an exact inorganic replica of the block copolymer microdomain.

Alternatives to block copolymer templates are assemblies of organic colloids, such as polystyrene latex particles or spherical polymer brushes. These colloids are commonly prepared *via* emulsion polymerization leading to narrowly dispersed particles. Controlling the assembly, large ordered arrays of the colloidal particles are accessible exhibiting crystal like structures (*e.g.* face-centered cubic).^{169,170} Filling the voids with metal oxide precursors a well-defined framework of the inorganic material is obtained after hydrolysis and removal of the colloidal

template.^{171,172} Starting with silica, up to now several other metal oxide frameworks have been templated this way, including IrO_2 , V_2O_5 and TiO_2 .¹⁷³⁻¹⁷⁵ Due to the high order in the lattice structures and the high refractive index of the metal oxides, photonic crystals can be obtained guiding the light.¹⁷⁶ Based on these observations DSCs, incorporating inverse opals of titania, showed improved light harvesting at the photonic band gap of the crystal.¹⁷⁷

Critical aspects of the above mentioned sacrificial templates are on the one hand the difficulty to individually control the pore size and wall thickness of the final porous material and on the other hand the removal of the template material. The latter commonly involves high temperature calcination processes to remove the organic template and to induce the crystallization of the metal oxide, but they impede the use of flexible plastic substrates for the devices. Further issues are either the poor degree of pore filling or the small aspect ratio of the length against the spatial distance in the patterned structures, which limits the active interface area and thus the efficiencies of the systems. Increasing the aspect ratio commonly causes the collapse of the structure while removing the template due to strong capillarity forces occurring with evaporation of the solvent.¹⁷⁸

NON-SACRIFICIAL BLOCK COPOLYMER TEMPLATES

To circumvent the bottlenecks of sacrificial templates, functional structure directing agents have to be developed, which facilitate a coordinative assembly of both the inorganic and the organic semiconductor. Therefore, several requirements have to be fulfilled (Figure 1–17): First, co-continuous domains for both hole and electron transport materials are necessary to guarantee the charge transport to the respective electrodes. Secondly, one block should have preferential binding properties for the inorganic material, to ensure a confinement of the inorganic semiconductor within the domain. Further, a sufficient content of inorganic semiconductor must be integrated, to guarantee a good charge percolation. Finally, the copolymer should permit the charge separation at the interphase of the inorganic and organic semiconductor.

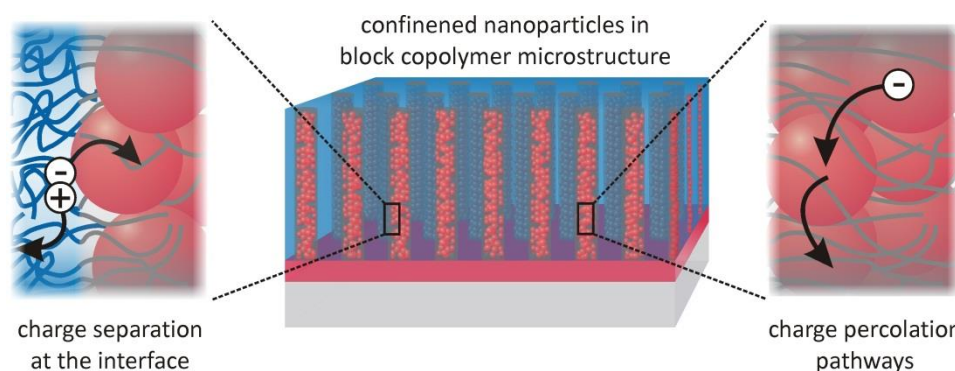


Figure 1–17. Scheme of an idealised hybrid device comprising a block copolymer microstructure and inorganic nanoparticles confined within the coordinative domain. Critical processes for charge generation are depicted in the magnifications, including the charge separation at the interface (left) and the charge percolation through the inorganic material (right).

Suitable structure directing agents are amphiphilic block copolymers, which bear segments to coordinate semiconducting nanoparticles or their precursors. Well-known hydrophilic polymers for coordination are poly(ethylene oxide) (PEO) and poly(vinyl pyridine) (P2VP or P4VP).^{166,179} Alternatively, negatively charged polyelectrolytes, featuring carboxylic acids or sulfonate groups, allow the coordination of metal precursors or positively charged particles.¹⁸⁰⁻¹⁸² A

comprehensive overview on amphiphilic polymers without electronic functions is given in reviews of Förster, Plantenberg and Antonietti.¹⁸³⁻¹⁸⁵ The following section is focused on structure directing block copolymers used for preparation of donor-acceptor microstructures.

Frey *et al.* utilized commercial emulsifiers or block copolymers (*e.g.* PEO-*b*-PPO) to gain control over the morphology of hybrid blends of TiO₂ and a hole conductor polymer (Figure 1–18).¹⁸⁶ Using time-resolved photoluminescence measurements and NMR analysis they studied the influence of composition and interaction on the organic/inorganic interface.¹⁸⁷ A crucial point comprises the influence of the coordinative block on charge separation at the interface of donor polymer and n-type inorganic semiconductor. The studies of Frey *et al.* clearly emphasize the importance of an intimate contact of both materials for efficient charge separation. In consequence amphiphilic functional block copolymers have to be rather electronically active components than solely coordinative.

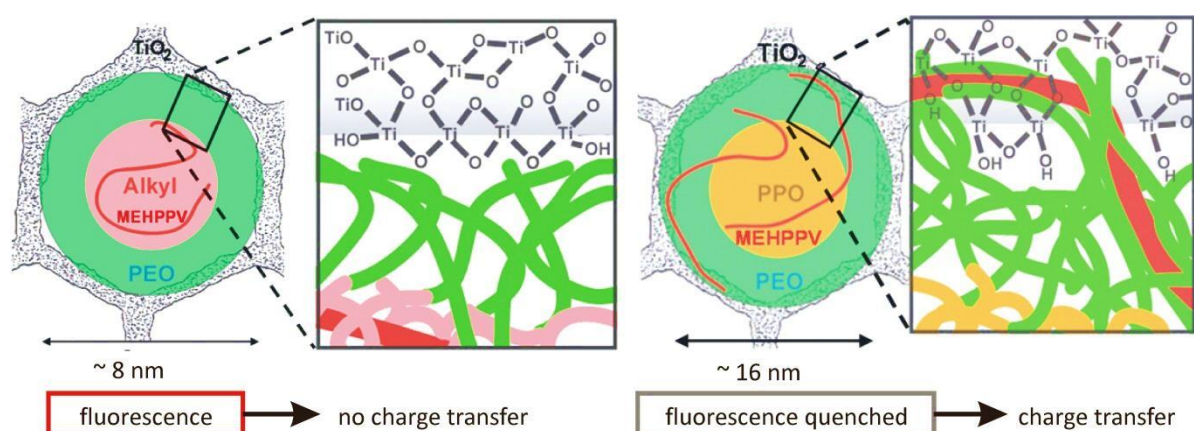


Figure 1–18. Schematic diagrams of mesostructured TiO₂ using blends of poly[2-methoxy-5-(20-ethyl-hexyloxy)-1,4-phenylenevinylene] (MEHPPV: red) and an amphiphilic structure directing agent. If the alkyl-ethyleneoxide C₈H₁₇-PEO₁₀ (alkyl: pink; PEO: green) is used, the conjugated polymer is confined in the hydrophobic part and separated from the TiO₂ (gray) (left). Thus no charge transfer is observed. In contrast using the triblock copolymer PEO₁₀₆-*b*-PPO₇₀-*b*-PEO₁₀₆ (PPO: yellow) an intimate contact between MEHPPV and TiO₂ is observed and the fluorescence is quenched indicating a good charge transfer (right) (adapted from ref. 187).

A promising approach to generate hybrid donor-acceptor structures relies on semiconducting amphiphilic block copolymers. Hence, the fraction of electronically inactive material can be significantly reduced. Synthesizing a functional block copolymer comprising PEO and a triphenylamine based hole conductor segment, Gutmann *et al.* were able to prepare self-assembled hybrid composites with TiO₂ (Figure 1–19).¹⁸⁸ Conductive scanning force microscopy studies revealed continuous percolation pathways in thicknesses up to 2 μm.¹⁸⁹

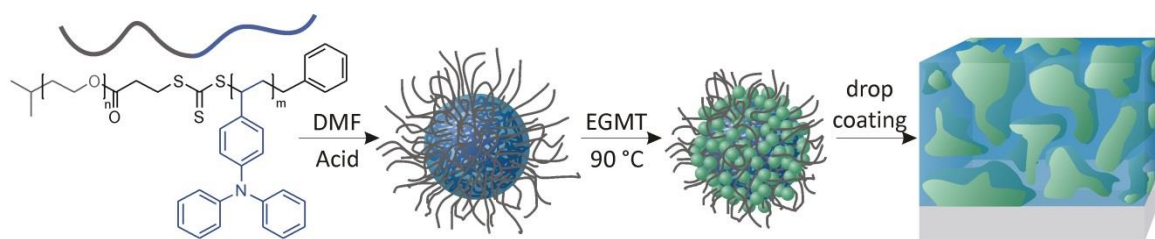


Figure 1–19. Formation of a microstructured hybrid device using the functional block copolymer poly(ethylene oxide)-*b*-polytriphenylamine (PEO-*b*-PTPA). First, the addition of HCl led to the formation of micelles. Adding the ethylene glycol modified titanate (EGMT) precursor and heating to 90°C induce the formation of TiO₂ (green) and a hybrid film can be formed by drop coating the solution.¹⁸⁸

A crucial aspect in the application of functional block copolymers is the preservation of the ordered morphology. Using tailor-made block copolymers prepared from a triphenyl diamine monomer and vinyl pyridine well-ordered lamellar structures were obtained. These block copolymers were able to confine CdSe:Te nanoparticles within the poly(vinyl pyridine) domain (Figure 1–20).¹⁹⁰

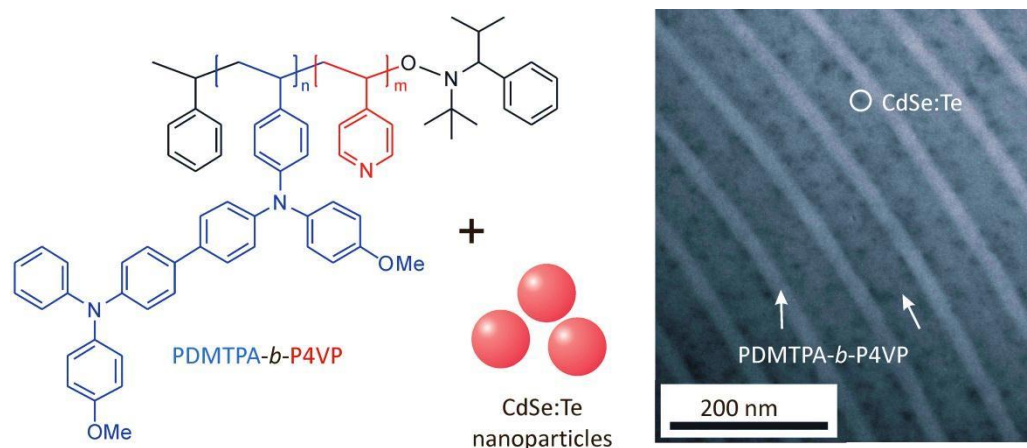


Figure 1–20. Scheme of the semiconducting amphiphilic block copolymer poly(vinyl-*N,N'*-bis(4-methoxyphenyl)-*N,N'*-diphenyl-(1,1'-biphenyl)-4,4'-diamine)-*block*-poly(4-vinylpyridine) (PDMTPD-*b*-P4VP) which can be used to create a microstructured hybrid composite with CdSe:Te nanocrystals. The TEM image (right) shows a lamellar morphology of the polymer (bright areas: PDMTPD; dark areas: P4VP; staining with I₂) confining the inorganic particles (0.5 vol%) within the P4VP domain. The sample was annealed at 170°C under N₂ for 2 days to obtain the equilibrium morphology (adapted from ref. 190).

As already mentioned above, a key issue for charge percolation through the inorganic nanoparticles is a sufficient amount of inorganic semiconductor confined in the coordinative domain. Electron conductivity measurements on composites of PS-*b*-P4VP and various amounts of CdSe clearly emphasize the positive effect of confinement on the transport properties. But they also reveal the importance of high volume ratios of at least 30 vol% inorganic semiconductor for sufficient contact.¹⁹¹ However, studies on CdS nanoparticles introduced into PS-*b*-P4VP bulk structures depict the loss of morphology control already at weight percentages of 28 wt% which corresponds to less than 10 vol% (Figure 1–21).¹⁹² Thus the combination of both sufficient nanoparticle accumulation and morphology control remains a challenging task for research on efficient hybrid photovoltaic devices.

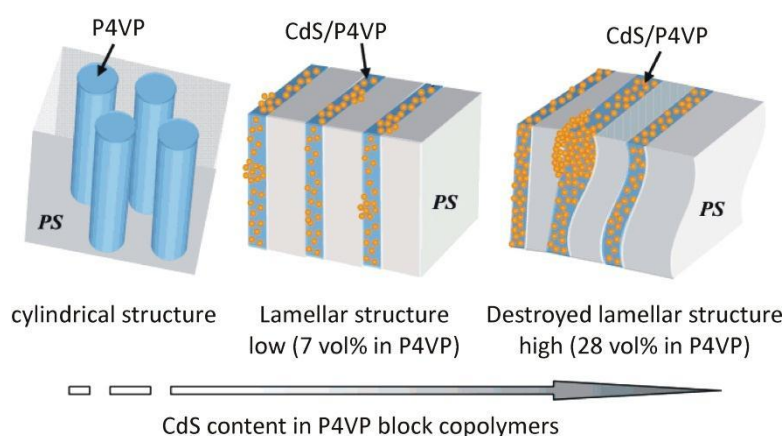


Figure 1–21. Schematic diagram showing the transformation of a hexagonal cylindrical morphology of the copolymer PS-*b*-P4VP to a lamellar order with introduction of 10 wt% CdS nanoparticles. The further addition of CdS (up to 28 wt%) leads to the aggregation of the nanoparticles and the disruption of the lamellar morphology (adapted from ref. 192).

ALIGNMENT OF MICRODOMAINS

A critical issue besides the general morphology lies within the correct alignment of the individual domains. Keeping the device structure in mind, key aspects are the transport pathways for electrons and holes towards the respective electrodes. Additionally, the recombination at the respective counter electrode should be blocked. Gyroid structures are ideal morphologies for Co-continuous transport pathways. However, these structures are only observed in a very narrow range of volume fractions of block copolymers. More common morphologies are hexagonal cylinders or lamellae. In these cases the domains of donor and acceptor have to be aligned perpendicular to the substrate to ensure charge transport towards electrodes (Figure 1–22).

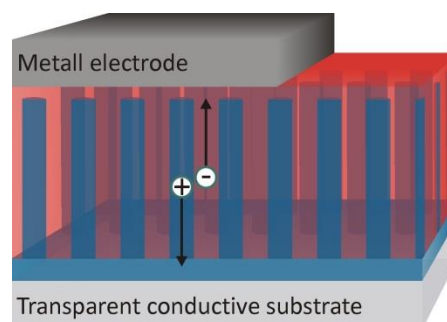


Figure 1–22. Exemplary scheme of an ideally microphase separated block copolymer with vertically aligned cylindrical structures consisting of donor (blue) and an acceptor (red) domains. Similar oriented lamellar structures would also apply.

Unfortunately block copolymers usually tend to orientate the domains parallel to the underlying substrate in thermodynamic equilibrium.¹⁹³ This effect is generally caused by the preferential attraction of one domain to the surface or the air, respectively. To overcome this limitation several methods have been applied, which are highlighted in comprehensive reviews of Hawker, Russell and Darling.^{156,193} The most important techniques are briefly summarized in the following.

A basic approach relies on the surface modification to balance the interface interaction of the polymers with the surface.¹⁹⁴ Due to the loss of preference, the block copolymer is able to self-assemble into highly ordered and vertically oriented domains.¹⁹⁵ A common way to adjust the interface attraction is the coverage with a defined random copolymer of the desired segments.^{196,197} Alternatively, the substrates can directly be patterned to facilitate the vertical self-assembly of the block copolymers (Figure 1–23).^{198,199} However, considering the solar cell device structure the interface to the electrodes should be selective transport materials to ensure the hole transport and block electrons or vice versa. This requirement necessitates the creation of a surface with balanced interaction and adapted functionality, which is by far more challenging.

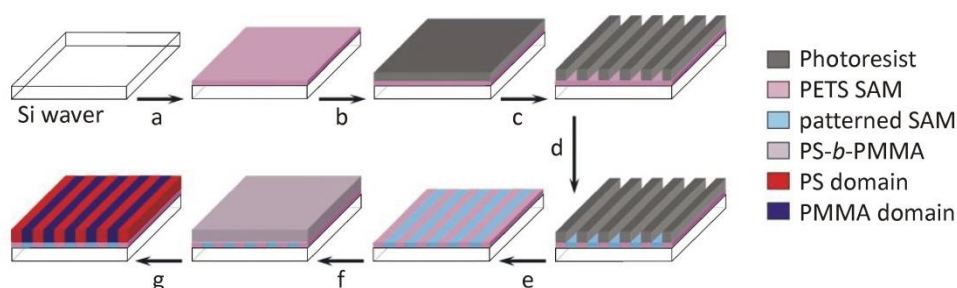


Figure 1–23. Top: scheme of the procedure to control the assembly of block-copolymer domains *via* patterned surfaces. a: self-assembled monolayer (SAM) of phenylethyltrichlorosilane (PETS), b: spin-coating of Photoresist, c: patterning by extreme ultraviolet interferometric lithography, d: conversion to chemical pattern irradiation with soft X-rays, e: removal of photoresist, f: coating with PS-*b*-PMMA copolymer, g: annealing. Chemically modified regions of the surface were preferentially wetted by the PMMA block. (adapted from ref. 198)

A crucial drawback of the mentioned methods is the limitation in layer thickness of the block copolymer.¹⁵⁶ The effect of substrate interaction is mainly restricted to the radius of gyration of the copolymer, while for thicker films the orientation is lost and a random orientation appears. In solar cells, efficient light harvesting necessitates layers of about 100 – 200 nm to absorb all incident light. An alternative approach towards vertical structures in thick layers is the application of strong electrical fields.^{201,202} A basic requirement for this method is a difference in the dielectric constant of the individual polymer segments. Another elegant method is based on solvent induced microphase separation.²⁰³ Using this method, large areas of ordered microstructures became accessible (Figure 1–24).²⁰⁰ A further interesting option for manipulation of the alignment relies on the addition of phase selective additives including nanoparticles. PS-*b*-P2VP could be reoriented adding CdSe nanoparticles, which are confined in the P2VP domain, but segregate to the interface to the substrate and air.²⁰⁴

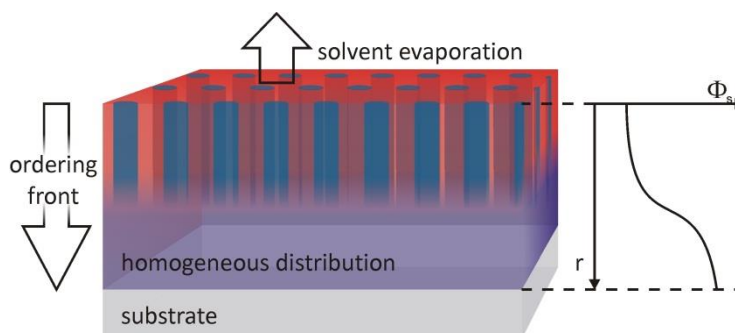


Figure 1–24. Schematic diagram of the controlled solvent evaporation in a thin block copolymer film. At the surface the concentration of the solvent (Φ_s) is low and the polymer undergoes microphase separation, while at the bottom the solvent concentration is high enough to mediate a homogeneous mixture. A gradient of Φ_s as a function of the depths r is established normal to the film surface and an ordering front propagates through the film.²⁰⁰

1.5 CHARACTERIZATION METHODS

MORPHOLOGY

Of central importance in this thesis are the morphologies of the developed polymers in bulk, in thin film or in solution. Common imaging tools comprise transmission or scanning electron microscopy (TEM and SEM)²⁰⁵ and atomic force microscopy (AFM).²⁰⁶ These methods give a direct image of the sample, but focus only on limited areas of individual spots and sections. A more comprehensive overview on the sample structure can be obtained with indirect scattering techniques, which include static and dynamic light scattering (SLS and DLS)^{207,208} and small angle X-ray scattering (SAXS).^{209,210} These methods are well-understood characterization methods, which are described in detail in the respective textbooks given above. However, a comprehensive characterization of the orientation and anisotropy in thin films requires more sophisticated methods such as grazing incident small angle X-ray spectroscopy (GISAXS).²¹¹ This technique is exceptionally useful to gain details of the morphology and domain orientation in the thin film. As it is not as common as the classical x-ray analysis, the basic principle is briefly summarized in the following.

In contrast to the bulk material, the morphology in thin films cannot only just assemble into more or less ordered structures, but it can also align in different directions, *e.g.* parallel or perpendicular to the substrate. Taking an ordinary X-ray vertically through the sample, neither the sample volume would be sufficient enough for a good resolution nor one is able to gain information on the orientation of the morphologies in comparison to the substrate. However, blazing the beam almost parallel to the substrate through the whole length of the thin film not only increases the test volume, but also distinguishes between scattering occurring at parallel or perpendicular oriented structures. A scheme of this principle including all important angles and scattering vectors is given in Figure 1–25.

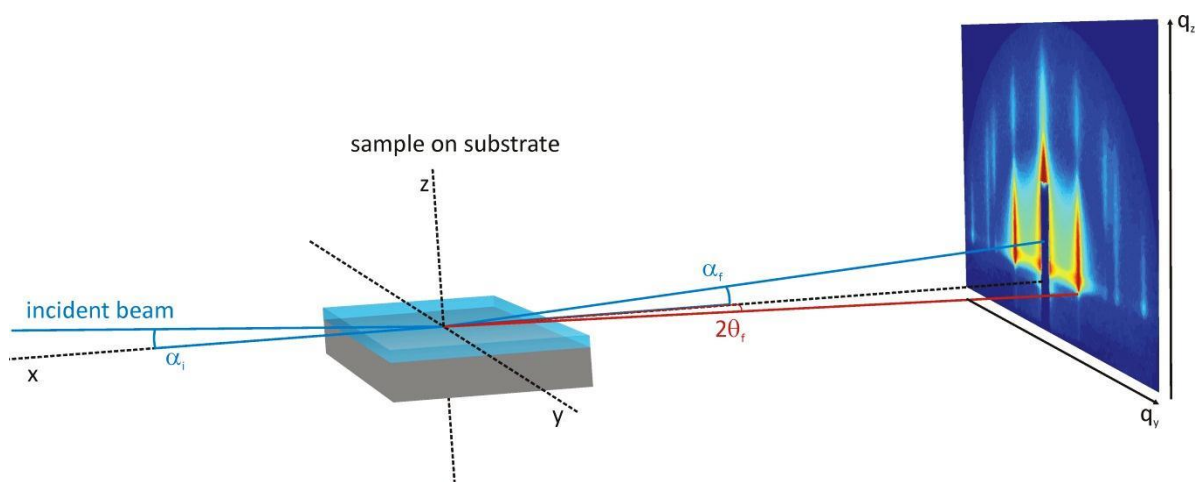


Figure 1–25. Schematic representation of the GISAXS geometry. The incident beam hits onto the sample at a very small incident angle α_i and is scattered in the direction $(2\theta_f, \alpha_f)$ by any electron density fluctuations, such as block copolymer domains.

In the experiment a monochromatic x-ray beam is directed onto the sample at a very small incident angle α_i with respect to the surface. The X-rays are scattered in the direction $(2\theta_f, \alpha_f)$ by

electron density fluctuations, *e.g.* block copolymer microdomains. At low incident angles the detector plane can be considered as parallel to the z -axis, which is perpendicular to the sample surface. In consequence, the scattered beams hit the detector plane either in the z -direction of the detector (scattering vector q_z) for structures oriented parallel to the substrate or in the y -direction (scattering vector q_y) for perpendicular alignment. In conclusion, this technique enables on the one hand the analysis of morphology and domain sizes, according to Bragg's law and on the other hand detailed information on orientation of these structures is accessible. More detailed information on this method can be found in the literature.²¹²⁻²¹⁴

CHARGE TRANSPORT IN BULK

A crucial factor in photovoltaic devices is the charge transport in the individual materials. In optimized devices electron and hole transport should be balanced and be reasonably high to ensure an optimum charge collection. The most important parameter in this context is the charge carrier mobility μ which is defined as the quotient of drift velocity v and the applied electrical field E :

$$\mu = \frac{v}{E}$$

The mobility itself is related to the electrical conductivity by

$$\sigma_c = ne\mu$$

where n is the number of charge carriers and e the electronic charge. In contrast to inorganic semiconductors, the band-model of electronic states does not apply for organic materials, due to less order in the materials and no continuous overlap of the electron orbitals. Instead, the charge transport can be described as a hopping process from one distinct localized state to another. These energy states are commonly related to the orbitals of single molecules. As the energy states are not uniform but dispersed (they follow a Gaussian distribution) due to molecular disorder in the material, the hopping charge transport is strongly depending on the thermal energy of the environment, *viz.* the temperature. A comprehensive overview on the physical aspects of charge transport in organic semiconductors is given by Bässler.²¹⁵

The determination of charge carrier mobility can be accomplished by several techniques, including organic field effect transistor (OFET)²¹⁶ measurements, time-of-flight (TOF)^{217,218} measurements and charge extraction by linearly increasing voltage (CELIV).^{219,220} A straightforward method for estimation of the bulk mobility in semiconductors is the space charge limited current (SCLC) method. Here, the material is sandwiched between two electrodes and the current-voltage (J - V) characteristics of the diode are recorded in the dark. To distinguish between hole and electron transport, the electrodes have to be carefully chosen to inject only holes and electrons. Therefore, the work function of the electrodes should match the respective energy levels of the semiconductor (HOMO for hole transport, LUMO for electron transport). To ensure an Ohmic contact, the energy level offset between the studied material and the electrode should not exceed 0.3 eV. Exemplary schemes of a hole-only and an electron-only device are depicted in Figure 1–26.

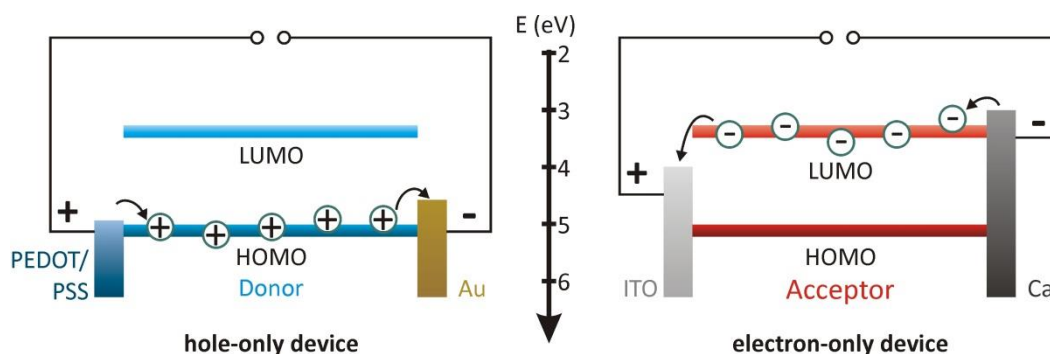


Figure 1–26. Exemplary schemes of a hole-only (left) and an electron-only (right) device. Common electrode pairs for hole-only devices are PEDOT/PSS – gold (Au) and for electron-only devices ITO – Ca (indium tin oxide and Calcium) can be used.

Maintaining the respective requirements, the current flow is not interfered by the charge injection, but it is only limited by the intrinsic charge carrier mobility of the semiconductor. Applying a bias, charges are injected at one electrode building the so called space charge. Depending on the mobility, a maximum of current flow is generated for a certain voltage. In consequence the mobility can be calculated according to Mott-Gurney's equation:

$$J = \frac{9}{8} \varepsilon_0 \varepsilon_r \mu \frac{V^2}{L^3}$$

where J is the current density, ε_0 is the vacuum permittivity, ε_r is the dielectric constant of the semiconductor, V is the applied voltage and L the thickness of the active layer. This equation is only valid, if the concentration of traps is low in comparison to the number of free carriers. However, in organic semiconductors traps may occur due to disorder or impurities (*e.g.* end-groups of the polymer chains) in the material. In consequence, these traps have to be filled and the charge transport mobility becomes field dependent, which is taken into account in the following equation:

$$J = \frac{9}{8} \varepsilon_0 \varepsilon_r \cdot \mu_0 \cdot \exp(0.89 \cdot \gamma \cdot \sqrt{\frac{V}{L}}) \cdot \frac{V^2}{L^3}$$

where μ_{0is} is the mobility at zero electric field and γ is the field activation parameter.

SOLAR CELL DEVICES

The photovoltaic device characterization mainly comprises two different measuring methods. The first is the recording of the current-voltage (J - V) characteristics and the second is the measurement of the spectral response, *viz.* the incident photon to current conversion efficiency (IPCE) for each wavelength, also called external quantum efficiency (EQE). Comparing various different photovoltaic devices necessitates general, uniform and equivalent measurement conditions. Therefore, standardized procedures and conditions have been established, including a generalized spectrum named AM 1.5 G, which is defined as sun light irradiance at a zenith angle of 48.19°, and an intensity set to 1000 W/m².²²¹

The key parameters for comparison of photovoltaic devices are the short circuit current density J_{sc} , the open circuit voltage V_{oc} , the fill factor (FF) and the power conversion efficiency (PCE) η . These values are estimated from the J - V characteristics of the solar cell. A representative plot is shown in Figure 1–27. J_{sc} is determined as the point of no counter voltage, the equivalent of a zero resistance. On the other hand at the point of zero current flow, *i.e.* an infinite resistance, the V_{oc} can be read-out. In an ideal case, the device should maintain the maximum current flow up to this voltage. However, due to internal series resistances and low parallel resistance the current decreases with increasing counter-voltage and the real device output is lower than in the ideal case. A measure for this loss is given by the fill factor, which is defined as quotient of the output at the maximum power point (MPP) and the ideal power output (product of J_{sc} and V_{oc}):

$$FF = \frac{J_{MPP} V_{MPP}}{J_{sc} V_{oc}}$$

where J_{MPP} and V_{MPP} are the current density and voltage at the maximum power point, respectively. According to this, the efficiency η is estimated as:

$$\eta = \frac{J_{MPP} V_{MPP}}{P_{light}} = \frac{FF J_{sc} V_{oc}}{P_{light}}$$

where P_{light} is the power of the incident light and P_{device} is the maximum obtained power from the device.

A key characteristic of devices is their spectral response at different wavelengths. Therefore, J_{sc} is measured for each wavelength and compared to the number of incident photons, giving the EQE or IPCE:

$$EQE = \frac{J_{sc}}{eN_0}$$

where e is the elementary charge and N_0 the incident photon flux density. The plot of EQE vs. wavelength gives a photovoltaic response spectrum of the device, which ideally matches with the absorption spectrum. In contrast, differences in these spectra give rise to loss processes and ineffective charge generation.

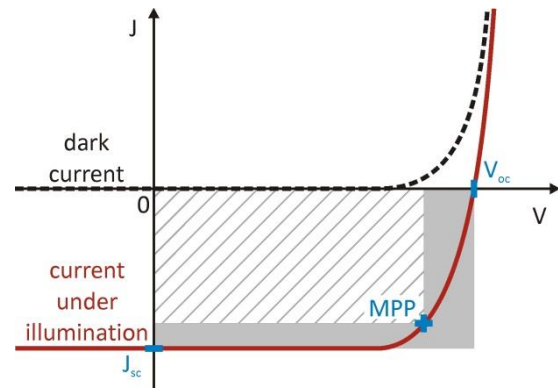


Figure 1–27. Representative current-voltage (J - V) characteristic of a typical photovoltaic device. The important parameters open circuit voltage (V_{oc}) and short circuit current density (J_{sc}) can be read out at the marked points. An ideal device would hold the J_{sc} up to the V_{oc} , however internal resistances cause energy losses and the real output is given as a product of current and voltage at the maximum power point (MPP). The fill factor is calculated as the ratio of the marked rectangular areas, *i.e.* real (lined) maximum power output and the ideal one (grey).

1.6 OBJECTIVE OF THE THESIS

The inherent reliability of inorganic semiconductors even under ambient conditions in combination with the convenient solution processability of polymer semiconductor turn hybrid composites into promising alternatives for photovoltaic devices with excellent cost-benefit ratio and long term stability. Key issues of hybrid devices are certainly the interface of inorganic and organic semiconductor and the morphology. Detailed investigations on these aspects are important to acquire a comprehensive understanding of the involved physical processes and to establish basic structure-property relationships.

This thesis is aimed at the development of novel organic dyes improving the light harvesting and tailor-made polymers, suitable for coordination of inorganic semiconductors and controlled alignment of the morphology (Figure 1–28).

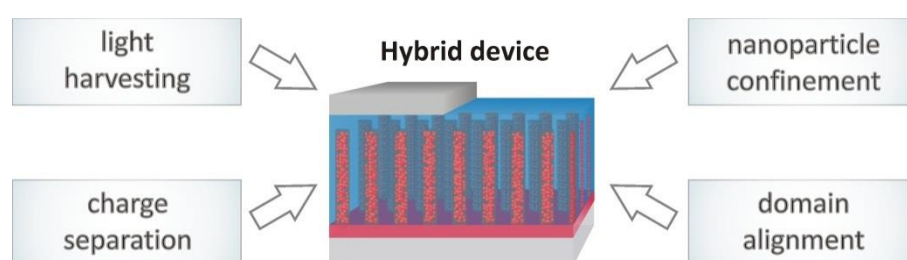


Figure 1–28. Schematic presentation of the main objectives of the thesis. The parameters of light harvesting, the nanoparticle confinement in one domain, the charge separation at the interface and the alignment of the morphology will be studied with the aim, to gain a better understanding of hybrid device properties and to reveal possible approaches towards optimization.

Broadening the spectral range of absorbed light is a central issue to improve the efficiency of hybrid devices. Therefore, the influence of structural modifications on the optical and electrical properties of organic dyes will be studied. Furthermore, the investigated sensitizers have to be examined in detail concerning their spectral response and efficiencies in photovoltaic devices.

In order to gain a better control on the morphology of hybrid devices, tailor-made amphiphilic polymers should be synthesized and characterized. Central aims are the controlled coordination of inorganic nanoparticles, the confinement of suitable amounts in one domain and a beneficial alignment of the microstructure for charge separation. Therefore, synthesis protocols for controlled polymerization of semiconducting and coordinative ambivalent polymers have to be established and optimized. Furthermore, preparation routes for the co-assembly of nanoparticles and functional polymers must be developed, to enable the integration of appropriate amounts of inorganic semiconductor selectively into one domain. Finally, the creation of well-defined morphologies necessitates the investigation of suitable tools for alignment and orientation in thin films. As the topic of hybrid solar cells is complex, not a comprehensive elucidation of all issues is expected. Nevertheless, the basic developments of this thesis should lay the foundation for improved control on the morphology of hybrid devices and thus contribute to a better understanding of the structure-property relations.

1.7 REFERENCES

- (1) H. Shirakawa, E. J. Louis, A. G. MacDiarmid, C. K. Chiang, A. J. Heeger, *J. Chem. Soc., Chem. Commun.* **1977**, 578-580.
- (2) A. J. Heeger, *Chem. Soc. Rev.* **2010**, *39*, 2354-2371.
- (3) A. J. Heeger, *Angew. Chem., Int. Ed.* **2001**, *40*, 2591-2611.
- (4) S. Kirchmeyer, K. Reuter, *J. Mater. Chem.* **2005**, *15*, 2077-2088.
- (5) M. Angelopoulos, *IBM J. Res. Dev.* **2001**, *45*, 57-75.
- (6) H. Naarmann, Polymers, Electrically Conducting in *Ullmann's Encyclopedia of Industrial Chemistry*; Wiley-VCH Verlag GmbH & Co. KGaA: **2000**.
- (7) J. Jang, Conducting Polymer Nanomaterials and Their Applications in *Emissive Materials Nanomaterials*; Springer Berlin Heidelberg: **2006**; Vol. 199, p 189-260.
- (8) M. S. AlSalhi, J. Alam, L. A. Dass, M. Raja, *Int. J. Mol. Sci.* **2011**, *12*, 2036-2054.
- (9) S. Tonzani, *Nature* **2009**, *459*, 312-314.
- (10) H. E. Katz, *Chem. Mater.* **2004**, *16*, 4748-4756.
- (11) J. H. Schon, A. Dodabalapur, Z. Bao, C. Kloc, O. Schenker, B. Batlogg, *Nature* **2001**, *410*, 189-192.
- (12) C. J. Brabec, S. Gowrisanker, J. J. M. Halls, D. Laird, S. Jia, S. P. Williams, *Adv. Mater.* **2010**, *22*, 3839-3856.
- (13) H. Letheby, *J. Chem. Soc.* **1862**, *15*, 161-163.
- (14) V. Meyer, *Ber.* **1883**, *16*, 1465-1478.
- (15) T. Yasui, *Bull. Chem. Soc. Jpn.* **1935**, *10*, 305-311.
- (16) J. Honzl, M. Tlustáková, *J. Polym. Sci., C Polym. Symp.* **1968**, *22*, 451-462.
- (17) S. L. Meisel, G. C. Johnson, H. D. Hartough, *J. Am. Chem. Soc.* **1950**, *72*, 1910-1912.
- (18) R. McNeill, R. Siudak, J. Wardlaw, D. Weiss, *Aust. J. Chem.* **1963**, *16*, 1056-1075.
- (19) H. Hoegl, *J. Phys. Chem.* **1965**, *69*, 755-766.
- (20) M. Sommer, S. M. Lindner, M. Thelakkat, *Adv. Funct. Mater.* **2007**, *17*, 1493-1500.
- (21) S. Barrau, T. Heiser, F. Richard, C. Brochon, C. Ngov, K. van de Wetering, G. Hadziioannou, D. V. Anokhin, D. A. Ivanov, *Macromolecules* **2008**, *41*, 2701-2710.
- (22) M.-A. Sato, S. Tanaka, K. Kaeriyama, *J. Chem. Soc., Chem. Commun.* **1986**, 873-874.
- (23) P. W. M. Blom, M. C. J. M. Vissenberg, *Mater. Sci. Eng., R* **2000**, *27*, 53-94.
- (24) U. Scherf, E. J. W. List, *Adv. Mater.* **2002**, *14*, 477-487.
- (25) R. D. McCullough, *Adv. Mater.* **1998**, *10*, 93-116.
- (26) Y.-J. Cheng, S.-H. Yang, C.-S. Hsu, *Chem. Rev.* **2009**, *109*, 5868-5923.
- (27) A. Facchetti, *Chem. Mater.* **2010**, *23*, 733-758.
- (28) Y. Liang, L. Yu, *Acc. Chem. Res.* **2010**, *43*, 1227-1236.
- (29) L. Bian, E. Zhu, J. Tang, W. Tang, F. Zhang, *Prog. Polym. Sci.* **2012**, *37*, 1292-1331.
- (30) Z. He, C. Zhong, X. Huang, W.-Y. Wong, H. Wu, L. Chen, S. Su, Y. Cao, *Adv. Mater.* **2011**, *23*, 4636-4643.
- (31) M. A. Green, K. Emery, Y. Hishikawa, W. Warta, E. D. Dunlop, *Prog. Photovolt: Res. Appl.* **2012**, *20*, 606-614.
- (32) F. C. Krebs, *Sol. Energy Mater.* **2009**, *93*, 394-412.
- (33) C. S. Tsai *Biomacromolecules*; Wiley-Liss: Hoboken, NJ, **2007**.
- (34) G. S. Manning, *Annu. Rev. Phys. Chem.* **1972**, *23*, 117-140.
- (35) S. Förster, M. Schmidt, *Adv. Polym. Sci.* **1995**, *120*, 51-133.
- (36) *Polyelectrolytes, special issue in Advances in colloid and interface science*; Elsevier: Amsterdam, **2010**; Vol. 158.
- (37) *Polyelectrolytes in Macromol. Symp.*; U. Scheler, Ed.; Wiley-VCH: Weinheim, **2004**; Vol. 211.
- (38) A. O. Patil, Y. Ikenoue, F. Wudl, A. J. Heeger, *J. Am. Chem. Soc.* **1987**, *109*, 1858-1859.

- (39) H. Jiang, P. Taranekar, J. R. Reynolds, K. S. Schanze, *Angew. Chem., Int. Ed.* **2009**, *48*, 4300-4316.
- (40) I. Haeldermans, I. Truijen, K. Vandewal, W. Moons, M. K. Van Bael, J. D. H. Haen, J. V. Manca, J. Mullens, *Thin Solid Films* **2008**, *516*, 7245-7250.
- (41) S. Shi, F. Wudl, *Macromolecules* **1990**, *23*, 2119-2124.
- (42) F. Huang, H. Wu, D. Wang, W. Yang, Y. Cao, *Chem. Mater.* **2004**, *16*, 708-716.
- (43) S. W. Thomas, G. D. Joly, T. M. Swager, *Chem. Rev.* **2007**, *107*, 1339-1386.
- (44) D. T. McQuade, A. E. Pullen, T. M. Swager, *Chem. Rev.* **2000**, *100*, 2537-2574.
- (45) K. E. Achyuthan, T. S. Bergstedt, L. Chen, R. M. Jones, S. Kumaraswamy, S. A. Kushon, K. D. Ley, L. Lu, D. McBranch, H. Mukundan, F. Rininsland, X. Shi, W. Xia, D. G. Whitten, *J. Mater. Chem.* **2005**, *15*, 2648-2656.
- (46) E. W. H. Jager, E. Smela, O. Inganäs, *Science* **2000**, *290*, 1540-1545.
- (47) K. Svennersten, K. C. Larsson, M. Berggren, A. Richter-Dahlfors, *Biochim. Biophys. Acta, Gen. Subj.* **2011**, *1810*, 276-285.
- (48) M. Berggren, A. Richter-Dahlfors, *Adv. Mater.* **2007**, *19*, 3201-3213.
- (49) C. Tan, M. R. Pinto, K. S. Schanze, *Chem. Commun.* **2002**, *0*, 446-447.
- (50) M. R. Pinto, B. M. Kristal, K. S. Schanze, *Langmuir* **2003**, *19*, 6523-6533.
- (51) H. Jiang, X. Zhao, K. S. Schanze, *Langmuir* **2006**, *22*, 5541-5543.
- (52) P. Kaur, H. Yue, M. Wu, M. Liu, J. Treece, D. H. Waldeck, C. Xue, H. Liu, *The Journal of Physical Chemistry B* **2007**, *111*, 8589-8596.
- (53) T. Kawai, T. Yamaue, K. Tada, M. Onoda, S.-H. Jin, S.-K. Choi, K. Yoshino, *Jpn. J. Appl. Phys., Part 2* **1996**, *35*, L741.
- (54) G. Decher, *Science* **1997**, *277*, 1232-1237.
- (55) J. K. Mwaura, M. R. Pinto, D. Witker, N. Ananthakrishnan, K. S. Schanze, J. R. Reynolds, *Langmuir* **2005**, *21*, 10119-10126.
- (56) J. Yang, A. Garcia, T.-Q. Nguyen, *Appl. Phys. Lett.* **2007**, *90*, 103514-103513.
- (57) G. K. V. V. Thalluri, J.-C. Bolsée, A. Gadisa, M. Parchine, T. Boonen, J. D'Haen, A. E. Boyukbayram, J. Vandenberg, T. J. Cleij, L. Lutsen, D. Vanderzande, J. Manca, *Sol. Energy Mater.* **2011**, *95*, 3262-3268.
- (58) C. J. Bhongale, M. Thelakkat, *Sol. Energy Mater.* **2010**, *94*, 817-822.
- (59) A. Garcia, R. Yang, Y. Jin, B. Walker, T.-Q. Nguyen, *Appl. Phys. Lett.* **2007**, *91*, 153502-153503.
- (60) J. C. deMello, N. Tessler, S. C. Graham, R. H. Friend, *Phys. Rev. B: Condens. Matter Mater. Phys.* **1998**, *57*, 12951-12963.
- (61) C. Hoven, R. Yang, A. Garcia, A. J. Heeger, T.-Q. Nguyen, G. C. Bazan, *J. Am. Chem. Soc.* **2007**, *129*, 10976-10977.
- (62) J. H. Seo, E. B. Namdas, A. Gutacker, A. J. Heeger, G. C. Bazan, *Adv. Funct. Mater.* **2011**, *21*, 3667-3672.
- (63) J. H. Seo, A. Gutacker, B. Walker, S. Cho, A. Garcia, R. Yang, T.-Q. Nguyen, A. J. Heeger, G. C. Bazan, *J. Am. Chem. Soc.* **2009**, *131*, 18220-18221.
- (64) J. H. Seo, A. Gutacker, Y. Sun, H. Wu, F. Huang, Y. Cao, U. Scherf, A. J. Heeger, G. C. Bazan, *J. Am. Chem. Soc.* **2011**, *133*, 8416-8419.
- (65) T. Yang, M. Wang, C. Duan, X. Hu, L. Huang, J. Peng, F. Huang, X. Gong, *Energy Environ. Sci.* **2012**, *5*, 8208-8214.
- (66) H. T. Nguyen, T.-Q. Nguyen, M. T. Nguyen, *Chem. Phys. Lett.* **2012**, *530*, 39-44.
- (67) K. Matyjaszewski, A. H. E. Müller *Controlled and Living Polymerizations*; Wiley-VCH: Weinheim, **2009**.
- (68) V. Coessens, T. Pintauer, K. Matyjaszewski, *Prog. Polym. Sci.* **2001**, *26*, 337-377.
- (69) C. J. Hawker, A. W. Bosman, E. Harth, *Chem. Rev.* **2001**, *101*, 3661-3688.
- (70) G. Moad, E. Rizzardo, S. H. Thang, *Aust. J. Chem.* **2005**, *58*, 379-410.

- (71) W. A. Braunecker, K. Matyjaszewski, *Prog. Polym. Sci.* **2007**, *32*, 93-146.
- (72) J. Chiefari, Y. K. Chong, F. Ercole, J. Krstina, J. Jeffery, T. P. T. Le, R. T. A. Mayadunne, G. F. Meijs, C. L. Moad, G. Moad, E. Rizzardo, S. H. Thang, *Macromolecules* **1998**, *31*, 5559-5562.
- (73) G. Moad, E. Rizzardo, S. H. Thang, *Polymer* **2008**, *49*, 1079-1131.
- (74) G. Moad, E. Rizzardo, S. H. Thang, *Polym. Int.* **2011**, *60*, 9-25.
- (75) N. Miyaura, K. Yamada, A. Suzuki, *Tetrahedron Lett.* **1979**, *20*, 3437-3440.
- (76) N. Miyaura, A. Suzuki, *J. Chem. Soc., Chem. Commun.* **1979**, *0*, 866-867.
- (77) K. Sonogashira, Y. Tohda, N. Hagihara, *Tetrahedron Lett.* **1975**, *16*, 4467-4470.
- (78) A. O. King, N. Okukado, E.-i. Negishi, *J. Chem. Soc., Chem. Commun.* **1977**, *0*, 683-684.
- (79) D. Milstein, J. K. Stille, *J. Am. Chem. Soc.* **1978**, *100*, 3636-3638.
- (80) A. Yokoyama, R. Miyakoshi, T. Yokozawa, *Macromolecules* **2004**, *37*, 1169-1171.
- (81) E. E. Sheina, J. Liu, M. C. Iovu, D. W. Laird, R. D. McCullough, *Macromolecules* **2004**, *37*, 3526-3528.
- (82) M. C. Iovu, E. E. Sheina, R. R. Gil, R. D. McCullough, *Macromolecules* **2005**, *38*, 8649-8656.
- (83) R. Miyakoshi, A. Yokoyama, T. Yokozawa, *J. Am. Chem. Soc.* **2005**, *127*, 17542-17547.
- (84) H. Komber, V. Senkovskyy, R. Tkachov, K. Johnson, A. Kiriy, W. T. S. Huck, M. Sommer, *Macromolecules* **2011**.
- (85) A. Kiriy, V. Senkovskyy, M. Sommer, *Macromol. Rapid Commun.* **2011**, *32*, 1503-1517.
- (86) A. Smeets, K. Van den Bergh, J. De Winter, P. Gerbaux, T. Verbiest, G. Koeckelberghs, *Macromolecules* **2009**, *42*, 7638-7641.
- (87) M. Jeffries-El, G. Sauvé, R. D. McCullough, *Macromolecules* **2005**, *38*, 10346-10352.
- (88) R. H. Lohwasser, M. Thelakkt, *Macromolecules* **2011**, *44*, 3388-3397.
- (89) R. Miyakoshi, K. Shimono, A. Yokoyama, T. Yokozawa, *J. Am. Chem. Soc.* **2006**, *128*, 16012-16013.
- (90) L. Huang, S. Wu, Y. Qu, Y. Geng, F. Wang, *Macromolecules* **2008**, *41*, 8944-8947.
- (91) M. C. Stefan, A. E. Javier, I. Osaka, R. D. McCullough, *Macromolecules* **2008**, *42*, 30-32.
- (92) Y. Zhang, K. Tajima, K. Hirota, K. Hashimoto, *J. Am. Chem. Soc.* **2008**, *130*, 7812-7813.
- (93) G. Tu, H. Li, M. Forster, R. Heiderhoff, L. J. Balk, U. Scherf, *Macromolecules* **2006**, *39*, 4327-4331.
- (94) M. C. Iovu, R. Zhang, J. R. Cooper, D. M. Smilgies, A. E. Javier, E. E. Sheina, T. Kowalewski, R. D. McCullough, *Macromol. Rapid Commun.* **2007**, *28*, 1816-1824.
- (95) M. C. Iovu, M. Jeffries-El, R. Zhang, T. Kowalewski, R. D. McCullough, *Journal of Macromolecular Science, Part A* **2006**, *43*, 1991-2000.
- (96) M. Urien, H. Erothu, E. Cloutet, R. C. Hiorns, L. Vignau, H. Cramail, *Macromolecules* **2008**, *41*, 7033-7040.
- (97) I. Botiz, S. B. Darling, *Macromolecules* **2009**, *42*, 8211-8217.
- (98) S. N. Patel, A. E. Javier, G. M. Stone, S. A. Mullin, N. P. Balsara, *ACS Nano* **2012**, *6*, 1589-1600.
- (99) A. E. Javier, S. N. Patel, D. T. Hallinan, V. Srinivasan, N. P. Balsara, *Angew. Chem., Int. Ed.* **2011**, *50*, 9848-9851.
- (100) C. Suspene, L. Miozzo, J. Choi, R. Gironda, B. Geffroy, D. Tondelier, Y. Bonnassieux, G. Horowitz, A. Yassar, *J. Mater. Chem.* **2012**, *22*, 4511-4518.
- (101) J. E. Hein, V. V. Fokin, *Chem. Soc. Rev.* **2010**, *39*, 1302-1315.
- (102) H. C. Kolb, M. G. Finn, K. B. Sharpless, *Angew. Chem., Int. Ed.* **2001**, *40*, 2004-2021.
- (103) R. Huisgen, G. Szeimies, L. Möbius, *Chem. Ber.* **1967**, *100*, 2494-2507.
- (104) A. S. Lang, M. Thelakkt, *Polym. Chem.* **2011**, *2*, 2213-2221.
- (105) G. H. Wannier, *Physical Review* **1937**, *52*, 191-197.
- (106) J. Frenkel, *Physical Review* **1931**, *37*, 17-44.
- (107) S. Karg, W. Riess, V. Dyakonov, M. Schwoerer, *Synth. Met.* **1993**, *54*, 427-433.

- (108) C. W. Tang, A. C. Albrecht, *J. Chem. Phys.* **1975**, *62*, 2139-2149.
- (109) C. W. Tang, S. A. VanSlyke, *Appl. Phys. Lett.* **1987**, *51*, 913-915.
- (110) G. Yu, K. Pakbaz, A. J. Heeger, *Appl. Phys. Lett.* **1994**, *64*, 3422-3424.
- (111) G. Yu, J. Gao, J. C. Hummelen, F. Wudl, A. J. Heeger, *Science* **1995**, *270*, 1789-1791.
- (112) G. Zhao, Y. He, Y. Li, *Adv. Mater.* **2010**, *22*, 4355-4358.
- (113) F. C. Jamieson, E. B. Domingo, T. McCarthy-Ward, M. Heeney, N. Stingelin, J. R. Durrant, *Chem. Sci.* **2012**.
- (114) Y. Sun, G. C. Welch, W. L. Leong, C. J. Takacs, G. C. Bazan, A. J. Heeger, *Nat. Mater.* **2011**.
- (115) B. A. Jones, A. Facchetti, M. R. Wasielewski, T. J. Marks, *J. Am. Chem. Soc.* **2007**, *129*, 15259-15278.
- (116) H. Usta, A. Facchetti, T. J. Marks, *Acc. Chem. Res.* **2011**, *44*, 501-510.
- (117) J. C. Hummelen, B. W. Knight, F. LePeq, F. Wudl, J. Yao, C. L. Wilkins, *J. Org. Chem.* **1995**, *60*, 532-538.
- (118) Y. Sun, J. A. Rogers, *Adv. Mater.* **2007**, *19*, 1897-1916.
- (119) W. U. Huynh, J. J. Dittmer, A. P. Alivisatos, *Science* **2002**, *295*, 2425-2427.
- (120) B. Sun, E. Marx, N. C. Greenham, *Nano Lett.* **2003**, *3*, 961-963.
- (121) I. Gur, N. A. Fromer, C.-P. Chen, A. G. Kanaras, A. P. Alivisatos, *Nano Lett.* **2006**, *7*, 409-414.
- (122) S. Dayal, N. Kopidakis, D. C. Olson, D. S. Ginley, G. Rumbles, *Nano Lett.* **2009**, *10*, 239-242.
- (123) S. D. Oosterhout, M. M. Wienk, S. S. van Bavel, R. Thiedmann, L. Jan Anton Koster, J. Gilot, J. Loos, V. Schmidt, R. A. J. Janssen, *Nat. Mater.* **2009**, *8*, 818-824.
- (124) W. J. E. Beek, M. M. Wienk, M. Kemerink, X. Yang, R. A. J. Janssen, *J. Phys. Chem. B* **2005**, *109*, 9505-9516.
- (125) D. V. Talapin, J.-S. Lee, M. V. Kovalenko, E. V. Shevchenko, *Chem. Rev.* **2009**, *110*, 389-458.
- (126) N. C. Greenham, X. Peng, A. P. Alivisatos, *Phys. Rev. B: Condens. Matter Mater. Phys.* **1996**, *54*, 17628-17637.
- (127) D. Yu, C. Wang, P. Guyot-Sionnest, *Science* **2003**, *300*, 1277-1280.
- (128) S. Fischer, A. Salcher, A. Kornowski, H. Weller, S. Förster, *Angew. Chem., Int. Ed.* **2011**, *50*, 7811-7814.
- (129) J. Liu, T. Tanaka, K. Sivula, A. P. Alivisatos, J. M. J. Frechet, *J. Am. Chem. Soc.* **2004**, *126*, 6550-6551.
- (130) S. Ren, L.-Y. Chang, S.-K. Lim, J. Zhao, M. Smith, N. Zhao, V. Bulović, M. Bawendi, S. Gradečak, *Nano Lett.* **2011**, *11*, 3998-4002.
- (131) N. Pradhan, B. Katz, S. Efrima, *J. Phys. Chem. B* **2003**, *107*, 13843-13854.
- (132) S. Dowland, T. Lutz, A. Ward, S. P. King, A. Sudlow, M. S. Hill, K. C. Molloy, S. A. Haque, *Adv. Mater.* **2011**, *23*, 2739-2744.
- (133) T. Rath, M. Edler, W. Haas, A. Fischereider, S. Moscher, A. Schenk, R. Trattnig, M. Sezen, G. Mauthner, A. Pein, D. Meischler, K. Bartl, R. Saf, N. Bansal, S. A. Haque, F. Hofer, E. J. W. List, G. Trimmel, *Adv. Energy Mater.* **2011**, *1*, 1046-1050.
- (134) B. O'Regan, M. Grätzel, *Nature* **1991**, *353*, 737-740.
- (135) A. Yella, H.-W. Lee, H. N. Tsao, C. Yi, A. K. Chandiran, M. K. Nazeeruddin, E. W.-G. Diao, C.-Y. Yeh, S. M. Zakeeruddin, M. Grätzel, *Science* **2011**, *334*, 629-634.
- (136) J. Hagen, W. Schaffrath, P. Otschik, R. Fink, A. Bacher, H.-W. Schmidt, D. Haarer, *Synth. Met.* **1997**, *89*, 215-220.
- (137) U. Bach, D. Lupo, P. Comte, J. E. Moser, F. Weissortel, J. Salbeck, H. Spreitzer, M. Grätzel, *Nature* **1998**, *395*, 583-585.
- (138) B. Peng, G. Jungmann, C. Jäger, D. Haarer, H.-W. Schmidt, M. Thelakkat, *Coord. Chem. Rev.* **2004**, *248*, 1479-1489.

- (139) M. K. Nazeeruddin, A. Kay, I. Rodicio, R. Humphry-Baker, E. Mueller, P. Liska, N. Vlachopoulos, M. Grätzel, *J. Am. Chem. Soc.* **1993**, *115*, 6382-6390.
- (140) J. Krüger, R. Plass, L. Cevey, M. Piccirelli, M. Grätzel, U. Bach, *Appl. Phys. Lett.* **2001**, *79*, 2085-2087.
- (141) J.-F. Yin, M. Velayudham, D. Bhattacharya, H.-C. Lin, K.-L. Lu, *Coord. Chem. Rev.* **2012**, *256*, 3008-3035.
- (142) M. M. Lee, J. Teuscher, T. Miyasaka, T. N. Murakami, H. J. Snaith, *Science* **2012**, *338*, 643-647.
- (143) I. Chung, B. Lee, J. He, R. P. H. Chang, M. G. Kanatzidis, *Nature* **2012**, *485*, 486-489.
- (144) A. Kojima, K. Teshima, Y. Shirai, T. Miyasaka, *J. Am. Chem. Soc.* **2009**, *131*, 6050-6051.
- (145) J. M. Ball, M. M. Lee, A. Hey, H. J. Snaith, *Energy Environ. Sci.* **2013**, *6*, 1739-1743.
- (146) J. Burschka, A. Dualeh, F. Kessler, E. Baranoff, N.-L. Cevey-Ha, C. Yi, M. K. Nazeeruddin, M. Grätzel, *J. Am. Chem. Soc.* **2011**, *133*, 18042-18045.
- (147) S. Erten-Ela, M. D. Yilmaz, B. Icli, Y. Dede, S. Icli, E. U. Akkaya, *Org. Lett.* **2008**, *10*, 3299-3302.
- (148) K. Willinger, M. Thelakkat, Photosensitizers in Solar Energy Conversion in *Photosensitizers in Medicine, Environment, and Security*; T. Nyokong, V. Ahsen, Eds.; Springer Netherlands: **2012**, p 527-617.
- (149) A. Mishra, Markus K. R. Fischer, P. Bäuerle, *Angew. Chem., Int. Ed.* **2009**, *48*, 2474-2499.
- (150) D. Gebeyehu, C. J. Brabec, N. S. Sariciftci, D. Vangeneugden, R. Kiebooms, D. Vanderzande, F. Kienberger, H. Schindler, *Synth. Met.* **2001**, *125*, 279-287.
- (151) J. E. Kroeze, N. Hirata, L. Schmidt-Mende, C. Orizu, S. D. Ogier, K. Carr, M. Grätzel, J. R. Durrant, *Adv. Funct. Mater.* **2006**, *16*, 1832-1838.
- (152) G. K. Mor, K. Shankar, M. Paulose, O. K. Varghese, C. A. Grimes, *Appl. Phys. Lett.* **2007**, *91*, 152111-152113.
- (153) P. Ravirajan, A. M. Peiró, M. K. Nazeeruddin, M. Grätzel, D. D. C. Bradley, J. R. Durrant, J. Nelson, *J. Phys. Chem. B* **2006**, *110*, 7635-7639.
- (154) X. Liu, W. Zhang, S. Uchida, L. Cai, B. Liu, S. Ramakrishna, *Adv. Mater.* **2010**, *9999*, NA.
- (155) Z. Nie, E. Kumacheva, *Nat. Mater.* **2008**, *7*, 277-290.
- (156) C. J. Hawker, T. P. Russell, *MRS Bulletin* **2005**, *30*, 952-966.
- (157) C. Park, J. Yoon, E. L. Thomas, *Polymer* **2003**, *44*, 6725-6760.
- (158) I. W. Hamley *The physics of block copolymers* Oxford Univ. Press: Oxford, **1999**.
- (159) M. L. Huggins, *J. Chem. Phys.* **1941**, *9*, 440-440.
- (160) P. J. Flory, *J. Chem. Phys.* **1941**, *9*, 660-660.
- (161) L. Leibler, *Macromolecules* **1980**, *13*, 1602-1617.
- (162) Y.-C. Tseng, S. B. Darling, *Polymers* **2010**, *2*, 470-489.
- (163) M. C. Orilall, U. Wiesner, *Chem. Soc. Rev.* **2011**, *40*, 520-535.
- (164) G. J. d. A. Soler-Illia, C. Sanchez, B. Lebeau, J. Patarin, *Chem. Rev.* **2002**, *102*, 4093-4138.
- (165) P. Yang, D. Zhao, D. I. Margolese, B. F. Chmelka, G. D. Stucky, *Nature* **1998**, *396*, 152-155.
- (166) G. J. d. A. A. Soler-Illia, C. Sanchez, *New J. Chem.* **2000**, *24*, 493-499.
- (167) E. L. Crepaldi, G. J. d. A. Soler-Illia, D. Grosso, F. Cagnol, F. Ribot, C. Sanchez, *J. Am. Chem. Soc.* **2003**, *125*, 9770-9786.
- (168) E. J. W. Crossland, M. Kamperman, M. Nedelcu, C. Ducati, U. Wiesner, D.-M. Smilgies, G. E. S. Toombes, M. A. Hillmyer, S. Ludwigs, U. Steiner, H. J. Snaith, *Nano Lett.* **2009**, *9*, 2807-2812.
- (169) M. Retsch, Z. Zhou, S. Rivera, M. Kappl, X. S. Zhao, U. Jonas, Q. Li, *Macromol. Chem. Phys.* **2009**, *210*, 230-241.
- (170) Z.-Z. Gu, A. Fujishima, O. Sato, *Chem. Mater.* **2002**, *14*, 760-765.
- (171) O. D. Velev, T. A. Jede, R. F. Lobo, A. M. Lenhoff, *Nature* **1997**, *389*, 447-448.
- (172) J. C. Brendel, Y. Lu, M. Thelakkat, *J. Mater. Chem.* **2010**, *20*, 7255-7265.

- (173) J. Hu, M. Abdelsalam, P. Bartlett, R. Cole, Y. Sugawara, J. Baumberg, S. Mahajan, G. Denuault, *J. Mater. Chem.* **2009**, *19*, 3855-3858.
- (174) L. Li, U. Steiner, S. Mahajan, *J. Mater. Chem.* **2010**, *20*, 7131-7134.
- (175) W. Dong, H. J. Bongard, F. Marlow, *Chem. Mater.* **2003**, *15*, 568-574.
- (176) S. John, *Phys. Rev. Lett.* **1987**, *58*, 2486-2489.
- (177) S. Guldin, S. Hüttner, M. Kolle, M. E. Welland, P. Müller-Buschbaum, R. H. Friend, U. Steiner, N. Tétreault, *Nano Lett.* **2010**, *10*, 2303-2309.
- (178) N. Haberkorn, J. S. Gutmann, P. Theato, *ACS Nano* **2009**, *3*, 1415-1422.
- (179) S. Malynych, I. Luzinov, G. Chumanov, *J. Phys. Chem. B* **2002**, *106*, 1280-1285.
- (180) M. Zhang, M. Drechsler, A. H. E. Müller, *Chem. Mater.* **2004**, *16*, 537-543.
- (181) K. D. Gatsouli, S. Pispas, E. I. Kamitsos, *J. Phys. Chem. C* **2007**, *111*, 15201-15209.
- (182) R. S. Yelamanchili, Y. Lu, T. Lunkenbein, N. Miyajima, L.-T. Yan, M. Ballauff, J. Brey, *Small* **2009**, *5*, 1326-1333.
- (183) S. Förster, M. Antonietti, *Adv. Mater.* **1998**, *10*, 195-217.
- (184) S. Förster, T. Plantenberg, *Angew. Chem., Int. Ed.* **2002**, *41*, 688-714.
- (185) Y. Liu, X. Wang, *Polym. Chem.* **2011**, *2*, 2741-2757.
- (186) S. Neyshtadt, M. Kalina, G. L. Frey, *Adv. Mater.* **2008**, *20*, 2541-2546.
- (187) S. Neyshtadt, J. P. Jahnke, R. J. Messinger, A. Rawal, T. Segal Peretz, D. Huppert, B. F. Chmelka, G. L. Frey, *J. Am. Chem. Soc.* **2011**, *133*, 10119-10133.
- (188) M. C. Lechmann, D. Kessler, J. S. Gutmann, *Langmuir* **2009**, *25*, 10202-10208.
- (189) M. C. Lechmann, S. A. L. Weber, J. Geserick, N. Husing, R. Berger, J. S. Gutmann, *J. Mater. Chem.* **2011**, *21*, 7765-7770.
- (190) S. Maria, A. S. Susha, M. Sommer, D. V. Talapin, A. L. Rogach, M. Thelakkat, *Macromolecules* **2008**, *41*, 6081-6088.
- (191) C.-P. Li, K.-H. Wei, J. Y. Huang, *Angew. Chem., Int. Ed.* **2006**, *45*, 1449-1453.
- (192) S.-W. Yeh, K.-H. Wei, Y.-S. Sun, U.-S. Jeng, K. S. Liang, *Macromolecules* **2005**, *38*, 6559-6565.
- (193) S. B. Darling, *Prog. Polym. Sci.* **2007**, *32*, 1152-1204.
- (194) T. P. Russell, E. Huang, L. Rockford, Block Copolymer Thin Films in *Encyclopedia of Materials: Science and Technology (Second Edition)*; Elsevier: Oxford, **2001**.
- (195) H.-C. Kim, T. P. Russell, *J. Polym. Sci. B Polym. Phys.* **2001**, *39*, 663-668.
- (196) P. Mansky, Y. Liu, E. Huang, T. P. Russell, C. Hawker, *Science* **1997**, *275*, 1458-1460.
- (197) D. Y. Ryu, K. Shin, E. Drockenmuller, C. J. Hawker, T. P. Russell, *Science* **2005**, *308*, 236-239.
- (198) S. Ouk Kim, H. H. Solak, M. P. Stoykovich, N. J. Ferrier, J. J. de Pablo, P. F. Nealey, *Nature* **2003**, *424*, 411-414.
- (199) L. Rockford, Y. Liu, P. Mansky, T. P. Russell, M. Yoon, S. G. J. Mochrie, *Phys. Rev. Lett.* **1999**, *82*, 2602-2605.
- (200) S. H. Kim, M. J. Misner, T. Xu, M. Kimura, T. P. Russell, *Adv. Mater.* **2004**, *16*, 226-231.
- (201) T. L. Morkved, M. Lu, A. M. Urbas, E. E. Ehrichs, H. M. Jaeger, P. Mansky, T. P. Russell, *Science* **1996**, *273*, 931-933.
- (202) T. Thurn-Albrecht, J. DeRouchey, T. P. Russell, H. M. Jaeger, *Macromolecules* **2000**, *33*, 3250-3253.
- (203) G. Kim, M. Libera, *Macromolecules* **1998**, *31*, 2569-2577.
- (204) Y. Lin, A. Boker, J. He, K. Sill, H. Xiang, C. Abetz, X. Li, J. Wang, T. Emrick, S. Long, Q. Wang, A. Balazs, T. P. Russell, *Nature* **2005**, *434*, 55-59.
- (205) R. F. Egerton *Physical principles of electron microscopy* Springer: New York, **2005**.
- (206) P. Eaton, P. West *Atomic force microscopy* Oxford Univ. Press: Oxford, **2010**.
- (207) *Light scattering* W. Brown, Ed.; Clarendon Press: Oxford, **1996**.
- (208) B. J. Berne, R. Pecora *Dynamic light scattering* Dover Publ.: Mineola, NY, **2000**.
- (209) *Small angle X-ray scattering* O. Glatter, Ed.; Acad. Press: London, **1982**.

-
- (210) N. Stribeck *X-ray scattering of soft matter* Springer: Berlin, **2007**.
- (211) J. Rivnay, S. C. B. Mannsfeld, C. E. Miller, A. Salleo, M. F. Toney, *Chemical Reviews Chem. Rev.* **2012**.
- (212) J. R. Levine, J. B. Cohen, Y. W. Chung, P. Georgopoulos, *J. Appl. Crystallogr.* **1989**, *22*, 528-532.
- (213) P. Müller-Buschbaum, *Anal. Bioanal. Chem.* **2003**, *376*, 3-10.
- (214) S. Dietrich, A. Haase, *Phys. Rep.* **1995**, *260*, 1-138.
- (215) H. Bässler, *Phys. Status Solidi B* **1993**, *175*, 15-56.
- (216) A. Dodabalapur, L. Torsi, H. E. Katz, *Science* **1995**, *268*, 270-271.
- (217) R. G. Kepler, *Physical Review* **1960**, *119*, 1226-1229.
- (218) J. O. H. LeBlanc, *J. Chem. Phys.* **1960**, *33*, 626-626.
- (219) G. Juška, K. Arlauskas, M. Viliūnas, K. Genevičius, R. Österbacka, H. Stubb, *Phys. Rev. B: Condens. Matter Mater. Phys.* **2000**, *62*, R16235-R16238.
- (220) G. Juška, K. Arlauskas, M. Viliūnas, J. Kočka, *Phys. Rev. Lett.* **2000**, *84*, 4946-4949.
- (221) S. Günes, N. S. Sariciftci, *Inorg. Chim. Acta* **2008**, *361*, 581-588.

2. OVERVIEW OF THE THESIS

This thesis focuses on the development and investigation of new materials for hybrid photovoltaic devices. In particular, the emphasis is on the synthesis, characterization and application of broadly absorbing light harvesting dyes and functional semiconducting amphiphilic polymers. It contains 7 publications of which 6 are presented in the chapters 3-8 and one is attached as appendix (chapter 9). Five of these manuscripts have already been published. A schematic overview of the main topics of this thesis is presented in Figure 2–1.

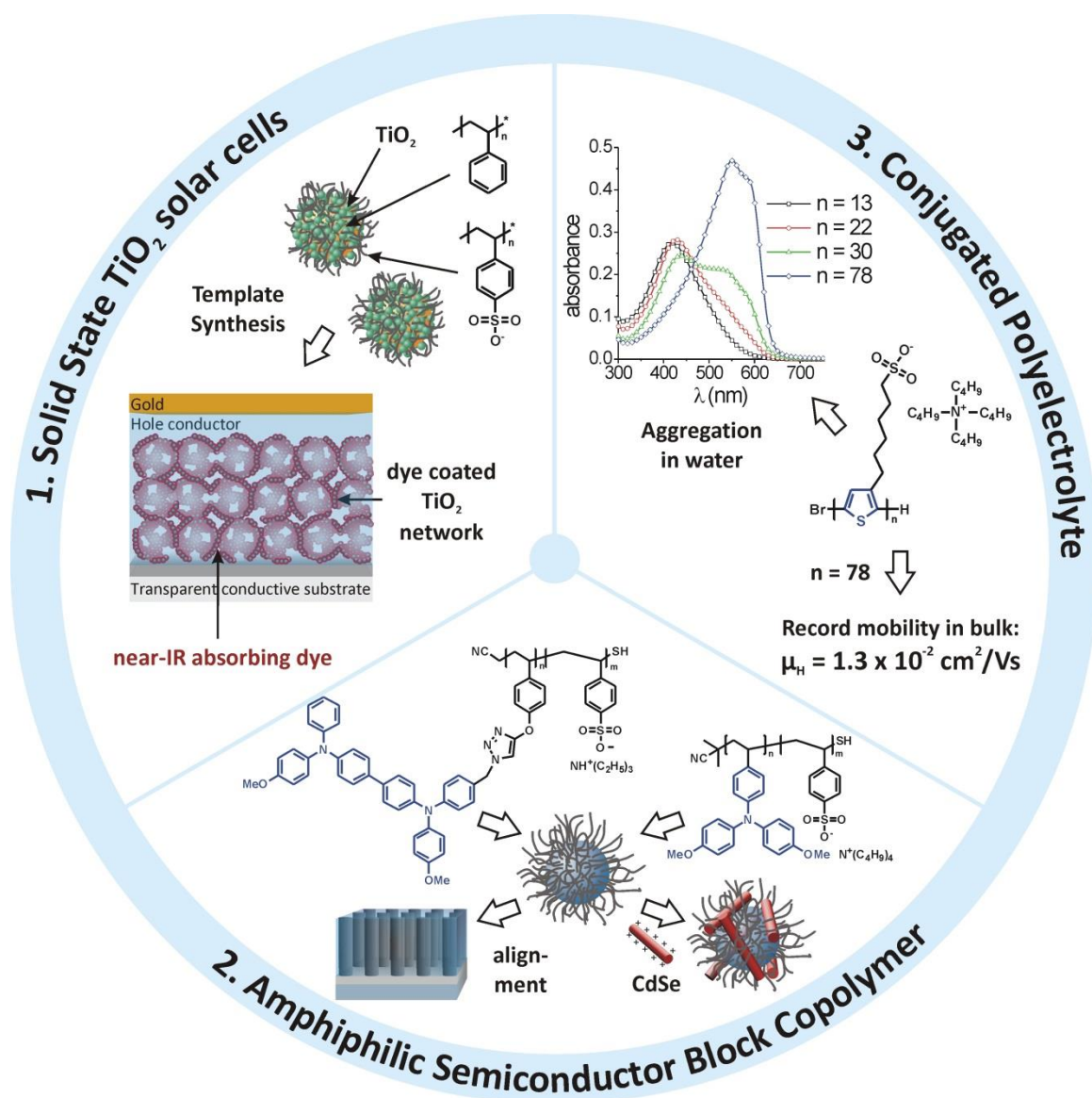


Figure 2–1. Overview of the thesis having an aim to optimize and understand hybrid photovoltaic devices. In the first part, alternative sensitizers for light harvesting were investigated and a new concept for the controlled preparation of mesoporous TiO₂ is presented using polymer brushes as templates (1.). Secondly, amphiphilic semiconducting block copolymers were synthesized for the self-assembly and alignment of hybrid composites (2.) The final part comprises the controlled synthesis and characterization of a conjugated polyelectrolyte which is an amphiphilic hole conductor comprising polar sulfonate groups and a hydrophobic conjugated backbone (3.).

The thesis is subdivided into three parts: 1. the investigation of light harvesting and the control of structure in SDSCs (solid state dye sensitized solar cells); 2. the synthesis of amphiphilic semiconductor block copolymers and their self-assembly; 3. The combination of hole transport and coordinative properties in an amphiphilic semiconductor conjugated polyelectrolyte. All the individual partitions of the work comprise innovative new approaches to address critical aspects including the light harvesting, the confinement of nanoparticles, the processability of hybrid composites and the organization of the morphology.

A crucial requirement to accomplish the aims of this thesis was the establishment of suitable synthesis procedures for the preparation of well-defined amphiphilic polymers. In consequence, various techniques were examined for their applicability to create these complex functional polymers including emulsion polymerization, controlled radical polymerization, catalyst transfer polymerizations and “click” chemistry (Figure 2–2).

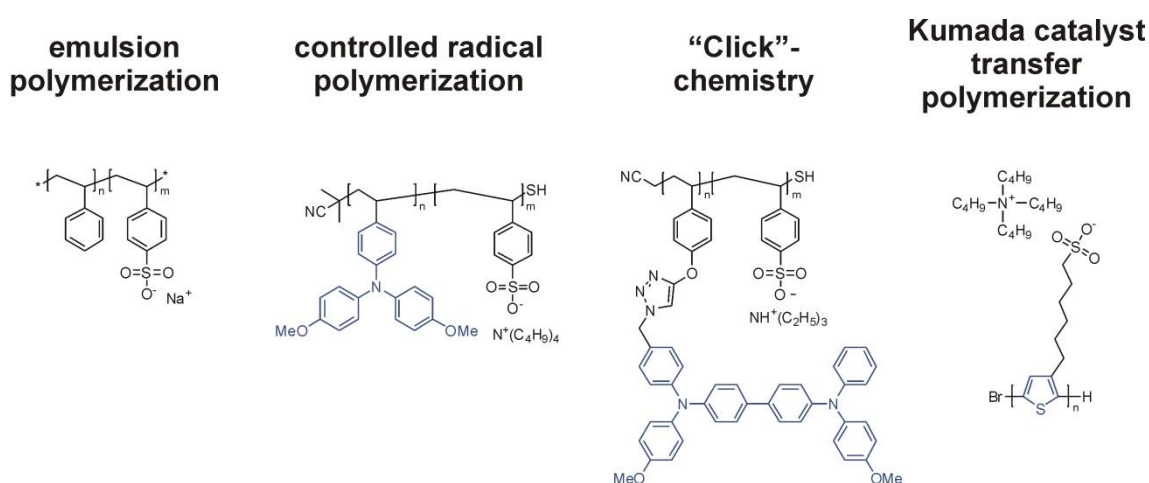


Figure 2–2. Overview of the examined synthesis procedures for the preparation of well-defined amphiphilic functional polymers. Sketches of the resulting polymers are shown below the respective method of polymerization.

The individual topics represent a step-by-step development of alternative concepts for hybrid devices starting from established solid state dye sensitized solar cells and leading to well-defined self-assembled composites. These three main topics of the thesis are briefly outlined in the following.

Investigation of light harvesting and the control of structure in SDSCs:

In the first part of the thesis basic studies on solid state dye sensitized solar cells (SDSC) are presented. Therefore we first examined the influence of pore size and structure of TiO₂-network on the performance of the solar cells. To gain control on the morphology of TiO₂ a novel templated synthesis of TiO₂ was introduced using spherical polyelectrolyte brushes. These brushes consist of a polystyrene core and a sodium polystyrene sulfonate corona which were synthesized *via* stepwise controlled emulsion polymerization. The sulfonate groups of the corona facilitated the catalytic growth of TiO₂ in the favorable anatase structure at room temperature, which otherwise usually requires high temperatures of more than 400°C. Variation of the TiO₂ content resulted in different morphologies of the inorganic network after calcination of the polymer template. A clear correlation between TiO₂ density as well as surface area and the obtained current was found, demonstrating the need for a dense phase of inorganic semiconductor which improves charge transport. This publication appears as appendix of the thesis (chapter 9), since part of this work was performed during my diploma thesis. Further to this work on the morphology of SDSC, we examined a new class of Boron-dipyrromethene (BODIPY) dyes and triphenyl diamine (TPD) based sensitizers. The BODIPY dyes are able to absorb red or near-IR light, while the TPD derivatives are organic sensitizers with suitable energy levels for injection and regeneration. The porous TiO₂ was prepared using a commercial paste which consists of a polymer template and anatase nanocrystals. The BODIPY dyes show response up to 900 nm. This broad absorption favors the harvesting of the whole visible light spectrum up to the IR region. However, the obtained current densities are higher for the TPD dye which is related to the more favorable energy levels of these dyes. Nevertheless, both publications highlight the potential of near-IR organic dyes for improved light harvesting (chapters 3 and 4).

Synthesis of amphiphilic semiconductor block copolymers and their self-assembly:

The second topic evolved out of the experience gained on the polyelectrolyte brush templates in chapter 9. We took advantage of the excellent coordination properties of polystyrene sulfonate and combined it with an electronically active triphenylamine block in order to accomplish a functional semiconducting micelle. In contrast to the previous inactive polystyrene based systems we established a direct access to a donor-acceptor composite without the need for a high temperature calcination. Therefore, well-defined block copolymers were synthesized *via* controlled reversible addition-fragmentation chain-transfer (RAFT) polymerization. The increased activity and steric demand of the semiconductor monomers necessitates crucial optimization of the polymerization. Accordingly, we scrutinized the influence of the most critical parameters such as temperature, solvent and the order of monomer addition on the resulting polymers. Finally, this optimization yielded narrowly distributed block copolymers. Upon self-assembly in water uniform micelles are created with a semiconducting core and a coordinative corona. Due to strong electrostatic attraction positively charged CdSe nanorods could be selectively attached to this negative shell forming a colloidal donor acceptor composite with suitable domain sizes of 10-20 nm (chapter 5). In order to simplify and extend the synthesis procedure established in chapter 5, we combined the RAFT process with the versatility of "click" chemistry. The controlled radical polymerization was used to create a well-defined scaffold polymer, poly(propargyl oxystyrene) with pendant alkyne groups. This precursor can be selectively clicked with any functional azide in a catalyzed azide-alkyne cycloaddition offering a

modular and versatile approach towards functional block copolymers. On this basis, we synthesized the amphiphilic semiconducting polymer poly(*N,N'*-bis(4-methoxyphenyl)-*N*-phenyl-*N'*-4-triazolylphenyl-(1,1'-biphenyl)-4,4'-diamine)-*block*-poly(triethylammonium styrene sulfonate) (PDMTPD-*b*-PEt₃NH⁺SS). The combination of RAFT and “click” reactions enabled a broad range of molecular weights while maintaining a narrow molecular weight distribution of the polymers. The morphology of the amphiphilic polymers was studied in the bulk and in thin films. For three different polymer compositions, phase separation was obtained in the bulk and aggregated micellar structures were formed in the as-cast thin film. After annealing in saturated solvent vapor the morphology could be transformed into vertically aligned domains. Depending on the block ratio a transition from lamellar to cylindrical structures was observed (chapter 6).

Combination of hole transport and coordinative properties in an amphiphilic semiconductor conjugated polyelectrolyte:

The third part of the thesis addresses the synthesis and characterization of conjugated polymers with ionic side chains. In particular, we aimed at the introduction of sulfonate groups, which previously have proven their beneficial coordination properties, and combine them with a polythiophene backbone suitable for electronic transport. Polythiophenes are known for their high hole mobility and the broad absorption spectrum in the visible region in comparison to triphenylamine based systems. Nevertheless, the focus was kept on the control of the polymerization including the molecular weight and a low polydispersity. Accordingly, the controlled Kumada catalyst transfer polymerization was used to synthesize a well-defined poly(3-(6-bromohexyl)thiophene) as precursor polymer. The reactive bromine side-group is suitable for several nucleophilic substitution reactions. In order to introduce sulfonate groups, a new substitution reaction using tetrabutylammonium sulfite was established gaining a quantitative exchange of the bromine group. In contrast to similar commercial polymers with broad molecular weight distribution and low regioregularity, the poly(6-(thiophen-3-yl)hexane-1-sulfonate) (PTHS) showed a specific aggregation behavior in solution as well as in thin films. In solution a clear dependence of aggregation on the molecular weight was observed. Furthermore, the influence of solvent and salt concentration on the optical properties and the aggregation was examined in detail. In solid-state the hole mobility of the bulk material was determined in a diode geometry. The observed mobility of $1.3 \pm 0.5 \times 10^{-2} \text{ cm}^2/\text{Vs}$ is among the highest values reported so far. In order to exclude any other conduction mechanism such as ion transport, impedance measurements were performed proving the pure semiconducting character of the material. The remarkably good transport properties are attributed to the formation of uniform aggregates in aqueous solution, which are maintained in the thin film. These results indicate that the well-controlled structures lead toward an enhancement of the charge transport properties (chapters 7 and 8).

In the following, the key results of all chapters are summarized with particular focus on the respective impact on the overall topic of the thesis. A detailed description of the experiments, all results and the respective conclusions are given in the chapters 3-9.

CONTROL OF PORE SIZE AND WALL THICKNESS IN TITANIA NETWORKS FOR SOLID STATE DYE SENSITIZED SOLAR CELLS (CHAPTER 9)

This contribution to the thesis is considered as a fundamental study to generate hybrid composites and uses amphiphilic polymers as templates for inorganic nanostructures. The template consists of spherical polyelectrolyte brushes, which are prepared *via* stepwise emulsion polymerization. The core is made of polystyrene (PS) and the corona consists of sodium polystyrene sulfonate (PSS) (Figure 2–3).

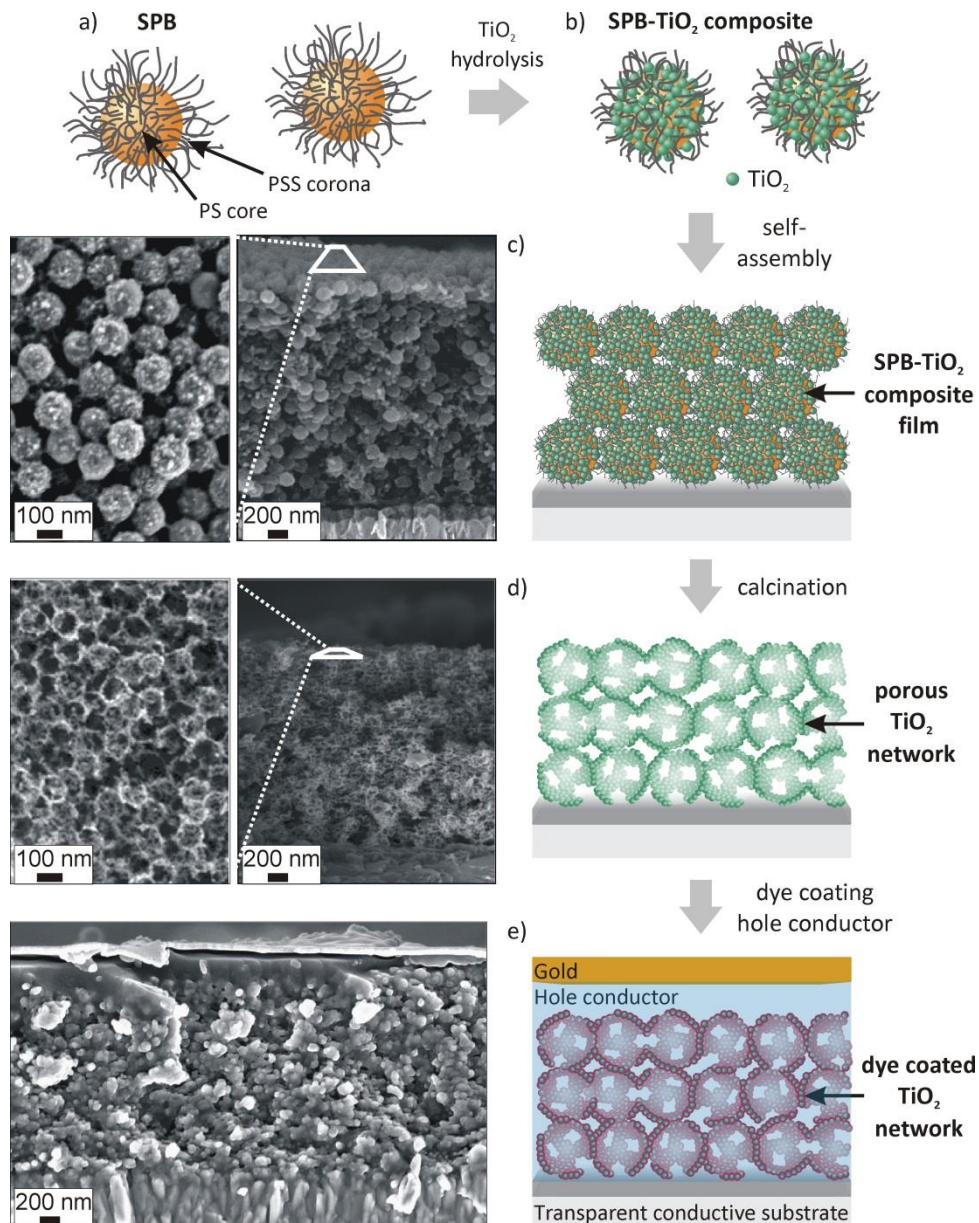


Figure 2–3. Scheme of the templated preparation of a hybrid solar cell using spherical polyelectrolyte brushes (SPB) as templates. a) SPBs consist of a polystyrene (PS) core and a polystyrene sulfonate (PSS) corona; b) composites are generated by hydrolysis of TiO₂ (anatase); c) the composites are assembled on a conductive substrate; d) the samples are calcinated at high temperatures to remove the template and to get the porous TiO₂ network; e) to complete the solar cell, the TiO₂ is sensitized with a dye and the network is backfilled with an organic hole conductor, the top contact is prepared by evaporation of gold. On the left, the preparation steps are documented with SEM images. For the steps c) and d) surface images with higher magnification are also given.

The emulsion polymerization gives a precise control over the core and shell diameter, respectively. TiO_2 is selectively hydrolyzed within the corona of the SPB particles, whereas the sulfonate groups catalyze the formation of pure anatase TiO_2 at room temperature. This crystal structure formation usually requires high crystallization temperatures of more than 400°C . The catalytic formation of anatase is unique for sulfonate groups, which makes them advantageous for the in-situ synthesis of TiO_2 to create hybrid composites. After the hydrolysis the resulting composite particles form stable dispersions in water, ethanol and glycerin. The latter two were used for the thin film assembly of the particles on a conductive substrate either by drop-casting (5 wt% dispersion in ethanol) or by blade-casting (10 wt% dispersion in glycerin). Much effort had to be spent on the assembly of uniform films which are crucial for device preparation. The best results were obtained for the glycerin dispersion casted with a $30\ \mu\text{m}$ blade gap. The film thickness was set to $2\ \mu\text{m}$, which is considered to be suitable for solid state dye sensitized solar cells (SDSC). Subsequently, the template was removed in a two-step calcination process at 500°C first under argon and finally in air. Due to the initial carbonization of the network the TiO_2 was solidified and a collapse of the structure was circumvented. The final device was prepared by sensitizing the TiO_2 with a metal-organic Ruthenium dye, backfilling the network with an organic hole conductor and evaporation of gold as counter electrode.

A key aspect of this work is the control of the resulting pore size by the diameter of the initial PS core and the TiO_2 wall thickness by the shell composition of the SPB composite particles. In consequence we examined different conditions for the TiO_2 hydrolysis varying the amount of water and the content of TiO_2 -precursor. The resulting composite particles were analyzed by cryo-TEM and after calcination the structure of the network was examined with high resolution SEM (Figure 2–4).

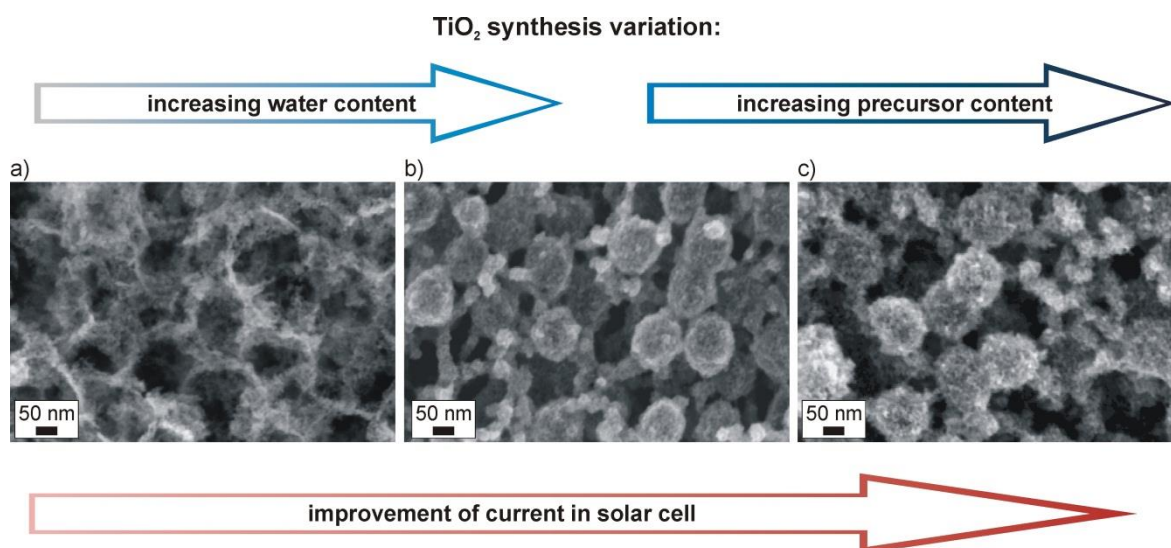


Figure 2–4. High resolution SEM images of the calcined TiO_2 networks prepared from different SPB composite particles. The arrows above the images indicate the variations on the TiO_2 hydrolysis conditions. The TiO_2 precursor was tetraethyl orthotitanate (TEOT). The overall ratios SPB/TEOT/water (wt/wt ratio) are 1/4/4 (a), 1/4/18 (b) and 1/6/18 (c). For each modification an increase of the current density of the respective SDSC was observed.

A critical factor in SDSCs is the available surface area for dye coating and its ratio with the overall amount of TiO_2 in the network, which is a measure for the density of the inorganic semiconductor. To evaluate this ratio we estimated the amount of dye absorbed using UV-vis spectroscopy and determined the mass of the mesoporous TiO_2 for a particular thickness of film.

For the sample with lowest water and precursor content, a finely branched thin TiO₂ network was obtained (Figure 2–4 a), which exhibited a large surface area but a low overall amount of TiO₂. The current density of the resulting device remained low due to the hampered charge transport through the very fine structure of the TiO₂ network. Increasing the water content during the hydrolysis results in a more compact structure of TiO₂ (Figure 2–4 b). Thus, the available surface area was reduced, but the resulting current density could still be enhanced as the transport properties were improved. Nevertheless, the best results were obtained after additionally increasing the precursor content during the hydrolysis of the TiO₂. The calcinated inorganic structure featured both a high available surface area due to fine branches and a compact, stabilizing framework of the inorganic semiconductor. This structure guaranteed an optimal balance between charge separation at the sensitized interface and charge transport to the electrodes *via* the dense TiO₂ walls. The comparison with optimized commercial pastes to form mesoporous TiO₂ confirms the importance of a compact framework for charge transport, as determined by the dye/TiO₂ ratio which is relatively low for the commercial TiO₂ sample. However, these pastes lack any control of the pore size and distribution, which is crucial for an entire filling of the network with the organic hole conductor in SDSCs. The presented approach thus offers a pathway to adjust both the pore size and the compactness of the TiO₂ framework individually. But an optimum quality of electron transport could not be reached here.

ORGANIC SENSITIZERS FOR SOLID STATE DYE SENSITIZED SOLAR CELLS (CHAPTER 3 AND 4)

One of the important processes in hybrid photovoltaic devices occurs at the interface of the organic and inorganic semiconductors. Therefore, much effort has been spent on the understanding of these processes including charge separation and recombination and the synthesis of dyes for improving the light harvesting. In this contribution, novel organic dyes were examined for their efficiency of light harvesting in SDSCs. 4,4-difluoro-4-bora-3a,4a-diaza-s-indacene (BODIPY) derivatives, which absorb in the red and near-IR spectrum of the sunlight, were studied (Figure 2–5). Furthermore, triphenyl diamine compounds also showing excellent stability in reversible redox processes were tested. This is crucial for charge transport and separation.

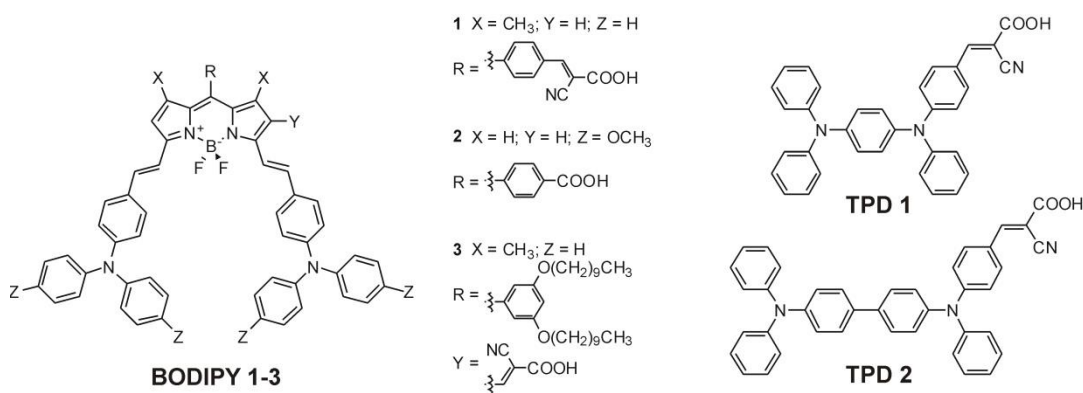


Figure 2–5. Overview of the investigated organic sensitizers, which were tested in solid state dye sensitized solar cells.

The BODIPY dyes show a broad absorption up to 900 nm with peak maxima at 699 nm (BODIPY 1), 746 nm (BODIPY 2) and 695 nm (BODIPY 3), at which the extinction coefficient was well above 6×10^5 l/(mol cm). In solar cells, external quantum efficiency measurements revealed that charges are generated over the whole absorption range. An important finding is the particular influence of the position and structure of the anchoring group on the charge generation. Despite the good π -conjugation of the BODIPY core and the triphenyl amine donor groups for all dyes, the electron injection seems favorable through the meso-position (R) at the BODIPY core via cyanoacetic acid anchor groups. However, at this position (R) the attached phenyl rings are tilted out of the π -conjugated system due to steric effects. The strong electron withdrawing effect of the cyanoacetic acid group (BODIPY 1) is beneficial for charge separation. Nevertheless, the overall efficiency of the BODIPY dyes remains low, which is due to the low driving force for charge separation caused by the small energy level offsets. Especially for electron injection into the TiO_2 , the lowest unoccupied molecular orbital (LUMO) should be sufficiently higher than the conduction band of the inorganic semiconductor to favor charge separation. Additionally, the highest occupied molecular orbital (HOMO) of the dye should be lower than that of the hole conductor for efficient dye regeneration. In contrast to the BODIPY dyes, the TPD based sensitizers offer suitable energy levels for charge separation but at the expense of the broad absorption. Nevertheless, these dyes show improved solar cell efficiencies in SDSCs. Particularly, the sensitizer TPD 2 was superior to TPD 1, which is due to its advantageous redox properties including an excellent stability for multiple reversible oxidation-reduction cycles. This feature makes the TPD dye interesting for application as hole conducting material either as small molecule or attached to a polymer backbone. This basic investigation of light harvesting organic molecules with excellent redox properties may lead to new building blocks for preparation of side-chain functionalized, semiconducting polymers.

SYNTHESIS OF SEMICONDUCTOR AMPHIPHILIC BLOCK COPOLYMERS (CHAPTER 5 AND 6)

This part of the work aimed at the design and synthesis of novel amphiphilic and semiconducting block copolymers comprising an amorphous hole conductor segment and a strongly charged polyelectrolyte block. Particular attention was paid to the control of the polymerization leading towards well-defined block copolymers with narrow molecular weight distribution which is a key requirement for microphase separation and morphology control of the polymer in solution and bulk. The choice of poly(bis(4-methoxyphenyl)-4'-vinylphenylamine) (PDMTPA) and poly(*N,N'*-bis(4-methoxyphenyl)-*N*-phenyl-*N'*-4-triazolylphenyl-(1,1'-biphenyl)-4,4'-diamine) (PDMTPD) as hole conducting blocks is based upon the excellent stability of triphenylamine derivatives and its amorphous character which favors a smooth film formation. Poly(styrene sulfonate) (PSS) blocks with variable counter ions were selected due to the high solubility in polar solvents including water or alcohols and the high charge density of the sulfonate groups enabling either the electrostatic attachment of inorganic particles or the catalytic formation of anatase TiO_2 . The inherent difference in solubility of both segments required the development of a smart synthesis strategy. Compatibility of the blocks for the synthesis was gained by suitable protection of the sulfonate group which can be easily removed after the block polymer formation. Using this strategy the harsh and uncontrolled conditions of a polymer analogous sulfonation can be avoided. In order to maintain control over the polymerization even with these complex

monomers the reversible addition-fragmentation chain transfer (RAFT) process was chosen due to its tolerance toward many functional groups.

Nevertheless, the direct polymerization of the semiconductor monomer (DMTPA) needed a careful optimization of conditions to obtain block copolymers with narrow molecular weight distribution. Factors such as polymerization sequence, temperature and solvent were varied. A scheme of the sequential RAFT polymerization toward poly(bis(4-methoxyphenyl)-4'-vinylphenylamine)-*block*-poly(neopentyl styrene sulfonate) (PDMPA-*b*-PNeoSS) is shown in Figure 2–6 a.

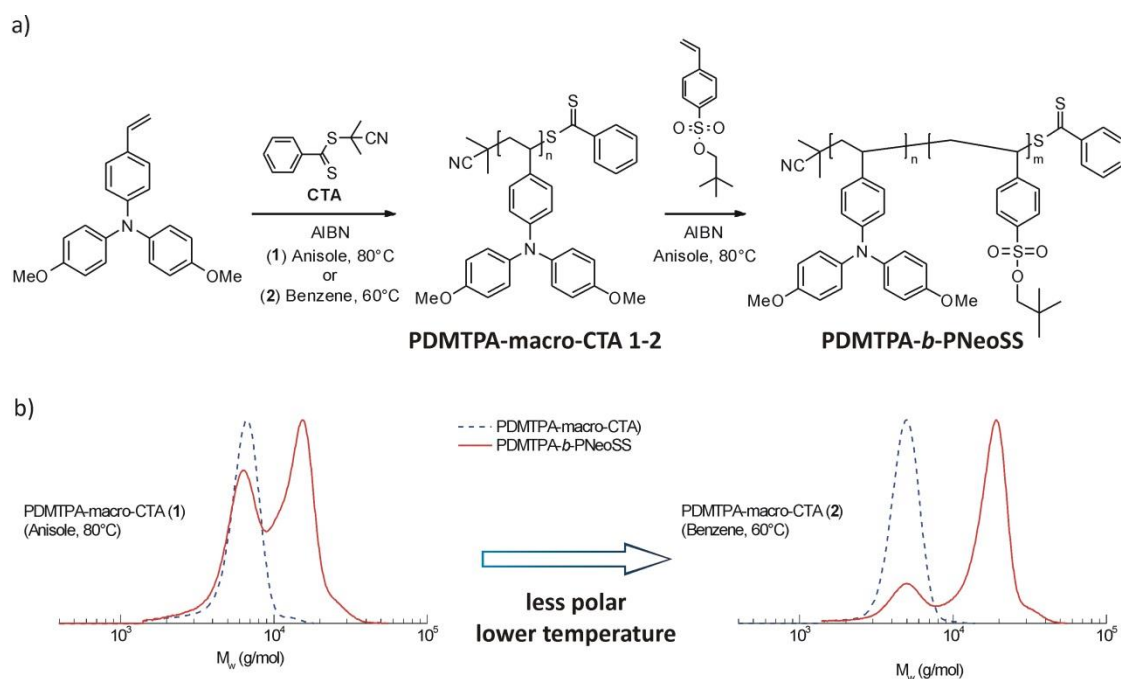


Figure 2–6. a) Scheme of the synthesis steps toward poly(bis(4-methoxyphenyl)-4'-vinylphenylamine)-*block*-poly(neopentyl styrene sulfonate) (PDMPA-*b*-PNeoSS), b) SEC traces of the macro-CTA prepared under the listed conditions (blue dotted line) and the respective block copolymer started from this macro CTA (red solid line). The arrow indicates the main changes in the polymerization conditions.

The sequence of monomer addition is a crucial factor in the formation of block copolymers using controlled radical polymerization techniques and relies on the different reactivity of the propagating radical chain end. In the presented system only the primary preparation of a PDMPA macro initiator (chain transfer agent: CTA) and the subsequent polymerisation of neopentyl styrene sulfonate (NeoSS) resulted in the diblock formation. Nevertheless, still a considerable amount of macro-CTA remained unreactive under the initially chosen conditions for the RAFT polymerization (anisole, 80°C) (Figure 2–6 b). The high reactivity of the DMTPA monomer facilitates a self-initiation process known for styrene monomers. This spontaneous formation of free radicals at high temperatures results in increased termination reactions, which result in the loss of the CTA during polymerization as confirmed by MALDI-Tof-MS analysis. By modifying temperature and the polarity of the surrounding medium this side reaction could be efficiently suppressed and the resulting block copolymer contained only a small fraction of remaining homopolymer (Figure 2–6 b), which could easily be removed. The low dipole moment of benzene in combination with low temperature restrained the side reaction most efficiently. With subsequent deprotection of the sulfonate group the final amphiphilic semiconducting block copolymer PDMPA-*b*-P₄N⁺SS was obtained.

These results showed that the direct synthesis of the semiconductor amphiphilic block copolymer PDMTPA-*b*-PBu₄N⁺SS *via* RAFT polymerization is possible. However, much effort had to be spent on the optimization of the polymerization conditions and the range of molecular weight was limited. In consequence, we developed a modular approach combining the advantages of RAFT and “click” chemistry. Therefore, a scaffold polymer was prepared bearing an alkyne group on every repeating unit suitable for an alkyne-azide cycloaddition. Trimethylsilyl propargyl oxystyrene (TMSPS) is conveniently accessible and its reactivity during the polymerization is comparable to other styrene derivatives allowing common polymerization conditions. After the growth of the second block the alkyne group can be deprotected and any functional building block can be introduced carrying an azide group. Accordingly, we designed the semiconducting amphiphilic block copolymer poly(*N,N'*-bis(4-methoxyphenyl)-*N*-phenyl-*N'*-4-triazolylphenyl-(1,1'-biphenyl)-4,4'-diamine)-*block*-poly(triethylammonium styrene sulfonate) (PDMTDP-*b*-PEt₃NH⁺SS). First, an azide-functionalized triphenyl diamine group was attached to the scaffold block copolymer poly(propargyl oxystyrene)-*block*-poly(2,2,2-trifluorethyl styrene sulfonate) (PPS-*b*-PTfeSS). After the final hydrolysis of the PTfeSS block, we obtained the amphiphilic semiconductor block copolymer PDMTDP-*b*-PEt₃NH⁺SS. The key synthesis steps are summarized in Figure 2–7.

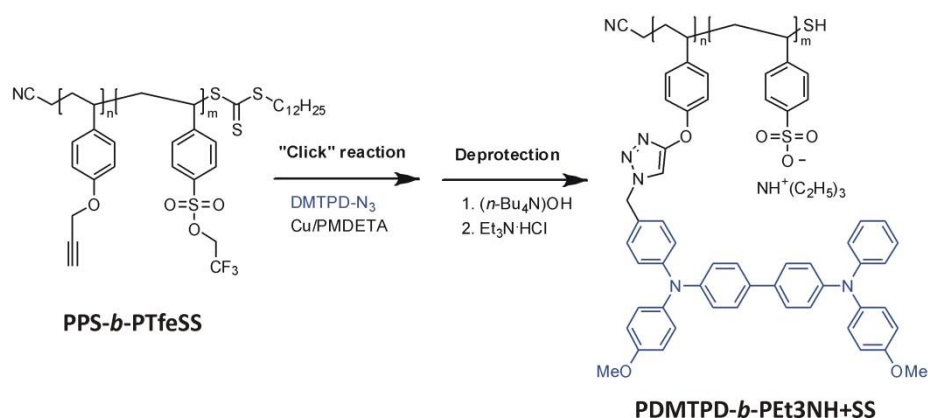


Figure 2–7. Schematic representation of the key synthesis steps to prepare the block copolymer poly(*N,N'*-bis(4-methoxyphenyl)-*N*-phenyl-*N'*-4-triazolylphenyl-(1,1'-biphenyl)-4,4'-diamine)-*block*-poly(triethylammonium styrene sulfonate) (PDMTDP-*b*-PEt₃NH⁺SS). In the first part a sequential RAFT block copolymerization is used to create the scaffold block copolymer poly(propargyl oxystyrene)-*block*-poly(2,2,2-trifluorethyl styrene sulfonate) (PPS-*b*-PTfeSS), which subsequently can be modified with a hole conductor group *via* “click” chemistry. Deprotection of sulfonate group gives the final amphiphilic semiconductor block copolymer. DMTPD-N₃: *N,N'*-bis(4-methoxyphenyl)-*N*-phenyl-*N'*-4-azidophenyl-(1,1'-biphenyl)-4,4'-diamine, PMDETA: *N,N,N',N',N''*-pentamethyldiethylenetriamine.

The polymerization of the scaffold polymer and the subsequent block formation proceeded smoothly yielding a well-defined polymer. After the “click” reaction, no residual alkyne groups were traceable proving a quantitative functionalization with the hole conductor moiety. On this basis we prepared two similar block copolymers whereas the molecular weight of the hole conductor segment was increased. In all cases a narrow molecular weight distribution and efficient functionalization was observed including a PDMTDP block of more than 60.000 g/mol. These results certainly reveal the potential of the combination of RAFT and “click” chemistry for designing functional block copolymers. In this case, a well-defined amphiphilic semiconducting block copolymer was created with a superior hole conductor group and high molecular weights in comparison to PDMTPA-*b*-PBu₄N⁺SS. Moreover, the key characteristics of an amorphous structure and a narrow molecular weight distribution were maintained.

MICELLE FORMATION AND PREPARATION OF HYBRID DONOR-ACCEPTOR COMPOSITES (CHAPTER 5)

In water, the block copolymer PDMTPA-*b*-PBU₄N⁺SS forms micelles with narrow size distribution consisting of a hydrophobic PDMTPA core and polystyrene sulfonate as corona. A hydrodynamic radius of 22 nm was determined by dynamic light scattering (DLS) and the core diameter was estimated to be approximately 16 nm in dried TEM samples (Figure 2–8).

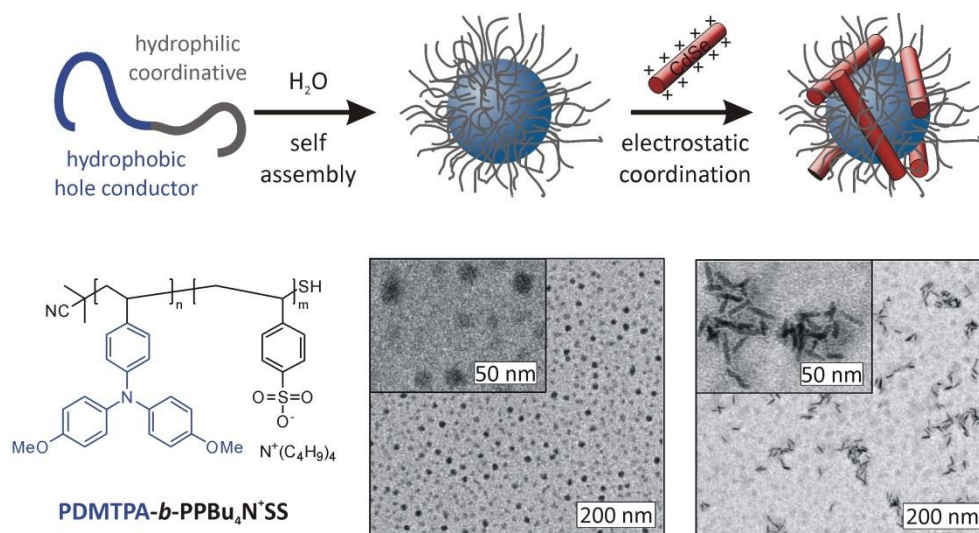


Figure 2–8. Schematic representation of the self assembly of the block copolymer PDMTPA-*b*-PBU₄N⁺SS into micelles upon addition of water and the subsequent attachment of positively charged CdSe nanorods to the negative shell of the micelles. For each step the respective TEM images are depicted below with insets of higher magnification. A scheme of the polymer is shown at the bottom left.

The negatively charged shell of PBU₄N⁺SS is suitable for the coordination of positively charged nanoparticles. Therefore, highly crystalline CdSe nanorods were synthesized at high temperatures using trioctylphosphine oxide (TOPO) as ligand. Substituting the ligand with the small 2-aminoethanethiol introduces positive charges on the surface of the CdSe. These particles could be simply attached to the semiconducting micelles by electrostatic attraction forming a hybrid donor-acceptor composite (Figure 2–8). Stable dispersions were obtained for nanorods/polymer weight ratios of up to 1/1. With regard to typical exciton diffusion lengths of 10 nm, the prepared composite exhibits ideal domain sizes for charge generation and transport. Moreover, the assembly in aqueous systems circumvents the needs for hazardous solvents for processing. In conclusion, the presented approach opens a promising new pathway for environmentally benign processing with further improving critical parameters such as confinement of nanoparticles and introduction of sufficient amounts of inorganic semiconductor for charge transport. The developed process is very versatile concerning the nature of the inorganic semiconductor and can be further combined with other polymerization techniques to introduce light absorbing polymers such as polythiophene.

VERTICAL ALIGNMENT OF MICRODOMAINS FOR AMPHIPHILIC SEMICONDUCTOR BLOCK COPOLYMERS (CHAPTER 6)

The three block copolymers PDMTPD-*b*-PEt₃NH⁺SS **1-3**, which feature a different block composition (**1**: 58 wt% PDMTPD, **2**: 72 wt% PDMTPD, **3**: 78 wt% PDMTPD), were used to examine the morphology in bulk and in thin film. Small angle X-ray scattering (SAXS) on the bulk sample revealed only one signal, which indicates microphase separated domains, but give no clear evidence for an ordered morphology. Nevertheless, the calculated d-spacing of the signal shifted consistently with the increase of molecular weight of the PDMTPD block. After thermal annealing above the T_g of the polymer no significant change was observed. This transition temperature is attributed to the PDMTPD block, however, no further transition was observed for the PEt₃NH⁺SS segment below the temperature of degradation. Thus, while the PDMTPD block becomes flexible, the strong interactions of the sulfonate groups prevent the mobility of the second block. Similar observations were found in the thin film after thermal annealing. In the as-cast film micellar structures were detected in the atomic force micrographs (AFM). After thermal annealing only a flattening of the surface was detectable, but no morphology transition occurred. The formation of micelles during the coating process could be proven *via* cryo-TEM of the polymer solution in DMF. Grazing incident small angle X-ray scattering (GISAXS) revealed no preferential orientation or order in the as-cast (Figure 2–9) or the thermally annealed film.

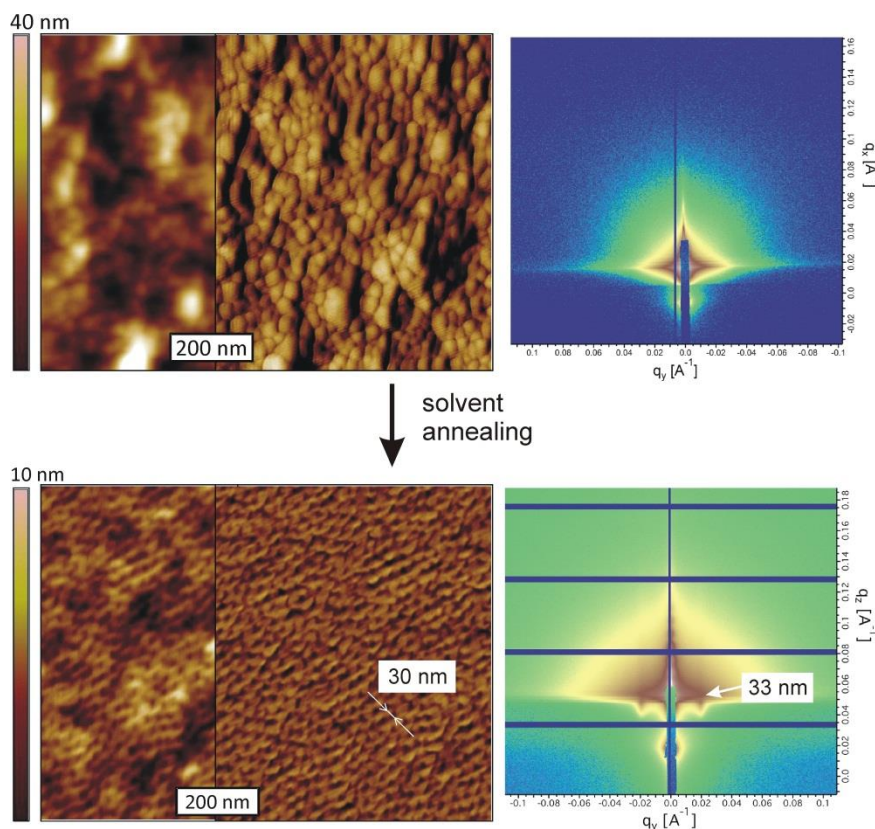


Figure 2–9. Atomic force micrographs (left: height image, right: phase image) and the respective grazing incident X-ray scattering patterns of thin films made of the block copolymer PDMTPD-*b*-PEt₃NH⁺SS with 79 wt% PDMTPD. The as-cast film is shown on the top, while at the bottom a film is shown, which was annealed in saturated DMF vapor for four days.

Alternatively, we studied the influence of saturated solvent vapor to induce a morphology transition. DMF was chosen since it solubilizes both blocks, but seems to be a preferential solvent for the $\text{PEt}_3\text{NH}^+\text{SS}$ block as observed during the micelle formation. After four days in saturated vapor, the samples were again analyzed by AFM and GISAXS. A clear transition of the dimple-type structures towards a more ordered cylindrical or lamellar morphology was observed (Figure 2–9). The GISAXS patterns revealed one discrete out-of-plane peak, which is correlated to a vertical orientation of the morphology. In combination with the surface topography from the AFM images a vertical lamellar or cylindrical morphology can be derived depending on the composition of the block copolymer. While for the polymer with 58 wt% of PDMTPD the morphology is lamellar, a clear transition to cylinders is observed for the high PDMTPD content (79 wt%). The opportunity of vertical alignment of an amphiphilic semiconducting block copolymer facilitates the application in various electronic devices ranging from batteries and sensors to hybrid photovoltaics. Moreover, an excellent reproducibility and the possible up-scaling of the synthesis are guaranteed by the convenience and versatility of the combination of RAFT and “click” chemistry. On basis of the presented approach, a large variety of functional moieties can be introduced and combined with coordination ability of the hydrophilic sulfonate block.

WELL-DEFINED CONJUGATED POLYELECTROLYTES BASED ON POLYTHIOPHENE: AGGREGATION IN SOLUTION AND ELECTRICAL PROPERTIES IN SOLID STATE (CHAPTER 7 AND 8)

Considering semiconducting organic materials, the most efficient systems are based on π -conjugated polymers. However, the control over the molecular weight, the molecular weight distribution and the end-group of these polymers is still a challenging task. While for poly(alkylthiophenes) controlled chain growth mechanisms are established, reports on well-defined functional or amphiphilic conjugated polymers suitable for hybrid devices are rare. In this work, the synthesis of a side-chain functionalized derivative of polythiophene, poly(6-(thiophen-3-yl)hexane-1-sulfonate) (PTHS) was developed combining the “living” Kumada catalyst transfer polymerization and a polymer analogous substitution (Figure 2–10).

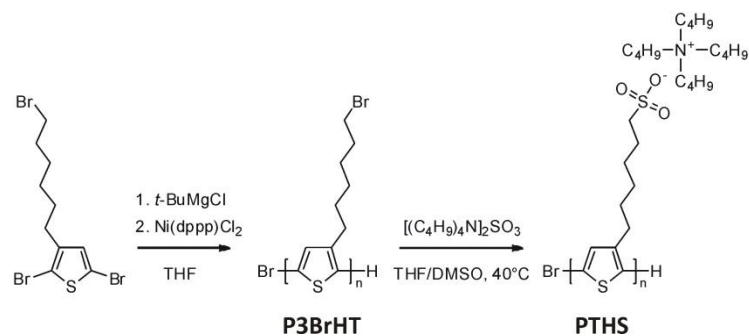


Figure 2–10. Reaction scheme of the synthesis procedure for the controlled preparation of the conjugated polyelectrolyte tetrabutylammonium poly(6-(thiophen-3-yl)hexane-1-sulfonate) (PTHS).

The resulting polymer tetrabutylammonium poly(6-(thiophen-3-yl)hexane-1-sulfonate) (PTHS) features a conjugated backbone and sulfonate groups attached to each side-chain. The optimized substitution reaction allowed a quantitative conversion of the bromine side groups into anionic sulfate groups which was determined *via* NMR spectroscopy (Figure 2–11 a).

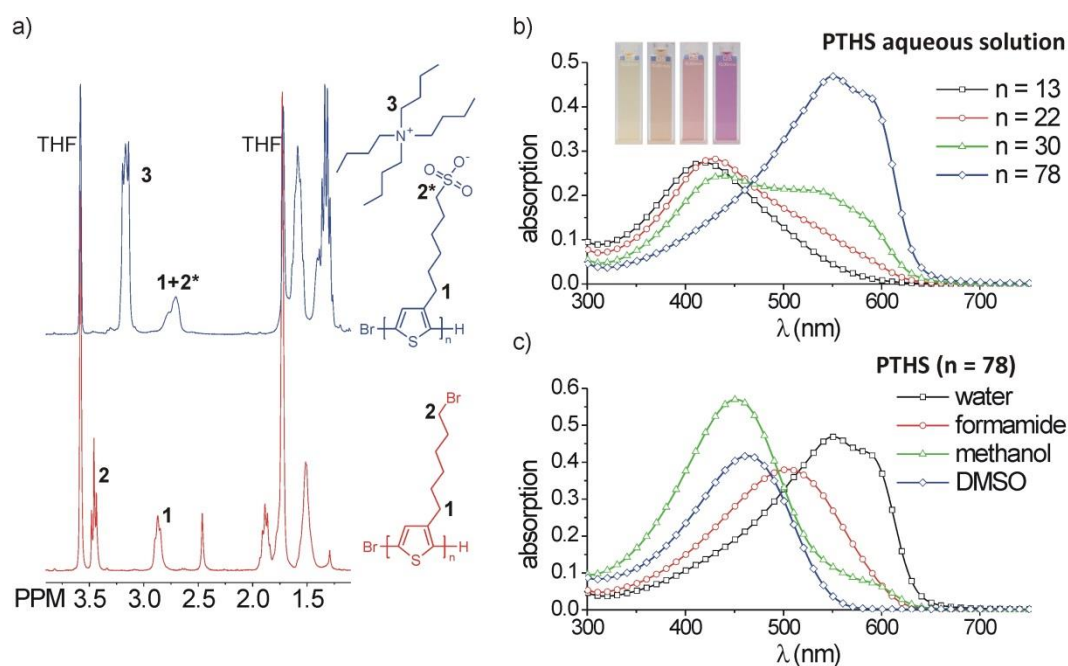


Figure 2–11. a) NMR spectra of the precursor polymer (bottom) and the resulting conjugated polyelectrolyte PTHS (top); the important signals are assigned with numbers. c) Absorption spectra of aqueous solutions of PTHS with different average degree of polymerization n . d) Absorption spectra of PTHS ($n = 78$) in various solvents.

After the substitution reaction, the polymer exhibits excellent solubility in water and other highly polar solvents. The optical properties of the conjugated polyelectrolytes in solution were studied in detail. In contrast to similar, but ill-defined polymers, this conjugated polyelectrolyte (CPE) shows specific aggregation features in aqueous solution, which are derived from the vibronic absorption bands in the UV-vis spectra. Furthermore, a strong dependency of the polymer aggregation on the molecular weight was observed in aqueous solution. A concentration dependent aggregation was detected for medium chain lengths, while short chains remain non-aggregated. Long polymer chains, however, are permanently aggregated. Further experiments revealed the dissolution of aggregates in organic solvents in contrast to water. This finding suggests that the hydrophobic character of the polymer backbone abets the aggregation in aqueous solution. Finally, we studied the influence of the salt concentration on aggregation in aqueous solution. A continuous disintegration of the aggregates is observed with increasing ionic strengths of the solution. The screening effect of the ions reduces the coulomb repulsion between adjacent repeating units and induces an enhanced flexibility to the polymer chain. Photoluminescence studies support the aggregation and deaggregation behavior observed under various conditions.

Complementary to the solution properties, we investigated the characteristics of the material in the solid state. The similarity in the UV-Vis absorption of an aqueous solution and the thin film reveals that the aggregated structure occurring in solution is maintained in the solid-state. In addition to the optical properties, the electrical properties were examined in detail. The underlying transport mechanisms were analyzed in impedance measurements and the hole transport mobility was determined from the current-voltage (J-V) characteristics of a PTHS thin film using the space charge limited current (SCLC) method. The J-V characteristics of the material (Figure 2–12 a) showed a quadratic dependence of current against voltage, which corroborates the semiconducting characteristics of the polymer. The plots showed no hysteresis and several

scan cycles confirm the reproducibility of the measurements. In comparison, other CPEs commonly featured strong hysteresis for continuous measurements, which is related to the reorganization of ions in the material according to the applied electrical field. To unambiguously determine the pure electron transport mechanism we analyzed the impedance spectra of the materials in thin film. The impedance data gave one semicircle in the Nyquist-plot, which is indicative for a semiconductor (Figure 2–12 b). A conductivity of 1.4×10^{-6} S/cm was estimated fitting the measured values with an equivalent circuit of a semiconductor, *viz.* a parallel connection of a capacitor and a resistor.

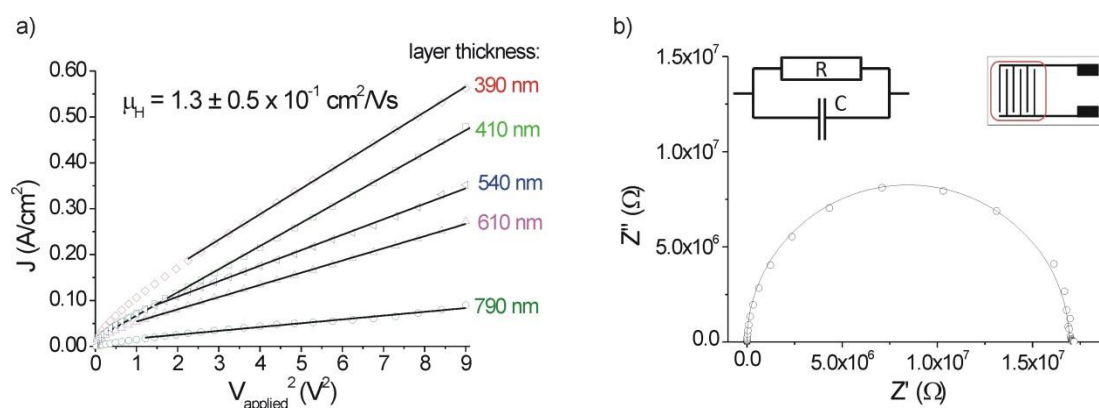


Figure 2–12. a) Current against voltage square (J - V^2) characteristics of a polymer thin film with different thicknesses measured in diode geometry; the hole carrier mobility μ_H was calculated according to the Mott-Gurney law for space charge limited current. b) Impedance data in the Nyquist representation of a thin film of PTHS; the respective fit was calculated on a parallel combination of a resistor and a capacitor (left inset) and the geometrical structure of the electrodes is shown in the right inset.

In consequence, we are able to exclude any ion motion in the PTHS thin film as evidenced by the impedance data and the fast temporal response of the current for different bias. From the J - V characteristics we estimated a hole carrier mobility of $(1.3 \pm 0.5) \times 10^{-2}$ cm^2/Vs in accordance to the Mott-Gurney law for SCLC and consistent for various thicknesses. This result outperforms the mobility of common P3HT and it is among the highest values reported in literature measured in a diode geometry. In conclusion, we created a narrowly distributed and highly regioregular conjugated polyelectrolyte by combining controlled polymerization techniques and polymer analogous reactions. These unique features facilitate the formation of aggregates, which are known to suppress the ion mobility and account for the excellent hole transport mobilities.

INDIVIDUAL CONTRIBUTIONS TO JOINT PUBLICATIONS

The results of this thesis were obtained in cooperation with other groups and are published or prepared as manuscripts for submission as denoted below. In the following the individual contributions of all authors are summarized and specified.

CHAPTER 3:

This work is published in **ORGANIC LETTERS** (2010, 12, 3812) under the title:

“Solid-State Dye-Sensitized Solar Cells Using Red and Near-IR Absorbing Bodipy Sensitizers”

by Safacan Kolemen, Yusuf Cakmak, Sule Erten-Ela, Yigit Altay, Johannes C. Brendel, Mukundan Thelakkat and Engin U. Akkaya.

I prepared and characterized all solar cells and was involved in the scientific discussion.

Safacan Kolemen, Yusuf Cakmak, Sule Erten-Ela and Yigit Altay synthesized and characterized all dyes and wrote the manuscript.

Mukundan Thelakkat and Engin U. Akkaya supervised the project and corrected the manuscript.

CHAPTER 4:

This work is published in **CHEMICAL PHYSICS LETTERS** (2011, 510, 93) under the title:

“Solid-state dye-sensitized solar cells fabricated with nanoporous TiO₂ and TPD dyes: Analysis of penetration behavior and I–V characteristics”

by Sule Erten-Ela, Johannes C. Brendel and Mukundan Thelakkat.

I prepared and characterized all solar cells and was involved in the scientific discussion.

Sule Erten-Ela synthesized and characterized all dyes and wrote the manuscript.

Mukundan Thelakkat supervised the project and corrected the manuscript.

CHAPTER 5

This work is published in **JOURNAL OF MATERIALS CHEMISTRY** (2012, 22, 24386) under the title:

“Semiconductor amphiphilic block copolymers for hybrid donor-acceptor nanocomposites“

by Johannes C. Brendel, Hubertus Burchardt and Mukundan Thelakkat.

I synthesized and characterized some of the polymers, wrote the publication and supervised Hubertus Burchardt during his Bachelor thesis.

Hubertus Burchardt synthesized and characterized most of the polymers during his Bachelor thesis under my guidance.

Mukundan Thelakkat supervised the project and corrected the manuscript.

CHAPTER 6

This work is published in **ACS NANO** (2013, *in print*, DOI: 10.1021/nn401877g) under the title:

“Vertical alignment of microdomains in semiconductor amphiphilic block copolymers thin films“

by Johannes C. Brendel, Feng Liu, Andreas S. Lang, Thomas P. Russell and Mukundan Thelakkat.

I synthesized and characterized all the polymers, prepared the thin films, conducted the AFM measurements and wrote the publication.

Feng Liu performed and analyzed the X-ray measurements and corrected the manuscript.

Andreas Lang synthesized the trimethylsilyl propargyl oxystyrene monomer and the DMTPD-azide.

Mukundan Thelakkat and Thomas P. Russell supervised the project and corrected the manuscript.

CHAPTER 7

This work is prepared for submission under the title:

“Optical Properties of Well-defined Conjugated Polyelectrolytes: Influence of Molecular Weight, Concentration, Solvent and Added Salt”

by Johannes C. Brendel, Martina Schmidt and Mukundan Thelakkat.

I characterized all the polymers and wrote the publication.

Martina Schmidt synthesized the polymers during her lab course under my guidance.

Mukundan Thelakkat supervised the project and corrected the manuscript.

CHAPTER 8

This work is submitted to **CHEMISTRY OF MATERIALS** under the title:

“Controlled Synthesis of a Conjugated Polyelectrolyte Leading to Excellent Hole Transport Mobility”

by Johannes C. Brendel, Gunter Hagen, Ralf Moos and Mukundan Thelakkat.

I synthesized and characterized all the polymers, prepared the thin films, conducted the electrical measurements and wrote the publication.

Gunter Hagen helped with the impedance measurements and analyzed the impedance data.

Mukundan Thelakkat and Ralf Moos supervised the project and corrected the manuscript.

CHAPTER 9: APPENDIX

This work is published in **JOURNAL OF MATERIALS CHEMISTRY** (2010, 20, 7255) under the title:

“Polymer templated nanocrystalline titania network for solid state dye sensitized solar cells“

by Johannes C. Brendel, Yan Lu and Mukundan Thelakkat.

I synthesized and characterized some of the template particles, prepared the composites, assembled and characterized the thin films, prepared the solar cells and wrote the publication.

Yan Lu synthesized most of the spherical polymer brush template particles, helped with the composite synthesis and corrected the manuscript.

Mukundan Thelakkat supervised the project and corrected the manuscript.

3. SOLID-STATE DYE-SENSITIZED SOLAR CELLS USING RED AND NEAR-IR ABSORBING BODIPY SENSITIZERS

Safacan Kolemen,^a Yusuf Cakmak,^b Sule Erten-Ela,^{c,d} Yigit Altay,^a
Johannes Brendel,^d Mukundan Thelakkat,^d and Engin U. Akkaya^{*,a,b}

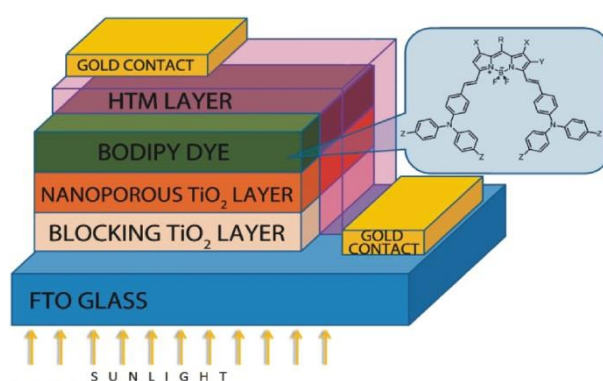
^a Department of Chemistry, Bilkent University, Ankara 06800, Turkey

^b UNAM-Institute of Materials Science and Nanotechnology, Bilkent University, Ankara 06800,
Turkey

^c Institute of Solar Energy, Ege University, Bornova, Izmir 35100, Turkey

^d Macromolecular Chemistry I, Applied Functional Polymers, University of Bayreuth, 95440
Bayreuth, Germany

*E-mail of corresponding author: eua@fen.bilkent.edu.tr



Published in *Organic Letters* **2010**, 12, 3812-3815.

ABSTRACT

Boron-dipyrrin dyes, through rational design, yield promising new materials. With strong electron-donor functionalities and anchoring groups for attachment to nanocrystalline TiO₂, these dyes proved useful as sensitizers in dye-sensitized solar cells. Their applicability in a solid-state electrolyte regime offers additional opportunities for practical applications.

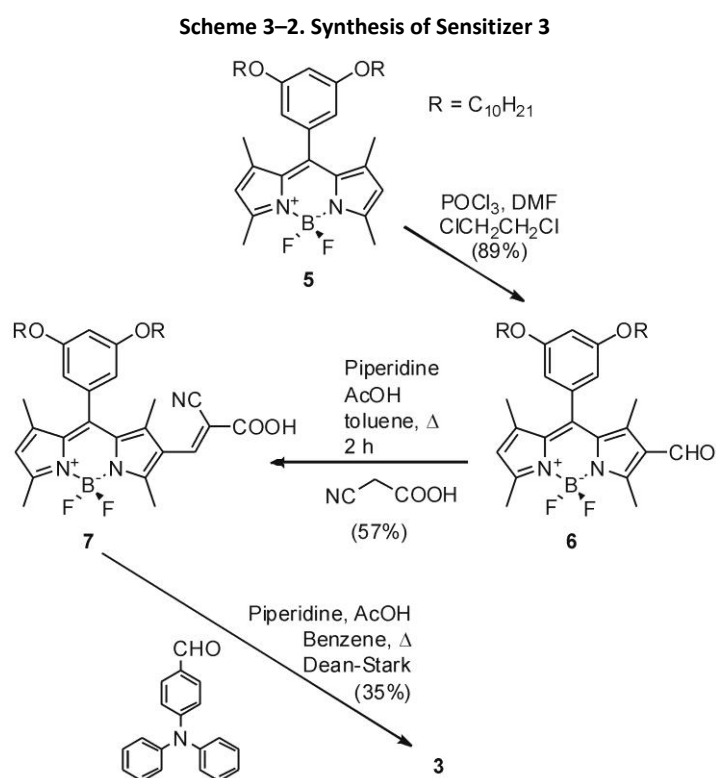
ARTICLE

Dye-sensitized solar cells (DSSC) are successful alternatives to more widely used traditional semiconductor-based designs. The DSSC technology is being vigorously developed through commercial enterprises.¹⁻⁷ In fact, in the European Union Photovoltaic Roadmap, it was suggested that by the year 2020, DSSCs are expected to be a significant contributor to renewable electricity generation.⁸ However, most people would agree that there is still room for improvement for a few components of a typical DSSC.⁹ This is perhaps more apparent for the electrolyte and the sensitizer dye component itself. For use as redox mediator, I⁻ and I₂ (to generate iodide/triiodide redox couple) is typically dissolved in organic solvents (such as acetonitrile). However, the use of solvents creates temperature stability problems, and because of the volatility of the solvents, sealing of the cell is crucial. Most plastics are not compatible with organic solvents, and thus the use of liquid electrolytes effectively precludes integration into flexible structures. Also, ruthenium dyes are expensive, and their preparation includes lengthy purification steps.¹⁰ Accurate engineering of the sensitization wavelength would also benefit from a replacement organic dye. Not surprisingly, a large number of laboratories around the world are actively pursuing potential candidates for sensitizers for DSSC applications.¹¹⁻²²

Boron-dipyrrin or Bodipy dyes are interesting chromophores with high quantum yields and absorptivity, typically with typical bright green fluorescence.²³⁻²⁵ We and others have found ways to transform these dyes to absorb essentially all colors of the rainbow and then some.²⁶⁻³⁴

A few years ago, we published the first report of a rationally functionalized Bodipy-based photosensitizer, taking advantage of some of the superior characteristics of this class of dyes.³⁵ Others followed with equally promising Bodipy derivatives.³⁶⁻⁴¹ Calculations at various levels of the theory suggested that excitation of the Bodipy chromophore results in significant reorganization of the electron distribution, setting up the scene for efficient electron transfer to nanocrystalline titania from the S₁ state of the dye.^{35,42} Needless to say, further optimization of the Bodipy derivatives may provide better sensitizers for use in DSSCs.

In order to bypass the limitations imposed by liquid electrolytes, one of the most common hole transport materials (HTM) is 2,2',7,7'-tetrakis(*N,N*-di-*p*-methoxyphenyl-amine)-9,9'-spirobifluorene (spiro-OMeTAD).^{22,43} In this work, our goal was to investigate the performance of rationally designed boron-dipyrrin sensitizers in connection with spiro-OMeTAD hole transport material. In our previous work, we synthesized sensitizer **1** (Figure 3–1) and reported its efficiency in a standard DSSC setup using a iodide/triiodide redox couple in solution as electrolyte.³⁵ In this work, however, we targeted two more boron-dipyrrin dyes, compounds **2** and **3**, in an attempt to clarify relative effects of various modifications on the efficiency. The rationale behind the two new sensitizers was as follows.



In the synthesis of sensitizer **3**, we first prepared 3,5-didecyloxyphenyl-substituted Bodipy **5**.²⁷ Formylation following the procedure in a recent report resulted in compound **6**.⁴⁴ Cyanoacetic acid reacts with the formyl-bodipy **6** in toluene, resulting in compound **7**. In the final step, a double Knoevenagel condensation with the appropriate aldehyde yields the target sensitizer **3**. All new compounds were analytically pure (Supporting Information).

First the absorbance spectra in solution (CHCl_3) (Figure 3–2) and as adsorbed on TiO_2 (Figure 3–3) were obtained. The chromophores in solution have strong absorption peaks in the red and near-IR regions of the visible spectrum. As expected, on absorption over titania, peaks are significantly broadened, suggesting aggregation of the sensitizers in the adsorbed film.

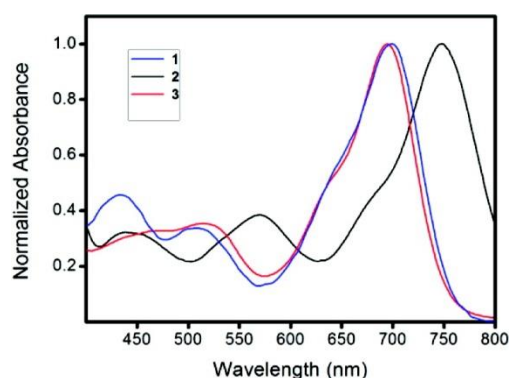


Figure 3–2. Normalized absorption spectra of the sensitizers in CHCl_3 .

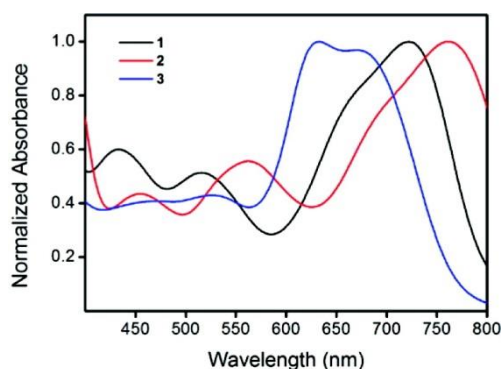


Figure 3-3. Normalized absorption spectra of the sensitizers adsorbed on nanocrystalline TiO₂.

The sensitizers **1-3** were further characterized by cyclic voltammetry and absorption spectroscopy in solution (Table 3-1). It is clear that the LUMO energies of the sensitizers are appropriate for efficient electron injection to TiO₂.

Table 3-1. Optical and Electrochemical Properties of Sensitizers 1-3

dye	λ_{\max} (abs) ^a (nm)	ϵ_{\max} ^a	E_{ox} ^b (mV)	E_{red} ^b (mV)	HOMO ^b (eV)	LUMO ^b (eV)
1	699	69500	680	-890	-5.09	-3.52
2	746	66000	560	-870	-5.05	-3.62
3	695	79000	720	-940	-5.21	-3.55

^a Absorption data were collected in CHCl₃.

^b Electrochemical data were collected in CH₂Cl₂. Potentials are quoted with reference to the internal ferrocene standard.

The solid-state cells were prepared as in the previous reports. For a brief procedure, please see Supporting Information. Incident photon to current conversion plots were obtained under standard conditions (AM 1.5G, 100 mW cm⁻²). The results show that the sensitizer **1** has the highest efficiency (Figure 3-4). Only beyond 800 nm, sensitizer **2** has IPCE values higher than those of **1**. For sensitizer **3**, IPCE values are below 1% in the 450-850 nm region.

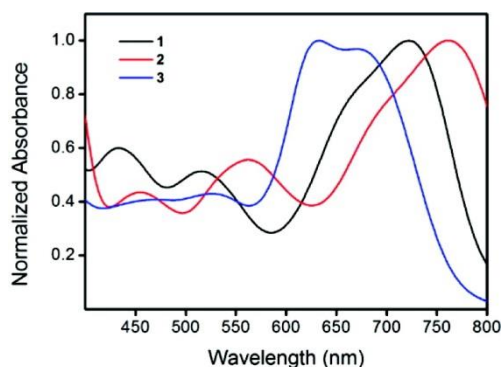


Figure 3-4. Incident photon to current conversion efficiency as a function of wavelength for the solid-state DSSCs prepared as described in Supporting Information.

The data can be interpreted as follows. As we suggested previously, the *meso* position (8 position) is particularly important. In the parent Bodipy and in other derivatives, theoretical calculations suggest that on excitation there is significant charge relocation on the *meso*

carbon.³⁵ Sensitizers **1** and **2** take advantage of this natural Bodipy tendency for charge relocation onto *meso*-carbon, by placing electron-acceptor/anchor groups on that position. The sensitizer **3** has the anchor group on a different position, forcing electron flow to an alternate position, apparently reducing the efficiency of charge injection. The data also suggest that the cyanoacetic acid derived anchor is better than a simple carboxylic acid group in their dual role of charge-withdrawing and anchoring group. As expected, the sensitizers have very low fluorescence emissions due to strong charge transfer characteristics of the diphenylaminophenyl substituent.

What is also remarkable is the near flat response of these sensitizers in the visible wavelengths. Actually, the response is one that could be expected from a black dye. Table 3–2 lists some cell parameters for the solid-state DSSCs prepared using these sensitizers.

Table 3–2. DSSC Performance Parameters of BODIPY Dyes^a

dye	V_{oc} (V)	J_{sc} (mA/cm ²)	f	η (%)
1	0.80	2.27	0.37	0.68
2	0.64	1.61	0.28	0.28
3	0.59	1.49	0.38	0.33

^a V_{oc} is the open-circuit potential, J_{sc} is the short circuit current, f is the fill factor, and η is the overall efficiency of the cell under standard conditions.

The overall conversion efficiency is highest for the sensitizer **1** ($\eta = 0.68\%$), which could be considered a respectable value for an organic dye with a solid-state redox mediator. It appears that solution properties only loosely translate into properties on titania. However, Bodipy-based sensitizers still hold significant promise as they can be derivatized as desired and the absorption peaks can be moved along the visible and near-IR region. It is interesting to note that one of the most efficient dyes in terms of monochromatic incident photon to current conversion is indeed a Bodipy dye. It looks like Bodipy dyes, which are known for their bright fluorescence, are likely to find novel applications as photosensitizers. We will continue in fine-tuning the Bodipy structure toward ever more efficient dyes for dye-sensitized solar cells through rational design.

REFERENCES

- (1) B. O'Regan, M. Grätzel, *Nature* **1991**, *353*, 737-740.
- (2) M. Grätzel, **2001**, *414*, 338-344.
- (3) R. Eisenberg, D. G. Nocera, *Inorg. Chem.* **2005**, *44*, 6799-6801.
- (4) N. Armaroli, V. Balzani, *Angew. Chem., Int. Ed.* **2007**, *46*, 52-66.
- (5) N. Robertson, *Angew. Chem., Int. Ed.* **2008**, *47*, 1012-1014.
- (6) N. S. Lewis, D. G. Nocera, *Proc. Natl. Acad. Sci. U. S. A.* **2006**, *103*, 15729-15735.
- (7) M. K. Nazeeruddin, *Coord. Chem. Rev.* **2004**, *248*, 1161-1164.
- (8) A. Jäger-Waldau, *Renewable and Sustainable Energy Rev.* **2007**, *11*, 1414-1437.
- (9) J.-H. Yum, P. Chen, M. Grätzel, M. K. Nazeeruddin, *ChemSusChem* **2008**, *1*, 699-707.
- (10) H. Choi, I. Raabe, D. Kim, F. Teocoli, C. Kim, K. Song, J.-H. Yum, J. Ko, M. K. Nazeeruddin, M. Grätzel, *Chem. Eur. J.* **2010**, *16*, 1193-1201.
- (11) A. Mishra, Markus K. R. Fischer, P. Bäuerle, *Angew. Chem., Int. Ed.* **2009**, *48*, 2474-2499.
- (12) Y. Ooyama, Y. Harima, *Eur. J. Org. Chem.* **2009**, *2009*, 2903-2934.
- (13) D. P. Hagberg, J.-H. Yum, H. Lee, F. De Angelis, T. Marinado, K. M. Karlsson, R. Humphry-Baker, L. Sun, A. Hagfeldt, M. Grätzel, M. K. Nazeeruddin, *J. Am. Chem. Soc.* **2008**, *130*, 6259-6266.
- (14) S. Ito, S. M. Zakeeruddin, R. Humphry-Baker, P. Liska, R. Charvet, P. Comte, M. K. Nazeeruddin, P. Péchy, M. Takata, H. Miura, S. Uchida, M. Grätzel, *Adv. Mater.* **2006**, *18*, 1202-1205.
- (15) S. Hwang, J. H. Lee, C. Park, H. Lee, C. Kim, C. Park, M.-H. Lee, W. Lee, J. Park, K. Kim, N.-G. Park, C. Kim, *Chem. Commun.* **2007**, 4887-4889.
- (16) S. Ito, H. Miura, S. Uchida, M. Takata, K. Sumioka, P. Liska, P. Comte, P. Pechy, M. Grätzel, *Chem. Commun.* **2008**, *0*, 5194-5196.
- (17) J. He, G. Benkö, F. Korodi, T. Polívka, R. Lomoth, B. Åkermark, L. Sun, A. Hagfeldt, V. Sundström, *J. Am. Chem. Soc.* **2002**, *124*, 4922-4932.
- (18) M. Velusamy, J.-H. Huang, Y.-C. Hsu, H.-H. Chou, K.-C. Ho, P.-L. Wu, W.-H. Chang, J. T. Lin, C.-W. Chu, *Org. Lett.* **2009**, *11*, 4898-4901.
- (19) J. Mei, K. R. Graham, R. Stalder, J. R. Reynolds, *Org. Lett.* **2010**, *12*, 660-663.
- (20) N. Koumura, Z.-S. Wang, S. Mori, M. Miyashita, E. Suzuki, K. Hara, *J. Am. Chem. Soc.* **2006**, *128*, 14256-14257.
- (21) J. T. Lin, P.-C. Chen, Y.-S. Yen, Y.-C. Hsu, H.-H. Chou, M.-C. P. Yeh, *Org. Lett.* **2008**, *11*, 97-100.
- (22) R. H. Lohwasser, J. Bandara, M. Thelakkat, *J. Mater. Chem.* **2009**, *19*, 4126-4130.
- (23) G. Ulrich, R. Ziesel, A. Harriman, *Angew. Chem., Int. Ed.* **2008**, *47*, 1184-1201.
- (24) R. Ziesel, G. Ulrich, A. Harriman, *New J. Chem.* **2007**, *31*, 496-501.
- (25) A. Loudet, K. Burgess, *Chem. Rev.* **2007**, *107*, 4891-4932.
- (26) O. Buyukcakir, O. A. Bozdemir, S. Kolemen, S. Erbas, E. U. Akkaya, *Org. Lett.* **2009**, *11*, 4644-4647.
- (27) Y. Cakmak, E. U. Akkaya, *Org. Lett.* **2009**, *11*, 85-88.
- (28) S. Erbas, A. Gorgulu, M. Kocakusakogullari, E. U. Akkaya, *Chem. Commun.* **2009**, 4956-4958.
- (29) Z. Dost, S. Atilgan, E. U. Akkaya, *Tetrahedron* **2006**, *62*, 8484-8488.
- (30) E. Deniz, G. C. Isbasar, O. A. Bozdemir, L. T. Yildirim, A. Siemiarczuk, E. U. Akkaya, *Org. Lett.* **2008**, *10*, 3401-3403.
- (31) K. Rurack, M. Kollmannsberger, J. Daub, *Angew. Chem., Int. Ed.* **2001**, *40*, 385-387.
- (32) K. Umezawa, Y. Nakamura, H. Makino, D. Citterio, K. Suzuki, *J. Am. Chem. Soc.* **2008**, *130*, 1550-1551.
- (33) D. Zhang, Y. Wen, Y. Xiao, G. Yu, Y. Liu, X. Qian, *Chem. Commun.* **2008**, 4777-4779.
- (34) S. Atilgan, I. Kutuk, T. Ozdemir, *Tetrahedron Lett.* **2010**, *51*, 892-894.

- (35) S. Erten-Ela, M. D. Yilmaz, B. Icli, Y. Dede, S. Icli, E. U. Akkaya, *Org. Lett.* **2008**, *10*, 3299-3302.
- (36) T. Rousseau, A. Cravino, T. Bura, G. Ulrich, R. Ziessel, J. Roncali, *Chem. Commun.* **2009**, *0*, 1673-1675.
- (37) T. Rousseau, A. Cravino, T. Bura, G. Ulrich, R. Ziessel, J. Roncali, *J. Mater. Chem.* **2009**, *19*, 2298-2300.
- (38) S. Hattori, K. Ohkubo, Y. Urano, H. Sunahara, T. Nagano, Y. Wada, N. V. Tkachenko, H. Lemmetyinen, S. Fukuzumi, *J. Phys. Chem. B* **2005**, *109*, 15368-15375.
- (39) J. C. Forgie, P. J. Skabara, I. Stibor, F. Vilela, Z. Vobecka, *Chem. Mater.* **2009**, *21*, 1784-1786.
- (40) C. Y. Lee, J. T. Hupp, *Langmuir* **2009**, *26*, 3760-3765.
- (41) D. Kumaresan, R. P. Thummel, T. Bura, G. Ulrich, R. Ziessel, *Chem. Eur. J.* **2009**, *15*, 6335-6339.
- (42) O. A. Bozdemir, R. Guliyev, O. Buyukcakil, S. Selcuk, S. Kolemen, G. Gulseren, T. Nalbantoglu, H. Boyaci, E. U. Akkaya, *J. Am. Chem. Soc.* **2010**, *132*, 8029-8036.
- (43) U. Bach, D. Lupo, P. Comte, J. E. Moser, F. Weissortel, J. Salbeck, H. Spreitzer, M. Grätzel, *Nature* **1998**, *395*, 583-585.
- (44) L. Jiao, C. Yu, J. Li, Z. Wang, M. Wu, E. Hao, *J. Org. Chem.* **2009**, *74*, 7525-7528.

SUPPORTING INFORMATION

Experimental Section:

General:

^1H NMR and ^{13}C NMR spectra were recorded on Bruker DPX-400 (operating at 400 MHz for ^1H NMR and 100 MHz for ^{13}C NMR) in CDCl_3 with tetramethylsilane as internal standard. All spectra were recorded at 25°C and coupling constants (J values) are given in Hz. Chemical shifts are given in parts per million (ppm). Absorption spectra were acquired using a Varian Cary-100 spectrophotometer. Mass spectra were recorded on Agilent Technologies 6530 Accurate-Mass Q-TOF LC/MS. Reactions were monitored by thin layer chromatography using Merck TLC Silica gel 60 F_{254} . Silica gel column chromatography was performed over Merck Silica gel 60 (particle size: 0.040-0.063 mm, 230-400 mesh ASTM). 4,4-difluoro-8-(3',5'-bis(decyloxy)phenyl)-1,3,5,7-tetramethyl-4-bora-3a,4a-diaza-s-indacene (**5**) was synthesized according to literature.¹ Compound **1** was synthesized according to our previous work.² All other reagents and solvents were purchased from Aldrich and used without further purification.

Fabrication Method of Solid State Dye Sensitized Solar Cells:

The $\text{SnO}_2:\text{F}$ covered glass was cut into 25x25 mm pieces. The transparent conducting glasses (TCO) covered with adhesive tape to control the thickness of the film and to provide non-coated areas for electrical contact and they were etched using Zn powder and 5% HCl acid solution. And then, FTO glasses were cleaned by using acetone, 2% Helmanex solution, distilled water and ethanol, respectively. After cleaning procedure, blocking layer was covered onto the FTO glasses. The films were sintered at 500°C . TiO_2 Solaronix paste was applied onto the TCO glass covered with blocking layer using screen printing technique; thin films of about 2 μm in thicknesses were prepared. Finally, temperature was increased gradually, the films were sintered at 500°C for 1 hour and temperature was cooled down to room temperature gradually. The TiO_2 electrodes were then immersed into the 0.5 mM dye solutions of BODIPYs and kept at room temperature overnight. TiO_2 -coated glasses with Bodipy dyes adsorbed on were washed with pure solvent. Afterwards, organic hole-transporting material (HTM) 2,2',7,7'-tetrakis-(*N,N*-di-*p*-methoxyphenylamine)-9,9'-pirobifluorene (spiro-OMeTAD) was covered on dye adsorbed TiO_2 films by using spin coater. 40 nm gold was evaporated as top electrodes.

Electrochemistry of BODIPY Derivatives:

E_{HOMO} and E_{LUMO} values of BODIPY derivatives were calculated using cyclic voltammograms. Solutions of BODIPY derivatives were prepared in dichloromethane (10^{-3} M). A three electrode cell was used consisting of glassy carbon working electrode, Pt wire counter electrode and Ag/AgCl reference electrode, all placed in a glass vessel. Tetrabutylammonium hexafluorophosphate (TBAPF_6), 0.1 M, was used as supporting electrolyte. Ferrocene was used as internal reference electrode. BODIPY derivatives show both reversible reduction and oxidation potential.

In calculations for compounds **2** and **3**, zero vacuum level belongs to ferrocene was taken as 4.8 eV and $E_{\text{ferrocene}}$ was 0.31 V.

E_{LUMO} level was calculated by using the formula of $E_{\text{LUMO}} = -(E_{1/2}(\text{red}) - E_{\text{fer.}} + 4.8)$.

E_{HOMO} level was calculated by using the formula of $E_{\text{HOMO}} = -(E_{1/2}(\text{ox}) - E_{\text{fer.}} + 4.8)$.

The conduction band of TiO_2 layer, $E_{\text{TiO}_2\text{CB}} = -4.2$ eV.

Calculations for compound **1** were done in our previous report.²

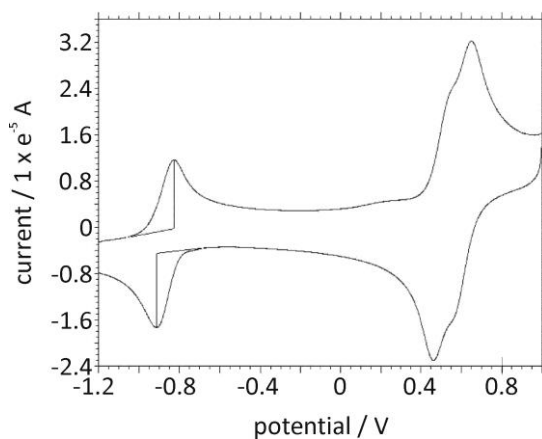


Figure 3–S1. Cyclic Voltammogram of **2**

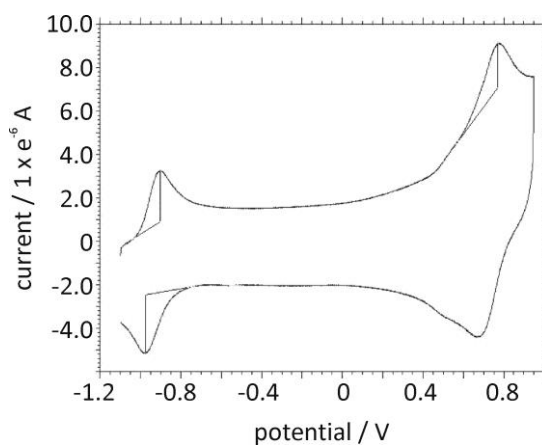


Figure 3–S2. Cyclic Voltammogram of **3**

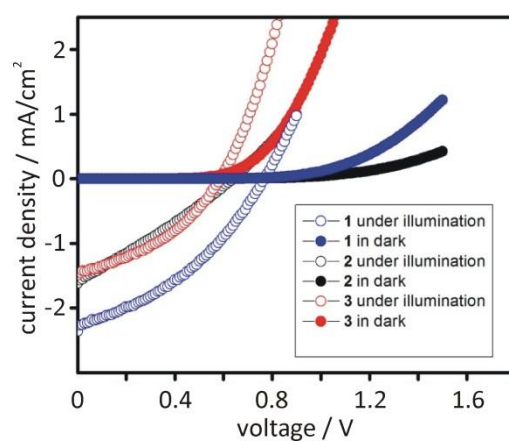
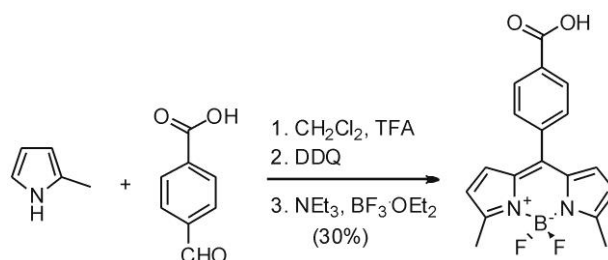
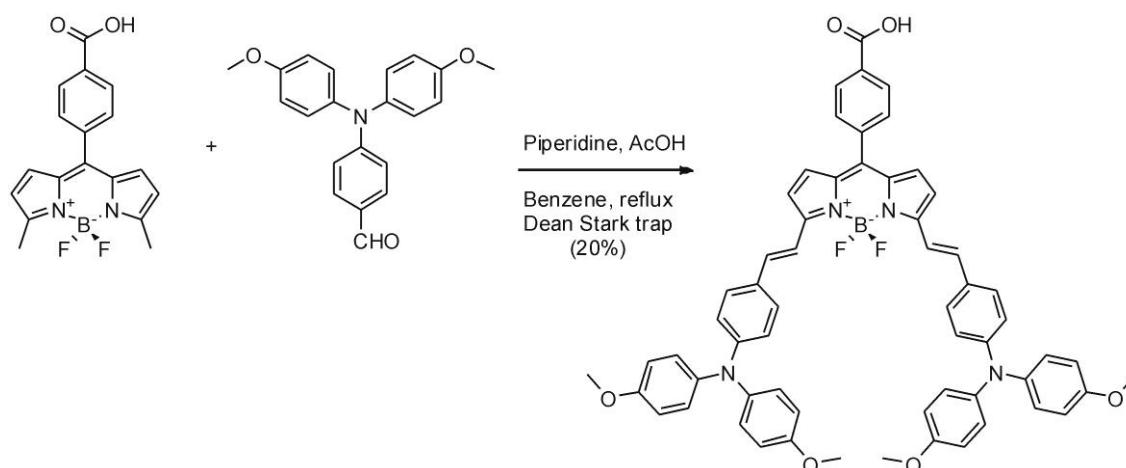


Figure 3–S3. I-V plots for the cells.

Synthesis:**Compound 4:**

To a 1 L round-bottomed flask containing 400 mL argon-degassed CH_2Cl_2 were added 2-methyl pyrrole (12.3 mmol, 1.0 g) and 4-carboxybenzaldehyde (6.0 mmol, 0.9 g). One drop of TFA was added and the solution was stirred under N_2 at room temperature for 1 day. After addition of a solution of DDQ (6.0 mmol, 1.36 g) in 100 mL of dichloromethane to the reaction mixture, stirring was continued for 30 min. 5 mL of Et_3N and 5 mL of $\text{BF}_3\cdot\text{OEt}_2$ were successively added and after 30 min, the reaction mixture was washed three times with water (50 x 100 mL) which was then extracted into the CHCl_3 (3 x 100 mL) and dried over anhydrous Na_2SO_4 . The solvent was evaporated and the residue was purified by silica gel column chromatography using (CHCl_3 : MeOH 95:5) as the eluant. Red solid (1.25 g, 30%).

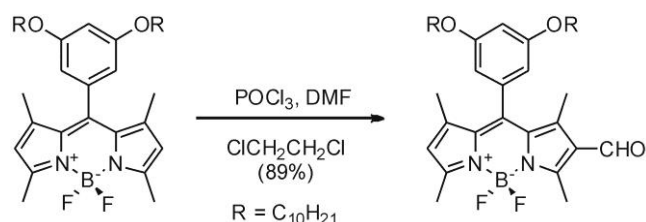
^1H NMR (400 MHz, CDCl_3): δ_{H} 8.25 (2H, d; $J = 7.6$ Hz, ArH), 7.65 (2H, d; $J = 7.7$ Hz, ArH), 6.70 (2H, s; ArH), 6.30 (2H, d; $J = 3.4$ Hz, ArH), 2.70 (6H, s; CH_3). ^{13}C NMR (100 MHz, CDCl_3): δ_{C} 170.5, 158.5, 140.9, 139.4, 134.5, 130.6, 130.5, 130.2, 130.0, 119.9, 15.0 ppm; MS (TOF-ESI): m/z : Calcd: 340.1195 $[\text{M}-\text{H}]^+$, Found: 340.1130 $[\text{M}-\text{H}]^+$, $\Delta = 19.1$ ppm.

Compound 2:

4 (0.88 mmol, 0.30 g) and *N,N*-di(4-methoxyphenyl)aminobenzaldehyde (3.53 mmol, 1.18 g) were added to a 100 mL round-bottomed flask containing 50 mL benzene and to this solution was added piperidine (0.3 mL) and acetic acid (0.3 mL). The mixture was heated under reflux by using a Dean Stark trap and reaction was monitored by TLC (CHCl_3 : MeOH 93:7): When all the starting material had been consumed, the mixture was cooled to room temperature and solvent was evaporated. Water (100 mL) added to the residue and the product was extracted into the chloroform (3 x 100 mL). Organic phase dried over Na_2SO_4 , evaporated and residue was purified

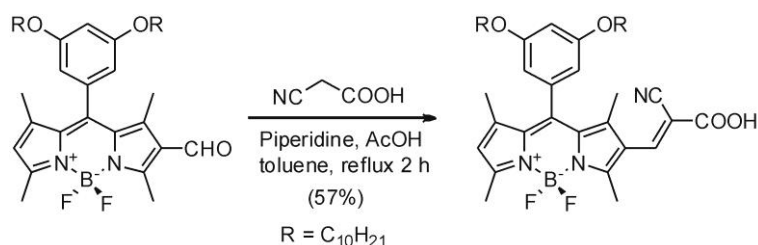
by silica gel column chromatography using (CHCl₃ : MeOH 93:7) as the eluant. Black waxy solid (0.17 g, 20%). ¹H NMR (400 MHz, DMSO-*d*₆): δ_H 8.25 (1H, s; COOH), 8.05 (2H, d; *J* = 8.3 Hz, *ArH*), 7.64 (2H, d; *J* = 8.2 Hz, *ArH*), 7.52 (2H, d; *J* = 17.2 Hz, *CH*), 7.38 (4H, d; *J* = 8.7 Hz, *ArH*), 7.32 (2H, d; *J* = 15.2 Hz, *CH*), 7.15 (2H, d; *J* = 4.6 Hz, *ArH*), 7.10-7.05 (8H, m; *ArH*), 6.95-6.85 (12H, m; *ArH*), 6.78 (2H, d; *J* = 4.6 Hz, *ArH*), 6.72 (4H, d; *J* = 8.5 Hz, *ArH*). ¹³C NMR (100 MHz, DMSO-*d*₆): δ_C 167.5, 156.9, 154.9, 150.2, 139.5, 138.2, 137.8, 135.4, 132.6, 131.0, 129.9, 129.8, 129.6, 129.3, 129.1, 128.0, 127.7, 120.2, 118.4, 117.6, 115.5, 55.7 ppm; MS (TOF-ESI): *m/z*: Calcd: 970.3713, Found: 970.3692, Δ = 2.2 ppm.

Compound 6:



A mixture of DMF (6 mL) and POCl₃ (6 mL) was stirred under argon for 5 min in the ice bath. After warming solution up to rt, it was stirred for additional 30 min. **5** (0.50 mmol, 158.0 mg) in 60 mL dichloroethane was added to the solution and temperature raised to 500°C. After stirring for 2 h, the mixture was cooled to rt and then poured in to iced cooled saturated aqueous solution of NaHCO₃ (150 mL). Then reaction mixture was stirred for 30 min after warming solution to rt. After 30 min. the mixture was washed with H₂O (2 x 100 mL). The product was extracted into the dichloromethane. Organic phase dried over Na₂SO₄. Reddish brown solid was obtained (157.0 mg, 89%). ¹H NMR (400 MHz, CDCl₃, 300 K): δ_H 10.02 (1H, s; CHO), 6.58 (1H, t; *J* = 2.61 Hz, *ArH*), 6.41 (2H, d; *J* = 2.20 Hz, *ArH*), 6.15 (1H, s; *ArH*), 3.92 (4H, t; *J* = 6.60 Hz, OCH₂), 2.81 (3H, s; CH₃), 2.60 (3H, s; CH₃), 1.85 (3H, s; CH₃), 1.75 (4H, m; CH₂), 1.42 (4H, m; CH₂), 1.40-1.15 (24H, m; CH₂), 0.85 (6H, t; *J* = 6.68 Hz, CH₃). ¹³C NMR (100 MHz, CDCl₃): δ_C 185.8, 161.4, 156.4, 147.3, 143.5, 142.9, 135.5, 133.8, 130.8, 129.5, 128.8, 126.3, 123.8, 106.1, 102.5, 68.5, 31.9, 29.5, 29.3, 29.1, 26.0, 22.7, 15.0, 14.7, 14.1, 13.0, 11.5 ppm; MS (TOF-ESI): *m/z*: Calcd: 664.4587 [M-H]⁺, Found: 664.4503 [M-H]⁺, Δ = 12.7 ppm.

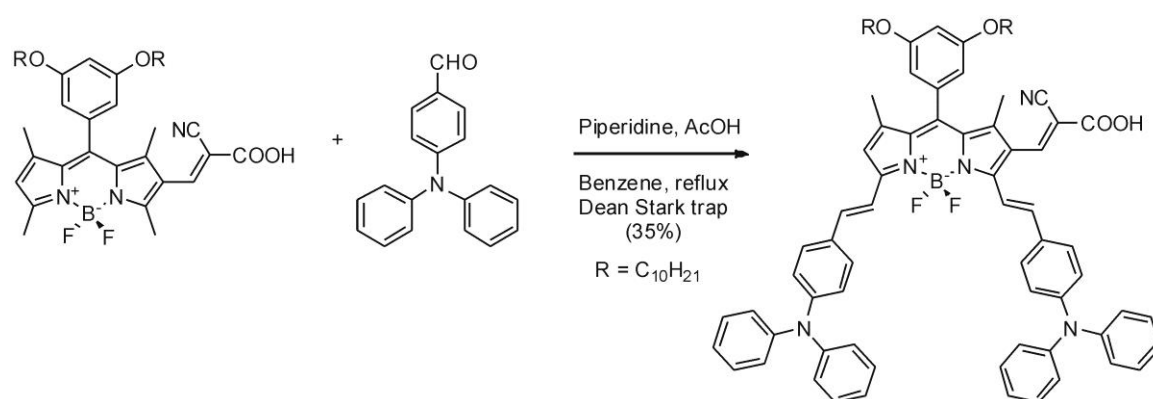
Compound 7:



6 (0.12 mmol, 83.0 mg) and cyanoacetic acid (0.49 mmol, 42.3 mg) were dissolved in toluene. One drop of piperidine and catalytic amount of acetic acid were added to the mixture under argon atmosphere. The reaction mixture was refluxed and stirred under argon for 3 h. Then mixture washed with water (2 x 50 mL). Organic phase dried over Na₂SO₄ and solvent was evaporated and the residue was purified by silica gel column chromatography using (CHCl₃ : MeOH 90:10) as the eluent. Red solid was obtained (50.0 mg, 57%). ¹H NMR (400 MHz,

CDCl₃): δ_{H} 8.18 (1H, s; CH), 6.55 (1H, s; ArH), 6.41 (2H, d; $J = 1.9$ Hz, ArH), 6.08 (1H, s; ArH), 3.91 (4H, t; $J = 6.5$ Hz, OCH₂), 2.57 (6H, s; CH₃), 1.80-1.68 (4H, m; CH₂), 1.63 (3H, s; CH₃), 1.59 (3H, s; CH₃), 1.48-1.37 (4H, m; CH₂), 1.45-1.18 (24H, m; CH₂), 0.86 (6H, t; $J = 6.8$ Hz, CH₃). ¹³C NMR (100 MHz, CDCl₃): δ_{C} 161.4, 153.7, 142.8, 140.6, 135.6, 133.4, 130.8, 123.9, 123.3, 106.1, 102.6, 68.5, 31.9, 29.6, 29.4, 29.3, 29.1, 25.9, 14.6, 14.1 ppm; MS (TOF-ESI): m/z : Calcd: 731.4645 [M-H]⁺, Found: 731.4585 [M-H]⁺, $\Delta = 8.2$ ppm.

Compound 3:



7 (0.12 mmol, 90.0 mg) and *N,N*-diphenylaminobenzaldehyde (0.37 mmol, 100.9 mg) were added to a 100 mL round-bottomed flask containing 50 mL benzene and to this solution was added piperidine (0.3 mL) and acetic acid (0.3 mL). The mixture was heated under reflux by using a Dean Stark trap and reaction was monitored by TLC (CHCl₃ : MeOH 93:7). When all the starting material had been consumed, the mixture was cooled to room temperature and solvent was evaporated. Water (100 mL) added to the residue and the product was extracted into the chloroform (3 x 100 mL). Organic phase dried over Na₂SO₄, evaporated and residue was purified by silica gel column chromatography using (CHCl₃ : MeOH 93:7) as the eluent. Green solid was obtained (52.2 mg, 35%). ¹H NMR (400 MHz, CDCl₃): δ_{H} 8.24 (1H, s; CH), 7.61-7.52 (1H, m; CH), 7.47 (2H, d; $J = 8.0$ Hz, ArH), 7.33-7.24 (6H, m; ArH), 7.21-7.08 (12H, m; ArH), 7.04-6.93 (8H, m; ArH), 6.90-6.69 (4H, m; ArH), 6.62 (1H, s; ArH), 6.46 (2H, s; ArH), 3.92-3.61 (4H, m; OCH₂), 1.89-1.54 (4H, m; CH₂), 1.52-1.49 (4H, m; CH₂), 1.48-1.12 (30H, m; CH₂, CH₃), 0.91-0.74 (6H, m; CH₃). ¹³C NMR (100 MHz, CDCl₃): δ_{C} 161.1, 148.5, 147.1, 147.0, 139.0, 136.4, 132.7, 129.4, 129.3, 128.9, 128.6, 125.4, 125.1, 124.8, 123.7, 123.3, 122.6, 122.3, 117.0, 106.8, 68.4, 31.9, 29.6, 29.5, 29.4, 29.3, 29.2, 26.0, 22.7, 14.7, 14.5, 14.1 ppm; MS (TOF-ESI): m/z : Calcd: 1241.6741 [M-H]⁺, Found: 1241.6790 [M-H]⁺, $\Delta = 3.9$ ppm.

References:

- (1) Y. Cakmak, E. U. Akkaya, *Org. Lett.* **2009**, *11*, 85-88.
- (2) S. Erten-Ela, M. D. Yilmaz, B. Icli, Y. Dede, S. Icli, E. U. Akkaya, *Org. Lett.* **2008**, *10*, 3299-3302.

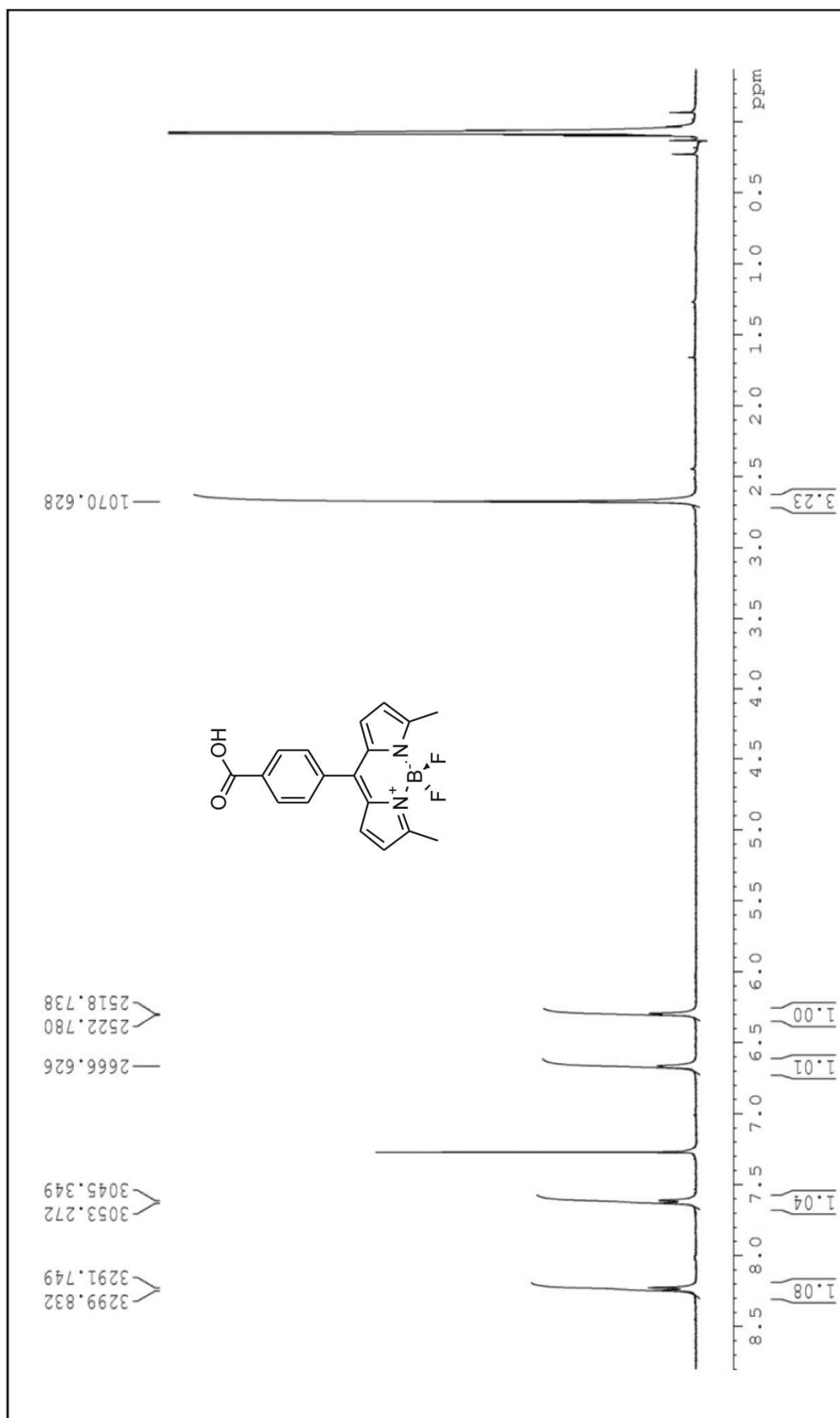


Figure 3-S4. ¹H NMR spectrum of compound 4

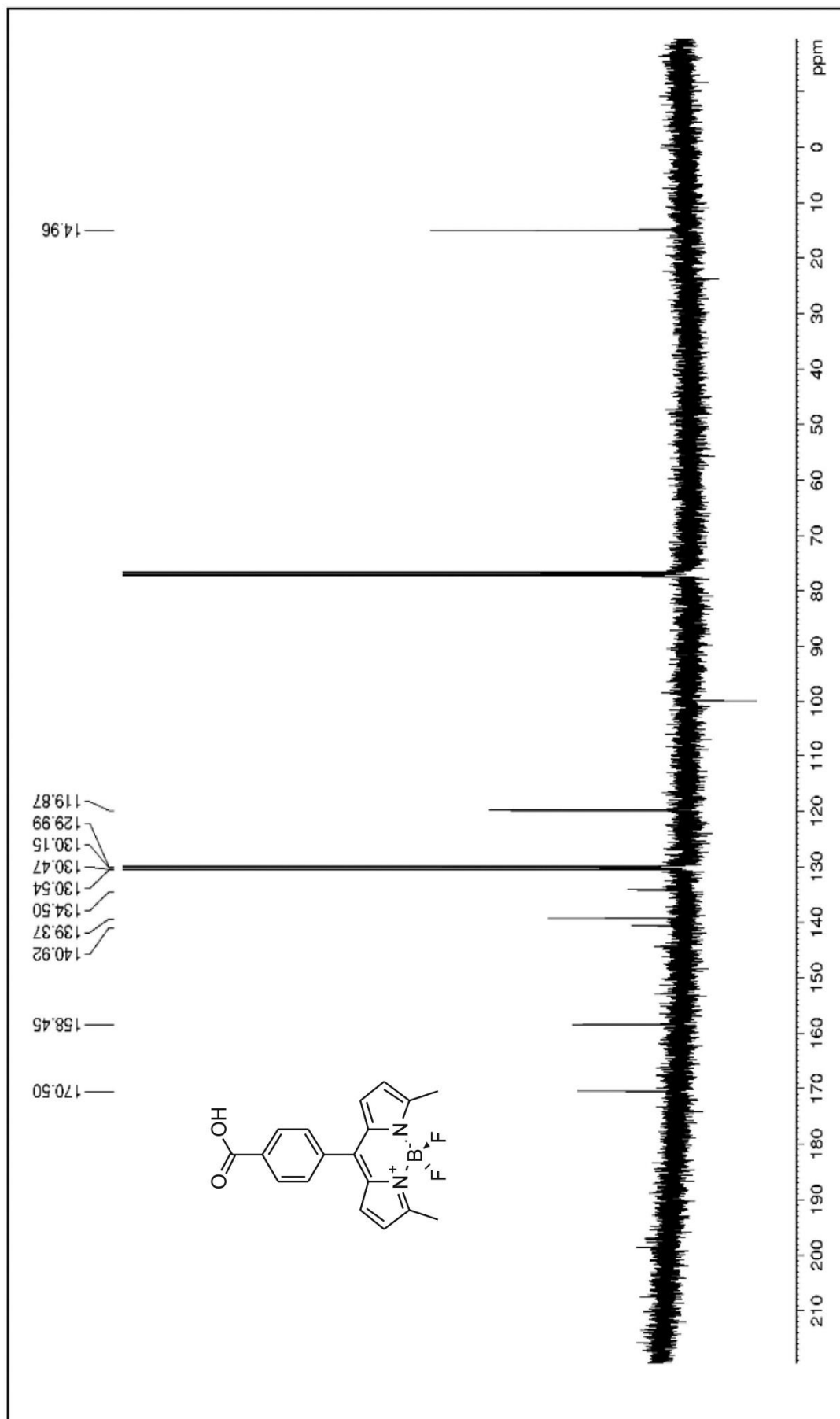


Figure 3– S5. ¹³C NMR spectrum of compound 4

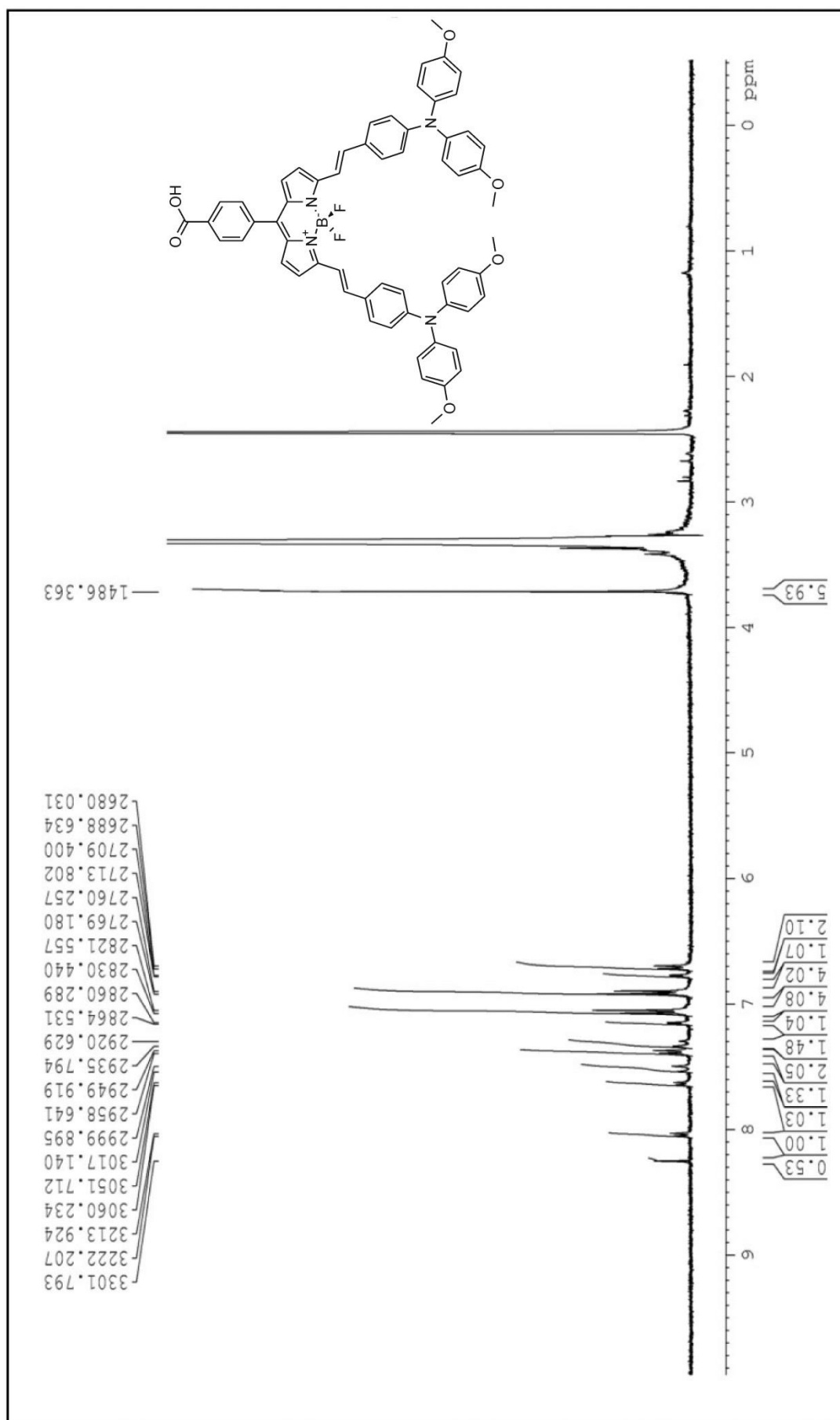


Figure 3- S6. ¹H NMR spectrum of compound 2

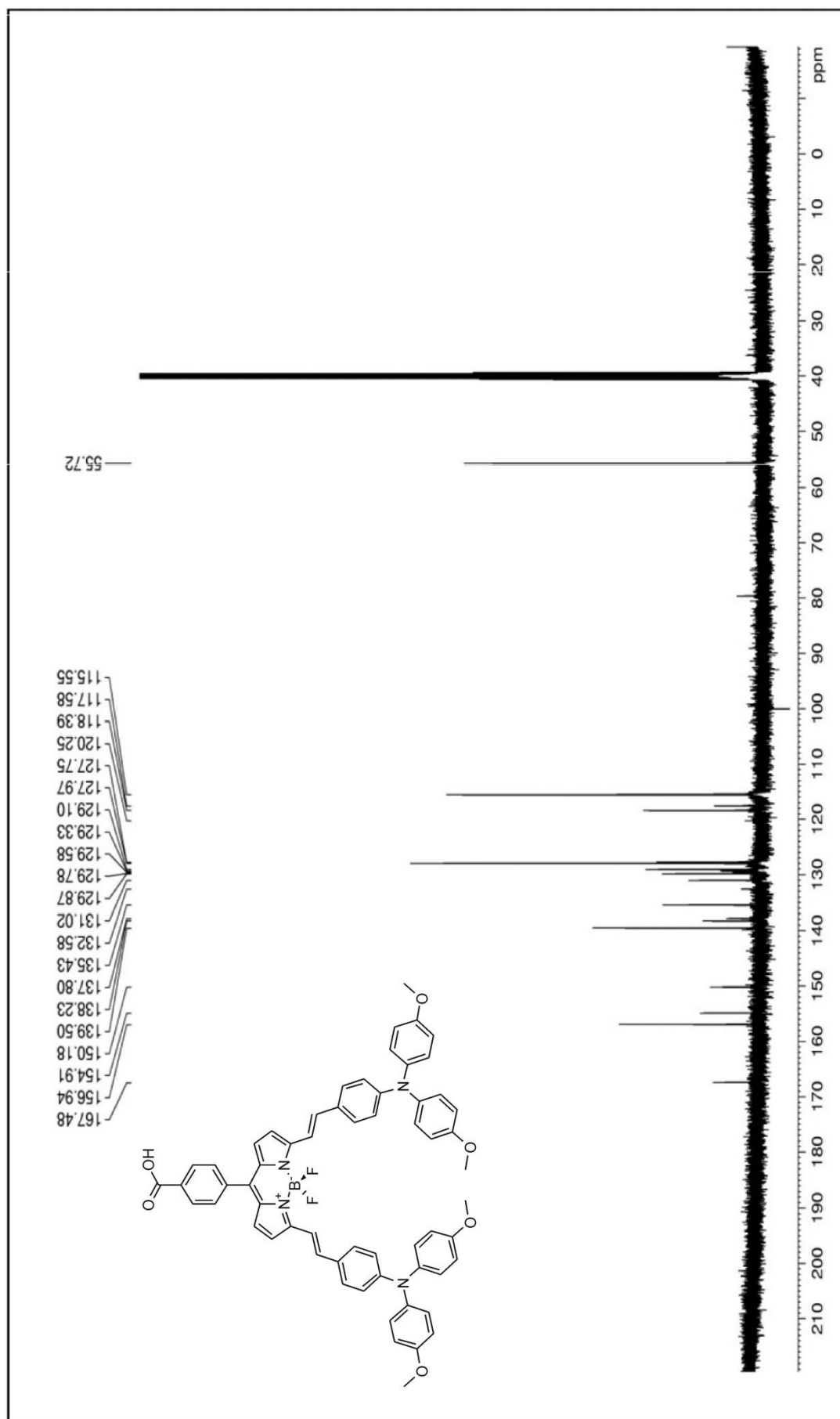


Figure 3–S7. ^{13}C NMR spectrum of compound 2

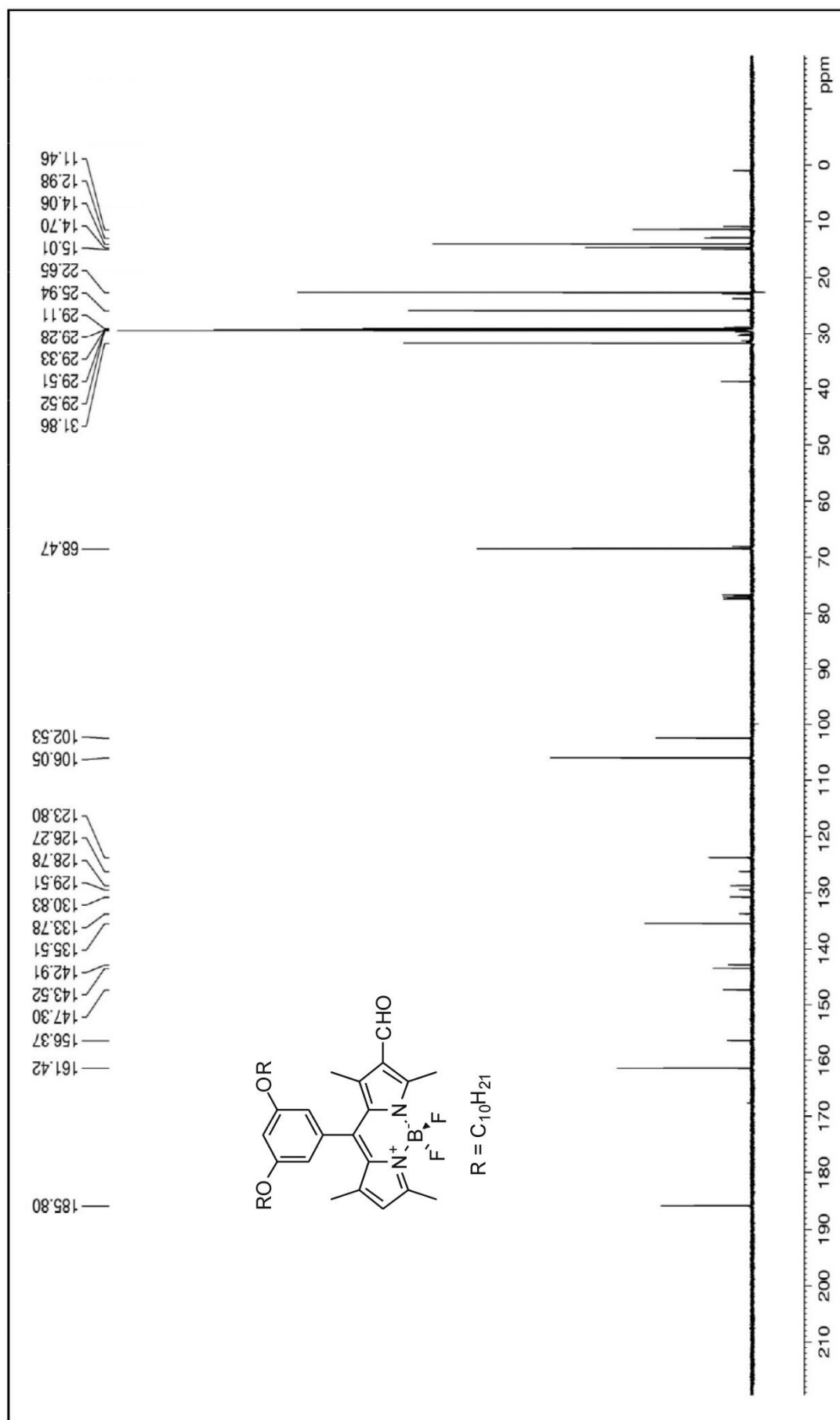


Figure 3– S9. ^{13}C NMR spectrum of compound 6

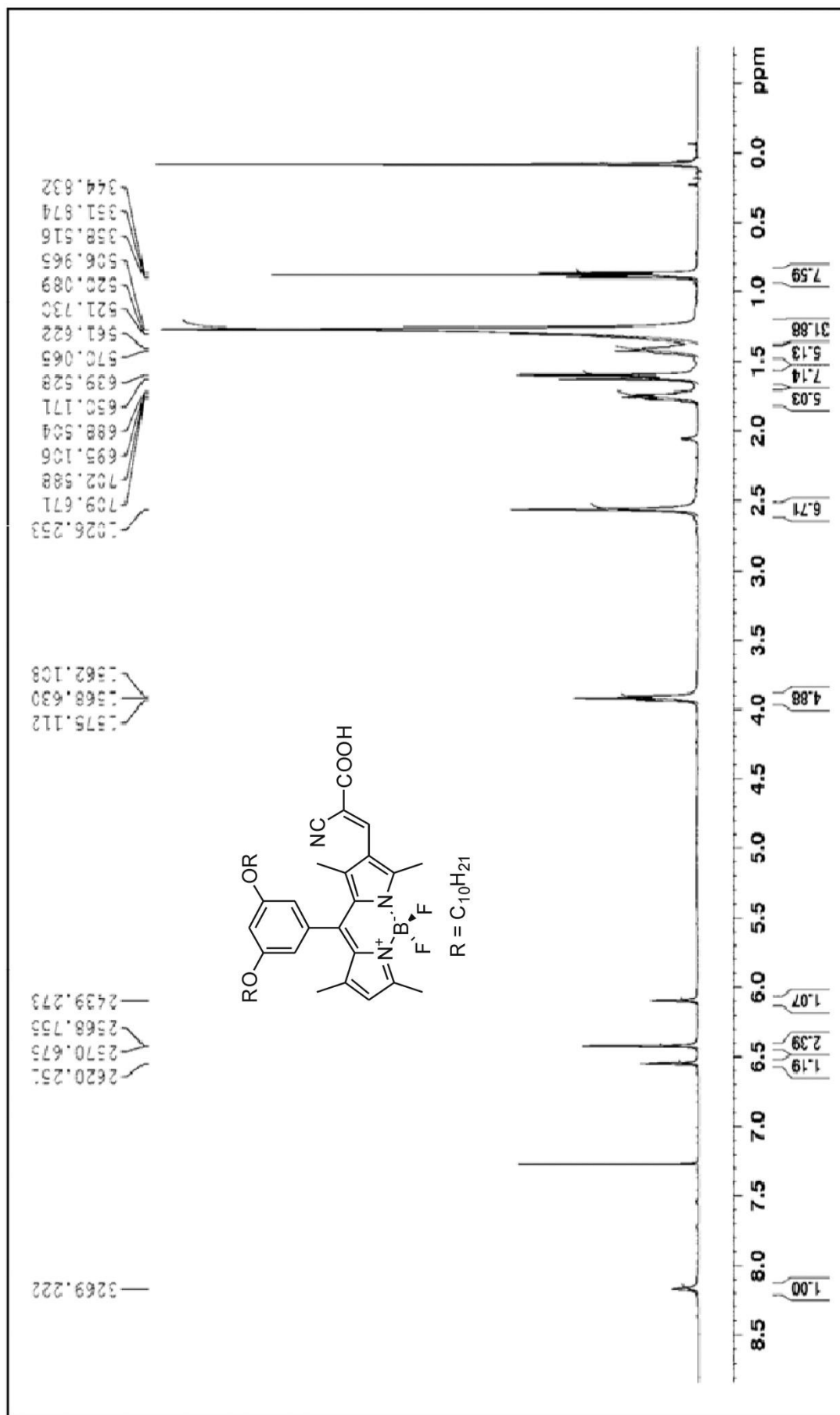


Figure 3-S10. ¹H NMR spectrum of compound 7

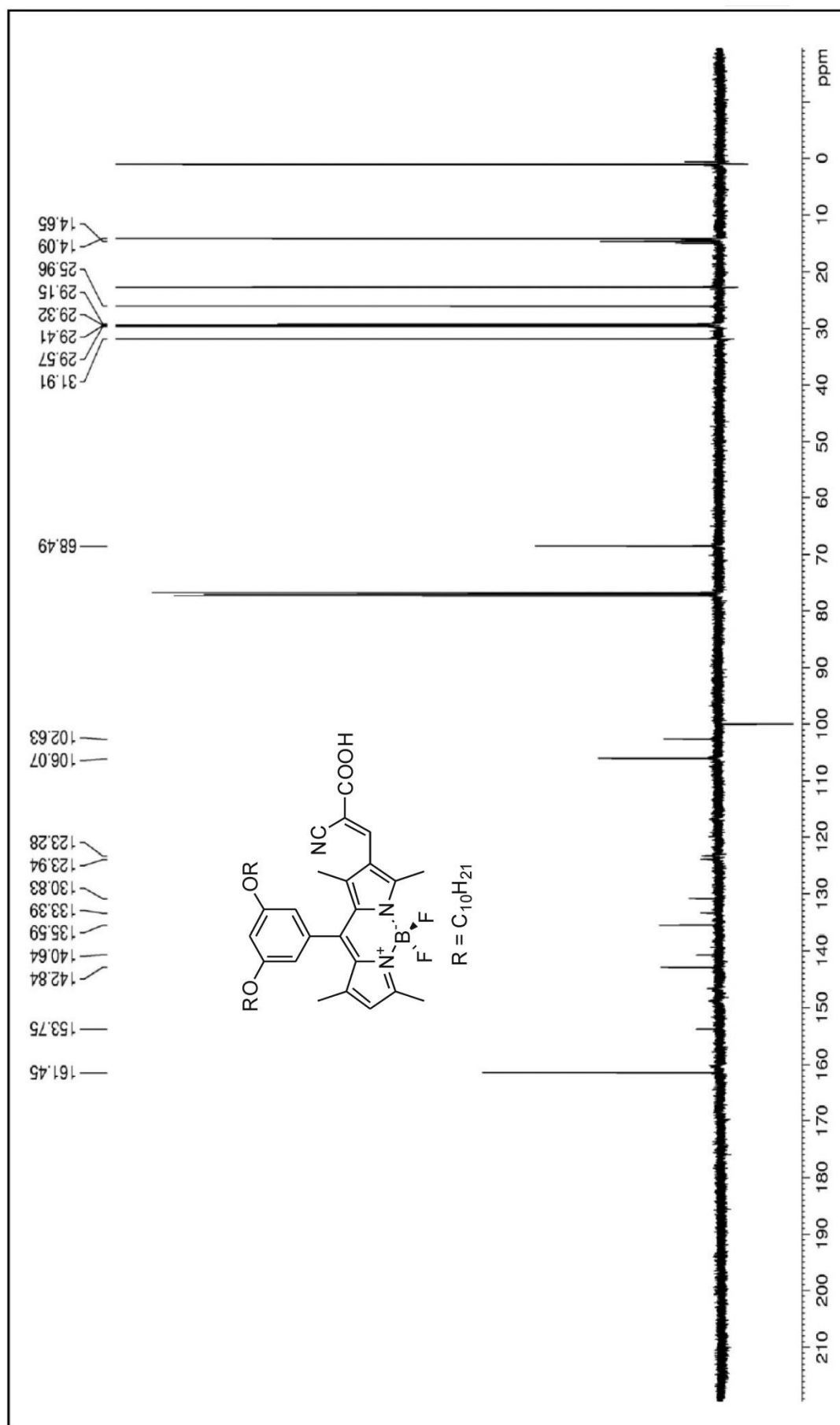


Figure 3-S11. ^{13}C NMR spectrum of compound 7

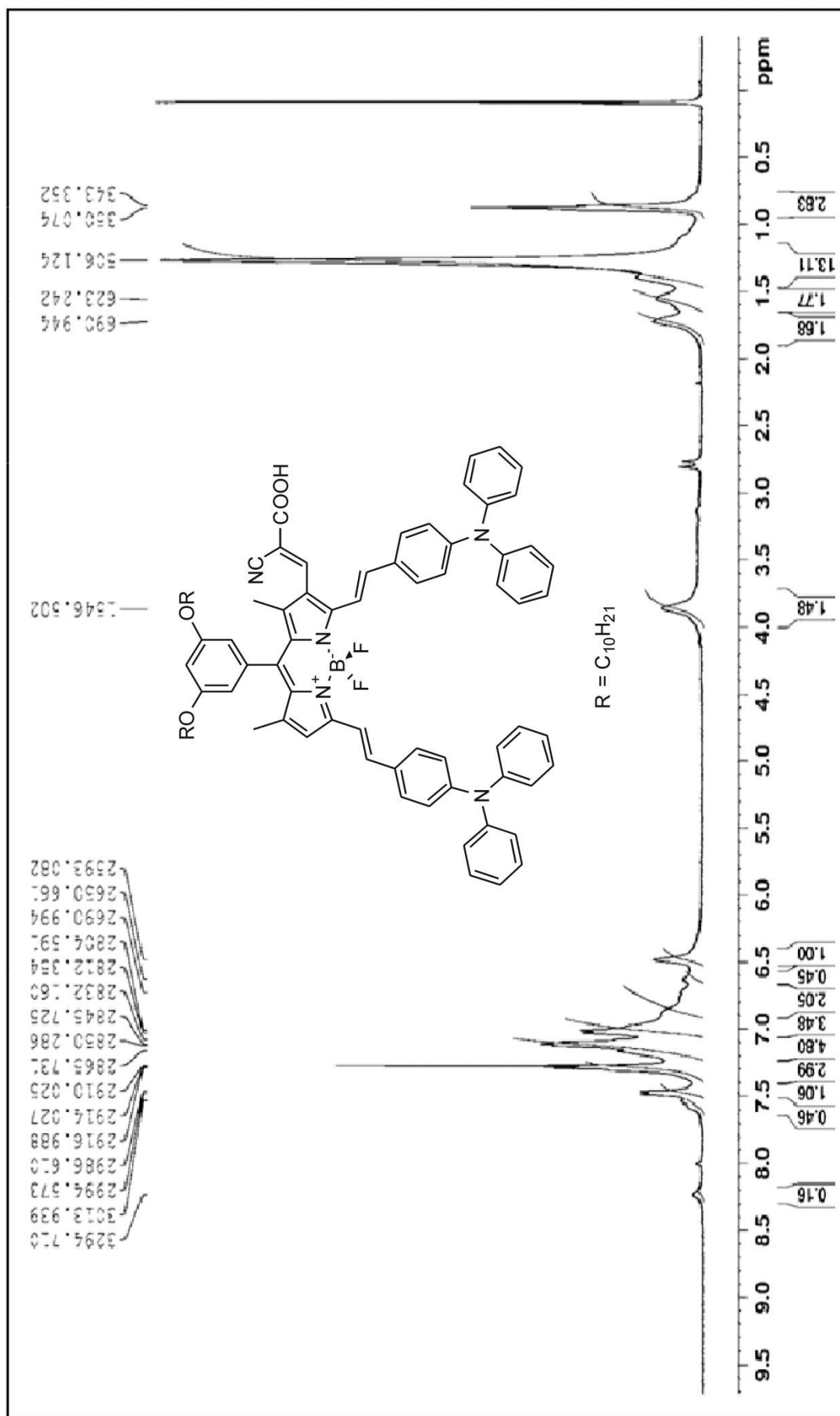


Figure 3-S12. ¹H NMR spectrum of compound 3

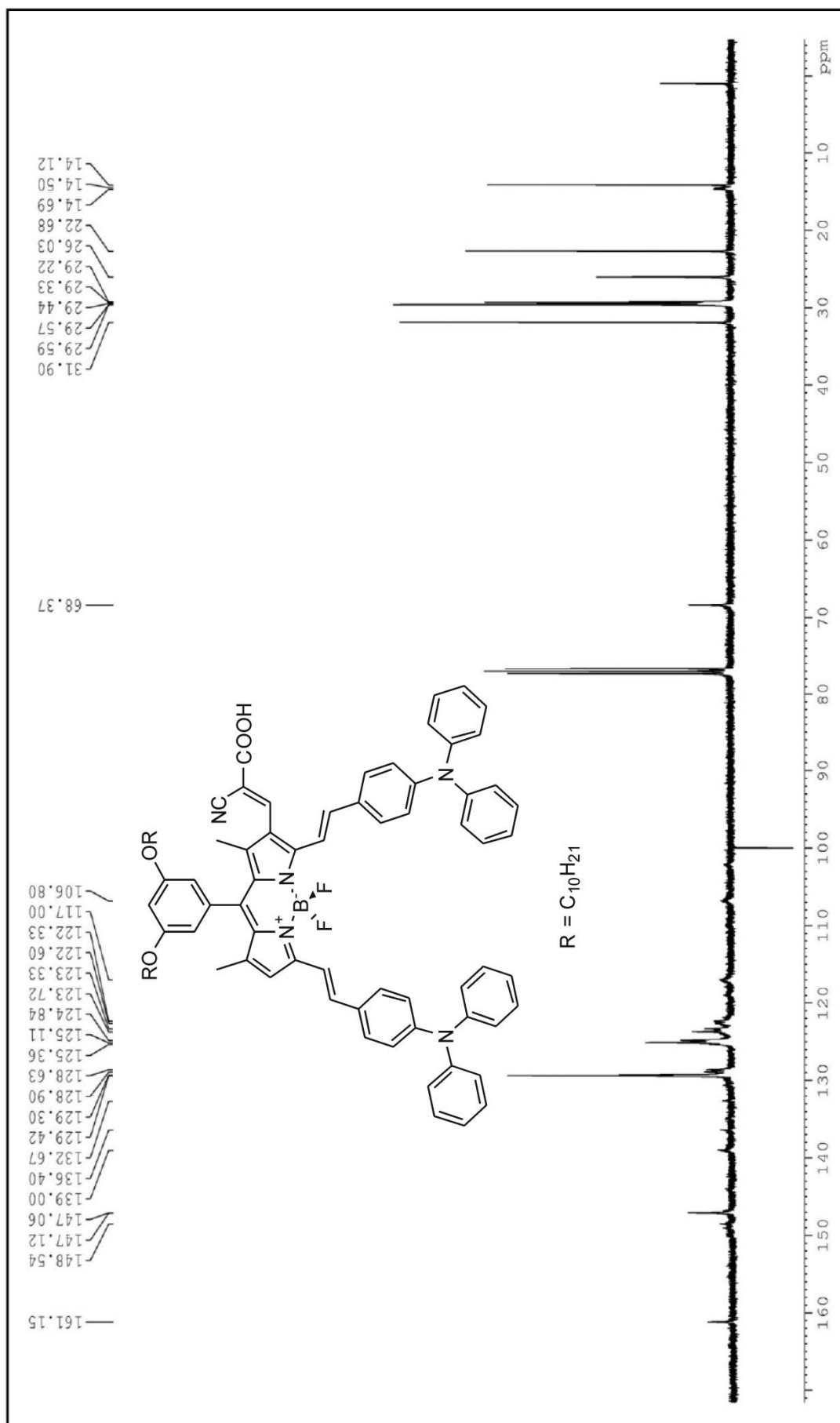


Figure 3– S13. ^{13}C NMR spectrum of compound 3

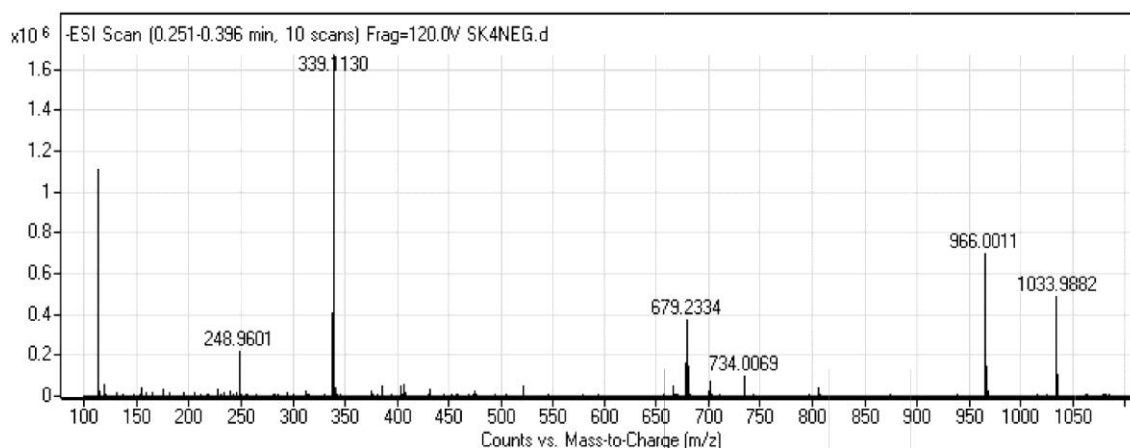


Figure 3-S14. Mass spectrum of compound 4

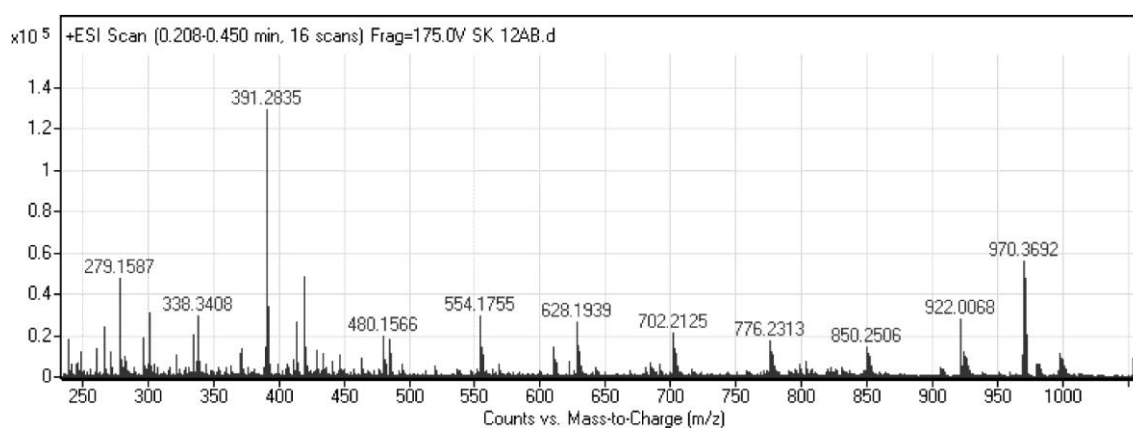


Figure 3-S15. Mass spectrum of compound 2

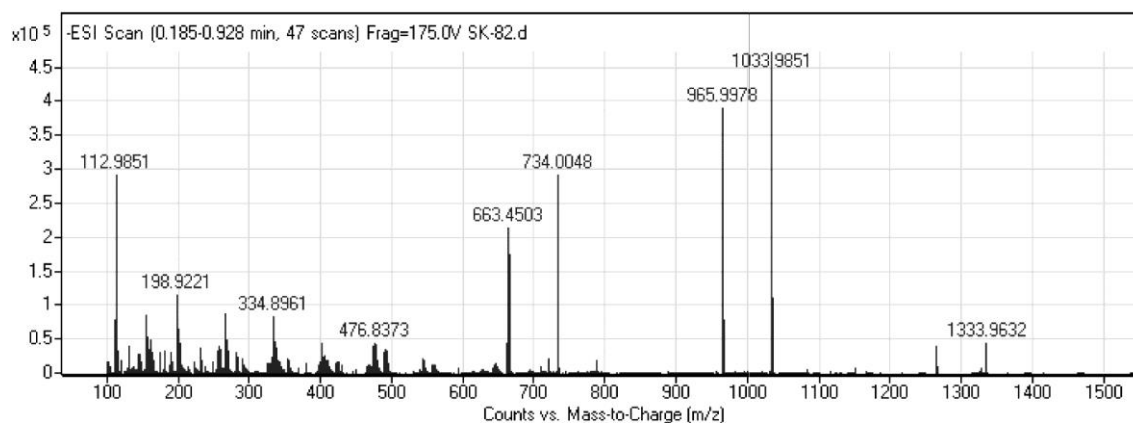


Figure 3-S16. Mass spectrum of compound 6

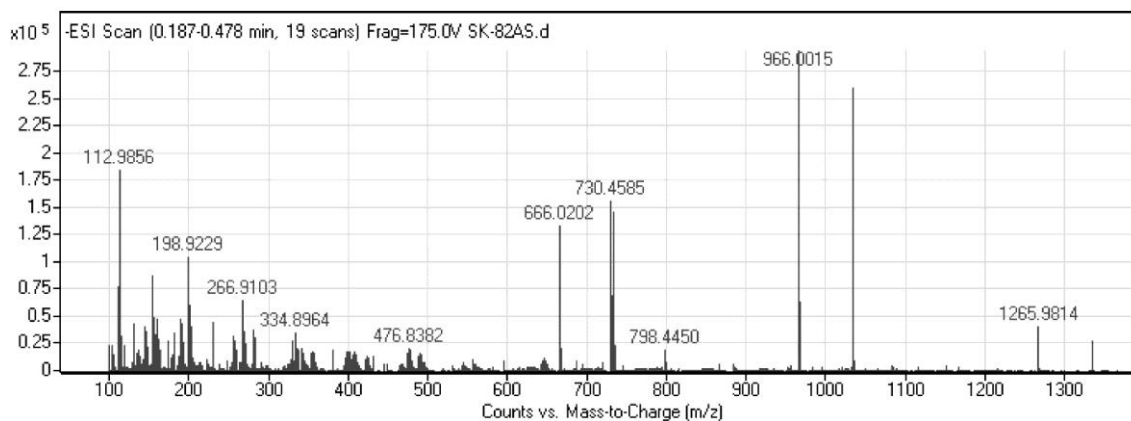


Figure 3-S17. Mass spectrum of compound 7

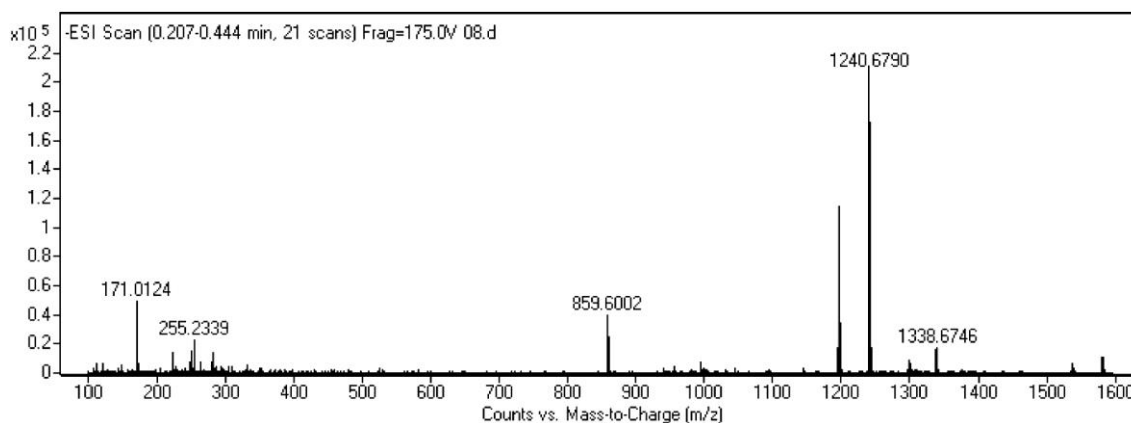


Figure 3-S18. Mass spectrum of compound 3

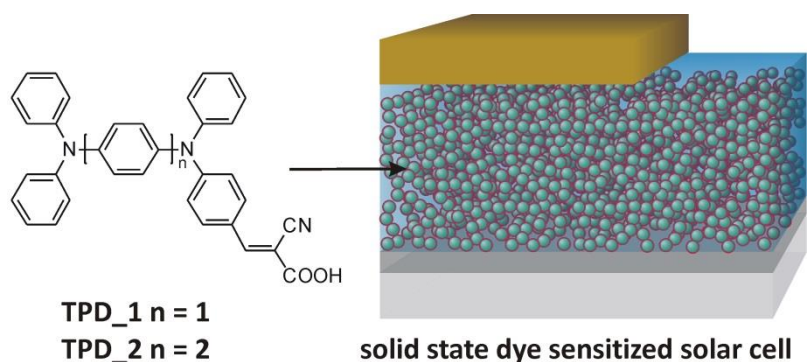
4. SOLID-STATE DYE-SENSITIZED SOLAR CELLS FABRICATED WITH NANOPOROUS TiO₂ AND TPD DYES: ANALYSIS OF PENETRATION BEHAVIOR AND I–V CHARACTERISTICS

Sule Erten-Ela,^{*,a,b} Johannes Brendel,^b Mukundan Thelakkat^b

^a Institute of Solar Energy, Ege University, Bornova, Izmir 35100, Turkey

^b Macromolecular Chemistry I, Applied Functional Polymers, University of Bayreuth, 95440 Bayreuth, Germany

*E-mail of corresponding author: sule.erten@ege.edu.tr



Published in *Chemical Physics Letters* **2011**, 510, 93-98.

ABSTRACT

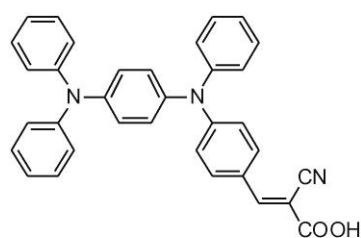
We present the synthesis, electrochemical properties and device-based investigation of triphenylene diamine (TPD) sensitizer with an extended π -system consisting of donor, electron conducting and anchoring group for solid-state dye-sensitized solar cells. Solid-state dye-sensitized solar cells were fabricated using blocking TiO₂-electrodes, nanoporous TiO₂-electrodes and the organic hole-transporting medium, HTM (spiro-OMeTAD) in a fluorine doped tin oxide/blocking TiO₂/nanoporous TiO₂/TPDs/hole transport material/Au configuration. Solid state dye sensitized solar cell consisting of TPD_2 as sensitizer on mesoporous TiO₂ shows the best results with a short-circuit current of 2.8 mA/cm², an open circuit voltage of 835 mV and an overall conversion efficiency of 0.97%.

INTRODUCTION

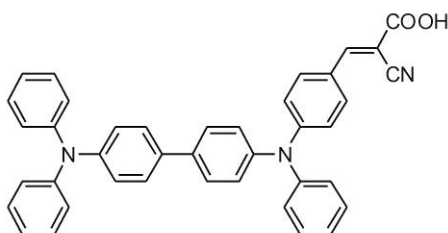
The first solar cell based on a nanoporous TiO₂ layer with an iodine–iodide electrolyte was realized by O'Regan and Grätzel in the 1990s.¹ The dye-sensitized solar cell is a non-conventional solar technology that has attracted much attention owing to its stability, low cost and device efficiency. Power-conversion efficiencies of over 11% have been achieved for devices that contain liquid electrolytes. The main problem of this cell type is the encapsulation of the liquid electrolyte. New investigations use an iodine-free solid organic hole transporting material (HTM) and instead of the liquid electrolyte.²⁻⁴ The ionic transport is replaced by electronic transport in the amorphous HTM. Solid-state devices that do not require a liquid electrolyte display an overall efficiency of 5%. Improvement of the efficiency of solid-state dye-sensitized solar cell requires optimization of their various components, such as the hole-transport material, sensitizer, mesoporous TiO₂ film, and the blocking layer.⁵ Solid-state dye-sensitized solar cells (SDSC) are promising due to their large potential to convert solar energy to electrical energy at low cost and their capabilities to solve the leakage or sealing problems that exist in liquid electrolyte dye-sensitized solar cells.⁶ A typical solid-state DSSC comprises a dye sensitized, mesoporous, nanocrystalline TiO₂ film interpenetrated by an organic semiconductor based hole transporting material (HTM), namely spiro-OMeTAD (2,2'-7,7'-tetrakis(*N,N*-diparamethoxyphenyl-amine 9,9'-spirobifluorene)). The function of the device is based upon a light induced charge separation reaction at the TiO₂/dye/HTM interface.^{7,8} In the state of the art solid-state dye-sensitized nanocrystalline-TiO₂ solar cell (SDSC), charge recombination is still one of the most limiting factors for device performance.⁹ Therefore, the question arises if it is possible to overcome this problem by developing new multifunctional materials which recombination processes can be decelerated.^{10,11} The interest in metal free, organic dyes with high extinction coefficients has grown in recent years. The organic dyes for DSSCs based on diphenylaniline as electron donor, published so far, include relatively complicated synthetic procedures, such as Stille or Suzuki couplings or more steps in the synthetic route. In order to investigate organic dyes and, in the longer run, prepare an efficient solar cell dye, a number of different organic dyes were designed and synthesized.¹²⁻¹⁴ Most organic sensitizers are constituted by donor, linker and acceptor moieties. Generally organic dyes used for efficient solar cells are required to possess a broad and intense spectral absorption in the visible light region.¹⁵⁻²⁵

Present study highlights the synthesis, electrochemical properties of triphenylene diamine dyes (TPD_1 and TPD_2) and their performance for solid state dye-sensitized solar cells using blocking

and nanoporous TiO₂ working electrodes. We have synthesized the TPD dyes (TPD₁ and TPD₂), with a general structure donor–linker–acceptor, D–L–A, where the triphenylene diamine moieties act as an electron donor and the cyanoacetic moieties act as the electron acceptor and as anchoring groups for attachment on the TiO₂. The dyes will be referred to as TPD₁ and TPD₂, respectively, according to the conjugation length (see Figure 4–1). To enhance the electron-donor ability of TPD₁, an extra phenylene unit was attached to the middle phenyl ring, leading to dye: TPD₂ for solid state dye sensitized solar cell device. Spectroscopic and electrochemical properties of TPD₁ and TPD₂ were characterized experimentally. Solid state dye sensitized solar cell performances of TPD dyes are also investigated. The penetration behavior of HTM into nanoporous TiO₂ layer has been determined by scanning electron microscopy (SEM) measurements. Both preparation and thickness of the compact TiO₂ layer were optimized using spray pyrolysis.



(Z)-2-cyano-3-{4-[[4-(diphenylamino) phenyl] (phenyl) amino] phenyl}acrylic acid, **TPD₁**



(Z)-2-(cyanomethyl)-3-{4-[[4'-(diphenylamino)biphenyl-4-yl](phenyl)amino]phenyl}acrylic acid, **TPD₂**

Figure 4–1. Molecular structures of TPD dyes.

EXPERIMENTAL SECTION

Materials

N,N'-Diphenyl-1,4-phenylenediamine, tetraphenylbenzidine, sodium-*tert*-butoxide, triphenyl phosphine, Pd(OAc)₂, POCl₃, cyanoacetic acid and piperidine were purchased from Aldrich. Solvents were supplied from Merck and were used without any further purification.

Synthesis and characterization of triphenylene diamines consisting of anchoring groups

The synthesis of TPD dyes is conducted in three steps with moderate yields. First reaction is Ullmann reaction to form the triphenylene diamine product. Second reaction is Vilsmeier reaction to form aldehyde product. Final reaction is Knoevenagel reaction which comprises condensation reaction of aldehyde product and cyano-acetic acid. This reaction gives the target compound TPDs. Synthetic route of TPD is given below in Figure 4–2.

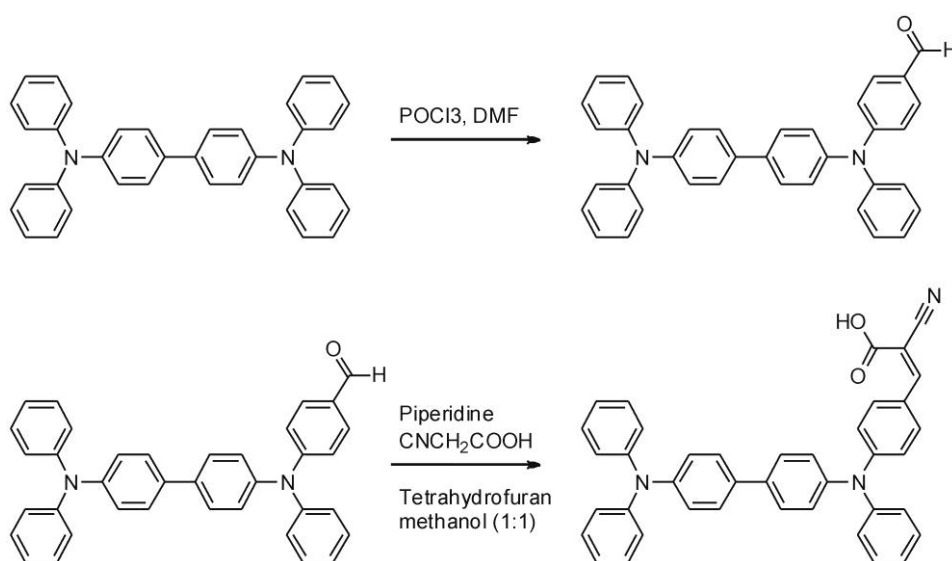


Figure 4–2. Synthetic route of TPD dyes consisting of anchoring groups, Vilsmeier reaction (a), Knoevenagel reaction (b).

Synthesis and characterization of TPD dyes

Synthesis method of TPD_1

1. Step: synthesis of 1,4-Bis(diphenylamino)benzene

N,N'-Diphenyl-1,4-phenylene diamine (0.01 mol, 2.6 g), sodium tert-butoxide (0.013 mol, 1.25), triphenyl phosphine (0.4 mmol, 0.1 g), Pd(OAc)₂ (0.2 mmol, 0.045 g) and 40 ml toluene are placed in a two-necked flask and stirred under argon atmosphere. And then, bromo benzene (0.024 mol, 2.6 ml) is added to the reaction. The reaction is refluxed for 24 h. After reaction finished, the solutions are waited for cooling to room temperature. It is extracted with ethyl acetate and distilled water. Organic phase is taken and filtered. Solvent is evaporated. Crude product is purified with column chromatography (chloroform:hexane ratio 3:2). 1,4-Bis(diphenylaminobenzene), gray crystals, (yield 85%). Molecular structure is analyzed with ¹H NMR spectrum, ¹H NMR (CDCl₃): (ppm), 7.25 (8H, m, Ar–H), 7.10 (8H, m, Ar–H), 6.99 (8H, m, Ar–H).

2. Step: synthesis of 4-[[4-(diphenylamino)phenyl](phenyl)amino]phenyl benzaldehyde

POCl₃ (1.36 mmol, 0.2 g) is stirred in DMF at 0 °C for 1 h under argon atmosphere. 1,4-Bis(diphenylamino)benzene (1.14 mmol, 471 mg) is added to reaction mixture and refluxed at 100 °C. After the reaction finished, solvent is evaporated. Crude product is purified by using column chromatography. 4-[[4-(Diphenylamino)phenyl](phenyl)amino]phenyl benzaldehyde, yellow crystals, (yield 90%). Molecular structure is analyzed with ¹H NMR spectrum. ¹H NMR (CDCl₃): (ppm), 9.79 (1H, s, –CHO), 7.68 (2H, d, Ar–H), 7.36 (2H, t, Ar–H), 7.28 (4H, t, Ar–H), 7.21 (3H, m, Ar–H), 7.12 (4H, d, Ar–H), 7.04 (8H, d, Ar–H).

3. Step: synthesis of (Z)-2-cyano-3-{4-[[4-(diphenylamino) phenyl] (phenyl) amino] phenyl}acrylic acid, TPD_1

To a solution of 4-[[4-(diphenylamino)phenyl](phenyl)amino]phenyl benzaldehyde (0.16 mmol, 72.3 mg) and cyanoacetic acid (0.32 mmol, 27.95 mg) in a mixture of tetrahydrofuran:methanol (1:1) is added catalytic amount of piperidine. Solution is stirred for 2 h at 40 °C. The solvent mixture is evaporated under reduced pressure and the resulting material is extracted with chloroform and 0.1 M HCl solution, washed with water, and dried over magnesium sulfate. The product is purified by column chromatography using silicagel and chloroform:methanol (2:0.5) as the eluent (yield 75%). Molecular structure is characterized by using IR, ¹H NMR, Mass and Elemental Analysis. IR (KBr): cm⁻¹, 3551, 3412, 2214, 1617, 1587, 1503, 1384, 1269, 1192, 833, 755, 696, 621, 480. ¹H NMR (DMSO-*d*₆): (ppm), 7.85 (1H, s, —CH=), 7.78 (2H, d, Ar–H), 7.40 (2H, t, Ar–H), 7.33 (4H, t, Ar–H), 7.18 (3H, m, Ar–H), 7.09 (10H, m, Ar–H), 6.92 (2H, d, Ar–H). HRMS (TOF ESI⁻): [M–H]⁻ = 506.2 (calcd. for C₃₄H₂₅N₃O₂ (507.2)). Calcd: C 80.45, H 4.96, N 8.28, O 6.30; found: C 80.43, H 4.93, N 8.28, O 6.30.

Synthesis method of TPD_2

Tetraphenylbenzidine was supplied from Aldrich company, aldehyde product and acrylic acid product were synthesized in the following procedure.

1. Step: synthesis of 4-[[4'-(diphenylamino)biphenyl-4-yl](phenyl)amino]benzaldehyde

POCl₃ (1.36 mmol, 0.2 g) is stirred in a two-necked flask at 0 °C for 1 h in dried DMF under argon atmosphere. After additional stirring for 1 h at room temperature, this solution is added to a stirred solution of 5 g (0.0097 mol) of *N,N'*-Bis(diphenyl)benzidine in 20 mL of 1,2-dichloroethane. This reaction mixture is stirred for another hour at 60 °C and allowed to cool to room temperature. And then, the mixture is poured into a solution of 10 g sodium acetate in 100 mL water, and this mixture is extracted three times with chloroform. The combined organic layers were washed twice with water and dried over magnesium sulfate. After filtration and evaporation of the solvent a yellow solid is obtained. The desired monoformylated product is isolated from this crude product by column chromatography using silica gel and solvent as the eluent, (yield 90%).

4-[[4'-(diphenylamino)biphenyl-4-yl](phenyl)amino]benzaldehyde, yellow crystals, Molecular structure is analyzed with ¹H NMR spectrum. ¹H NMR (CDCl₃): (ppm), 9.83 (1H, s, –CHO), 7.71 (2H, d, Ar–H), 7.55 (2H, t, Ar–H), 7.48 (2H, t, Ar–H), 7.21 (21H, m, Ar–H).

2. Step: synthesis of (Z)-2-(cyanomethyl)-3-{4-[[4'-(diphenylamino)biphenyl-4-yl](phenyl)amino]phenyl}acrylic acid, TPD_2

To a solution of 4-[[4'-(diphenylamino)biphenyl-4-yl](phenyl)amino]benzaldehyde (0.16 mmol, 72.3 mg) and cyanoacetic acid (0.32 mmol, 27.95 mg) in a mixture of tetrahydrofuran:methanol (1:1) is added catalytic amount of piperidine. The solution is stirred for 2 h at 40 °C. The solvent mixture is evaporated under reduced pressure and the resulting material is extracted with chloroform 0.1 M HCl solution washed with water, and dried over magnesium sulfate. The product is purified by column chromatography using silicagel and chloroform:methanol (2:0.5) as the eluent (yield 75%). Molecular structure is characterized by using IR, ¹H NMR, Mass and Elemental Analysis. IR (KBr): cm⁻¹, 3551, 3412, 3031, 2214, 1583, 1487, 1392, 1323, 1270, 1178, 1074, 1028, 1003, 959, 818, 788, 749, 723, 693, 667. ¹H NMR (DMSO-*d*₆): (ppm), 7.88 (1H, s, —CH=), 7.79 (2H, d, Ar–H), 7.60 (4H, q, Ar–H), 7.36 (6H, m, Ar–H), 7.15 (5H, m, Ar–H), 7.10 (10H, m, Ar–H).

HRMS (TOF ESI⁻): [M–H]⁻ = 582.3 (calcd. for C₄₀H₂₉N₃O₂ (583)). Calcd: C 82.31, H 5.01, N 7.20, O 5.48; found: C 82.33, H 5.00, N 7.23, O 5.48.

RESULTS AND DISCUSSION

Electrochemistry of triphenylene diamines consisting of anchoring groups

E_{HOMO} and E_{LUMO} values of triphenylene diamines comprising anchoring groups were calculated by using cyclic voltammograms. Solutions of TPD dyes were prepared in dichloromethane (10^{-3} M). A three electrode cell set-up employed for the measurements consisted of glassy carbon working electrode, Pt wire counter electrode and Ag/AgCl reference electrode, all placed in a glass vessel. Tetrabutylammonium hexafluorophosphate (TBAPF₆), 0.1 M, was used as supporting electrolyte. Ferrocene was used as internal reference electrode.

Table 4–1. Solid state dye sensitized solar cell efficiencies for TPD_1 and TPD_2 using nanoporous TiO₂ paste and Redox potentials of TPD derivatives.

	V_{oc}^a (mV)	I_{sc}^b (mA/cm ²)	FF ^c	η^d (%)	$E_{\text{oxidation}}^e$ (Volt)	$E_{\text{reduction}}^f$ (Volt)	$E_{\text{ferrocene}}^g$ (Volt)	E_{HOMO}^h (eV)	E_{LUMO}^i (eV)	E_{BandGap}^j
TPD_1	805	2.05	0.53	0.87	0.79	-1.43	0.31	5.28	3.06	2.22
TPD_2	835	2.80	0.42	0.97	0.85	-1.08	0.39	5.26	3.33	1.93

^a Open-circuit voltage

^b Short-circuit photocurrent.

^c Fill factor.

^d Overall solar-light-to-electrical conversion efficiency η .

^e First oxidation potentials of TPDs.

^f Reduction potentials of TPDs.

^g Potentials of ferrocene, internal reference electrode.

^h HOMO energy level of TPDs.

ⁱ LUMO energy level of TPDs.

^j Energy Band Gap of TPDs.

Figure 4–3, Figure 4–4 and Table 4–1 summarize the voltammetric behavior of 10^{-3} M solutions of TPDs. TPD derivatives show both reduction and oxidation potential in Figure 4–3 and Figure 4–4. E_{HOMO} and E_{LUMO} levels are calculated from the onset potentials of oxidation and reduction and by assuming the energy level of ferrocene/ferrocenium (Fc/Fc⁺) to be 4.8 eV below the vacuum level.^{26,27}

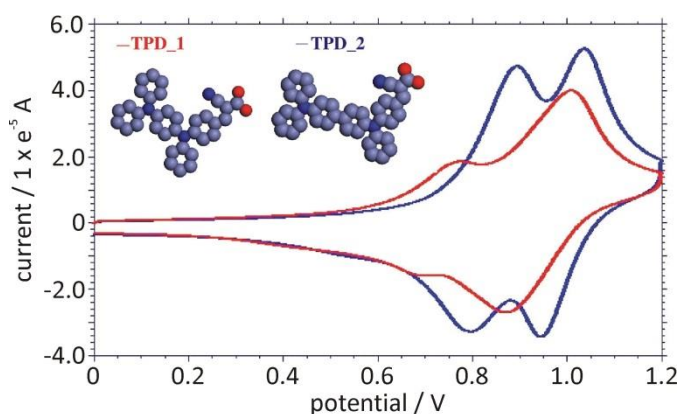


Figure 4–3. Cyclic voltammogram of TPDs in positive region.

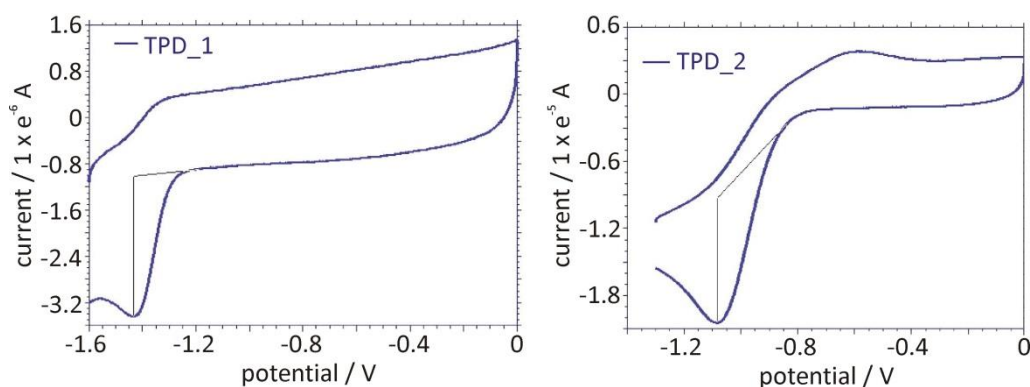


Figure 4–4. Cyclic voltammogram of TPDs in negative region.

The oxidation of TPD_1 and TPD_2, respectively, proceeds by two successive one-electron oxidations. The addition of the extra phenylene substituent to TPD_1 increases the first oxidation potential of the TPD_2 by ca. 0.06 V. The oxidation products for TPDs are stable on the voltammetric time scale at least several minutes in the solvents. Reduction processes were observable for TPD molecules because of cyanoacetic acid side chain within the solvent window. Additional phenylene group to TPD_1 shifts the reduction potential by ca. 0.35 V. Voltammetric results show that the extra phenylene group effects the first oxidation potential and reduction potential of TPD_1. Phenylene substitution to TPD_1 also greatly effects the E_{HOMO} and E_{LUMO} values and E_{BandGap} of TPD_2. TPD_2 has lower band gap than TPD_1 (Table 4–1). According to E_{LUMO} data of TPD_1 and TPD_2, electrons can be injected into the conduction band of TiO₂ easily.

Photovoltaic device fabrication and characterization of Solid state dye sensitized solar cells

The SnO₂:F covered glass was cut into 25 × 25 mm pieces. The transparent conducting glasses (TCO) covered with adhesive tape to control the thickness of the film and to provide non-coated areas for electrical contact and they were etched using Zn powder and 5% HCl acid solution. And then, FTO glasses were cleaned by using acetone, 2% Helmanex solution, distilled water and ethanol, respectively. After cleaning procedure, blocking layer was covered onto the FTO glasses. The films were sintered at 500 °C. TiO₂ paste was applied onto the TCO glass covered with blocking layer using screen printing technique; thin films of about 2 μm in thicknesses were prepared. Finally, temperature was increased gradually, the films were sintered at 500 °C for 1 h and temperature was cooled down to room temperature gradually. The TiO₂ electrodes were then immersed into the 0.5 mM dye solutions of TPDs and kept at room temperature overnight. TiO₂-coated glasses with TPD dyes adsorbed on were washed with pure solvent. Afterwards, organic hole-transporting material (HTM) 2,2',7,7'-tetrakis-(*N,N*-di-*p*-methoxyphenyl-amine)-9,9'-pirobifluorene (spiro-OMeTAD) was covered on dye adsorbed TiO₂ films by using spin coater. 40 nm gold was evaporated as top electrodes.

Figure 4–5 shows the schematic representation of a solid state dye sensitized solar cell which consists of transparent conductive oxide layer, compact TiO₂ layer; a dye adsorbed on mesoporous nanocrystalline-titanium dioxide acting as *n*-type semiconductor layer; hole transport material and a gold counter electrode.

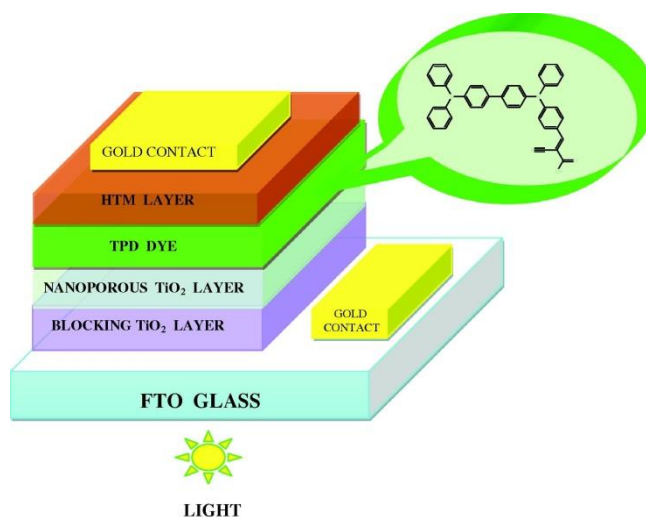


Figure 4–5. Schematic representation of a solid state dye sensitized solar cell.

I–V data collection is made by using Keithley 2400 Source-Meter and LabView data acquisition software. I–V characteristic of dye sensitized solar cell in dark and under illumination is shown in Figure 4–6.

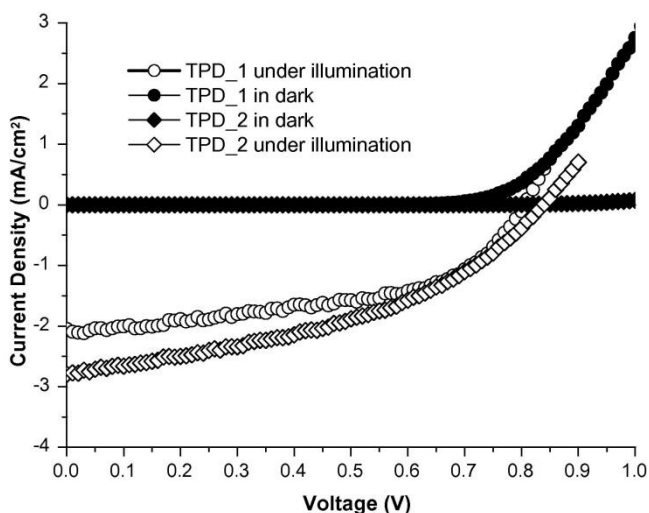


Figure 4–6. I–V curve of TPD dyes.

Performances of solid state dye sensitized solar cells

The photovoltaic performances of solid state solar cells based on the different sensitizers of TPD_1 and TPD_2 under AM 1.5 illumination are summarized in Figure 4–6 and Table 4–1. The penetration behavior of HTM into nanoporous TiO₂ layer has been determined by scanning electron microscopy (SEM) measurements in Figure 4–7. Both preparation and thickness of the compact TiO₂ layer were optimized using spray pyrolysis. The studies revealed that an optimum film thickness of 130–150 nm of compact TiO₂ yielded the best rectifying behavior and SDSC performance. In this work, our goal was to investigate the performance of TPD sensitizers in connection with spiro-OMeTAD hole transport material. SEM pictures show that the thicknesses of nanoporous TiO₂ paste and HTM layer are 2.1 μm and 257 nm, respectively, (Figure 4–7).

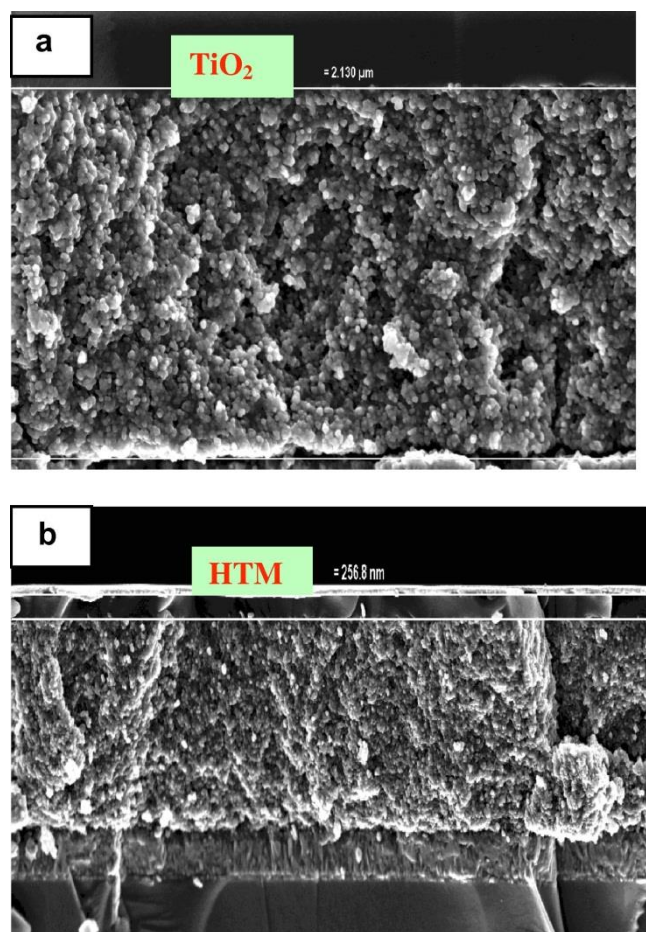


Figure 4–7. SEM pictures of solid state solar cells; TiO₂ thickness = 2.130 μm (a), HTM thickness = 256.8 nm (b).

We fabricated solid state devices several times to ensure optimization and reproducibility of the devices based on TPDs. Experiments show that these thicknesses are optimum values for solid state dye sensitized solar cells. The reproducibility and optimization parameters of TPD_1 and TPD_2 dyes show satisfactory efficiencies on thin TiO₂ films by increasing π -conjugation, the E_{HOMO} and E_{LUMO} energy levels were tuned, which was further supported by electrochemistry experiments. Solar cells based on TPD_2 yielded the highest efficiency (Table 4–1). As seen in Table 4–1, the efficiencies improve significantly from the dye TPD_1 to TPD_2, as 0.87% and 0.97%, respectively. The solar cell with TPD_2 sensitizer gives the highest efficiency as compared to the TPD_1 sensitizers. When we compare the J_{sc} values of TPDs, short circuit current density of TPD_2 are higher than the TPD_1, as 2.8 mAcm⁻², 2.05 mAcm⁻², respectively. Also, V_{oc} value of TPD_2 (835 mV) are higher than TPD_1 (805 mV).

In line with these statements, we now report the best efficiency under standard conditions obtained for a solid state dye sensitized solar cell based on TPD_2 dye that performs 835 mV open circuit voltage, 2.8 mA/cm² short-circuit current, 0.42 fill factor and 0.97% overall conversion efficiency.

CONCLUSION

In this study, we have successfully synthesized two metal-free organic dyes (TPD_1 and TPD_2) which consist of donor group and cyano acrylic acid acceptors bridged by an ethylene unit. We discussed the spectroscopic and device-based investigation of efficiently operating solid-state dye-sensitized solar cells using TPDs. Our results prove that more electron-rich donor part leads to better efficiency for solid state dye sensitized solar cell performance and show promising for future.

ACKNOWLEDGEMENTS

We acknowledge the Project support funds to Scientific Research Council of Turkey (TUBITAK) and to European Science Foundation (ESF). I thank Mechanical Engineer M.Sc. Cagatay Ela for proofreading and his support.

REFERENCES

- (1) B. O'Regan, M. Grätzel, *Nature* **1991**, *353*, 737-740.
- (2) J. Hagen, W. Schaffrath, P. Otschik, R. Fink, A. Bacher, H.-W. Schmidt, D. Haarer, *Synth. Met.* **1997**, *89*, 215-220.
- (3) M. K. Nazeeruddin, A. Kay, I. Rodicio, R. Humphry-Baker, E. Mueller, P. Liska, N. Vlachopoulos, M. Grätzel, *J. Am. Chem. Soc.* **1993**, *115*, 6382-6390.
- (4) M. Thelakkat, J. Hagen, D. Haarer, H.-W. Schmidt, *Synth. Met.* **1999**, *102*, 1125-1128.
- (5) J.-H. Yum, P. Chen, M. Grätzel, M. K. Nazeeruddin, *ChemSusChem* **2008**, *1*, 699-707.
- (6) M. Grätzel, **2001**, *414*, 338-344.
- (7) M. Grätzel, *J. Photochem. Photobiol., A* **2004**, *164*, 3-14.
- (8) S. Handa, H. Wietasch, M. Thelakkat, J. R. Durrant, S. A. Haque, *Chem. Commun.* **2007**, 1725-1727.
- (9) U. Bach, D. Lupo, P. Comte, J. E. Moser, F. Weissortel, J. Salbeck, H. Spreitzer, M. Grätzel, *Nature* **1998**, *395*, 583-585.
- (10) A. Hagfeldt, M. Grätzel, *Acc. Chem. Res.* **2000**, *33*, 269-277.
- (11) C. S. Karthikeyan, K. Peter, H. Wietasch, M. Thelakkat, *Sol. Energy Mater.* **2007**, *91*, 432-439.
- (12) T. Kitamura, M. Ikeda, K. Shigaki, T. Inoue, N. A. Anderson, X. Ai, T. Lian, S. Yanagida, *Chem. Mater.* **2004**, *16*, 1806-1812.
- (13) M. Velusamy, K. R. Justin Thomas, J. T. Lin, Y.-C. Hsu, K.-C. Ho, *Org. Lett.* **2005**, *7*, 1899-1902.
- (14) D. P. Hagberg, T. Edvinsson, T. Marinado, G. Boschloo, A. Hagfeldt, L. Sun, *Chem. Commun.* **2006**, 2245-2247.
- (15) R. Chen, X. Yang, H. Tian, L. Sun, *J. Photochem. Photobiol., A* **2007**, *189*, 295-300.
- (16) S.-L. Li, K.-J. Jiang, K.-F. Shao, L.-M. Yang, *Chem. Commun.* **2006**, 2792-2794.
- (17) R. Chen, X. Yang, H. Tian, X. Wang, A. Hagfeldt, L. Sun, *Chem. Mater.* **2007**, *19*, 4007-4015.
- (18) J. Tang, W. Wu, J. Hua, J. Li, X. Li, H. Tian, *Energy Environ. Sci.* **2009**, *2*, 982-990.
- (19) S. Wenger, P.-A. Bouit, Q. Chen, J. Teuscher, D. D. Censo, R. Humphry-Baker, J.-E. Moser, J. L. Delgado, N. Martín, S. M. Zakeeruddin, M. Grätzel, *J. Am. Chem. Soc.* **2010**, *132*, 5164-5169.
- (20) P.-A. Bouit, C. Villegas, J. L. Delgado, P. M. Viruela, R. Pou-Amérigo, E. Ortí, N. Martín, *Org. Lett.* **2011**, *13*, 604-607.

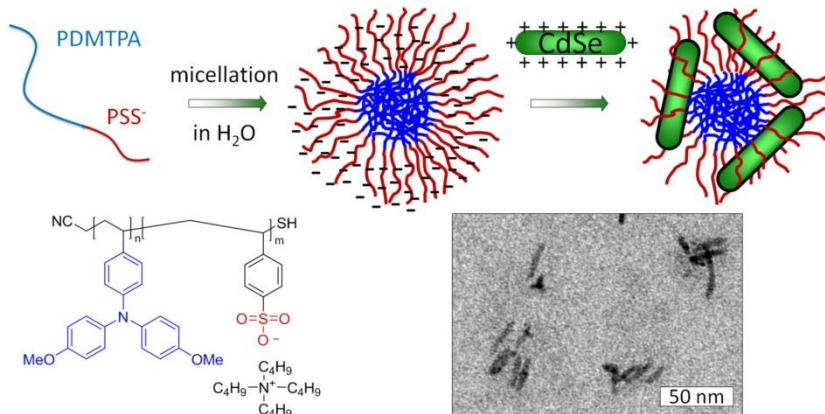
- (21) A. Hagfeldt, G. Boschloo, L. Sun, L. Kloo, H. Pettersson, *Chem. Rev.* **2010**, *110*, 6595-6663.
- (22) S. Kolemen, O. A. Bozdemir, Y. Cakmak, G. Barin, S. Erten-Ela, M. Marszalek, J.-H. Yum, S. M. Zakeeruddin, M. K. Nazeeruddin, M. Gratzel, E. U. Akkaya, *Chem. Sci.* **2011**, *2*, 949-954.
- (23) S. Kolemen, Y. Cakmak, S. Erten-Ela, Y. Altay, J. Brendel, M. Thelakkat, E. U. Akkaya, *Org. Lett.* **2010**, *12*, 3812-3815.
- (24) S. Erten-Ela, S. Cogal, G. Turkmen, S. Icli, *Current Applied Physics* **2010**, *10*, 187-192.
- (25) S. Erten-Ela, G. Turkmen, *Renewable Energy* **2011**, *36*, 1821-1825.
- (26) J. Pommerehne, H. Vestweber, W. Guss, R. F. Mahrt, H. Bässler, M. Porsch, J. Daub, *Adv. Mater.* **1995**, *7*, 551-554.
- (27) Q. Sun, H. Wang, C. Yang, Y. Li, *J. Mater. Chem.* **2003**, *13*, 800-806.

5. SEMICONDUCTOR AMPHIPHILIC BLOCK COPOLYMERS FOR HYBRID DONOR-ACCEPTOR NANOCOMPOSITES

Johannes C. Brendel, Hubertus Burchardt and Mukundan Thelakkat*

Macromolecular Chemistry I, Applied Functional Polymers, University of Bayreuth, 95440
Bayreuth, Germany

*E-mail of corresponding author: mukundan.thelakkat@uni-bayreuth.de



Published in *Journal of Materials Chemistry* **2012**, *22*, 24386-24393.

ABSTRACT

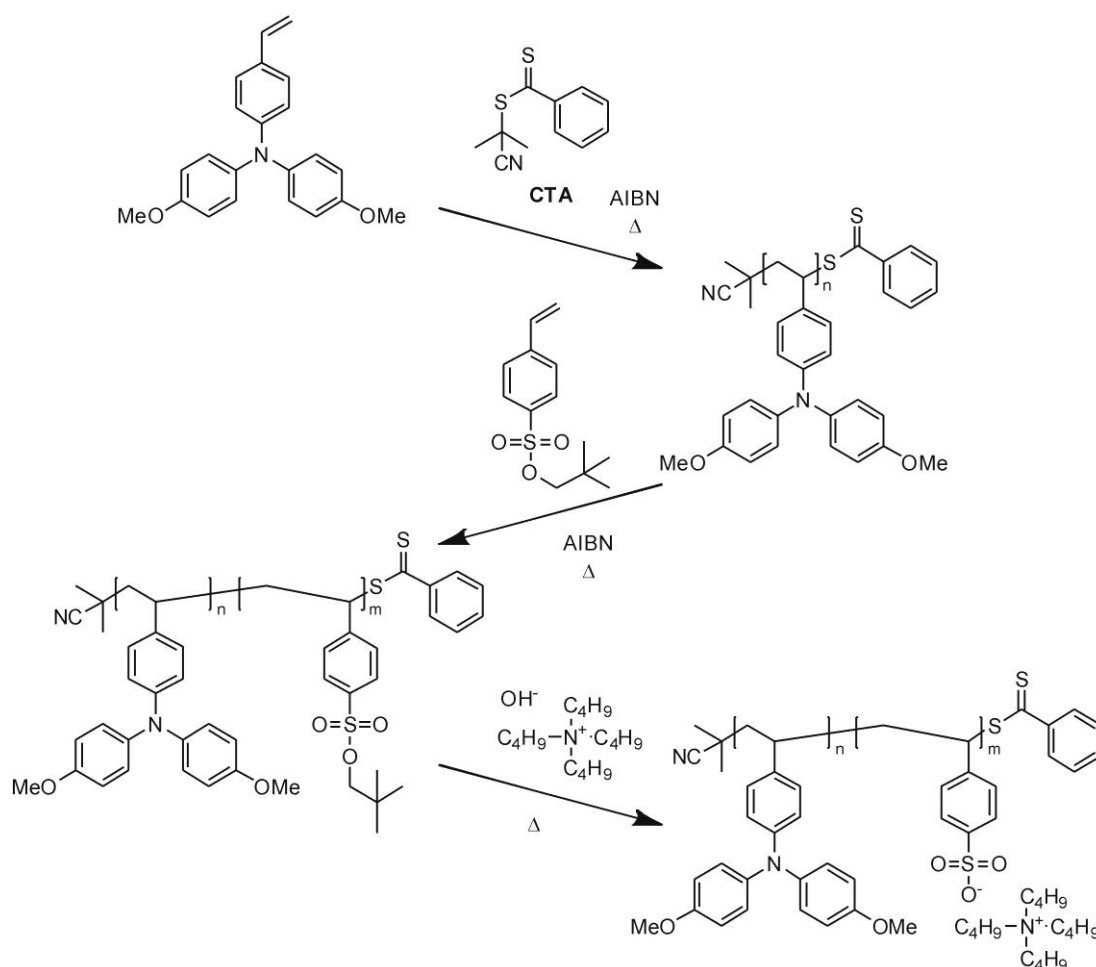
Block copolymers feature unique properties for organizing in well-defined pattern on length scales of several tenths of nanometers. This special attribute enables the formation of ideal donor and acceptor domains for photovoltaic devices in the size of the exciton diffusion length. Thus we designed an amphiphilic block copolymer, able to act as hole conductor and to coordinate inorganic semiconductor nanoparticles as electron acceptors. Utilizing controlled radical polymerization techniques, defined polymers were synthesized consisting of triphenylamine pendant groups in the hole conductor block and a hydrophilic polystyrene sulfonate block. This particular combination creates narrow distributed micelles in aqueous solution exhibiting domain sizes suitable for photovoltaic applications. The strong anionic sulfonate groups offer high loading capacities for modified cationic nanoparticles. To guarantee a broad absorption and good conductivity, we synthesized cationic CdSe nanorods and combined them with our hole conductor micelles. The advantage of high loading combined with the processability from aqueous dispersions promises a novel “green” alternative for preparation of hybrid solar cells with controlled domain sizes in the desired length scale.

INTRODUCTION

Considering the last decades of research a countless number of publications were presented on block copolymers (BCP), due to their unique morphologies with nanoscale domain sizes and highly ordered structures in bulk and solution.^{1,2} The self-assembly process of these materials is considered to be ideal for “Bottom-up” approaches towards patterned functional thin films.^{3,4} Referring to photovoltaic devices these unique properties perfectly match the desired interface distance in the range of the exciton diffusion length.^{5,6} However, the synthesis of functional BCPs for highly efficient solar cells remains challenging. So far only few reports could prove the advantages of BCPs on solar cells, including the stability of the equilibrated morphology and improved device efficiency. Hashimoto and co-workers synthesized stiff conjugated block copolymers of poly(3-hexylthiophene) (P3HT) and fullerenes attached to the side chains of a second polythiophene block.⁷ As a result the stability of the devices was preserved under long term annealing tests due to the equilibrated morphology. In contrast blends of materials are trapped in a non-equilibrium state and on a long time-scale the morphology reaches an undesirable macrophase separated equilibrium state. We and others have earlier shown the advantages of donor-acceptor BCPs, using perylene as electron acceptor.^{8,9} Here, the copolymer exhibited superior device efficiencies compared to the corresponding blend.^{8,10} However, the number of soluble, stable and efficient organic electron acceptors is limited. Promising alternatives are n-type inorganic semiconductor nanoparticles, due to their high stability and electron transport mobilities.¹¹ Combinations of inorganic semiconductors in various shape and form are well studied in blend devices with donor polymers.¹² However due to the strong tendency to aggregate high contents of nanoparticles are necessary to guarantee good charge percolation pathways.¹³ While blend devices of homopolymers and nanoparticles suffer from the lack of control of morphology and interface, BCPs featuring coordinative groups are able to organize the particles in microphase domains.¹⁴ Here the amount of particles required can be much less than in usual blends due to advantages of confinement.¹⁵ This is the attractiveness of self-assembled systems compared to usual blends. Despite the various detailed studies on self-

assembled hybrid materials,¹⁶⁻²¹ to our knowledge only few reports combine functional hole conductor BCPs with inorganic semiconductors suitable for solar cell applications. Lechman *et al.* prepared hybrid devices utilizing the amphiphilic polymer poly(ethylene oxide)-*b*-polytriphenylamine (PEO-*b*-PTPA), whereat titanium dioxide was hydrolyzed in the PEO-block using sol-gel chemistry precursors.²² Secondly, hybrid structures could be generated with poly(vinyl-*N,N'*-bis(4-methoxyphenyl)-*N,N'*-diphenyl-(1,1'-biphenyl)-4,4'-diamine)-blockpoly(4-vinylpyridine) (PDMPD-*block*-P4VP). CdSe nanoparticles could be selectively incorporated into the P4VP phase of the lamellar morphology.²³ Motivated by the requirement of novel materials on this promising field, we synthesized the new amphiphilic BCP poly(bis(4-methoxyphenyl)-4'-vinylphenylamine)-*block*-poly(tetrabutylammonium styrene sulfonate) (PDMTPA-*b*-PBu₄N⁺) (Scheme 5–1).

Scheme 5–1. Synthesis of poly(4,4'-dimethoxytriphenylamine)-*block*-poly(tetrabutylammonium styrene sulfonate) (PDMTPA-*b*-PBu₄N⁺SS) using 2-cyan-2-propylbenzodithioat as chain transfer agent (CTA)



PDMTPA is an amorphous hole conductor polymer well-studied in our group before.²⁴ Hole mobilities up to $5 \times 10^{-5} \text{ cm}^2/\text{Vs}$ were found.²⁵ As hydrophilic block we chose PBu₄N⁺, due to its sufficient solubility and the high charge density even at low pH. As previously reported, the sulfonate groups feature the catalytic crystallization of TiO₂ at room temperature.^{26,27} Furthermore, the strong coulomb interactions of the polyelectrolyte enable high loading capacities with oppositional charged nanoparticles, while maintaining a high solubility.²⁸ The close arrangement of the nanoparticles is crucial for the percolation of charges and conductivity.

The desired block copolymer was synthesized by reversible addition fragmentation chain transfer polymerization (RAFT). Therefore, we first needed to optimize the polymerization conditions in order to get well-defined molecular weights and low polydispersities.²³ The sulfonated block was prepared *via* polymerization of the protected monomer, neopentyl styrene sulfonate (NeoSS). This allows the use of common high boiling solvents such as anisole or toluene and the neopentyl group can be easily removed afterwards.^{29,30} The resulting amphiphilic polymer was studied for its morphology in aqueous solution by dynamic light scattering (DLS) and transmission electron microscopy (TEM). We combined these micelles with highly crystalline CdSe nanorods to ensure the absorption of visible light and good electron transport. The particles can be modified with aminoethanethiol hydrochlorid to get a high positive surface charge gaining the solubility in water.³¹ Due to the strong attraction to the negative charged PBU₄N⁺-block, mixing of both components results in a stable colloidal solution of donor and acceptor materials in water.

RESULTS AND DISCUSSION

During the last decade RAFT polymerization has become an important technique among the controlled radical polymerizations for macromolecule design.³²⁻³⁴ But actually there are only a few reports on the polymerization of functional semiconductor monomers.³⁵ Due to the large size of these monomers compared to simple styrene or acrylate monomers and the sensitivity against radical oxidation, particular attention has to be paid on the polymerization conditions. Crucial for well-defined block copolymers by RAFT is the order of monomer addition.³⁶ Especially triphenylamine monomers (TPA) are able to stabilize the propagating radical altering the reactivity of the active chain end. In consequence we first prepared the individual homopolymers PDMPA and poly(neopentyl styrene sulfonate) (PNeoSS) and verify their ability to initiate the respective counterpart. Both polymerizations were carried out using 2-cyan-2-propylbenzodithioat as chain transfer agent (CTA) and under 80°C in anisole, which is a suitable high boiling solvent for both monomers. Both the resulting homopolymers showed narrow molecular weight distributions (Figure 5–1), which implies good control on the RAFT polymerization of the monomers.

Then, we studied the sequential polymerization of DMTPA using the macro-CTA PNeoSS under similar conditions. The GPC trace of sample PNeoSS-*b*-PDMPA displays no significant shift of the main peak in comparison to the macro-CTA (Figure 5–2). Furthermore a broad underlying peak was formed characteristic for a free radical polymerization. This indicates that PNeoSS was not able to initiate the DMTPA and a broadly distributed homopolymer was formed beside the macro-CTA. Changing the synthesis condition such as variation of temperature and concentration unfortunately had no influence on this process (Figure 5–S1 in supplementary information).

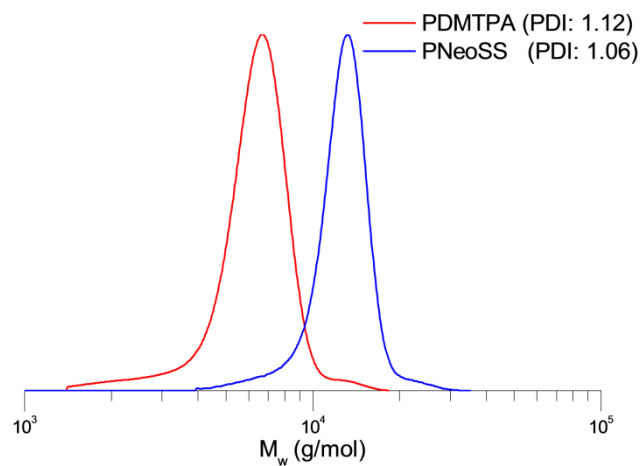


Figure 5–1. GPC-Plots of the homopolymers poly(bis(4-methoxyphenyl)-4'-vinylphenylamine) (PDMTPA, red) and poly(neopentyl styrene sulfonate) (PNeoSS, blue), eluent: THF, calibration with polystyrene.

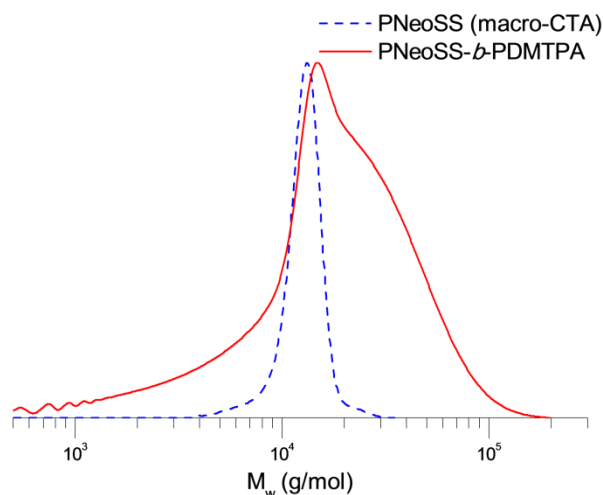


Figure 5–2. Comparison of GPC plots of the initiating macro-CTA PNeoSS (dashed line) and the resulting block copolymer PNeoSS-*b*-PDMTPA (continuous line).

Alternatively we started the polymerization of NeoSS as second monomer from PDMTPA as macro CTA. Here the GPC traces clearly indicated in the formation of a block copolymer. However, a second peak was observed at original elution volume of PDMTPA (Figure 5–3).

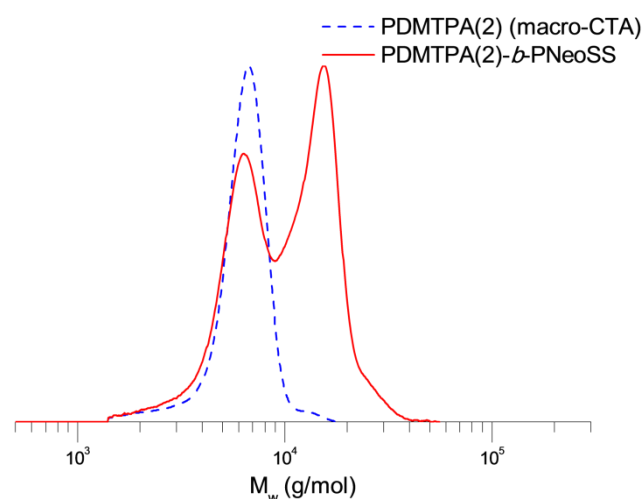


Figure 5–3. Comparison of GPC plots of the initiating macro-CTA PDMTPA (dashed line) and the resulting block copolymer PDMTPA-*b*-PNeoSS (continuous line).

This suggests that a considerable part of the macro-CTA remained unreactive. Keeping a retarded initiation in mind, one could expect a statistical distribution covering the macro-CTA and the associated BCPs, resulting in one broad peak. But the fact that a bimodal distribution indicates that the main part of the PDMTPA homopolymer was able to initiate the controlled polymerization of NeoSS, while a second part remained without addition of further monomer units. In consequence, the functional chain transfer end group of the PDMTPA must be partially disabled or lost. As no intermediate steps of purification are involved in the macro-CTA synthesis, this process must already occur during the polymerization of DMTPA. For verification we altered the conditions of the macro-CTA synthesis and consequently tested the macro-initiator efficiency of the macro-CTAs prepared in different solvents and under different temperatures keeping the concentration and ratio of components the same. Thus, the temperature was varied from 60 to 100°C and secondly the polarity of the media was changed. A summary of these reactions and the corresponding polymer characteristics are given in Table 5–1.

Table 5–1. Synthesis conditions and characterization for the macro-CTAs and the respective block copolymers.

	ratio monomer/CTA/AIBN	T	solvent	M_n (kg/mol) ^a	M_{p1} (kg/mol) ^{a, b}	M_{p2} (kg/mol) ^{a, b}	PDI
macro-CTA							
PDMTPA(1)	50 / 1 / 0.2	60°C	Anisole	3.21	3.66	-	1.09
PDMTPA(2)	50 / 1 / 0.2	80°C	Anisole	5.80	6.64	-	1.12
PDMTPA(3)	50 / 1 / 0.2	100°C	Anisole	4.97	5.73	-	1.11
PDMTPA(4)	50 / 1 / 0.2	60°C	Benzene	4.52	4.94	-	1.07
BCP							
PDMTPA(1)- <i>b</i> -PNeoSS	100 / 1 / 0.4	80°C	Anisole	4.78	4.06	8.55	1.30
PDMTPA(2)- <i>b</i> -PNeoSS	100 / 1 / 0.4	80°C	Anisole	8.67	6.31	15.23	1.28
PDMTPA(3)- <i>b</i> -PNeoSS	100 / 1 / 0.4	80°C	Anisole	8.77	5.73	15.47	1.34
PDMTPA(4)- <i>b</i> -PNeoSS	100 / 1 / 0.4	80°C	Anisole	11.55	5.00	18.95	1.37

^a GPC was calibrated with polystyrene as standard.

^b M_p was defined as molecular weight of single peaks.

The reduced reaction temperature (60°C) in anisole of the macro-CTA **PDMPA(1)** reduced the polymerization rate, so that only a conversion of 44% was reached after 22 h. All other samples were stopped at higher conversions of 55-60%, yielding similar molecular weights and narrow distributions. Those macro-CTAs were then employed in the polymerization of NeoSS under conditions summarized in Table 5–1. The GPC plots of the resulting BCPs and the respective macro-CTAs are shown in Figure 5–4.

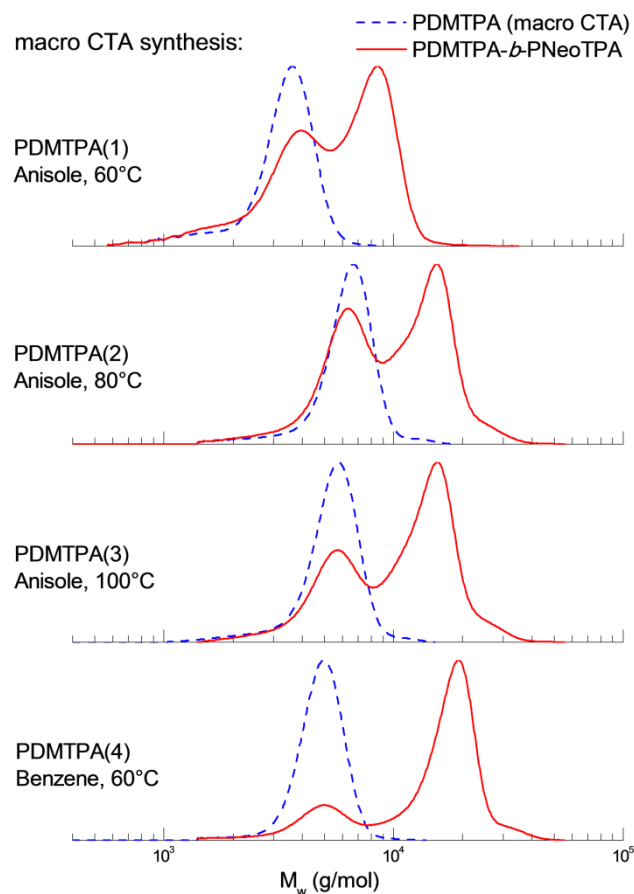


Figure 5–4. GPC-Traces of the samples **PDMPA(1)-b-PNeoSS**, **PDMPA(2)-b-PNeoSS**, **PDMPA(3)-b-PNeoSS** and **PDMPA(4)-b-PNeoSS** (solid lines) and the respective macro CTAs (dashed lines). The variations in synthesis of the macro CTA are shown on the left, while the BCP was formed under equal conditions (experimental section).

By rising the temperature for the macro-CTA synthesis from 60°C to 80°C the amount of unreactive **PDMPA** increased slightly. Considerable improvements were observed at high temperatures of 100°C, but still a substantial part of the macro-CTA remained unreactive in polymerization using macro-CTA **PDMPA(3)**. The best result was obtained with macro-CTA **PDMPA(4)** by changing the solvent from anisole to benzene and thus reducing the polarity of the surrounding medium. Despite a small part of unreacted homopolymer was still visible, a low polydispersity index (PDI) of 1.37 was reached for the as-synthesized BCP. The final polymer **PDMPA(4)-b-PNeoSS** was purified by preparative GPC to remove the last traces of the homopolymer. The GPC trace of the final polymer is shown in Figure 5–5. These results obviously prove the influence of the initial macro-CTA synthesis on the final initiator efficiency.

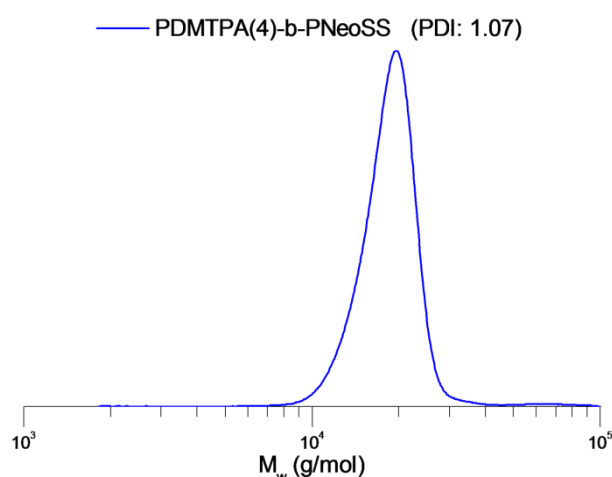


Figure 5–5. GPC-Trace of the purified sample PDMTPA(4)-b-PNeoSS.

Further evidence for a loss of the chain transfer agent was attained by matrix-assisted laser desorption/ionization time-of-flight (MALDI-TOF) measurements, which provides detailed information on the end-group distribution. For comparison the measurements of macro-CTAs PDMTPA(2) and PDMTPA(4) are plotted in Figure 5–6.

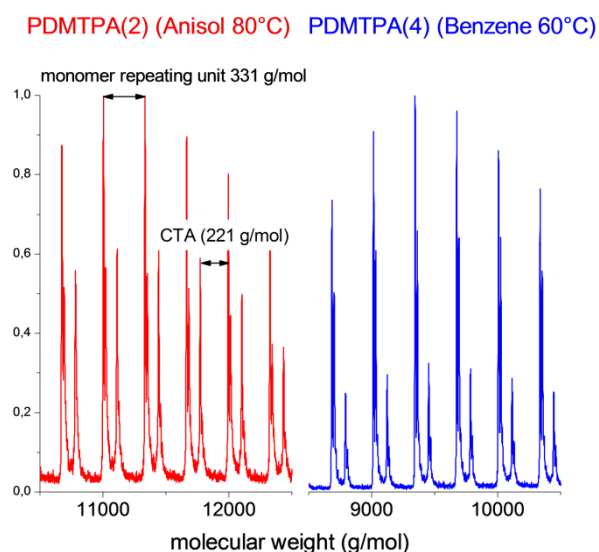


Figure 5–6. Matrix-assisted laser desorption/ionization time-of-flight measurement of macro-CTA PDMTPA(2) and PDMTPA(4). The major peak series corresponds to macro CTA and the minor one to homopolymer with dead chain ends.

The full MALDI spectra of all samples are given in the supporting information (Figure 5–S2 - Figure 5–S5 in supporting information). The second peak series clearly indicate a change in the polymer end groups. The difference of 221 g/mol correlates well with the loss of the chain transfer agent 2-cyan-2-propylbenzodithioat. Furthermore comparing the intensities of the second peak the ratio of active species to dead chain end moieties decreases from macro-CTA

PDMTPA(2) to **PDMTPA(4)**. This is in good agreement with the GPC traces of the block copolymers, where the part of unreactive homopolymer decreases, too.

The lost CTA is possibly caused by the formation of additional free radicals, which terminate the active polymer. As the polymer distribution remains narrow, this process seems to be suppressed at the beginning of the polymerization, but increases drastically with higher conversion. For styrene monomers self-initiation and radical formation is already well studied and we assumed a similar process for this system.^{2,37} Therefore the polymerization was examined under similar conditions, without using any AIBN initiator. GPC traces at different reaction times evidently present the formation of oligomers first and higher molecular weight polymers after 23 h (Figure 5–S6 in supporting information). In comparison to the self-initiation radical polymerization of styrene, here first a cycloaddition step is involved.³⁷ The electron donating effect of the nitrogen in the triphenylamine monomer and the increased number of active phenyl rings enhance this effect. Free hydrogen radicals are created in this reaction to retain the aromaticity in the resulting molecule after the cycloaddition, which may start or quench a radical polymerization. However, for a detailed mechanism further studies have to be accomplished on this phenomenon, which are not part of this research. But the presented results certainly depict the importance of detailed kinetic studies in optimization of synthesis of functional block copolymers.

With a well-defined polymer in hand, we consequently studied the assembly and coordination properties of PDMTPA-*b*-PSS. After deprotection of the sulfonate groups, the BCP showed a distinct amphiphilic character. The complete deprotection was confirmed by NMR analysis (Figure 5–S7 in supporting information). Thus the polymer showed micelle formation in aqueous solutions. These assembly structures were characterized by dynamic light scattering (DLS) to obtain the hydrodynamic radius R_h . For consistent values we measured the decay rate Γ , calculated from the autocorrelation function (1. order of cumulant fit), for multiple angles θ and plotted it against q^2 with $q = 4\pi n/\lambda \cdot \sin(\theta/2)$ (n : refractive index; λ : wavelength of laser). The respective linear slope of the plot is correlated to the diffusion coefficient D by $\Gamma = Dq^2$. With D the hydrodynamic radius R_h can be calculated to $R_h = (k_B T)/(6\pi\eta D)$ (k_B : Boltzmann constant; T : temperature; η : viscosity of the medium).

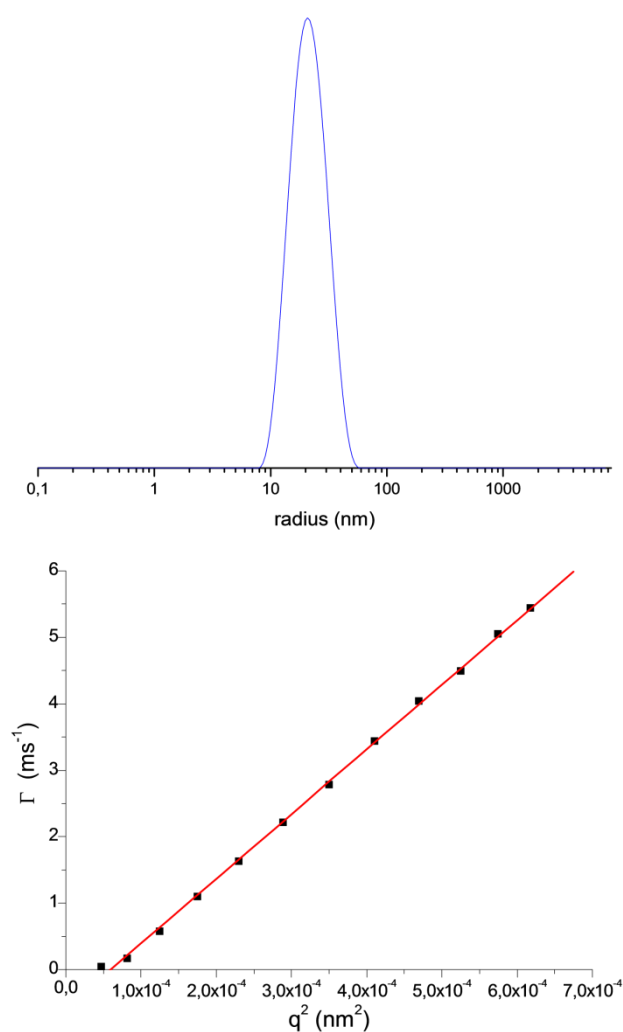


Figure 5–7. Plot of Γ against q^2 for various measured angles (top) and a representative distribution of micelles for an angle of 120° (bottom).

The plot in Figure 5–7 clearly displays a linear relation between Γ and q^2 . From the slope a hydrodynamic radius R_h of $22 \text{ nm} \pm 0.23 \text{ nm}$ was determined. While this value reflects the size of the micelles in solution, including the hydrated polyelectrolyte shell, adjacent transmission electron micrographs (TEM) of the dried micelles stained with Ruthenium tetroxide reveal a core diameter of approximately 16 nm (Figure 5–8).

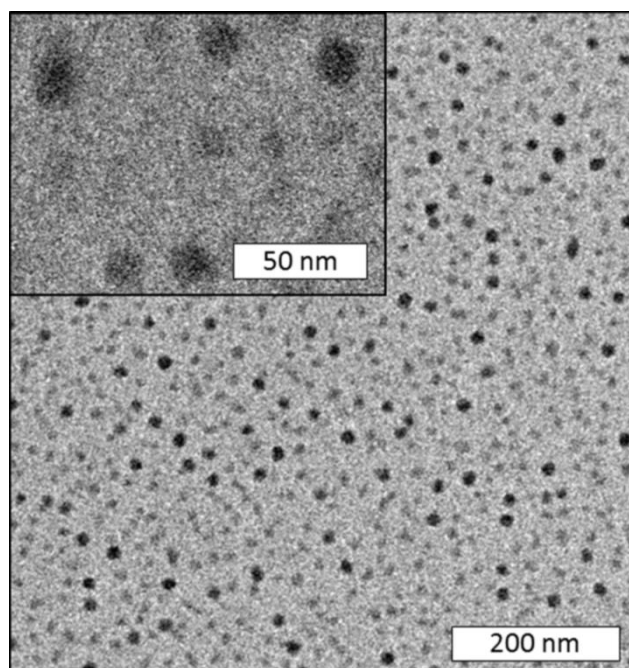


Figure 5–8. Transmission electron micrographs of the dried micelles stained with Ruthenium tetroxide.

The respective individual sizes of the core and the shell (~ 14 nm) is in good agreement with theoretical values for a coiled solid PDMPA-block and a highly stretched $\text{PBu}_4\text{N}^+\text{SS}$ -block, which is characteristic for strong polyelectrolytes in deionised water.³⁸ Aqueous dispersions of those micelles are stable and showed no precipitation, even after storage under ambient conditions for several months.

We have studied earlier the coordination capabilities of PSS containing spherical polyelectrolyte brushes.^{26,28} Building upon this experience, we studied the coordination abilities of the PDMPA-*b*- PBu_4N^+ micelles. In contrast to the spherical colloidal particles, no time-consuming solvent exchange is necessary, as the micelles can be freeze dried and well dispersed in various suitable polar solvents. Non-toxic solvents such as water or alcohols are highly preferred in technological applications. Therefore, we focused on a system using water soluble semiconductor nanoparticles.³⁹ Furthermore, to guarantee an efficient absorption of the visible light, the particles need to have good absorption coefficients in this range. CdSe nanoparticles fulfil these requirements and they are well studied in solar cells.^{11,12} A general scheme of this colloidal assembly route is shown in Figure 5–9.

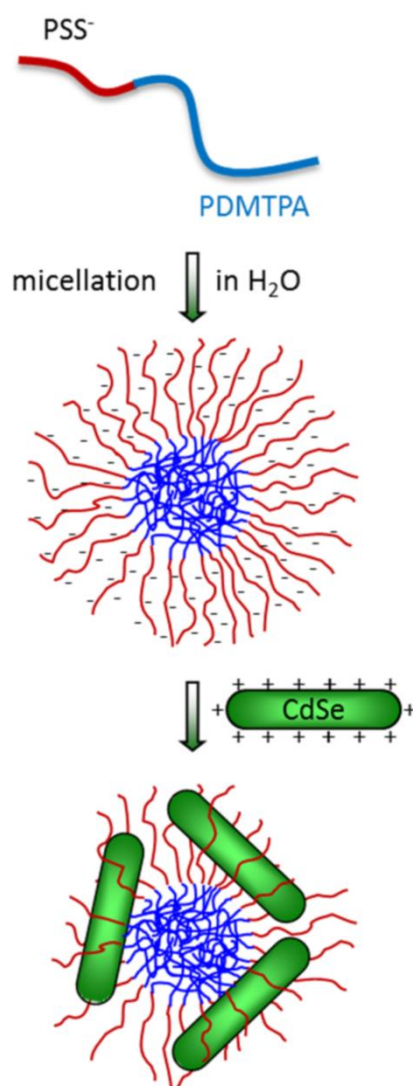


Figure 5–9. General preparation scheme of hybrid colloidal composites.

Recently Zentel *et al.* presented a comparable BCP in combination with CdSe quantum dots for application in light emitting devices.⁴⁰ A similar colloidal arrangement was shown by Winnik *et al.* using commercial block copolymers.⁴¹ The synthesis of CdSe nanoparticles in various shape and high crystallinity is well controlled using various phosphonic acid ligands.^{42,43} To enable the solubility in water we exchanged this ligand with the hydrophilic 2-aminoethanethiol (AET) according to Krauss *et al.*³¹ The resulting nanoparticles exhibit a good solubility in water and good absorption up to 630 nm (Figure 5–10). According to literature the HOMO and LUMO levels of PDMTA are at 5.0 eV and 1.8 eV respectively.⁶ CdSe nanoparticles of similar shape typically have a conduction band edge at 6.2 eV and a valence band edge at 4.4 eV.⁴⁴ Thus this system fulfil the requirements for charge transfer. Transmission electron micrographs show uniformly distributed CdSe nanoparticles with an average diameter of 5 nm and length of 21 nm (Figure 5–S8 in supporting information).

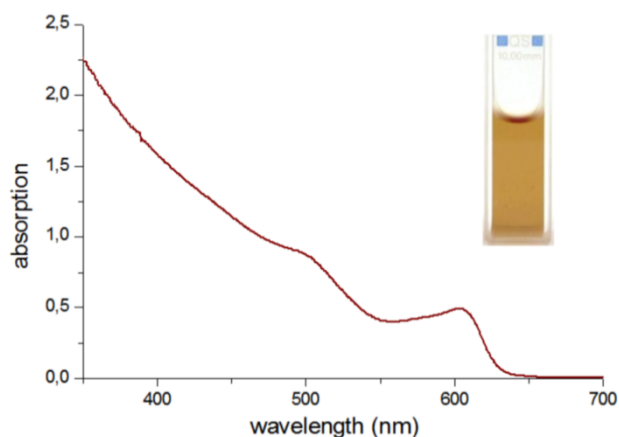


Figure 5–10. Absorption of the prepared CdSe nanoparticles with 2-aminoethanethiol ligand in water (0.5 mg/ml).

The positively charged AET ligands not only convey the water solubility, but also yield a strong coulombic interaction between the nanoparticles and the negatively charged sulfonate groups. By mixing both solutions the nanocrystals immediately attach to the negative charged micelles. The strong driving force is attributed to the enthalpy benefit from the release of multiple counterions by exchanging with a single particle. These strong interactions enable a high loading capacity in comparison to uncharged polymers like polyvinylpyridine, while maintaining the stability of the dispersions.²⁸ Composites of the CdSe nanoparticles and the PDMTPA-*b*-PBu₄N⁺ micelles are shown in the transmission electron micrographs in Figure 5–11. The weight ratio of nanoparticles against polymer was as high as 1 : 1.

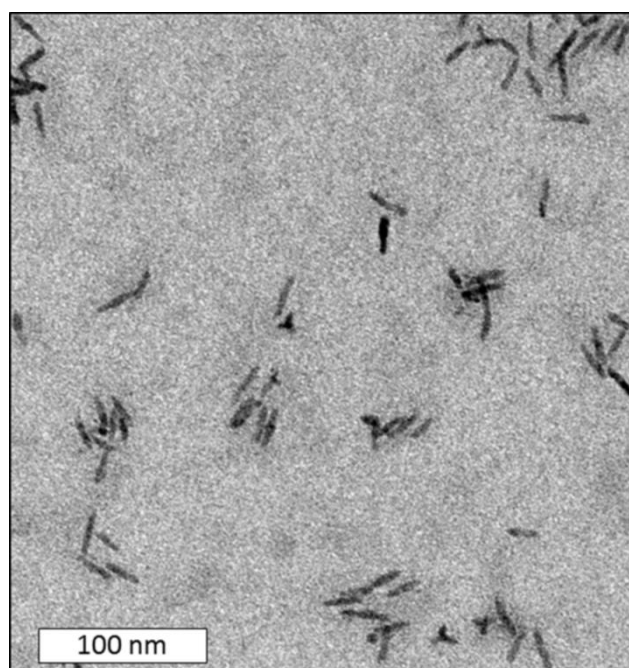


Figure 5–11. Transmission electron micrographs of the CdSe nanorods attached to the block copolymer micelles.

Only few single nanoparticles are obviously seen in the images, which confirm the strong interaction. The high loading facilitates a better packing of the nanoparticles, which is crucial for high charge carrier mobility.¹⁵ A major advantage of this separate synthesis of polymer and inorganic semiconductor is the variability of the nanoparticle synthesis. In literature the preparation of several highly crystalline nanoparticles is well-known and they all can be combined with these micelle structures by electrostatic interaction.⁴⁵

Finally the resulting donor-acceptor (D-A) micelles can be used to prepare devices with microstructures on the length scale of the exciton diffusion length. A general scheme of this concept with spherical nanoparticles is shown in Figure 5–12. The nanocomposite micelles can be assembled on to a conducting substrate and dried to get a smooth film, which can be annealed or pressed above T_g to get bicontinuous domains. The amorphous PDMPA softens and forms a continuous phase. Simultaneously the particles aggregate to create the required percolation once the concentration increases on drying and annealing as shown in Figure 5–12. In such a system charge transfer and transport required for a solar cell are feasible.

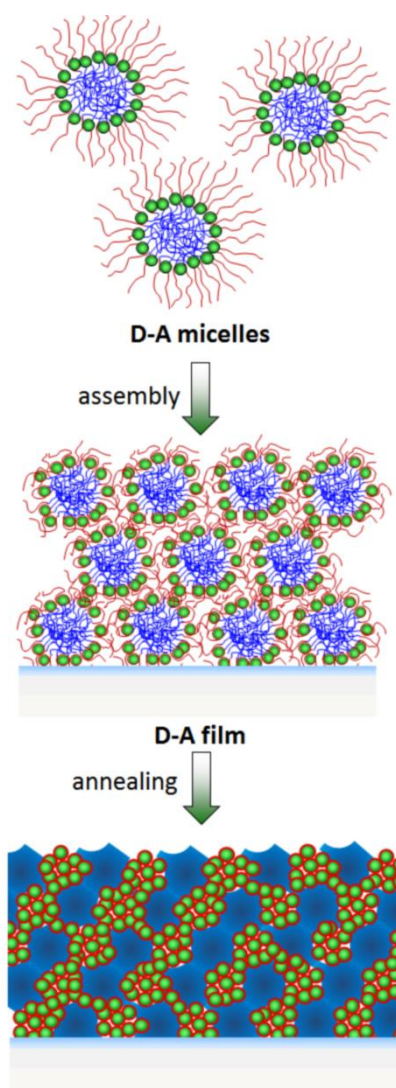


Figure 5–12. General scheme for the preparation of a donor-acceptor (D-A) microstructure from hybrid colloidal nanocomposites.

CONCLUSION

The ability of block copolymers to create domains in the nanometer scale reveals them to be ideal for structured organic or hybrid solar cells. Here we developed an innovative colloidal organization of inorganic semiconductors and semiconductor amphiphilic block copolymers. The polymer consists of a wellknown hole conductor block and a water soluble styrene sulfonate block, able to coordinate nanoparticles by electrostatic interaction. We optimized the synthesis conditions to accomplish narrow distributions and create well-defined micelle dispersions. Crucial in this context are the order of monomer addition and the reactivity of the triphenylamine monomer. The latter resulted in the loss of the chain transfer agent during the homopolymerization. This caused bimodal distributions during the block copolymer formation. By altering the temperature and solvent polarity the side reaction could be minimized and thus the ratio of unreactive homopolymer reduced. After hydrolysis of the sulfonate protection groups the block copolymer formed uniform and stable micelles in aqueous solutions. The highly charged sulfonate groups are strong coordinating groups especially for electrostatic interaction with charged nanoparticles. Ideal semiconductors for this approach are CdSe nanorods. They combine both good absorption in the visible spectrum of light and high electron mobility. By exchanging the typical phosphine ligands with a positive charged aminoethanethiol the particles can be attached to our hole conductor micelles. In consequence we created semiconductor colloids including both a donor material and an acceptor. The domain sizes are defined by the micelle core and the nanoparticle size, which can be adjusted in individual reactions. As the system is based on an aqueous dispersion no hazardous solvents are necessary for processing enabling large scale industrial fabrication. The strong electrostatic interaction of the sulfonate polymer allows high loading capacities while maintaining the good solubility. In combination with other polymerization techniques all kind of functional polymers such as polythiophenes or low band-gap polymers can be integrated into this environmentally benign processing of devices from water. Furthermore various inorganic semiconductors such as TiO_2 or CuInS_2 are interesting alternatives which can easily be incorporated. In conclusion this approach opens a promising pathway towards defined donor-acceptor hybrid systems using semiconductor amphiphilic block copolymers.

ACKNOWLEDGEMENT

Financial support from SFB 840 and Bayerische Eliteförderung are kindly acknowledged. Furthermore we thank Melanie Förtsch and Katharina Neumann for the TEM and MALDI measurements respectively.

REFERENCES

- (1) S. Förster, M. Antonietti, *Adv. Mater.* **1998**, *10*, 195-217.
- (2) P. J. Flory, *J. Am. Chem. Soc.* **1937**, *59*, 241-253.
- (3) J. Weickert, R. B. Dunbar, H. C. Hesse, W. Wiedemann, L. Schmidt-Mende, *Adv. Mater.* **2011**, *23*, 1810-1828.
- (4) J. Y. Cheng, C. A. Ross, H. I. Smith, E. L. Thomas, *Adv. Mater.* **2006**, *18*, 2505-2521.
- (5) P. D. Topham, A. J. Parnell, R. C. Hiorns, *J. Polym. Sci. B Polym. Phys.* **2011**, *49*, 1131-1156.
- (6) M. Sommer, S. Hüttner, M. Thelakkat, *J. Mater. Chem.* **2010**, *20*, 10788-10797.
- (7) S. Miyanishi, Y. Zhang, K. Tajima, K. Hashimoto, *Chem. Commun.* **2010**, *46*, 6723-6725.
- (8) M. Sommer, A. S. Lang, M. Thelakkat, *Angew. Chem., Int. Ed.* **2008**, *47*, 7901-7904.
- (9) Q. Zhang, A. Cirpan, T. P. Russell, T. Emrick, *Macromolecules* **2009**, *42*, 1079-1082.
- (10) M. Sommer, S. M. Lindner, M. Thelakkat, *Adv. Funct. Mater.* **2007**, *17*, 1493-1500.
- (11) M. Skompska, *Synth. Met.* **2010**, *160*, 1-15.
- (12) W. U. Huynh, J. J. Dittmer, A. P. Alivisatos, *Science* **2002**, *295*, 2425-2427.
- (13) K. F. Jeltsch, M. Schädel, J.-B. Bonekamp, P. Niyamakom, F. Rauscher, H. W. A. Lademann, I. Dumsch, S. Allard, U. Scherf, K. Meerholz, *Adv. Funct. Mater.* **2012**, *22*, 397-404.
- (14) Y. Lin, A. Boker, J. He, K. Sill, H. Xiang, C. Abetz, X. Li, J. Wang, T. Emrick, S. Long, Q. Wang, A. Balazs, T. P. Russell, *Nature* **2005**, *434*, 55-59.
- (15) C.-P. Li, K.-H. Wei, J. Y. Huang, *Angew. Chem., Int. Ed.* **2006**, *45*, 1449-1453.
- (16) A. C. Balazs, T. Emrick, T. P. Russell, *Science* **2006**, *314*, 1107-1110.
- (17) N. Haberkorn, M. C. Lechmann, B. H. Sohn, K. Char, J. S. Gutmann, P. Theato, *Macromol. Rapid Commun.* **2009**, *30*, 1146-1166.
- (18) S.-W. Yeh, K.-H. Wei, Y.-S. Sun, U.-S. Jeng, K. S. Liang, *Macromolecules* **2005**, *38*, 6559-6565.
- (19) A. Haryono, W. H. Binder, *Small* **2006**, *2*, 600-611.
- (20) Y. Lin, V. K. Daga, E. R. Anderson, S. P. Gido, J. J. Watkins, *J. Am. Chem. Soc.* **2011**, *133*, 6513-6516.
- (21) Q. Zhang, S. Gupta, T. Emrick, T. P. Russell, *J. Am. Chem. Soc.* **2006**, *128*, 3898-3899.
- (22) M. C. Lechmann, S. A. L. Weber, J. Geserick, N. Husing, R. Berger, J. S. Gutmann, *J. Mater. Chem.* **2011**, *21*, 7765-7770.
- (23) S. Maria, A. S. Susha, M. Sommer, D. V. Talapin, A. L. Rogach, M. Thelakkat, *Macromolecules* **2008**, *41*, 6081-6088.
- (24) S. Hüttner, M. Sommer, U. Steiner, M. Thelakkat, *Appl. Phys. Lett.* **2010**, *96*, 073503-073503.
- (25) E. M. Barea, G. Garcia-Belmonte, M. Sommer, S. Hüttner, H. J. Bolink, M. Thelakkat, *Thin Solid Films* **2010**, *518*, 3351-3354.
- (26) J. C. Brendel, Y. Lu, M. Thelakkat, *J. Mater. Chem.* **2010**, *20*, 7255-7265.
- (27) Y. Lu, M. Hoffmann, R. S. Yelamanchili, A. Terrenoire, M. Schrinner, M. Drechsler, M. W. Möller, J. Brey, M. Ballauff, *Macromol. Chem. Phys.* **2009**, *210*, 377-386.
- (28) R. S. Yelamanchili, Y. Lu, T. Lunkenbein, N. Miyajima, L.-T. Yan, M. Ballauff, J. Brey, *Small* **2009**, *5*, 1326-1333.
- (29) H. Okamura, Y. Takatori, M. Tsunooka, M. Shirai, *Polymer* **2002**, *43*, 3155-3162.
- (30) S. C. Miller, *J. Org. Chem.* **2010**, *75*, 4632-4635.
- (31) J. M. Haremza, M. A. Hahn, T. D. Krauss, S. Chen, J. Calcines, *Nano Lett.* **2002**, *2*, 1253-1258.
- (32) H. Kakwere, S. Perrier, *Polym. Chem.* **2011**, *2*, 270-288.
- (33) M. Siau, B. S. Hawkett, S. Perrier, *J. Polym. Sci., Part A: Polym. Chem.* **2012**, *50*, 187-198.

- (34) G. Moad, E. Rizzardo, S. H. Thang, *Polymer* **2008**, *49*, 1079-1131.
- (35) G. Moad, M. Chen, M. Haussler, A. Postma, E. Rizzardo, S. H. Thang, *Polym. Chem.* **2011**, *2*, 492-519.
- (36) Y. K. Chong, J. Krstina, T. P. T. Le, G. Moad, A. Postma, E. Rizzardo, S. H. Thang, *Macromolecules* **2003**, *36*, 2256-2272.
- (37) F. R. Mayo, *J. Am. Chem. Soc.* **1968**, *90*, 1289-1295.
- (38) S. Förster, N. Hermsdorf, C. Bottcher, P. Lindner, *Macromolecules* **2002**, *35*, 4096-4105.
- (39) R. Sondergaard, M. Helgesen, M. Jorgensen, F. C. Krebs, *Adv. Energy Mater.* **2011**, *1*, 68-71.
- (40) J. Kwak, W. K. Bae, M. Zorn, H. Woo, H. Yoon, J. Lim, S. W. Kang, S. Weber, H.-J. Butt, R. Zentel, S. Lee, K. Char, C. Lee, *Adv. Mater.* **2009**, *21*, 5022-5026.
- (41) M. Wang, S. Kumar, A. Lee, N. Felorzabihi, L. Shen, F. Zhao, P. Froimowicz, G. D. Scholes, M. A. Winnik, *J. Am. Chem. Soc.* **2008**, *130*, 9481-9491.
- (42) W. Wang, S. Banerjee, S. Jia, M. L. Steigerwald, I. P. Herman, *Chem. Mater.* **2007**, *19*, 2573-2580.
- (43) Z. A. Peng, X. Peng, *J. Am. Chem. Soc.* **2000**, *123*, 183-184.
- (44) S. A. McClure, B. J. Worfolk, D. A. Rider, R. T. Tucker, J. A. M. Fordyce, M. D. Fleischauer, K. D. Harris, M. J. Brett, J. M. Buriak, *ACS Appl. Mater. Interfaces* **2009**, *2*, 219-229.
- (45) M. Kruszynska, H. Borchert, J. Parisi, J. Kolny-Olesiak, *J. Am. Chem. Soc.* **2010**, *132*, 15976-15986.

SUPPORTING INFORMATION**Experimental section***Materials and characterization*

¹H NMR spectra were recorded in chloroform on a Bruker Avance 250 spectrometer at 300 MHz. The spectra were calibrated according to solvent signals. Size exclusion chromatography (SEC) measurements were carried out in THF using a UV detector from Waters and a mixed-C PL-Gel (PL) column. Polystyrene was used as external standard and 1,2-dichlorobenzene as an internal standard for calibration. Matrix-assisted laser desorption ionization spectroscopy with time-of-flight detection mass spectroscopy (MALDI-TOF MS) measurements were performed on a Bruker Reflex I using *trans*-2-[3-(4-*tert*-Butylphenyl)-2-methyl-2-propenylidene]malononitrile (DCTB) with silver trifluoroacetate (AgTFA) as matrix and a mixture of 1000:1 (matrix:polymer). The laser intensity was set to around 20%. The reflection mode was calibrated with a fullerite mixture from Sigma-Aldrich (CAS 131159-39-2).

Octadecylphosphonic acid (98%, ABCR) was recrystallized from toluene prior to use. All other reagents were purchased from Sigma-Aldrich or ABCR and used as received. Neopentyl styrene sulfonate (NeoSS) was prepared according to known procedures.

Synthesis of Bis(4-methoxyphenyl)-4'-vinylphenylamine (DMTPA)

Sodium *tert*-butoxide (5.04 g, 52.4 mmol), Palladium(II) acetate (0.094 g, 0.420 mmol), 4-Bromoanisole (7.90 ml, 62.9 mmol) and 4-Vinylaniline (2.5 g, 20.98 mmol) were dissolved in Toluene (80 ml) and degassed with an Argon stream for 30 min. Tri-*tert*-butylphosphine (0.424 g, 2.098 mmol) was added and the reaction was stirred for 12 h at 100°C. The reaction mixture was filtered through Alox B and washed with Aceton. The organic layer was concentrated using a rotary evaporator. The crude product was purified by column chromatography with toluene. After evaporation of the solvent the oil was added to degassed hexane and stored at 4°C for crystallization as a white solid (4 g, 72%);

¹H-NMR (300 MHz, CD₂Cl₂): δ 7.26 (d, *J* = 8.6 Hz, 2H), 7.07 (d, *J* = 9.0 Hz, 4H), 6.83-6.92 (m, 6H), 6.67 (dd, *J* = 17.6 Hz, *J* = 10.9 Hz, 1H), 5.62 (dd, *J* = 17.6 Hz, *J* = 0.8 Hz, 1H), 5.12 (dd, *J* = 10.9 Hz, *J* = 0.8 Hz, 1H), 3.81 (s, 6H); MS (*m/z*, M⁺) 331 (57.3).

Synthesis of PNeoSS homopolymer

Under Argon, NeoSS (2 g, 7.86 mmol), 2-cyanopropan-2-yl benzodithioate (23.2 mg, 0.11 mmol) and 2,2'-Azobisisobutyronitrile (3.4 mg, 0.021 mmol) were added to a 5 mL schlenk flask and dissolved in 2 ml Anisole. The reaction mixture was degassed by three freeze-thaw cycles and the reaction was started in an oil bath at 80°C. The reaction was stopped after 18 h by immersing the flask into an ice bath. For purification the reaction mixture was diluted with few chloroform and added to hexane for precipitation of the polymer. The solid polymer was filtered off and dissolved again in a small amount of chloroform. After the second precipitation in hexane no further monomer could be detected by NMR.

M_w (SEC) = 12900 g/mol, PDI = 1.06; $^1\text{H-NMR}$ (300 MHz, CDCl_3): δ 7.93-7.46 (m, $-\text{O-SO}_2-\text{C}_3\text{H}_2=\text{C}_3\text{H}_2-$, 2H), 7.00-6.36 (m, $-\text{SO}_3-\text{C}_3\text{H}_2=\text{C}_3\text{H}_2-$, 2H), 3.92-3.60 (m, $-\text{O-CH}_2-\text{C}(\text{CH}_3)_3$, 2H), 2.22-1.70 (m, $-\text{CH}_2\text{CH-C}_6\text{H}_4-\text{SO}_3^-$, 1H), 1.69-1.04 (m, $-\text{CH}_2\text{CH-C}_6\text{H}_4-\text{SO}_3^-$, 2H), 1.02-0.76 (m, $-\text{OCH}_2-\text{C}(\text{CH}_3)_3$, 9H).

Synthesis of PDMTPA(1)

Under Argon, DMTPA (2 g, 6.03 mmol), 2-cyanopropan-2-yl benzodithioate (26.7 mg, 0.12 mmol) and 2,2'-Azobisisobutyronitrile (4.0 mg, 0.024 mmol) were added to a 5 mL schlenk flask and dissolved in 2 ml Anisole. The reaction mixture was degassed by three freeze-thaw cycles and the reaction was started in an oil bath at 60°C. The reaction was stopped after 22 h by immersing the flask into an ice bath. For purification the reaction mixture was diluted with few THF and added to hexane for precipitation of the polymer. The solid polymer was filtered off and dissolved again in a small amount of THF. After the second precipitation in hexane no further monomer could be detected by NMR.

M_w (SEC) = 3510 g/mol, PDI = 1.09; $^1\text{H-NMR}$ (300 MHz, C_6D_6): δ 7.23-6.50 (m, $\text{CH}_3-\text{O-C}_6\text{H}_4-\text{N-}$, $-\text{CH}_2\text{CH-C}_6\text{H}_4-\text{N-}$, 12H), 3.45-3.17 (m, $\text{CH}_3-\text{O-C}_6\text{H}_4-\text{N-}$, 6H), 2.78-2.23 (m, $-\text{CH}_2\text{CH-C}_6\text{H}_4-\text{N-}$, 1H), 2.07-1.59 (m, $-\text{CH}_2\text{CH-C}_6\text{H}_4-\text{N-}$, 2H).

Synthesis of PDMTPA(2)

The same procedure as for PMDTPA(1) was used except the temperature was raised to 80°C and the polymerization was stopped after 4 h. M_w (SEC) = 6440 g/mol, PDI = 1.12.

Synthesis of PDMTPA(3)

Here the temperature was 100°C and the polymerization was stopped after 1 h. M_w (SEC) = 5510 g/mol, PDI = 1.11.

Synthesis of PDMTPA(4)

To lower the polarity of the surrounding medium benzene was used as solvent and the temperature was kept at 60°C. The polymerization was stopped after 22 h. M_w (SEC) = 4840 g/mol, PDI = 1.07.

Synthesis of PNeoSS-b-PDMTPA

Under Argon, PNeoSS (0.25 g), DMTPA (0.55 g, 1.66 mmol) and 2,2'-Azobisisobutyronitrile (0.5 mg, 0.003 mmol) were added to a 5 mL schlenk flask and dissolved in 1.6 ml Anisole. The reaction mixture was degassed by three freeze-thaw cycles and the reaction was started in an oil bath at 80°C. The reaction was stopped after 6 h by immersing the flask into an ice bath. For purification the reaction mixture was diluted with few THF and added to hexane for precipitation of the polymer. The solid polymer was filtered off and dissolved again in a small amount of THF. After the second precipitation in hexane no further monomer could be detected by NMR.

M_w (SEC) = 23560 g/mol, PDI = 2.60; $^1\text{H-NMR}$ (300 MHz, C_6D_6): δ 7.93-7.46 (m, $-\text{O}-\text{SO}_2-\text{C}_3\text{H}_2=\text{C}_3\text{H}_2-$, 2H), 7.23-6.50 (m, $\text{CH}_3-\text{O}-\text{C}_6\text{H}_4-\text{N}-$, $-\text{CH}_2\text{CH}-\text{C}_6\text{H}_4-\text{N}-$, $-\text{SO}_3-\text{C}_3\text{H}_2=\text{C}_3\text{H}_2-$, 14H), 4.15-3.69 (m, $-\text{SO}_2-\text{O}-\text{CH}_2-\text{C}(\text{CH}_3)_3$, 2H), 3.45-3.17 (m, $\text{CH}_3-\text{O}-\text{C}_6\text{H}_4-\text{N}-$), 6H), 2.78-2.23 (m, $-\text{CH}_2\text{CH}-\text{C}_6\text{H}_4-$, 1H), 2.07-1.59 (m, $-\text{CH}_2\text{CH}-\text{C}_6\text{H}_4-$, 2H), 1.04-0.63 (m, $-\text{OCH}_2-\text{C}(\text{CH}_3)_3$, 9H).

Synthesis of PDMTPA(1-4)-b-PNeoSS

All polymerizations were carried out under equal conditions. Therefore the ratio of macro-CTA/NeoSS/AIBN was kept at 1/100/0.4. A representative synthesis proceeded as follows. Under Argon, PDMTPA(1) (0.2 g), NeoSS (0.85 g, 3.33 mmol) and 2,2'-Azobisisobutyronitrile (1.1 mg, 0.007 mmol) were added to a 5 mL schlenk flask and dissolved in 1 ml Anisole. The reaction mixture was degassed by three freeze-thaw cycles and the reaction was started in an oil bath at 80°C. The reaction was stopped after 22 h by immersing the flask into an ice bath. For purification the reaction mixture was diluted with few THF and added to hexane for precipitation of the polymer. The solid polymer was filtered off and dissolved again in a small amount of THF. After the second precipitation in hexane no further monomer could be detected by NMR.

PDMTPA(1)-b-PNeoSS: M_w (SEC) = 6220 g/mol, PDI = 1.30;

PDMTPA(2)-b-PNeoSS: M_w (SEC) = 11100 g/mol, PDI = 1.28;

PDMTPA(3)-b-PNeoSS: M_w (SEC) = 11790 g/mol, PDI = 1.34;

PDMTPA(4)-b-PNeoSS: M_w (SEC) = 15860 g/mol, PDI = 1.37;

$^1\text{H-NMR}$ (300 MHz, C_6D_6): δ 7.93-7.46 (m, $-\text{O}-\text{SO}_2-\text{C}_3\text{H}_2=\text{C}_3\text{H}_2-$, 2H), 7.23-6.50 (m, $\text{CH}_3-\text{O}-\text{C}_6\text{H}_4-\text{N}-$, $-\text{CH}_2\text{CH}-\text{C}_6\text{H}_4-\text{N}-$, $-\text{SO}_3-\text{C}_3\text{H}_2=\text{C}_3\text{H}_2-$, 14H), 4.15-3.69 (m, $-\text{SO}_2-\text{O}-\text{CH}_2-\text{C}(\text{CH}_3)_3$, 2H), 3.45-3.17 (m, $\text{CH}_3-\text{O}-\text{C}_6\text{H}_4-\text{N}-$), 6H), 2.78-2.23 (m, $-\text{CH}_2\text{CH}-\text{C}_6\text{H}_4-$, 1H), 2.07-1.59 (m, $-\text{CH}_2\text{CH}-\text{C}_6\text{H}_4-$, 2H), 1.04-0.63 (m, $-\text{OCH}_2-\text{C}(\text{CH}_3)_3$, 9H).

Deprotection of the sulfonate group

PDMPA(4)-*b*-PNeoSS (0.1 g) was dissolved in DMF (7 ml) and degassed by an argon stream for 30 min. After addition of a 1M tetrabutylammonium hydroxide solution in methanol (3 ml, 4.65 mmol) the mixture was stirred for 2.5 h at 150°C. To remove the methanol and the resulting neopentanol a distillation bridge was attached to the flask. After cooling to room temperature, methanol was added dropwise to induce the micelle formation. This dispersion was dialyzed first against methanol and secondly against purified water.

¹H-NMR (300 MHz, C₆D₆): δ 7.80-7.08 (m, -O-SO₂-C₃H₂=C₃H₂-, 2H), 6.99-5.94 (m, CH₃-O-C₆H₄-N-, -CH₂CH-C₆H₄-N-, -SO₃-C₃H₂=C₃H₂-, 14H), 3.89-3.34 (m, CH₃-O-C₆H₄-N-), 6H), 3.29-2.88 (m, +N(-CH₂-CH₂-CH₂-CH₃)₄, 8H), 1.97-1.34 (m, -CH₂CH-C₆H₄-, -CH₂CH-C₆H₄-, 1H), 1.66-1.39 (m, +N(-CH₂-CH₂-CH₂-CH₃)₄, 8H), 1.36-1.13 (m, +N(-CH₂-CH₂-CH₂-CH₃)₄, 8H), 0.96-0.80 (m, +N(-CH₂-CH₂-CH₂-CH₃)₄, 12H).

Synthesis of CdSe nanorods

The CdSe particles were prepared according to published procedures with slight modifications. (ref cdse) cadmium oxide (0.205 g, 1.60 mmol), tri-*n*-octylphosphine oxide (3.00 g, 7.76 mmol), octadecylphosphonic acid (0.97 g, 2.91 mmol) and methylphosphonic acid (0.03 g, 0.29 mmol) were loaded into a schlenk flask and then heated to 320°C under argon until all the cadmium oxide reacted to give a transparent solution. The solution was kept at 320°C for 10 min and then it was cooled to room temperature under argon flow. After aging for at least 48 h, the mixture was directly used without further purification. Selenium (0.06 g, 0.80 mmol) was stirred in tri-*n*-octylphosphine (1.48 g, 4.00 mmol) over night to obtain the injection solution. This solution was injected to the Cd solution at 320°C. The crystals were allowed to grow for 8 min at 300°C, after which the heating bath was removed and the mixture was allowed to cool down to room temperature. Chloroform (5 ml) was added into the flask at ~50°C and the nanorods were precipitated out by addition of methanol (10-15 ml). For purification the CdSe nanorods were separated by centrifugation and decantation and then dissolved in chloroform. This procedure was repeated several times to remove the residual ligands.

For the ligand exchange, the cadmium selenide nanoparticles (0.20 g) were dispersed in DCM (100 ml) and poured into a schlenk flask. Aminoethanethiol hydrochloride (6 g, 52.8 mmol) was added and the dispersion was degassed with an argon stream for 30 min. For exchange of the phosphonic acid ligands the mixture was refluxed for 20 h. For precipitation of the particles Ethanol (100 ml) was added to the hot solution and the mixture was refluxed for another hour. For purification the particles were dispersed in methanol and centrifuged five times to remove the residual ligands. Finally the particles were dried, redispersed in water solution and filtered through a 0.2 μm Nylon filter to remove larger aggregates.

Block copolymerization starting from PNeoSS as macro-CTA

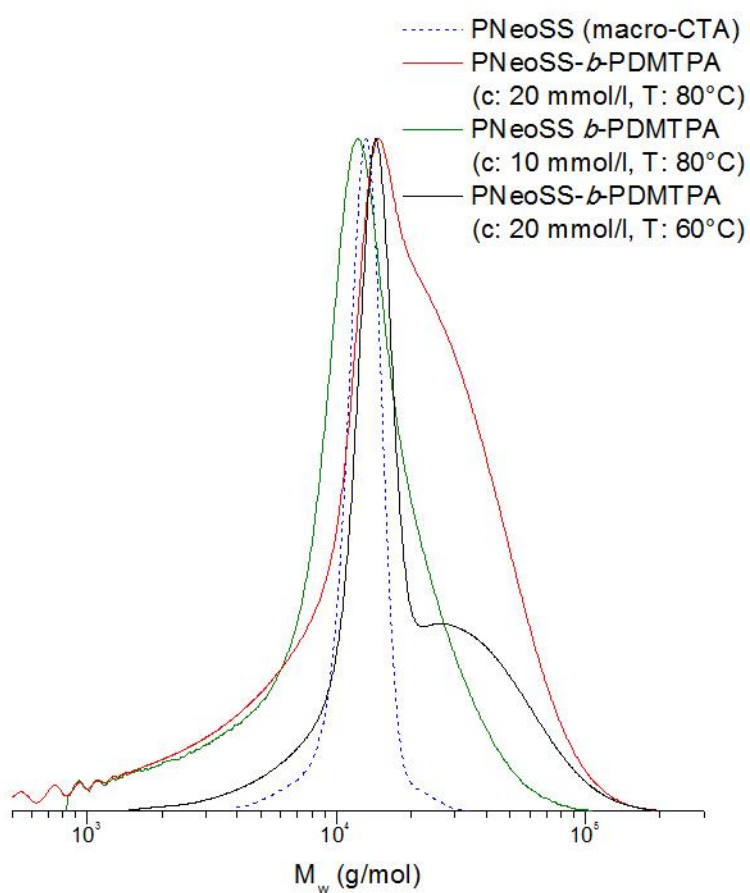


Figure 5–S1. GPC traces of the resulting block copolymers starting from PNeoSS. The dashed line presents the macro-CTA. The reaction ratios macro-CTA/DMTPA/AIBN were kept at 1/100/0.4. The temperature and concentration were varied according to the values given in the plot.

Matrix-assisted laser desorption/ionization time-of-flight (MALDI-TOF) measurements of the macro-CTAs PDMTPA(1), PDMTPA(2), PDMTPA(3) and PDMTPA(4)

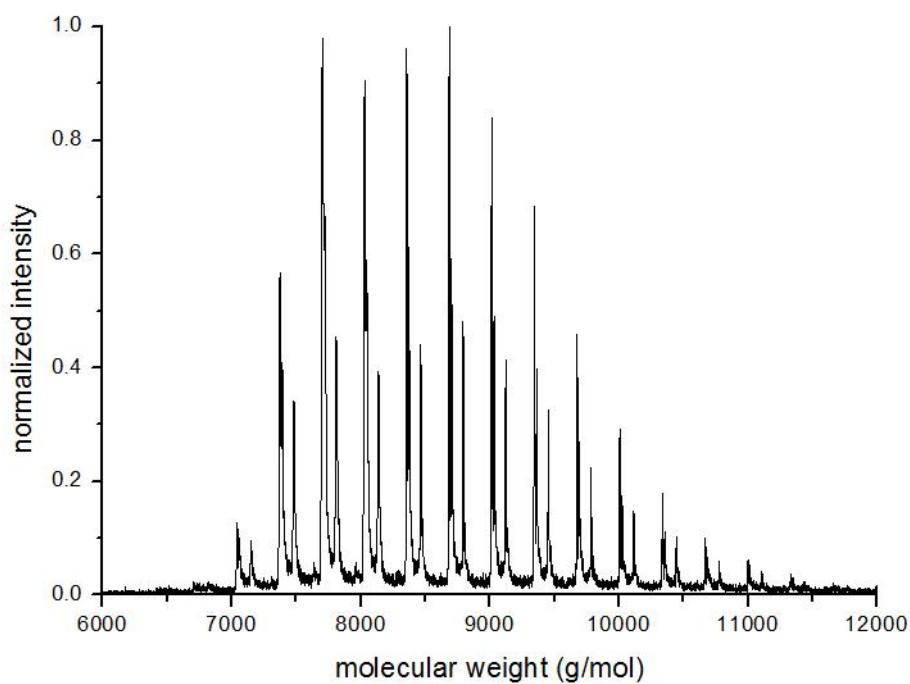


Figure 5-S2. MALDI spectrum of PDMTPA(1).

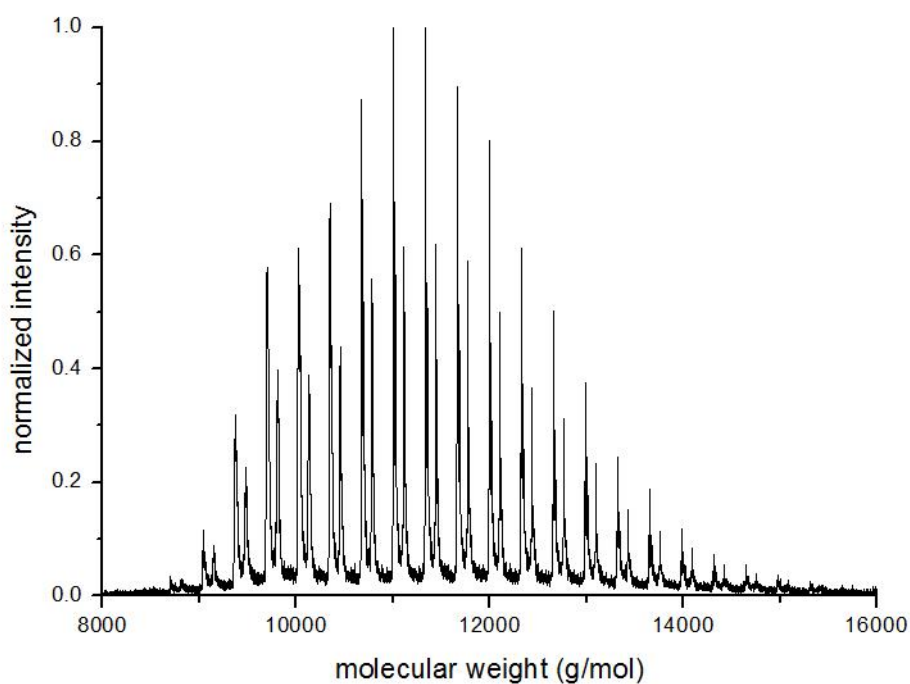


Figure 5-S3. MALDI spectrum of PDMTPA(2).

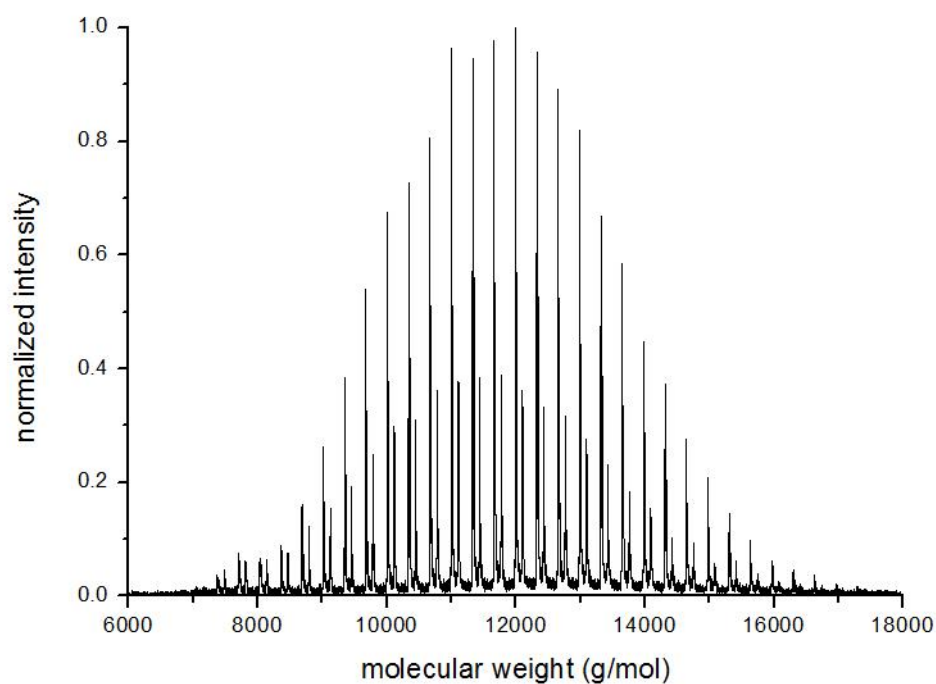


Figure 5-S4. MALDI spectrum of PDMTPA(3).

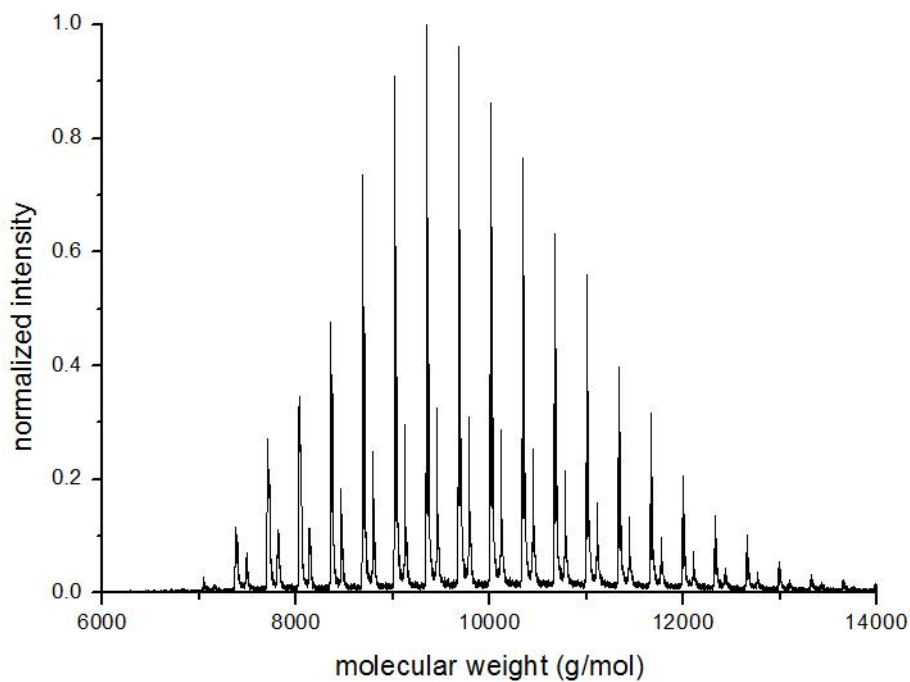


Figure 5-S5. MALDI spectrum of PDMTPA(4).

Self-initiation test of the DMTPA monomer

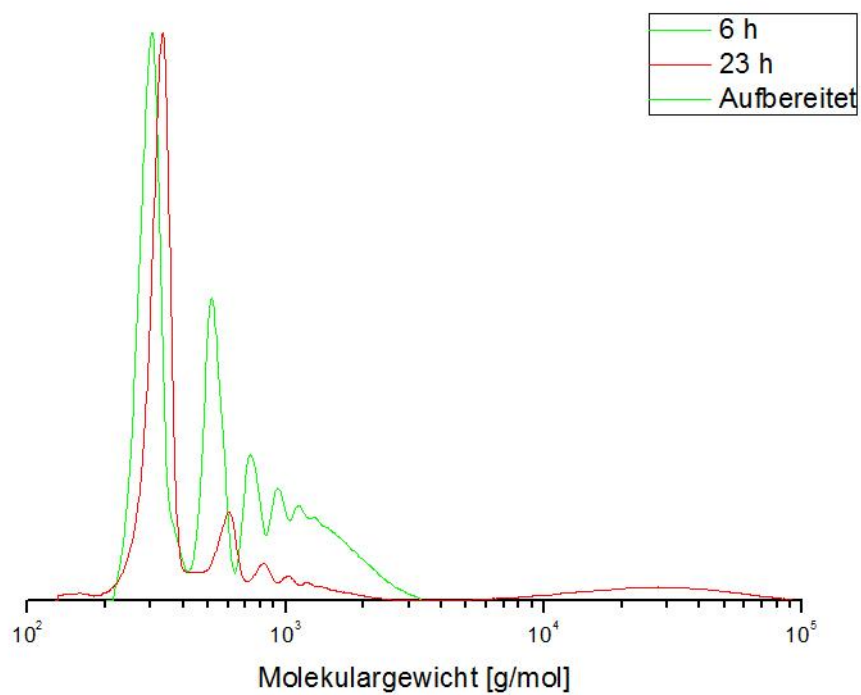


Figure 5-S6. GPC traces of samples taken from a polymerization of DMTPA without AIBN initiator.

Deprotection of sulfonate groups

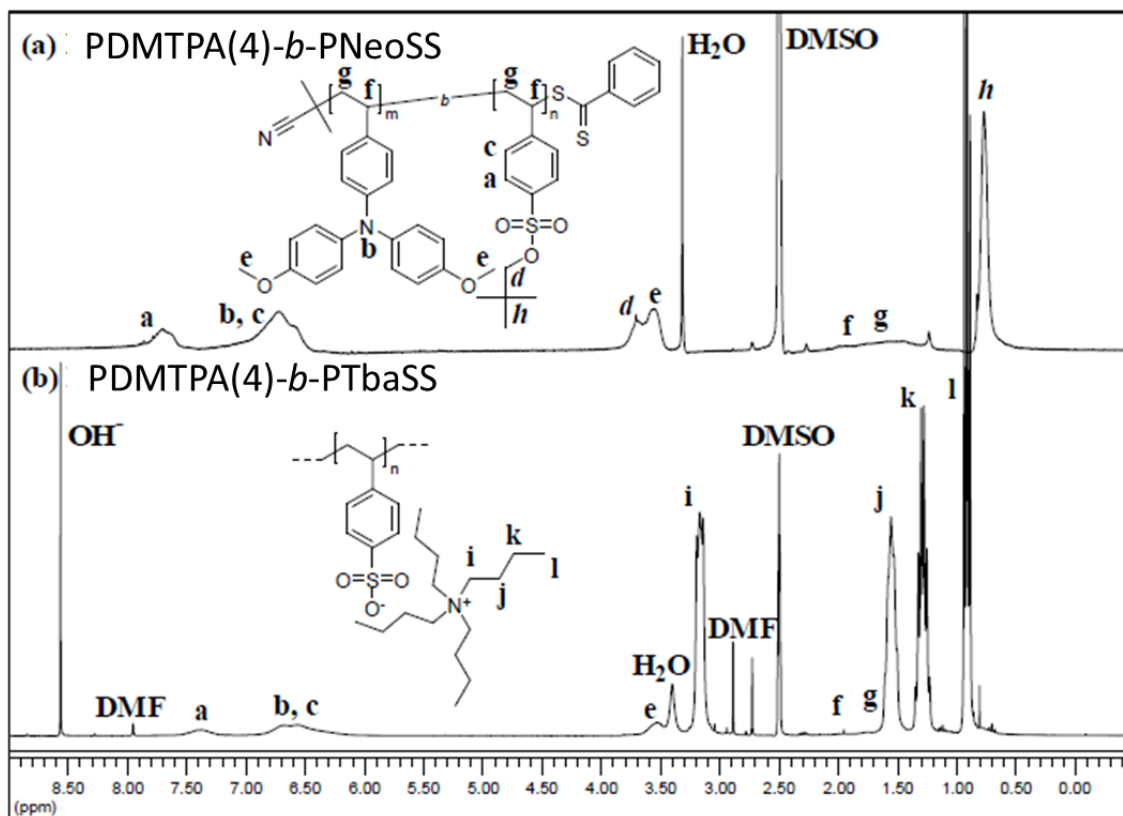


Figure 5–S7. NMR-spectra of the block copolymer PDMTPA(4)-*b*-PNeoSS and the deprotected polymer PDMTPA(4)-*b*-PTbaSS.

TEM of the CdSe nanoparticles

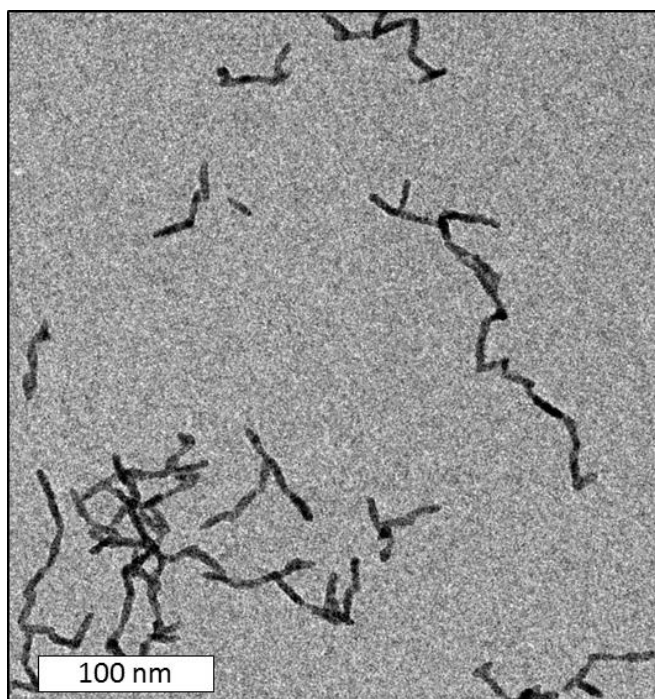


Figure 5–S8. Transmission electron micrograph of the prepared CdSe nanoparticles.

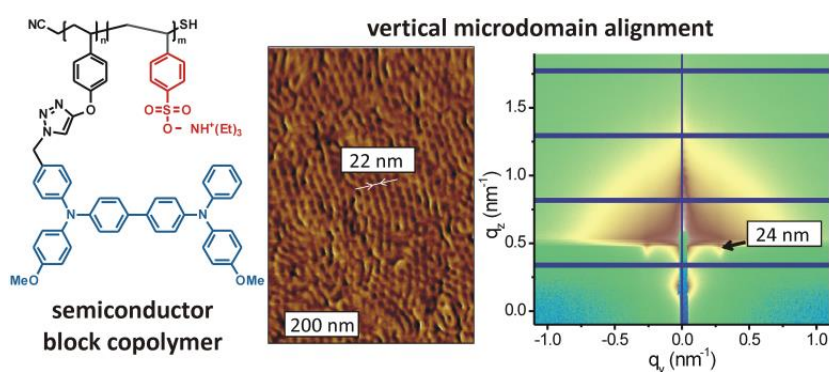
6. MACROSCOPIC VERTICAL ALIGNMENT OF NANODOMAINS IN THIN FILMS OF SEMICONDUCTOR AMPHIPHILIC BLOCK COPOLYMERS

Johannes C. Brendel,^a Feng Liu,^b Andreas S. Lang,^a Thomas P. Russell,^b Mukundan Thelakkat^{*a}

^a Applied Functional Polymers, Macromolecular Chemistry I, University of Bayreuth, 95440 Bayreuth, Germany

^b Polymer Science and Engineering Department, University of Massachusetts, Amherst, Massachusetts 01003

*E-mail of corresponding author: mukundan.thelakkat@uni-bayreuth.de



Published in *ACS Nano* **2013**, *in print*, DOI: DOI: 10.1021/nn401877g.

ABSTRACT

Though several techniques have been reported on the alignment of conventional block copolymers, the macroscopic vertical orientation of semiconductor block copolymer microdomains in thin films has still not been accomplished. Here, we report the control on the alignment of nanostructures in a semiconductor amphiphilic block copolymer comprising an amorphous triphenylamine hole conductor block and a hydrophilic poly(styrene sulfonate) segment. Three different compositions with a hole conductor content of 57, 72, and 79 wt% were synthesized using a combination of controlled reversible addition/fragmentation transfer polymerization and “click” chemistry. All polymers feature a narrow molecular weight distribution. Cryo-TEM reveals the formation of micelles in DMF solutions of the amphiphilic copolymer having nanoscopic dimensions. The micelle size correlates well with the X-ray analysis of dried bulk samples. Atomic force microscopy (AFM) confirms the micellar structure in the as-cast films. Thermal annealing causes an aggregation of micelles but did not lead to morphologies known for conventional block copolymers. However, annealing in saturated DMF vapor induces a morphology transition and a vertical orientation of the microdomains which was determined by grazing incidence small-angle X-ray scattering and AFM. The morphology varies from lamella to cylinders with increasing content of the hole-conductor block. The orientation arises from the controlled evaporation of the solvent, a mechanism that is similar to that observed for conventional block copolymers. Our approach demonstrates the macroscopic vertical alignment of nanodomains in semiconductor block copolymers which is a key requirement for applications in hybrid devices.

INTRODUCTION

The organization in nanoscopic domains and their alignment are crucial aspects for emerging technologies such as nanomembranes, lithography, microelectronics or organic photovoltaics. Therefore, numerous strategies have been devised to generate periodic patterns on the nanoscale including etching processes or removable templates.^{1,2} A promising route toward controlled microdomains is based on the self-organization of block copolymers which self-assemble into well-ordered morphologies ranging from spherical to cylindrical to lamellar domains.^{3,4} The size and structure is dictated by the molecular weights and the volume fractions of the individual blocks, respectively. However, most applications require precise control over orientation and alignment of microdomains.^{5,6} While the distinct interaction of the individual blocks with the surface usually favors a parallel alignment, vertical orientation can be achieved by use of an external field. So far electric fields, patterned substrates or controlled solvent interactions have been used to control the spatial orientation of the microdomains.⁷⁻¹² The latter has gained increasing attention due to its simplicity, versatility and suitability for many applications.¹³⁻¹⁵ The effect of solvents annealing on the alignment of polystyrene-polybutadiene-polystyrene triblock copolymers was first examined by Kim *et al.*¹⁶ Later, detailed work was presented on the orientation of ABC triblock copolymers controlling the evaporation rate of the solvent.¹⁷ Using polystyrene-*b*-poly(ethylene oxide) copolymers, the systematic treatment with benzene vapor leads to well-defined patterns which could be extended to large area macroscopic arrays in combination with structured sapphire substrates.^{18,19} And recently, ordered patterns of vertically oriented lamellae with large period distances were obtained

combining thermal and solvent annealing.²⁰ However, up to now no alignment studies on semiconductor block copolymers have been reported except the very recent publication of Goldberg-Oppenheimer *et al.* in which a block copolymer carrying perylenebisimide pendant groups was aligned using hierarchical electrohydrodynamic lithography.²¹

In this work, we present a block copolymer comprising a semiconductor block and a hydrophilic segment. As hole conductor we use poly(*N,N'*-bis(4-methoxyphenyl)-*N*-phenyl-*N'*-4-triazolyphenyl-(1,1'-biphenyl)-4,4'-diamine (PDMPD). The tetraphenylbenzidine group is well-known for its highly reversible oxidation and hole transport properties. Charge carrier mobilities of $1 \times 10^{-3} \text{ cm}^2/\text{Vs}$ have been observed in side-chain functionalized polymers.²² Another important point for selecting PDMPD building block for this work is the amorphous nature of the PDMPD block so that solvent vapor treatment earlier reported for conventional coil-coil block copolymers can be adapted here.²³

Poly(triethylammonium styrene sulfonate) (PEt₃NH⁺SS) features some unique properties as hydrophilic block due to the strong ionic sulfonate group. These groups are permanently charged down to a pH of 1 turning them into ideal counterparts for metal salt precursors or electrostatically stabilized inorganic nanoparticles which do not necessitate any insulating ligands for solubilization.²⁴⁻²⁶ Furthermore, the sulfonate groups are known to catalyze the hydrolysis of TiO₂ precursors to the anatase structure at low temperatures of 40°C which is otherwise usually observed at temperatures above 400°C.^{27,28}

The bulk morphology of the prepared semiconductor amphiphilic block copolymer before and after thermal annealing was analyzed with small-angle X-ray scattering (SAXS). Solution structures in DMF were examined using cryo transmission electron microscopy (TEM). Furthermore, thin films were prepared and characterized. The orientation and morphology of as-cast, thermal annealed and solvent treated thin films were analyzed with atomic force microscopy (AFM) and grazing incidence small-angle X-ray scattering (GISAXS).

RESULTS AND DISCUSSION

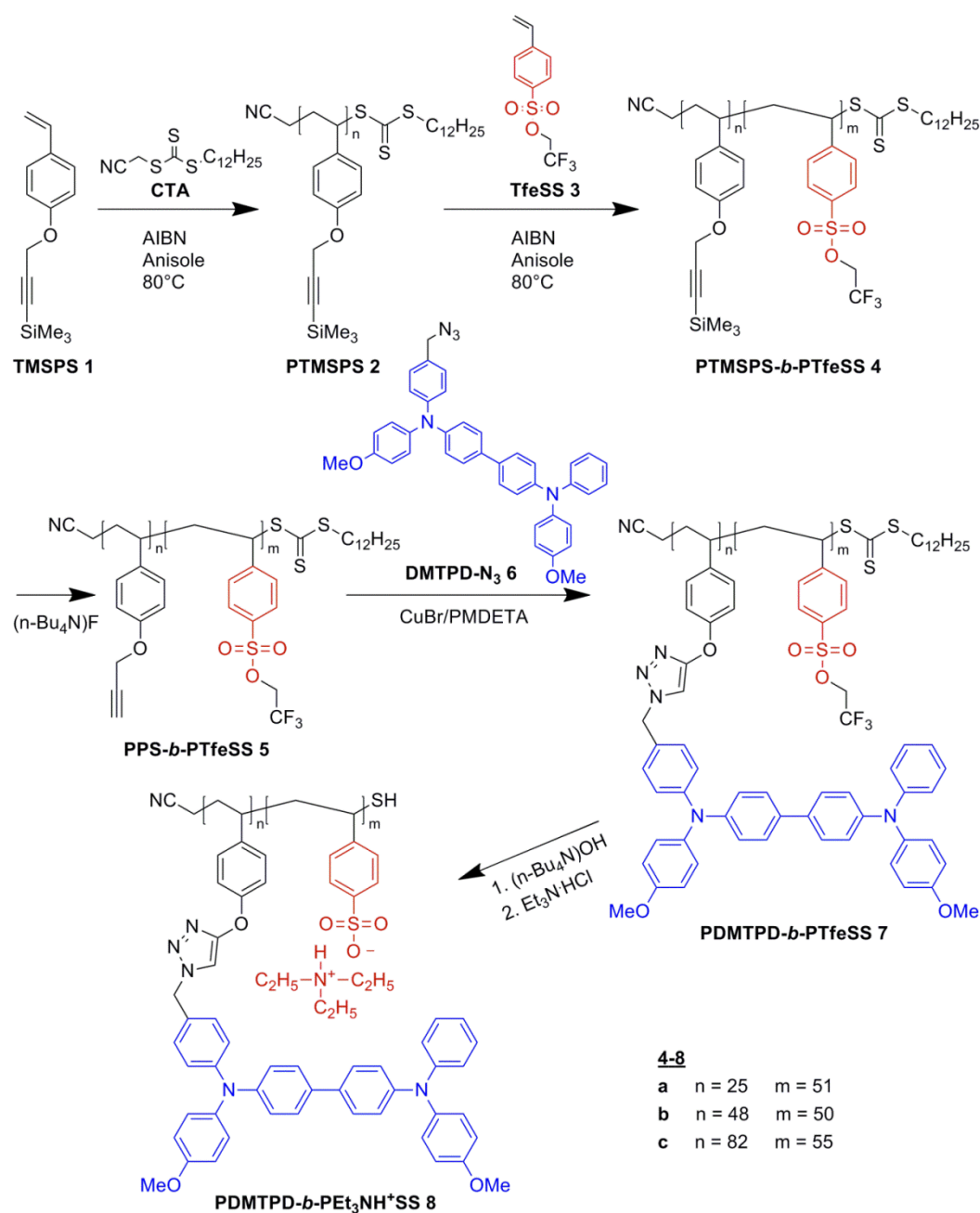
Synthesis

Among the controlled polymerization techniques, the reversible addition-fragmentation chain transfer (RAFT) process is a versatile tool for preparation of functional polymers.²⁹⁻³¹ The required chain transfer agents (CTA) are already commercially available and optimized for various types of monomers. Nevertheless, the controlled polymerization of bulky and reactive monomers, as they are used for electronic applications, remains challenging.^{32,33} Recently, we presented a combined approach using controlled radical polymerizations and copper-catalyzed azide-alkyne cycloaddition (CuAAC, “click” chemistry) to prepare well defined polymers carrying perylene bisimide groups.³⁴ The advantage of well-defined scaffold polymers from controlled polymerization techniques along with the flexibility and high yields of “click”-reactions makes it a versatile route toward tailor-made functional polymers.

Accordingly, we prepared the desired block copolymer PDMPD-*b*-PEt₃NH⁺SS **8** in a multistep synthesis, presented in Scheme 6–1. First the precursor polymer poly(4-(3-trimethylsilylpropargyloxy)styrene)-*block*-poly(2,2,2-trifluorethyl styrene sulfonate) (PTMSPS-*b*-PTfeSS **4**) was polymerized *via* stepwise RAFT polymerization using *S*-cyanomethyl-*S*-dodecyltrithiocarbonate as CTA. The monomer 4-(3-trimethylsilylpropargyloxy)styrene (TMSPS **1**) was prepared according to literature procedures.³⁴ After deprotection of the alkyne

group, the hole conductor moiety was attached by CuAAC of the azide *N,N'*-bis(4-methoxyphenyl)-*N*-phenyl-*N'*-4-azidophenyl-(1,1'-biphenyl)-4,4'-diamine dimethoxy triphenyl diamine (DMTPD- N_3 **6**). The detailed synthesis procedure for DMTPD- N_3 is given in the Supporting Information (Figure 6–S1). The resulting poly(*N,N'*-bis(4-methoxyphenyl)-*N*-phenyl-*N'*-4-triazolylphenyl-(1,1'-biphenyl)-4,4'-diamine)-*block*- poly(2,2,2-trifluorethyl styrene sulfonate) (PDMPD-*b*-PTfeSS **7**) was converted to poly(*N,N'*-bis(4-methoxyphenyl)-*N*-phenyl-*N'*-4-triazolylphenyl-(1,1'-biphenyl)-4,4'-diamine)-*block*- poly(triethylammonium styrene sulfonate) *via* basic hydrolysis of the sulfonate ester.

Scheme 6–1. Synthesis procedure for poly(*N,N'*-bis(4-methoxyphenyl)-*N*-phenyl-*N'*-4-triazolylphenyl-(1,1'-biphenyl)-4,4'-diamine)-*block*- poly(triethylammonium styrene sulfonate). (AIBN, 2,2'-Azobis(2-methylpropionitrile); PMDETA, *N,N,N',N',N''*-pentamethyldiethylenetriamine)



Characterization

The individual intermediates were characterized by NMR and SEC measurements to ensure that no side reactions occur and a well-defined polymer was formed. The SEC traces of selected steps are shown in Figure 6–1a.

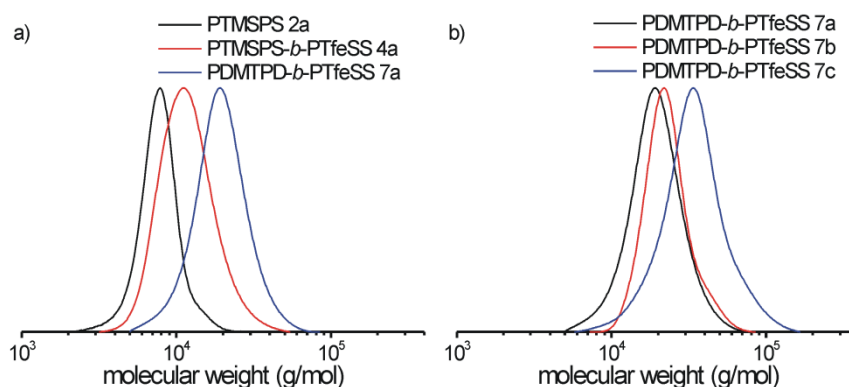


Figure 6–1. a) Normalized SEC traces of the intermediate steps poly(4-(3-trimethylsilylpropargyloxy)styrene) (PTMSPS 2a: black), poly(4-(3-trimethylsilylpropargyloxy)styrene)-*block*-poly(2,2,2-trifluorethyl styrene sulfonate) (PTMSPS-*b*-PTfeSS 4a: red) and poly(*N,N'*-bis(4-methoxyphenyl)-*N*-phenyl-*N'*-4-triazolylphenyl-(1,1'-biphenyl)-4,4'-diamine)-*block*- poly(2,2,2-trifluorethyl styrene sulfonate) (PDMTPD-*b*-PTfeSS 7a: blue). b) Normalized SEC traces of the different block copolymer precursors PDMTPD-*b*-PTfeSS 7a, PDMTPD-*b*-PTfeSS 7b and PDMTPD-*b*-PTfeSS 7c. The final polymers PDMTPD-*b*-PEt₃NH⁺SS could not be measured in SEC due to a strong interaction of the polyelectrolyte with the column material. The SEC was calibrated according to polystyrene standards.

In all cases a narrow distribution was retained. Only for the large molecular weight polymers (PDMTPD-*b*-PTfeSS 7c) some interchain coupling was detected, which can be related to disulfide coupling after partial loss of the CTA end-group or alkyne-alkyne coupling reactions. Nevertheless, the diblock copolymer formation and all polymer analogous reaction steps can be assumed to be quantitative, since no residual peaks of macro-CTA or precursor polymers were observed in SEC (Figure 6–1a). As no residual alkyne protons were traceable in NMR analysis, we conclude > 95% (considering the error limit of NMR) “click” efficiency for the CuAAC. The number average molecular weights M_n , the polydispersity indices (PDI) and the average molecular weights calculated from the NMR spectra are summarized in Table 6–1.

Table 6–1. M_n and PDI Measured by SEC and an Average Molecular Weight Calculated from the NMR Spectra for the Intermediate Steps in the Synthesis of PDMTPD-*b*-PEt₃NH⁺SS **8a, for All Nonionic Precursors PDMTPD-*b*-PTfeSS **7a-c** and the Respective Final Polymers PDMTPD-*b*-PEt₃NH⁺SS **8a-c****

sample	M_n (SEC) ^{b)}	PDI (SEC) ^{b)}	MW (NMR) ^{c)}	wt% PDMTPD
PTMSPS 2a	7.3 kg/mol	1.09	6.1 kg/mol	-
PTMSPS- <i>b</i> -PTfeSS 4a	10.7 kg/mol	1.17	19.5 kg/mol	-
PDMTPD- <i>b</i> -PTfeSS 7a	17.6 kg/mol	1.17	33.0 kg/mol	58 wt%
PDMTPD- <i>b</i> -PTfeSS 7b	21.6 kg/mol	1.12	50.0 kg/mol	72 wt%
PDMTPD- <i>b</i> -PTfeSS 7c	30.1 kg/mol	1.26	77.6 kg/mol	81 wt%
PDMTPD- <i>b</i> -PEt ₃ NH ⁺ SS 8a ^{a)}	-	-	34.0 kg/mol	57 wt%
PDMTPD- <i>b</i> -PEt ₃ NH ⁺ SS 8b ^{a)}	-	-	51.0 kg/mol	72 wt%
PDMTPD- <i>b</i> -PEt ₃ NH ⁺ SS 8c ^{a)}	-	-	79.0 kg/mol	79 wt%

a) The final polymer PDMTPD-*b*-PEt₃NH⁺SS could not be measured by SEC due to strong interactions with the column material.

b) The SEC was calibrated according to polystyrene standards.

c) For calculation of the PTMSPS block, the ratio of the signals at 4.63 ppm and 3.22 ppm of the polymer and the RAFT end-group, respectively, were taken. The MW of the PTfeSS block was calculated from the ratio of the two blocks, viz. the signals at 4.82 ppm (PTfeSS) and 4.67 ppm (PTMSPS).

Accordingly, we prepared three different block copolymers varying the composition of the individual blocks. The block copolymers **8a**, **8b** and **8c** contain 57, 72 and 79 wt% of PDMTPD, respectively. The characteristics of the final polymers PDMTPD-*b*-PEt₃NH⁺SS **8a-c** and the respective precursors PDMTPD-*b*-PTfeSS **7a-c** are also included in Table 6–1, whereas the SEC traces of the precursors are shown in Figure 6–1b. Details on the SEC analysis of all intermediate steps for the different block copolymers are given in the supporting information (Figure 6–S2). To prove a unimodal growth of the second block the samples were additionally monitored in SEC with different eluent (THF with 0.25 % tetrabutylammonium bromide salt which was added to reduce the interaction of the polymer with the column) (Figure 6–S3). All polymers exhibit narrow molecular weight distributions. Assuming densities of 1-1.2 g/ml, which is common for amorphous polymers, sample PDMTPD-*b*-PEt₃NH⁺SS **8a** possesses a volume ratio suitable for a lamellar morphology. On the other hand, PDMTPD-*b*-PEt₃NH⁺SS **8b** should lead to cylindrical domains and PDMTPD-*b*-PEt₃NH⁺SS **8c** may even form a spherical morphology in thin films.

The thermal characterization of the polymers reveals a decomposition onset of 300-310°C independent of the composition. In the differential scanning calorimetry (DSC) the individual block copolymers show only one T_g , which shifts to higher values for increasing number of PDMTPD repeating units (Figure 6–S4). For PDMTPD-*b*-PEt₃NH⁺SS **8a** we found a T_g of 144°C, for PDMTPD-*b*-PEt₃NH⁺SS **8b** 162°C and for PDMTPD-*b*-PEt₃NH⁺SS **8c** 178°C. No difference was found for the precursor polymers PDMTPD-*b*-PTfeSS **7a-c**. The T_g values are in the same range as those reported for DMTPD pendant homopolymers.²²

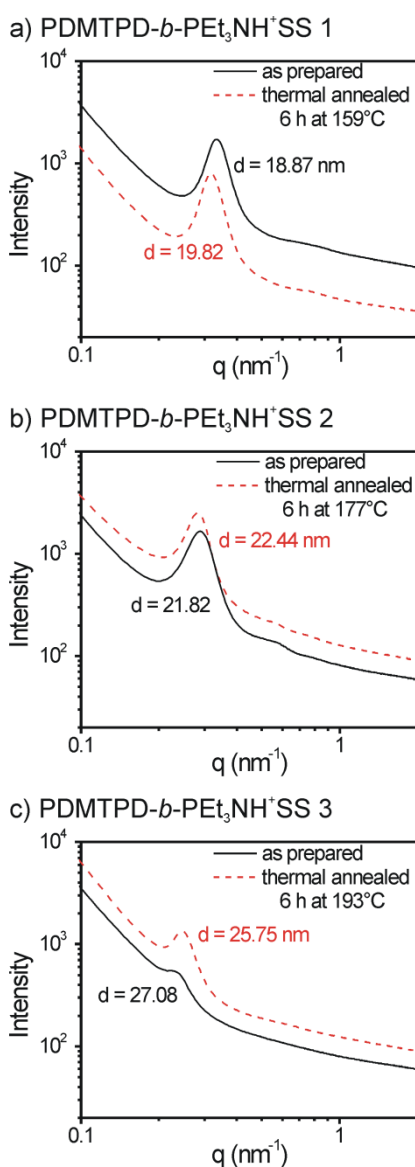


Figure 6–2. Small-angle X-ray spectroscopy (SAXS) results on bulk samples of the different block copolymers a) PDMTPD-*b*-PEt₃NH⁺SS **8a**, b) PDMTPD-*b*-PEt₃NH⁺SS **8b** and c) PDMTPD-*b*-PEt₃NH⁺SS **8c**; black solid line: before annealing over T_g , red dashed line: after annealing over T_g for 6 h. The distances d are calculated from the respective peak maxima.

Two-dimensional small-angle X-ray scattering (SAXS) of bulk samples was performed at the National Synchrotron Light Source (NSLS) at the Brookhaven National Laboratory (BNL). One-dimensional SAXS profiles were obtained by circular averaging of the corresponding two-dimensional scattering patterns. The results are shown in Figure 6–2. As we can see, all these samples show a certain length scale of phase separation defined by the major peak in the scattering profiles. For sample PDMTPD-*b*-PEt₃NH⁺SS **8a**, a center-to-center distance of 18.9 nm was calculated from the major peak. Increasing the PDMTTPA content to 72 % (**8b**) the feature size of the phase separation is increased to 21.8 nm. Further increase of PTMTTPA content (**8c**) elevates the phase separation size to 25.7 nm. It has to be noted we can only see first order correlation in the scattering profiles. No microdomain nanostructures, as observed in conventional AB-diblock copolymers such as cylinders or lamellae, are found. Thermal annealing

slightly increases the center-to-center distances for all three samples with data labeled in Figure 6–2. Although the PDMTPD-block becomes flexible, the strong interactions of the sulfonate groups in $\text{PEt}_3\text{NH}^+\text{SS}$ may prevent the movement of the polymer chains.

Analysis of Thin Films

The block copolymers PDMTPD-*b*- $\text{PEt}_3\text{NH}^+\text{SS}$ **8a-c** were deposited on a silicon substrate covered with a thin layer of ZnO by spin-casting a 10 wt% solution of the polymers in DMF resulting in a layer of approximately 150 nm. The morphology was examined by AFM and GISAXS.^{35, 36} The untreated films of PDMTPD-*b*- $\text{PEt}_3\text{NH}^+\text{SS}$ show no repetitive pattern, but spherical structures for all the samples as observed in AFM which arise from the formation of micelles (Figure 6–3). Further evidence for micelle formation could be observed exemplarily in cryo-TEM images of a solution of the polymer PDMTPD-*b*- $\text{PEt}_3\text{NH}^+\text{SS}$ **8c** in DMF (Figure 6–S5). The average size of the micelles in the images was estimated to be 27 nm which is in very good agreement with the SAXS signal of the bulk samples ($d = 27.08$ nm before annealing) and the structure sizes found in the AFM micrographs (average size 28 nm) for the sample PDMTPD-*b*- $\text{PEt}_3\text{NH}^+\text{SS}$ **8c**. This effect further explains the high roughness of the films which is caused by the aggregation of the micelles during the drying process.

The size of the spherical structures grows with increasing content of PDMTPD from 22 nm (**8a**) to 24 nm (**8b**) and finally to 28 nm on block copolymer **8c**. During the casting process, the soft micelles are flattened and, in consequence, the sizes are slightly larger than the average distance found in the SAXS analysis of the dried bulk samples (19, 22 and 27 nm). Nevertheless, the increase in structure size from block copolymer **8a** to **8b** and **8c** is comparable in both AFM and SAXS. GISAXS analysis of all thin films gave no evidence for order in the morphology of those films (Figure 6–S6).

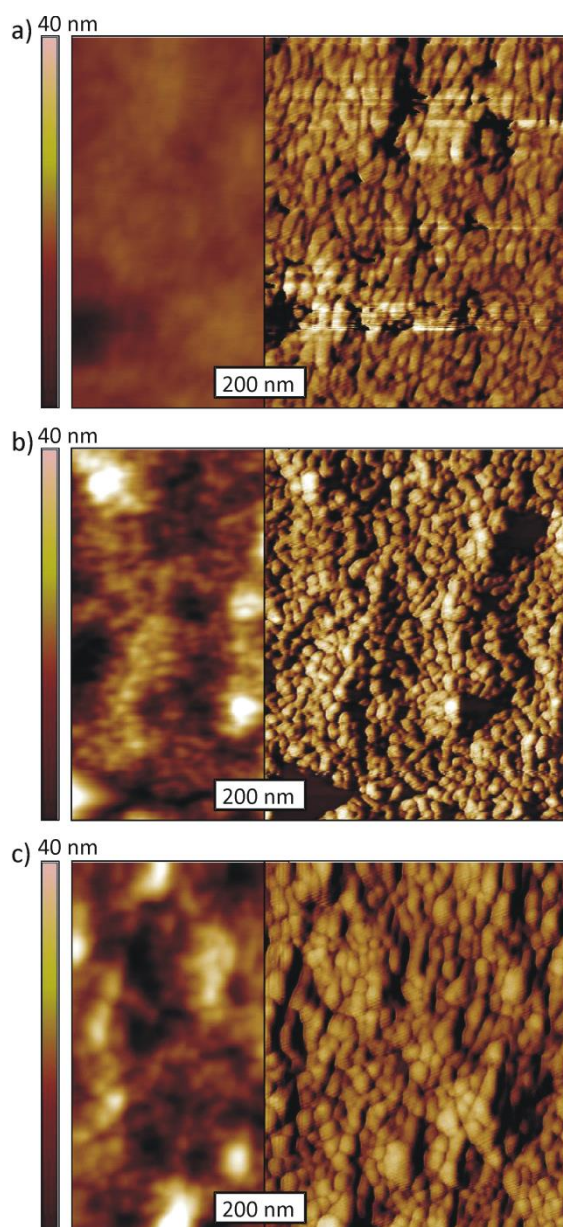


Figure 6–3. AFM height (left) and phase (right) images of thin films made by spin-casting a 10 wt% solution of PDMTPD-*b*-PEt₃NH⁺SS 8a (a), PDMTPD-*b*-PEt₃NH⁺SS 8b (b) and PDMTPD-*b*-PEt₃NH⁺SS 8c (c) in DMF.

To promote the self-assembly, the films were annealed either by thermal treatment above T_g or by continuous exposure to saturated solvent vapor. Analogous to the bulk samples, thermal annealing did not significantly alter the structure in the thin films. Only the PDMTPD phase was able to rearrange slightly leading to an increased aggregation of the micelles during the annealing. The GISAXS measurements and AFM images are given in the Supporting Information (Figure 6–S7 and Figure 6–S8). Alternatively, the effects of continuous solvent annealing in DMF vapor were examined. DMF is an excellent solvent for PEt₃NH⁺SS, while it is only a moderate solvent for PDMTPD. The preferential interaction of DMF with the PEt₃NH⁺SS block should lead to a strong swelling of its domain, while the PDMTPD domains take up less solvent. For solvent annealing the samples were kept in sealed chambers with a solvent reservoir and were analyzed after 4 days of annealing. We chose this long time period to enable the reorganization of the

polymer chains in accordance with experience in previous experiments. Since the sterically demanding DMTPD side groups restrict the chain movement a long time scale was chosen. The AFM images of the resulting thin films are depicted in Figure 6–4.

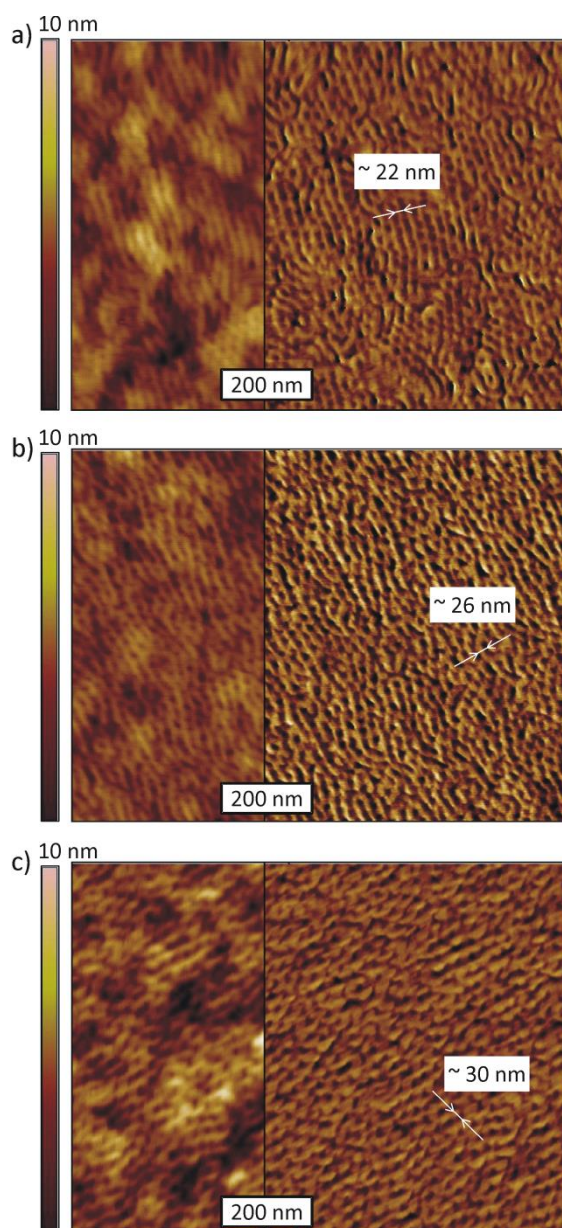


Figure 6–4. AFM height (left) and phase (right) images of thin films made by spin-casting a 10 wt% solution of PDMTPD-*b*-PEt₃NH⁺SS **8a** (a), PDMTPD-*b*-PEt₃NH⁺SS **8b** (b) and PDMTPD-*b*-PEt₃NH⁺SS **8c** (c) in DMF. The films were annealed in saturated DMF vapor for 4 days.

The surface patterns in the AFM images clearly reveal a reorganization of the block copolymer toward more ordered domains in contrast to the as-spun films (Figure 6–3). The microdomains feature lamellar morphology in polymer **8a** and cylinder morphology in sample **8c** with domain sizes changing from 21 nm to 30 nm. Images with lower magnification give evidence for a uniform large scale effect of the solvent vapor treatment (Figure 6–S9). Furthermore, discrete peaks emerge in the in-plane GISAXS pattern which confirm a morphology oriented perpendicular to the substrate (Figure 6–5).

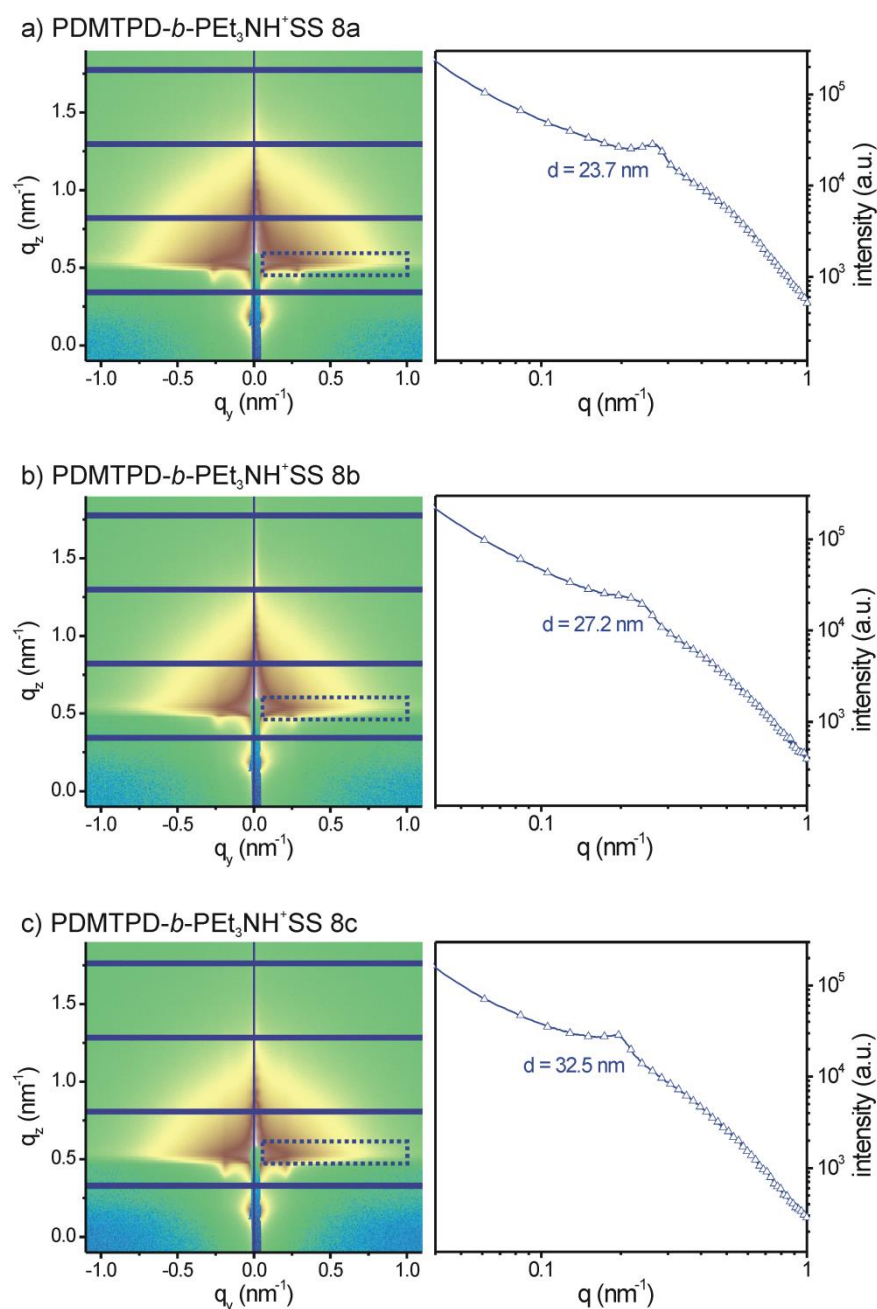


Figure 6–5. GISAXS measurements of the solvent annealed thin films made of PDMTPD-*b*-PET₃NH⁺SS **8a** (a), PDMTPD-*b*-PET₃NH⁺SS **8b** (b) and PDMTPD-*b*-PET₃NH⁺SS **8c** (c); the plots on the right show the indicated in-plane line cuts (dotted rectangle) out of the full pattern (left). For each signal, the calculated *d*-spacing is assigned.

No out of plane signals arise corroborating an exclusively vertical orientation of the block copolymer domains in the film. In conjunction with the AFM images, a vertical lamellar structure can be attributed for the sample PDMTPD-*b*-PET₃NH⁺SS **8a** indicated by the meander like structures on the surface. However, these forms are regularly interrupted. Keeping the weight ratio of PDMTPD/PET₃NH⁺SS of 58/42 in mind, a lamellar morphology is expected, but the strong dipole interactions of the sulfonate groups may interfere with a full morphology transition from micelles in the as-cast state to a lamellar morphology after annealing. In sample PDMTPD-*b*-

PEt₃NH⁺SS **8b** (PDMTDP/PEt₃NH⁺SS of 72/28), the cylindrical structure becomes more pronounced, although some areas still show short lamellae sections. The sample PDMTDP-*b*-PEt₃NH⁺SS **8c**, with a ratio of 79/21, clearly depicts a dot-like surface representative for vertical aligned cylinders. In contrast to the expected equilibrium morphologies which are commonly observed by thermal annealing of conventional diblock copolymers, solvent treatment may alter the volume ratios due to a preferential interaction with one block. Similar observations were found for polystyrene-*block*-poly(vinyl pyridine) copolymers treated with various compositions of toluene and THF vapor which clearly influence the resulting morphology transition from micelles to cylindrical microdomains.³⁷ Here, we observe a similar transition with the selective solvent DMF but in film thicknesses exceeding the period size of the polymer (Figure 6–6). In consequence, we assume a solvent evaporation effect causing the vertical alignment of the block copolymer similar as that observed for PS-*b*-PEO copolymers.¹⁸ In this case, a gradient of solvent in the thin film induces the orientation propagating through the film during solvent evaporation.

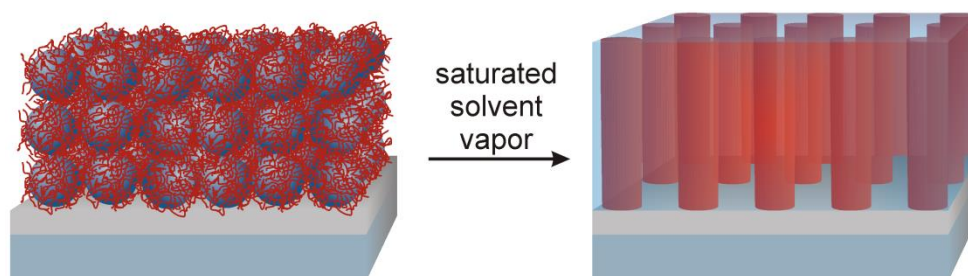


Figure 6–6. Schematic representation of the morphology transition from nonordered micelles toward vertically aligned cylindrical microdomains upon treatment with saturated solvent vapor.

CONCLUSIONS

In conclusion, we demonstrated the alignment of a functional amphiphilic block copolymer comprising the semiconducting segment PDMTPA and a hydrophilic polyanion block PEt₃NH⁺SS in vertical oriented microdomains upon solvent annealing. A key requirement for this control on morphology is first of all the preparation of well-defined block copolymers which is still a challenge for bulky functional groups. Therefore, we established a synthesis procedure combining the advantages of RAFT polymerization with the “click” chemistry approach to obtain narrowly distributed block copolymers with defined segment lengths. Utilizing this synthesis technique, we prepared three different compositions of variable PDMTDP content. The copolymers form micelles in DMF solutions which were retained in the as-cast thin films. Thermal treatment of the polymers did not notably affect the morphology either in the bulk or in the thin film. This can be attributed to the strong interactions of the ionic sulfonate groups suppressing the reorientation of the polymer chains. However, treating the thin films with saturated vapor of DMF induces a morphology transition. Thus, a lamellar morphology was obtained for the copolymer with low PDMTDP content. Increasing the content alters the structure toward cylindrical microdomains oriented perpendicular to the substrate which was supported by AFM and GISAXS measurements. While this perpendicular orientation was so far only reported for conventional block copolymers, we, for the first time, demonstrated the

controlled vertical alignment of a semiconductor block copolymer. This promising development is suitable for a wide range of applications in hybrid systems, since the hydrophilic block enables the incorporation of inorganic materials.^{38,39} Furthermore, due to the versatility of the combination of RAFT and “click” chemistry, this modular synthetic procedure can conveniently be extended to a large variety of functional groups.

EXPERIMENTAL SECTION

Materials and Methods

The synthesis of poly(propargyl oxystyrene) was shown elsewhere.¹ The chain transfer agent (CTA) *S*-cyanomethyl-*S*-dodecyltrithiocarbonate (97%) was purchased from ABCR Germany. Dimethylformamide (99.8%) was purchased from Sigma-Aldrich. PMDETA ($\geq 98\%$) was purchased from Fluka. CuBr (98%) was bought from Acros. All reagents were used without further purification unless otherwise noted. ¹H NMR (300 MHz) spectra were recorded on a Bruker AC 300 spectrometer and calibrated according to the respective solvent resonance signal. SEC measurements were carried out either in pure THF or in THF with 0.25% tetrabutylammoniumbromide with two Varian MIXED-C columns (300 x 7.5 mm) at room temperature and at a flow rate of 0.5 mL/min using UV (Waters model 486) with 254 nm detector wavelength and refractive index (Waters model 410) detectors. Polystyrene in combination with *o*-DCB as an internal standard was used for calibration. Differential scanning calorimetry experiments were conducted at heating rates of 10 K·min⁻¹ under N₂ atmosphere with a Perkin-Elmer Diamond DSC calibrated with indium. Thermogravimetry measurements were conducted on a Mettler Toledo TGA/SDTA 851^e under N₂ atmosphere at a heating rate of 10 K/min. Temperature of decomposition (T_{onset}) was calculated from the onset of the respective curve. Atomic force microscopy was conducted on a Dimension 3100 Nanoscope IV instrument with a closed-loop XY tip-scanner in the tapping mode. Thermal annealing was conducted under N₂ above the estimated T_g . For solvent annealing, the samples were kept in a closed vessel with a respective solvent reservoir.

Two-dimensional small-angle X-ray scattering (SAXS) was performed at the beamline X27C, National Synchrotron Light Source (NSLS), Brookhaven National Laboratory (BNL). The wavelength of incident X-ray was 0.1371 nm. Scattering signals were collected by a marCCD 2D detector with a resolution of 79 mm/pixel. Typical exposure time was between 30 and 120 s. All the SAXS data presented here are raw data without background subtraction. One-dimensional SAXS profiles were obtained by circular averaging of the corresponding two-dimensional scattering patterns. Grazing incidence small-angle X-ray scattering (GISAXS) was carried out at beamline 7.3.3 Advanced Light Source (ALS), Lawrence Berkeley National Lab (LBNL). An X-ray beam was impinged onto the sample at 0.2° grazing angle slightly above the critical angle of the polymer film ($R_c = 0.16^\circ$) but below the critical angle of Si substrates ($R_c = 0.28^\circ$). The wavelength of X-rays used was 1.240 Å, and the scattered intensity was detected by using a Pilatus 1M detector with image sizes of 981 x 1043 pixels.

Synthesis Procedures for the Preparation of the Block Copolymers

A detailed synthesis procedure is representatively given for the sample PDMPD-*b*-PEt₃NH⁺SS **8a**. The conditions were kept constant for all samples, but the amounts of reagents were adjusted to obtain the desired molecular weights.

Poly(4-(3-trimethylsilylpropargyloxy)styrene) (PTMSPS 2a)

Under nitrogen, 4-(3-trimethylsilylpropargyloxy)styrene (3 g, 13.3 mmol), *S*-cyanomethyl-*S*-dodecyltrithiocarbonate (0.085 g, 0.27 mmol) and 2,2'-azobisisobutyronitrile (8.8 mg, 0.05 mmol) were dissolved in 3 mL Anisole. The reaction mixture was degassed by 5 freeze-thaw cycles and the reaction was started in an oil bath at 80 °C. After 4.5 h the reaction was stopped at a conversion of approximately 50% by immersing the flask into an ice bath. For purification the polymer was diluted with chloroform and precipitated in methanol twice. Filtration gave 1.3 g (80%) of yellowish powder of poly(4-(3-trimethylsilylpropargyloxy)styrene). ¹H NMR (300 MHz, CHCl₃): δ (ppm) 6.9–6.18 (br m, 100H, *ArH*), 4.63 (s, 50H, –OCH₂), 3.22 (t, 2H, –S-CH₂-C₁₁H₂₃), 2.10–0.92 (br m, 97H, backbone CH, CH₂, CN-CH₂-S-, –S-CH₂-C₁₀H₂₀-CH₃), 0.90 (t, 3H, –C₁₁H₂₂-CH₃), 0.23 (m, 225H, SiMe₃). SEC: M_n = 7300 g mol⁻¹; PDI = 1.09.

PTMSPS 2b

4-(3-trimethylsilylpropargyloxy)styrene (2.7 g, 11.6 mmol), *S*-cyanomethyl-*S*-dodecyltrithiocarbonate (0.037 g, 0.12 mmol), 2,2'-azobisisobutyronitrile (3.8 mg, 0.02 mmol). ¹H NMR (300 MHz, CHCl₃): δ (ppm) 6.9–6.18 (br m, 192H, *ArH*), 4.63 (s, 96H, –OCH₂), 3.22 (t, 2H, –S-CH₂-C₁₁H₂₃), 2.10–0.92 (br m, 166H, backbone CH, CH₂, CN-CH₂-S-, –S-CH₂-C₁₀H₂₀-CH₃), 0.90 (t, 3H, –C₁₁H₂₂-CH₃), 0.23 (m, 432H, SiMe₃). SEC: M_n = 11500 g mol⁻¹; PDI = 1.11.

PTMSPS 2c

4-(3-trimethylsilylpropargyloxy)styrene (2.7 g, 11.6 mmol), *S*-cyanomethyl-*S*-dodecyltrithiocarbonate (0.037 g, 0.12 mmol), 2,2'-azobisisobutyronitrile (3.8 mg, 0.02 mmol). ¹H NMR (300 MHz, CHCl₃): δ (ppm) 6.9–6.18 (br m, 328H, *ArH*), 4.63 (s, 164H, –OCH₂), 3.22 (t, 2H, –S-CH₂-C₁₁H₂₃), 2.10–0.92 (br m, 268H, backbone CH, CH₂, CN-CH₂-S-, –S-CH₂-C₁₀H₂₀-CH₃), 0.90 (t, 3H, –C₁₁H₂₂-CH₃), 0.23 (m, 738H, SiMe₃). SEC: M_n = 11500 g mol⁻¹; PDI = 1.11.

*Poly(4-(3-trimethylsilylpropargyloxy)styrene)-block-poly(2,2,2-trifluoroethyl styrene sulfonate) (PTMSPS-*b*-PTfeSS 4a)*

Under nitrogen, PTMSPS **2a** (0.5 g, 0.08 mmol), 2,2,2-trifluoroethyl 4-vinylbenzenesulfonate (2.2 g, 8.2 mmol) and 2,2'-azobisisobutyronitrile (4.1 mg, 0.025 mmol) were dissolved in 1.2 mL 2-butanone. The reaction mixture was degassed by 5 freeze-thaw cycles and the reaction was started in an oil bath at 80 °C. After 140 min the reaction was stopped by immersing the flask into an ice bath. For purification the polymer was diluted with THF and precipitated in methanol twice. Filtration gave 1.1 g (66%) of yellowish powder of poly(4-(3-trimethylsilylpropargyloxy)styrene)-*block*-poly(2,2,2-trifluoroethyl styrene sulfonate). ¹H NMR (300 MHz, DMSO-*d*₆): δ (ppm) 7.83–7.50 (m, 102H, aromatic –CH=C-SO₃-), 7.00–6.18 (br m, 202H, other *ArH*), 4.82 (s, 102H, –SO₃-CH₂-CF₃), 4.67 (s, 50H, –OCH₂), 2.14–1.01 (br m, 250H, backbone CH, CH₂, CN-CH₂-S-, –S-CH₂-C₁₀H₂₀-CH₃), 0.84 (t, 3H, –C₁₁H₂₂-CH₃), 0.12 (m, 225H, SiMe₃). SEC: M_n = 10700 g mol⁻¹; PDI = 1.17.

PTMSPS-b-PTfeSS 4b

PTMSPS **2b** (0.5 g, 0.04 mmol), 2,2,2-trifluoroethyl 4-vinylbenzenesulfonate (1.2 g, 4.4 mmol) and 2,2'-azobisisobutyronitrile (2.2 mg, 0.013 mmol). ^1H NMR (300 MHz, DMSO- d_6): δ (ppm) 7.83-7.50 (m, 100H, aromatic $-\text{CH}=\text{C}-\text{SO}_3^-$), 7.00–6.18 (br m, 292H, other ArH), 4.82 (s, 100H, $-\text{SO}_3-\text{CH}_2-\text{CF}_3$), 4.67 (s, 96H, $-\text{OCH}_2$), 2.14–1.01 (br m, 316H, backbone CH, CH_2 , $\text{CN}-\text{CH}_2-\text{S}-$, $-\text{S}-\text{CH}_2-\text{C}_{10}\text{H}_{20}-\text{CH}_3$), 0.84 (t, 3H, $-\text{C}_{11}\text{H}_{22}-\text{CH}_3$), 0.12 (m, 432H, SiMe $_3$). SEC: $M_n = 13000 \text{ g mol}^{-1}$; PDI = 1.18.

PTMSPS-b-PTfeSS 4c

PTMSPS **2c** (0.5 g, 0.026 mmol), 2,2,2-trifluoroethyl 4-vinylbenzenesulfonate (0.7 g, 2.6 mmol) and 2,2'-azobisisobutyronitrile (1.3 mg, 0.008 mmol). ^1H NMR (300 MHz, DMSO- d_6): δ (ppm) 7.83-7.50 (m, 110H, aromatic $-\text{CH}=\text{C}-\text{SO}_3^-$), 7.00–6.18 (br m, 438H, other ArH), 4.82 (s, 110H, $-\text{SO}_3-\text{CH}_2-\text{CF}_3$), 4.67 (s, 164H, $-\text{OCH}_2$), 2.14–1.01 (br m, 433H, backbone CH, CH_2 , $\text{CN}-\text{CH}_2-\text{S}-$, $-\text{S}-\text{CH}_2-\text{C}_{10}\text{H}_{20}-\text{CH}_3$), 0.84 (t, 3H, $-\text{C}_{11}\text{H}_{22}-\text{CH}_3$), 0.12 (m, 738H, SiMe $_3$). SEC: $M_n = 16900 \text{ g mol}^{-1}$; PDI = 1.32.

Poly(4-propargyloxy)styrene)-block-poly(2,2,2-trifluorethyl styrene sulfonate) (PPS-b-PTfeSS 5a)

For deprotection of the alkyne group PTMSPS-*b*-PTfeSS **4a** (0.9 g, 0.046 mmol) was dissolved in THF (46.2 mL) and degassed with Argon for 10 min. At -20°C a degassed 1 M solution of tetrabutylammonium fluoride trihydrate and acetic acid (5.08 mL, 2.54 mmol) in THF was added dropwise. After 30 min at -20°C the temperature was raised to ROOM TEMPERATURE and the mixture was stirred for another 2 h. The resulting polymer was precipitated twice in methanol to remove the tetrabutylammonium salts. Filtration gave the deprotected polymer (0.66 g, 82%) as white powder. ^1H NMR (300 MHz, DMSO- d_6): δ (ppm) 7.83-7.50 (m, 102H, aromatic $-\text{CH}=\text{C}-\text{SO}_3^-$), 7.00–6.18 (br m, 202H, other ArH), 4.82 (s, 102H, $-\text{SO}_3-\text{CH}_2-\text{CF}_3$), 4.67 (s, 50H, $-\text{OCH}_2$), 3.47 (s, 25H, $-\text{C}\equiv\text{CH}$), 2.14–1.01 (br m, 250H, backbone CH, CH_2 , $\text{CN}-\text{CH}_2-\text{S}-$, $-\text{S}-\text{CH}_2-\text{C}_{10}\text{H}_{20}-\text{CH}_3$), 0.84 (t, 3H, $-\text{C}_{11}\text{H}_{22}-\text{CH}_3$). SEC: $M_n = 9800 \text{ g mol}^{-1}$; PDI = 1.13.

PPS-b-PTfeSS 5b

PTMSPS-*b*-PTfeSS **4b** (0.65 g, 0.026 mmol), 1 M solution of tetrabutylammonium fluoride trihydrate and acetic acid (3.17 mL, 1.6 mmol). ^1H NMR (300 MHz, DMSO- d_6): δ (ppm) 7.83-7.50 (m, 100H, aromatic $-\text{CH}=\text{C}-\text{SO}_3^-$), 7.00–6.18 (br m, 292H, other ArH), 4.82 (s, 100H, $-\text{SO}_3-\text{CH}_2-\text{CF}_3$), 4.67 (s, 96H, $-\text{OCH}_2$), 3.47 (s, 48H, $-\text{C}\equiv\text{CH}$), 2.14–1.01 (br m, 316H, backbone CH, CH_2 , $\text{CN}-\text{CH}_2-\text{S}-$, $-\text{S}-\text{CH}_2-\text{C}_{10}\text{H}_{20}-\text{CH}_3$), 0.84 (t, 3H, $-\text{C}_{11}\text{H}_{22}-\text{CH}_3$). SEC: $M_n = 11200 \text{ g mol}^{-1}$; PDI = 1.18.

PPS-b-PTfeSS 5c

PTMSPS-*b*-PTfeSS **4c** (0.65 g, 0.026 mmol), 1 M solution of tetrabutylammonium fluoride trihydrate and acetic acid (3.17 mL, 1.6 mmol). ^1H NMR (300 MHz, DMSO- d_6): δ (ppm) 7.83-7.50 (m, 110H, aromatic $-\text{CH}=\text{C}-\text{SO}_3^-$), 7.00–6.18 (br m, 438H, other ArH), 4.82 (s, 110H, $-\text{SO}_3-\text{CH}_2-\text{CF}_3$), 4.67 (s, 164H, $-\text{OCH}_2$), 3.47 (s, 82H, $-\text{C}\equiv\text{CH}$), 2.14–1.01 (br m, 433H, backbone CH, CH_2 , $\text{CN}-\text{CH}_2-\text{S}-$, $-\text{S}-\text{CH}_2-\text{C}_{10}\text{H}_{20}-\text{CH}_3$), 0.84 (t, 3H, $-\text{C}_{11}\text{H}_{22}-\text{CH}_3$). SEC: $M_n = 11700 \text{ g mol}^{-1}$; PDI = 1.36.

Poly(N,N'-bis(4-methoxyphenyl)-N-phenyl-N'-4-triazolylphenyl-(1,1'-biphenyl)-4,4'-diamine)-block-poly(2,2,2-trifluorethyl styrene sulfonate) (PDMTPD-b-PTfeSS 7a)

Under nitrogen, PPS-*b*-PTfeSS **5a** (0.28 g, 0.016 mmol) and DMTPD-N₃ **6** (0.29 g, 0.47 mmol) were dissolved in THF (8.7 mL) and degassed with Argon for 20 min. To start the reaction a degassed 5 mM solution of Copper(I) bromide and *N,N,N',N',N*-pentamethyldiethylenetriamine (0.94 mL, 4.7 μmol) in THF was added dropwise and the mixture was stirred overnight. The solvent was reduced under vacuum and the concentrated polymer was precipitated in diethyl ether. To remove the copper catalyst the polymer was dissolved in THF and passed an Alox N column. Finally it was again precipitated in methanol. Filtration gave 0.36 g (70%) of yellow polymer. ¹H NMR (300 MHz, THF-*d*₈): δ (ppm) 8.03-7.51 (m, 127H, Triazol-*H*, aromatic –CH=C-SO₃-), 7.42-6.14 (br m, 702H, other ArH), 5.31 (br s, 50H, -N-CH₂-DMTPD), 4.96 (s, 102H, -SO₃-CH₂-CF₃), 4.69 (s, 50H, -OCH₂), 3.67-3.54 (m, 150H, OCH₃), 2.19–1.01 (br m, 250H, backbone CH, CH₂, CN-CH₂-S-, -S-CH₂-C₁₀H₂₀-CH₃), 0.84 (t, 3H, -C₁₁H₂₂-CH₃). SEC: M_n = 17600 g mol⁻¹; PDI = 1.17.

PDMTPD-b-PTfeSS 7b

PPS-*b*-PTfeSS **5b** (0.5 g, 0.024 mmol), DMTPD-N₃ **6** (0.86 g, 1.42 mmol), 5 mM solution of Copper(I) bromide and *N,N,N',N',N*-pentamethyldiethylenetriamine (2.84 mL, 0.014 mmol). ¹H NMR (300 MHz, THF-*d*₈): δ (ppm) 8.03-7.51 (m, 148H, Triazol-*H*, aromatic –CH=C-SO₃-), 7.42-6.14 (br m, 1252H, other ArH), 5.31 (br s, 96H, -N-CH₂-DMTPD), 4.96 (s, 100H, -SO₃-CH₂-CF₃), 4.69 (s, 96H, -OCH₂), 3.67-3.54 (m, 288H, OCH₃), 2.19–1.01 (br m, 316H, backbone CH, CH₂, CN-CH₂-S-, -S-CH₂-C₁₀H₂₀-CH₃), 0.84 (t, 3H, -C₁₁H₂₂-CH₃). SEC: M_n = 21600 g mol⁻¹; PDI = 1.12.

PDMTPD-b-PTfeSS 7c

PPS-*b*-PTfeSS **5c** (0.25 g, 8.9 μmol), DMTPD-N₃ **6** (0.54 g, 0.89 mmol), 5 mM solution of Copper(I) bromide and *N,N,N',N',N*-pentamethyldiethylenetriamine (1.78 mL, 8.9 μmol). ¹H NMR (300 MHz, THF-*d*₈): δ (ppm) 8.03-7.51 (m, 192H, Triazol-*H*, aromatic –CH=C-SO₃-), 7.42-6.14 (br m, 2078H, other ArH), 5.31 (br s, 164H, -N-CH₂-DMTPD), 4.96 (s, 110H, -SO₃-CH₂-CF₃), 4.69 (s, 164H, -OCH₂), 3.67-3.54 (m, 492H, OCH₃), 2.19–1.01 (br m, 433H, backbone CH, CH₂, CN-CH₂-S-, -S-CH₂-C₁₀H₂₀-CH₃), 0.84 (t, 3H, -C₁₁H₂₂-CH₃). SEC: M_n = 30100 g mol⁻¹; PDI = 1.26.

Poly(N,N'-bis(4-methoxyphenyl)-N-phenyl-N'-4-triazolylphenyl-(1,1'-biphenyl)-4,4'-diamine)-block-poly(tetrabutylammonium styrene sulfonate) (PDMTPD-b-PEt₃NH⁺SS 8a)

PDMTPD-*b*-PTfeSS **7a** (0.2 g, 6.13 μmol) was dissolved in DMSO (5 mL). A 1 M solution of tetrabutylammonium hydroxide (1.35 mL, 1.35 mmol) in methanol was slowly added and the mixture was stirred for 24 h. The resulting polymer was precipitated in ethyl acetate and redissolved in DMF (5 mL). For exchange of the counterion, a 1 M solution of triethylamine hydrochloride (1.0 mL, 1.0 mmol) was slowly added and the polymer was again precipitated in ethyl acetate. After filtration 0.18 g (87%) of a yellow polymer were obtained. To prove the deprotection, the NMR was conducted in deuterated DMSO, which gives the best resolution for the ionic block. However, the segment comprising DMTPD aggregates in DMSO forming micellar structures. In consequence, the signals of this block are not fully resolved in the NMR analysis and they are only partially considered in the following overview. ¹H NMR (300 MHz, DMSO-*d*₆): δ (ppm) 9.10-8.86 (s, Et₃NH⁺), 7.96-6.14 (br m, all ArH), 3.70-3.23 (br m, OCH₃), 3.15-2.88 (q,

$(\text{CH}_3\text{-CH}_2)_3\text{-NH}^+$, 2.19–1.01 (br m, backbone CH, CH₂, CN-CH₂-S-, -S-CH₂-C₁₀H₂₀-CH₃, $(\text{CH}_3\text{-CH}_2)_3\text{-NH}^+$), 0.84 (t, 3H, -C₁₁H₂₂-CH₃).

PDMTPD-b-PEt₃NH⁺SS 8b

PDMTPD-*b*-PTfeSS **7b** (0.2 g, 4.0 μmol), 1 M solution of tetrabutylammonium hydroxide (1.35 mL, 1.35 mmol), 1 M solution of triethylamine hydrochloride (1.0 mL, 1.0 mmol). ¹H NMR (300 MHz, DMSO-*d*₆): δ (ppm) 9.10-8.86 (s, Et₃NH⁺), 7.96-6.14 (br m, all ArH), 3.70-3.23 (br m, OCH₃), 3.15-2.88 (q, $(\text{CH}_3\text{-CH}_2)_3\text{-NH}^+$), 2.19–1.01 (br m, backbone CH, CH₂, CN-CH₂-S-, -S-CH₂-C₁₀H₂₀-CH₃, $(\text{CH}_3\text{-CH}_2)_3\text{-NH}^+$), 0.84 (t, 3H, -C₁₁H₂₂-CH₃).

PDMTPD-b-PEt₃NH⁺SS 8c

PDMTPD-*b*-PTfeSS **7c** (0.2 g, 2.58 μmol), 1 M solution of tetrabutylammonium hydroxide (1.35 mL, 1.35 mmol), 1 M solution of triethylamine hydrochloride (1.0 mL, 1.0 mmol). ¹H NMR (300 MHz, DMSO-*d*₆): δ (ppm) 9.10-8.86 (s, Et₃NH⁺), 7.96-6.14 (br m, all ArH), 3.70-3.23 (br m, OCH₃), 3.15-2.88 (q, $(\text{CH}_3\text{-CH}_2)_3\text{-NH}^+$), 2.19–1.01 (br m, backbone CH, CH₂, CN-CH₂-S-, -S-CH₂-C₁₀H₂₀-CH₃, $(\text{CH}_3\text{-CH}_2)_3\text{-NH}^+$), 0.84 (t, 3H, -C₁₁H₂₂-CH₃).

ASSOCIATED CONTENT

Supporting Information: Synthesis of the monomers, detailed characterization of polymers including SEC and DSC, cryo-TEM of polymer solution in DMF, GISAXS analysis of as-cast and thermal annealed films, AFM images of thermal annealed samples, large area AFM images of solvent annealed samples. This material is available free of charge *via* the Internet at <http://pubs.acs.org>.

ACKNOWLEDGMENT

We thank X. Shen and B. Toga for the help with the preparation, GISAXS and TGA measurements. K. Neumann and M. Förtsch are acknowledged for the SEC and TEM measurements, respectively. Financial support from SFB 840 and the Elitenetzwerk Bayern (ENB), Macromolecular Science, (BCP synthesis and characterization) are kindly acknowledged. OPV characterization was supported by Polymer-Based Materials for Harvesting Solar Energy, an Energy Frontier Research Center funded by the U.S. Department of Energy, Office of Science, Office of Basic Energy Sciences under contract DE-SC0001087. BCP alignment and GISAXS characterization was supported by the U.S. Department of Energy, Office of Basic Energy Sciences under contract DOE-DE-FG02-45612.

REFERENCES

- (1) M. C. Orilall, U. Wiesner, *Chem. Soc. Rev.* **2011**, *40*, 520-535.
- (2) N. Haberkorn, M. C. Lechmann, B. H. Sohn, K. Char, J. S. Gutmann, P. Theato, *Macromol. Rapid Commun.* **2009**, *30*, 1146-1166.
- (3) S. Förster, M. Antonietti, *Adv. Mater.* **1998**, *10*, 195-217.
- (4) L. Tsarkova, G. J. A. Sevink, G. Krausch, Nanopattern Evolution in Block Copolymer Films: Experiment, Simulations and Challenges in *Complex Macromolecular Systems I*; A. H. E. Müller, H.-W. Schmidt, Eds.; Springer Berlin Heidelberg: **2010**; Vol. 227, p 33-73.
- (5) S. B. Darling, *Prog. Polym. Sci.* **2007**, *32*, 1152-1204.
- (6) C. J. Hawker, T. P. Russell, *MRS Bulletin* **2005**, *30*, 952-966.
- (7) T. Thurn-Albrecht, J. Schotter, G. A. Kästle, N. Emley, T. Shibauchi, L. Krusin-Elbaum, K. Guarini, C. T. Black, M. T. Tuominen, T. P. Russell, *Science* **2000**, *290*, 2126-2129.
- (8) T. L. Morkved, M. Lu, A. M. Urbas, E. E. Ehrichs, H. M. Jaeger, P. Mansky, T. P. Russell, *Science* **1996**, *273*, 931-933.
- (9) L. Rockford, Y. Liu, P. Mansky, T. P. Russell, M. Yoon, S. G. J. Mochrie, *Phys. Rev. Lett.* **1999**, *82*, 2602-2605.
- (10) S. Ouk Kim, H. H. Solak, M. P. Stoykovich, N. J. Ferrier, J. J. de Pablo, P. F. Nealey, *Nature* **2003**, *424*, 411-414.
- (11) J.-B. Chang, J. G. Son, A. F. Hannon, A. Alexander-Katz, C. A. Ross, K. K. Berggren, *ACS Nano* **2012**, *6*, 2071-2077.
- (12) H. Jung, D. Hwang, E. Kim, B.-J. Kim, W. B. Lee, J. E. Poelma, J. Kim, C. J. Hawker, J. Huh, D. Y. Ryu, J. Bang, *ACS Nano* **2011**, *5*, 6164-6173.
- (13) S. Hüttner, M. Sommer, A. Chiche, G. Krausch, U. Steiner, M. Thelakkat, *Soft Matter* **2009**, *5*, 4206-4211.
- (14) S. Park, J.-Y. Wang, B. Kim, J. Xu, T. P. Russell, *ACS Nano* **2008**, *2*, 766-772.
- (15) D. H. Lee, S. Park, W. Gu, T. P. Russell, *ACS Nano* **2011**, *5*, 1207-1214.
- (16) G. Kim, M. Libera, *Macromolecules* **1998**, *31*, 2569-2577.
- (17) K. Fukunaga, H. Elbs, R. Magerle, G. Krausch, *Macromolecules* **2000**, *33*, 947-953.
- (18) S. H. Kim, M. J. Misner, T. Xu, M. Kimura, T. P. Russell, *Adv. Mater.* **2004**, *16*, 226-231.
- (19) S. Park, D. H. Lee, J. Xu, B. Kim, S. W. Hong, U. Jeong, T. Xu, T. P. Russell, *Science* **2009**, *323*, 1030-1033.
- (20) E. Kim, H. Ahn, S. Park, H. Lee, M. Lee, S. Lee, T. Kim, E.-A. Kwak, J. H. Lee, X. Lei, J. Huh, J. Bang, B. Lee, D. Y. Ryu, *ACS Nano* **2013**, *7*, 1952-1960.
- (21) P. Goldberg-Oppeneheimer, D. Kabra, S. Vignolini, S. Hüttner, M. Sommer, K. Neumann, M. Thelakkat, U. Steiner, *Chem. Mater.* **2013**, *25*, 1063-1070.
- (22) S. Hüttner, M. Sommer, U. Steiner, M. Thelakkat, *Appl. Phys. Lett.* **2010**, *96*, 073503-073503.
- (23) C.-L. Liu, C.-H. Lin, C.-C. Kuo, S.-T. Lin, W.-C. Chen, *Prog. Polym. Sci.* **2011**, *36*, 603-637.
- (24) K. D. Gatsouli, S. Pispas, E. I. Kamitsos, *J. Phys. Chem. C* **2007**, *111*, 15201-15209.
- (25) R. S. Yelamanchili, Y. Lu, T. Lunkenbein, N. Miyajima, L.-T. Yan, M. Ballauff, J. Brey, *Small* **2009**, *5*, 1326-1333.
- (26) J. C. Brendel, H. Burchardt, M. Thelakkat, *J. Mater. Chem.* **2012**, *22*, 24386-24393.
- (27) J. C. Brendel, Y. Lu, M. Thelakkat, *J. Mater. Chem.* **2010**, *20*, 7255-7265.
- (28) Y. Lu, M. Hoffmann, R. S. Yelamanchili, A. Terrenoire, M. Schrinner, M. Drechsler, M. W. Möller, J. Brey, M. Ballauff, *Macromol. Chem. Phys.* **2009**, *210*, 377-386.
- (29) G. Moad, E. Rizzardo, S. H. Thang, *Aust. J. Chem.* **2005**, *58*, 379-410.
- (30) G. Moad, M. Chen, M. Haussler, A. Postma, E. Rizzardo, S. H. Thang, *Polym. Chem.* **2011**, *2*, 492-519.
- (31) C. Boyer, V. Bulmus, T. P. Davis, V. Ladmiral, J. Liu, S. b. Perrier, *Chem. Rev.* **2009**, *109*, 5402-5436.

- (32) S. Maria, A. S. Susha, M. Sommer, D. V. Talapin, A. L. Rogach, M. Thelakkat, *Macromolecules* **2008**, *41*, 6081-6088.
- (33) M. Sommer, A. S. Lang, M. Thelakkat, *Angew. Chem., Int. Ed.* **2008**, *47*, 7901-7904.
- (34) A. S. Lang, M. Thelakkat, *Polym. Chem.* **2011**, *2*, 2213-2221.
- (35) P. Müller-Buschbaum, *Anal. Bioanal. Chem.* **2003**, *376*, 3-10.
- (36) J. R. Levine, J. B. Cohen, Y. W. Chung, P. Georgopoulos, *J. Appl. Crystallogr.* **1989**, *22*, 528-532.
- (37) S. Park, J.-Y. Wang, B. Kim, W. Chen, T. P. Russell, *Macromolecules* **2007**, *40*, 9059-9063.
- (38) M. C. Lechmann, D. Kessler, J. S. Gutmann, *Langmuir* **2009**, *25*, 10202-10208.
- (39) A. E. Javier, S. N. Patel, D. T. Hallinan, V. Srinivasan, N. P. Balsara, *Angew. Chem., Int. Ed.* **2011**, *50*, 9848-9851.

SUPPORTING INFORMATION

Experimental

Synthesis of monomers

Synthesis of *N,N'*-bis(4-methoxyphenyl)-*N*-phenyl-*N'*-4-azidophenyl-(1,1'-biphenyl)-4,4'-diamine dimethoxy triphenyl diamine (DMTPD-N₃ 6):

Starting material for the synthesis was the DMTPD-aldehyde which was synthesized according to literature procedures published elsewhere.²

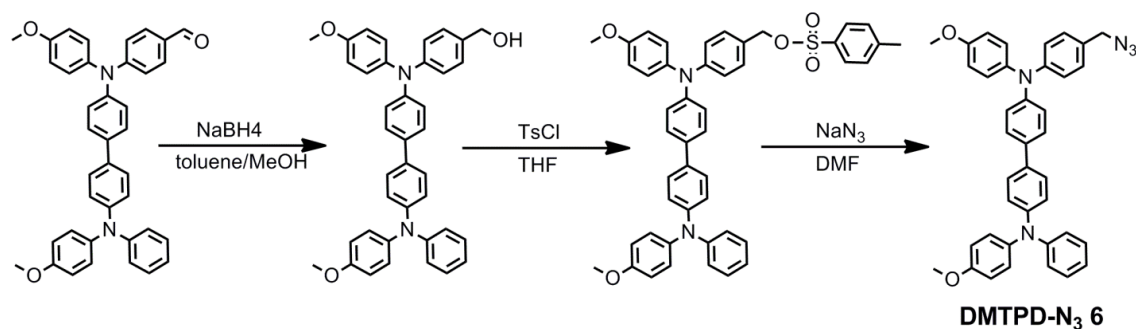


Figure 6–S1. Synthesis of an azide carrying DMTPD-N₃ 6 starting from the DMTPD-mono aldehyde.

Dimethoxy triphenyl diamine alcohol (DMTPD-OH)

DMTPD-aldehyde (0.72 g, 1.3 mmol) was dissolved in 15 mL of a 1:1 mixture of dry toluene and dry ethanol under inert gas atmosphere. NaBH₄ (95 mg, 2.50 mmol) was added and the reaction was stirred for 2h at RT. The progress of the reaction was controlled by thin film chromatography. The solvents were evaporated, the residue was washed with H₂O two times, filtered and dried. The light yellow powder weighed 720 mg (99.5%). ¹H NMR (300 MHz, DMSO-d₆): δ (ppm) 7.52-6.83 (m, 24 H, ArH), 5.11 (t, 1 H, *J* = 5.2 Hz, CH₂OH), 4.43 (d, 2H, *J* = 4.0 Hz, CH₂OH), 3.74 (s, 6H, OCH₃).

Dimethoxy triphenyl diamine tosylate (DMTPD-Tos)

DMTPD-OH (579 mg, 1.00 mmol) was dissolved in 15 mL of THF under inert gas atmosphere. Triethylamine (0.7 mL) was added to the solution which was stirred for 10 min. Subsequently, tosylchloride (1.91 g, 10.0 mmol) was added and the reaction was stirred for 24 h at RT. The solvents were evaporated, dissolved in CHCl₃ and washed with a solution of NH₄Cl in H₂O. The organic phase was dried with sodium sulphate, filtered and evaporated. The raw product was further purified by column chromatography over silica cyclohexane:ethyl acetate 2:1 to remove side products. The pure fraction was flushed from the column with DCM:MeOH 1:1 afterwards. The fractions containing the product were evaporated. The light yellow powder weighed 558 mg (76.1%). ¹H NMR (300 MHz, DMSO-d₆): δ (ppm) 7.61-6.83 (m, 28H, ArH_{TPD}, ArH_{Tosyl}), 4.36 (s, 2H, CH₂O), 3.76 (s, 6H, OCH₃), 2.10 (s, 3H, ArCH₃).

Dimethoxy triphenyl diamine azide (DMTPD-N₃ 6)

DMTPD-Tosylat (550 mg, 0.75 mmol) was dissolved in dry DMF under inert gas atmosphere. NaN₃ (97 mg, 1.50 mmol) was added and the reaction was heated to 100°C for 3 h. After cooling to RT the reaction was quenched with 10 mL of H₂O. The product was extracted with CHCl₃, the organic phase was dried with sodium sulfate, filtered and evaporated. For further purification, the compound was cleaned by column chromatography over silica with a gradient of hexanes:ethyl acetate 9:1 to 5:1. The product was obtained as a light yellow powder and weighed 330 mg (72.8%). ¹H NMR (300 MHz, DMSO-d₆): δ (ppm) 7.56-6.88 (m, 24H, ArH), 4.36 (s, 2H, CH₂N₃), 3.75 (s, 6H, OCH₃).

Synthesis of 2,2,2-trifluorethyl 4-vinylbenzenesulfonate (TfeSS 3):

Under Argon, Sodium styrenesulfonate (10 g, 43.6 mmol) was added in small portions to thionyl chloride (15.93 ml, 218 mmol) with 10 min at 0°C while stirring. To the resulting suspension DMF (22 ml) was added dropwise under cooling. The reaction system became homogeneous and it was stirred for 3 h at RT. The mixture was poured into ice water to quench unreacted thionyl chloride. The organic layers were extracted with diethyl ether and washed with 2% HCl solution and water repeatedly. The mixture was dried over sodium sulfate and the solvent was removed under reduced pressure. The product 4-vinylbenzene-1-sulfonyl chloride (8.5 g, yield: 96%) was immediately frozen to suppress the hydrolysis of the sulfonyl chloride and was used without further purification.

2,2,2-Trifluoroethanol (3.42 ml, 45.3 mmol) and triethylamine (6.43 ml, 46.1 mmol) was dissolved in CH₂Cl₂ (41.9 ml) and cooled to 0°C. Styrene sulfonyl chloride (8.5 g, 41.9 mmol) was dropwise added to the solution and kept for 2 h at 0°C. After stirring at RT overnight the reaction mixture was washed twice with water and the organic layer was dried over sodium sulphate. The solvent was removed under reduced pressure and the raw product was purified by column chromatography (DCM:pentane 1:2) to obtain 10 g (90%) of a viscous oil, which crystallized at 4°C.

Size exclusion chromatography (SEC)

Eluent: pure THF

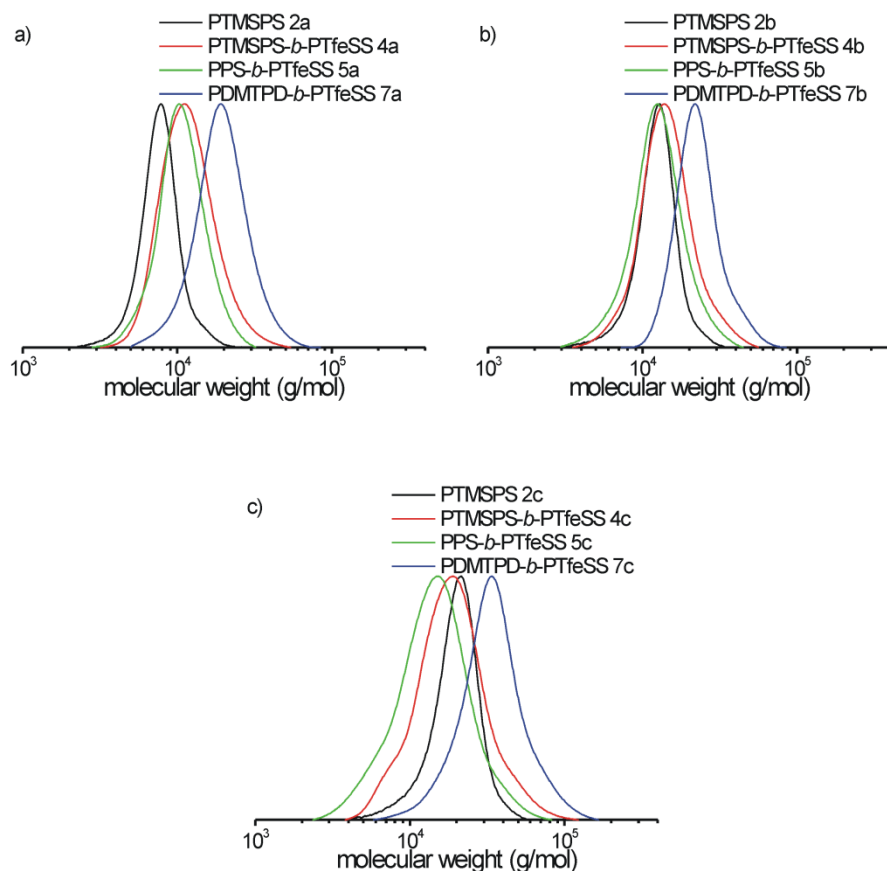


Figure 6–S2. Normalized SEC traces of the intermediate steps to the different polymers PDMTPD-*b*-PEt₃NH⁺SS 8a (a), PDMTPD-*b*-PEt₃NH⁺SS 8b (b) and PDMTPD-*b*-PEt₃NH⁺SS 8c (c). PTMSPS 2: black, PTMSPS-*b*-PTfeSS 4: red, PPS-*b*-PTfeSS 5: green and PDMTPD-*b*-PTfeSS 7: blue. The final polymers PDMTPD-*b*-PEt₃NH⁺SS could not be measured in SEC, due to a strong interaction of the polyelectrolyte with the column material. The eluent was THF and the SEC was calibrated according to polystyrene standards.

Eluent: THF with 0.25% tetrabutylammoniumbromide

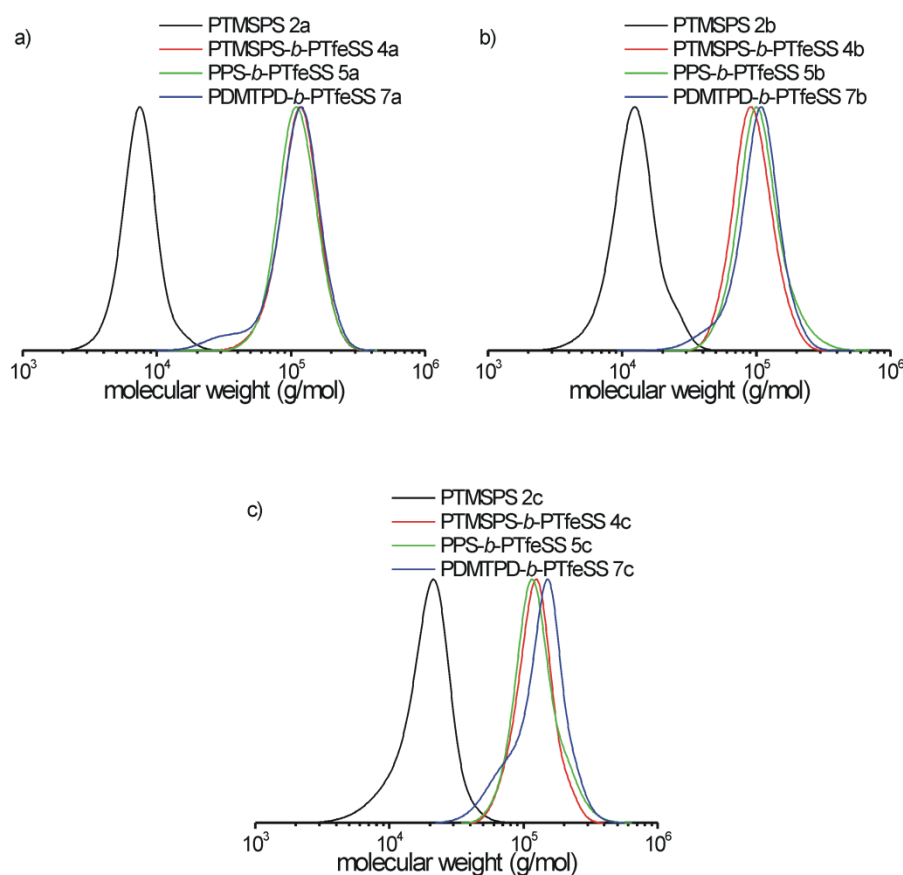


Figure 6-S3. Normalized SEC traces of the intermediate steps to the different polymers PDMTPD-*b*-PEt₃NH⁺SS 8a (a), PDMTPD-*b*-PEt₃NH⁺SS 8b (b) and PDMTPD-*b*-PEt₃NH⁺SS 8c (c). PTMSPS 2: black, PTMSPS-*b*-PTfeSS 4: red, PPS-*b*-PTfeSS 5: green and PDMTPD-*b*-PTfeSS 7: blue. The final polymers PDMTPD-*b*-PEt₃NH⁺SS could not be measured in SEC, due to a strong interaction of the polyelectrolyte with the column material. Here, the eluent was THF with 0.25% tetrabutylammoniumbromide and the SEC was calibrated according to polystyrene standards.

Differential scanning calorimetry (DSC)

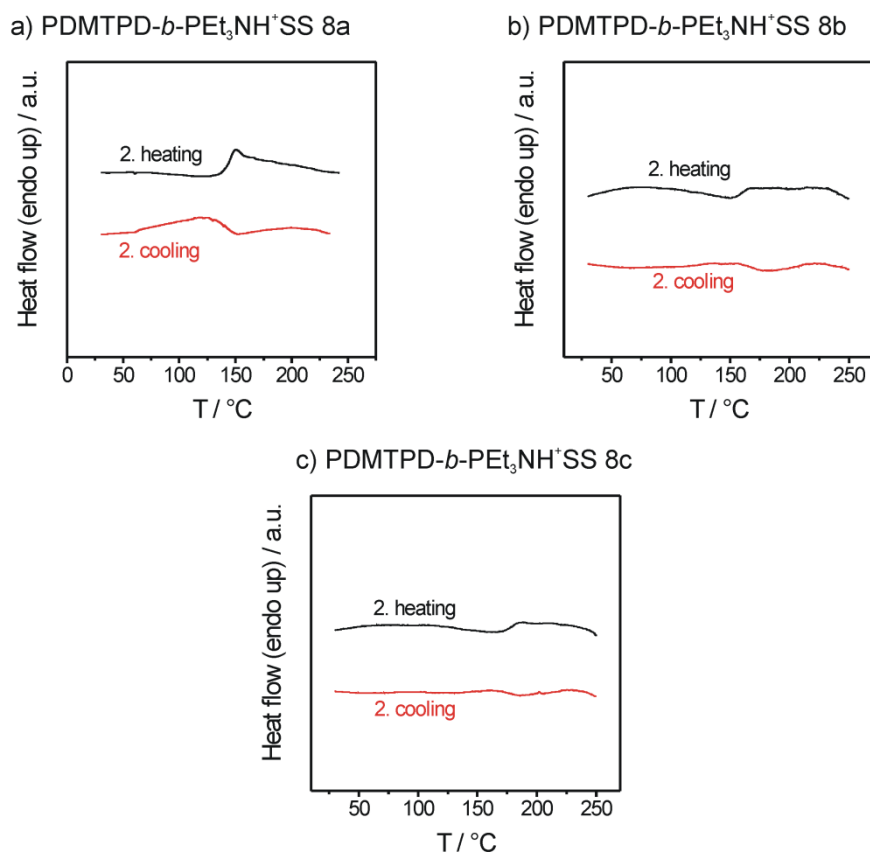


Figure 6–S4. Differential scanning calorimetry (DSC) traces of the polymers PDMTPD-*b*-PEt₃NH⁺SS 8a (a), PDMTPD-*b*-PEt₃NH⁺SS 8b (b) and PDMTPD-*b*-PEt₃NH⁺SS 8c (c) measured at 10 K/min. The individual polymers show only one T_g at 144 °C (a), 162 °C (b) and 178 °C (c) respectively.

Cryo-TEM

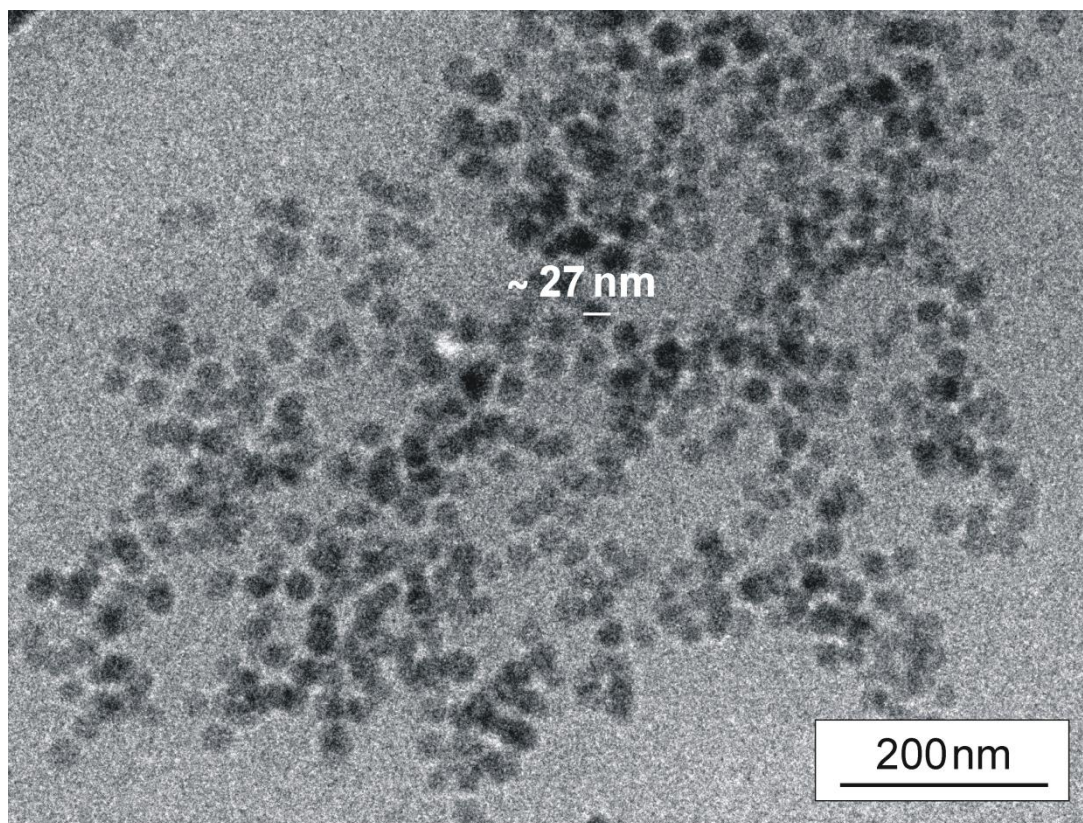


Figure 6–S5. Typical Cryo-transmission electron micrograph of a 1 wt% solution of PDMTPD-*b*- PEt₃NH⁺SS 8c in DMF.

Grazing incident small angle X-ray scattering (GISAXS)

Full scattering patterns of as cast samples:

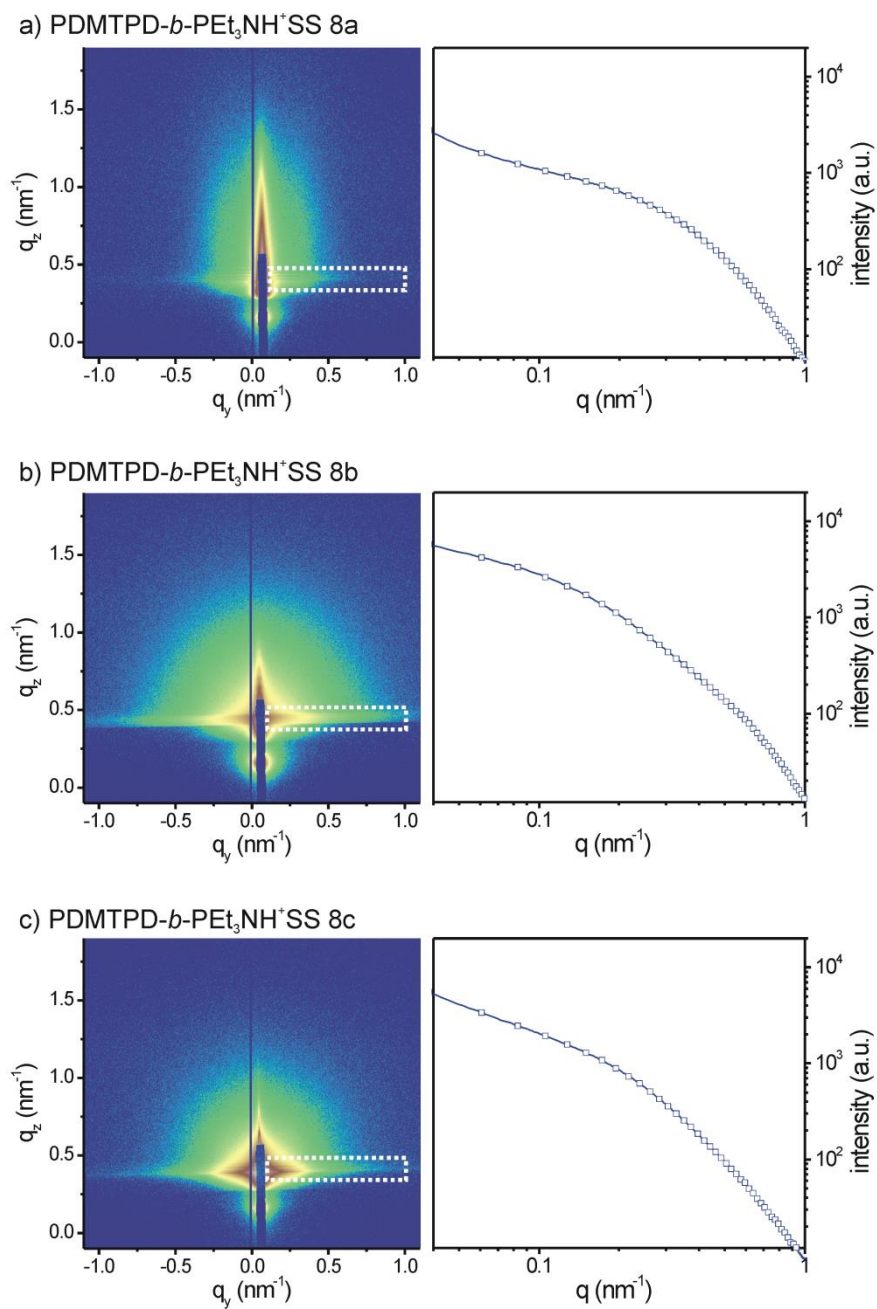


Figure 6–S6. Grazing incident small angle X-ray scattering patterns of the thin films made by spin coating a 10 wt% solution of PDMTPD-*b*-PEt₃NH⁺SS 8a (a), PDMTPD-*b*-PEt₃NH⁺SS 8b (b) and PDMTPD-*b*-PEt₃NH⁺SS 8c (c) in DMF.

Full scattering patterns of thermal annealed samples:

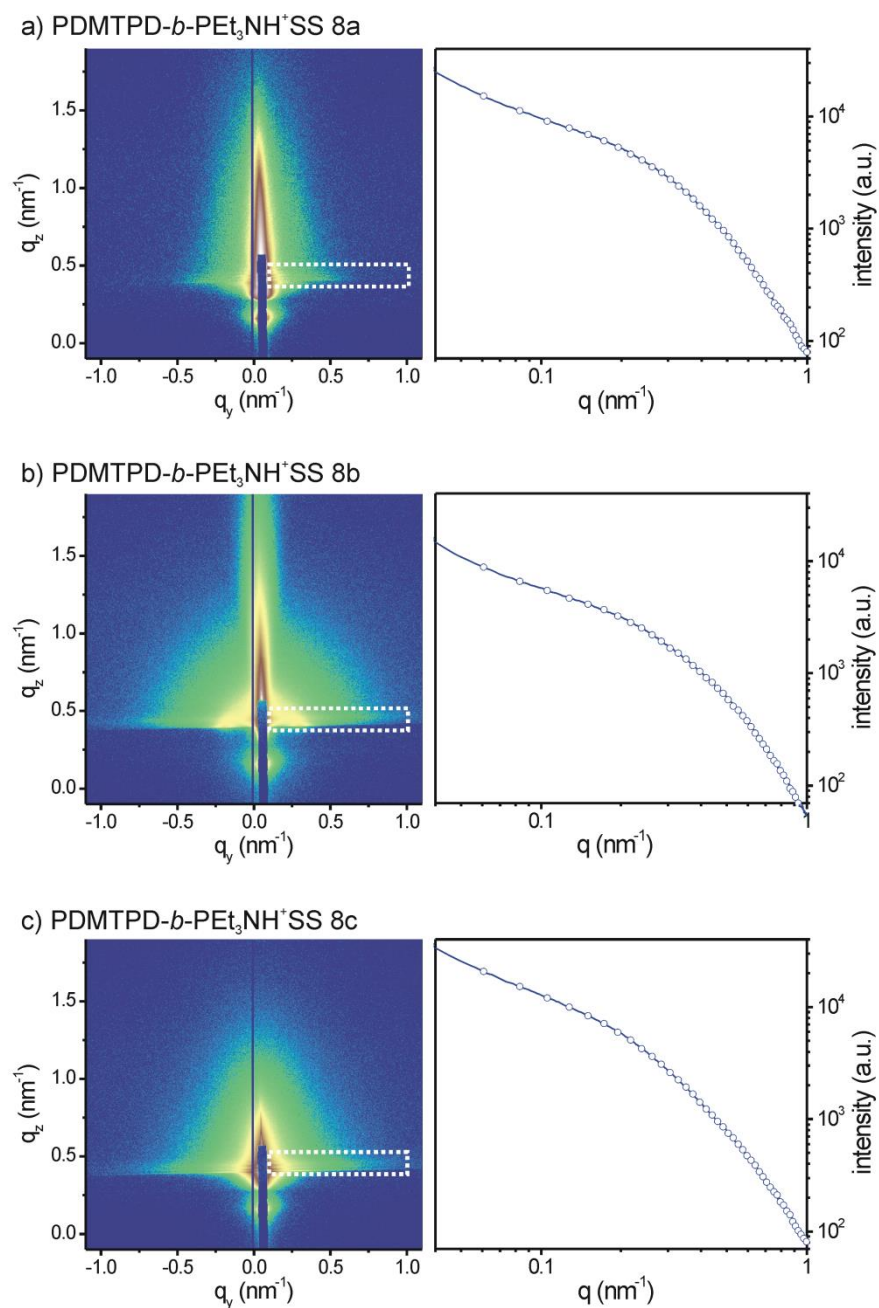


Figure 6-S7. Grazing incident small angle X-ray scattering patterns of the thin films made by spin coating a 10 wt% solution of PDMTPD-*b*-PEt₃NH⁺SS 8a (a), PDMTPD-*b*-PEt₃NH⁺SS 8b (b) and PDMTPD-*b*-PEt₃NH⁺SS 8c (c) in DMF. The films were annealed at 159°C (a), 177°C (b) and 193°C (c) for 6 h.

Atomic force microscopy (AFM)

*PDMTPD-*b*-PEt₃NH⁺SS 3 before and after thermal annealing:*

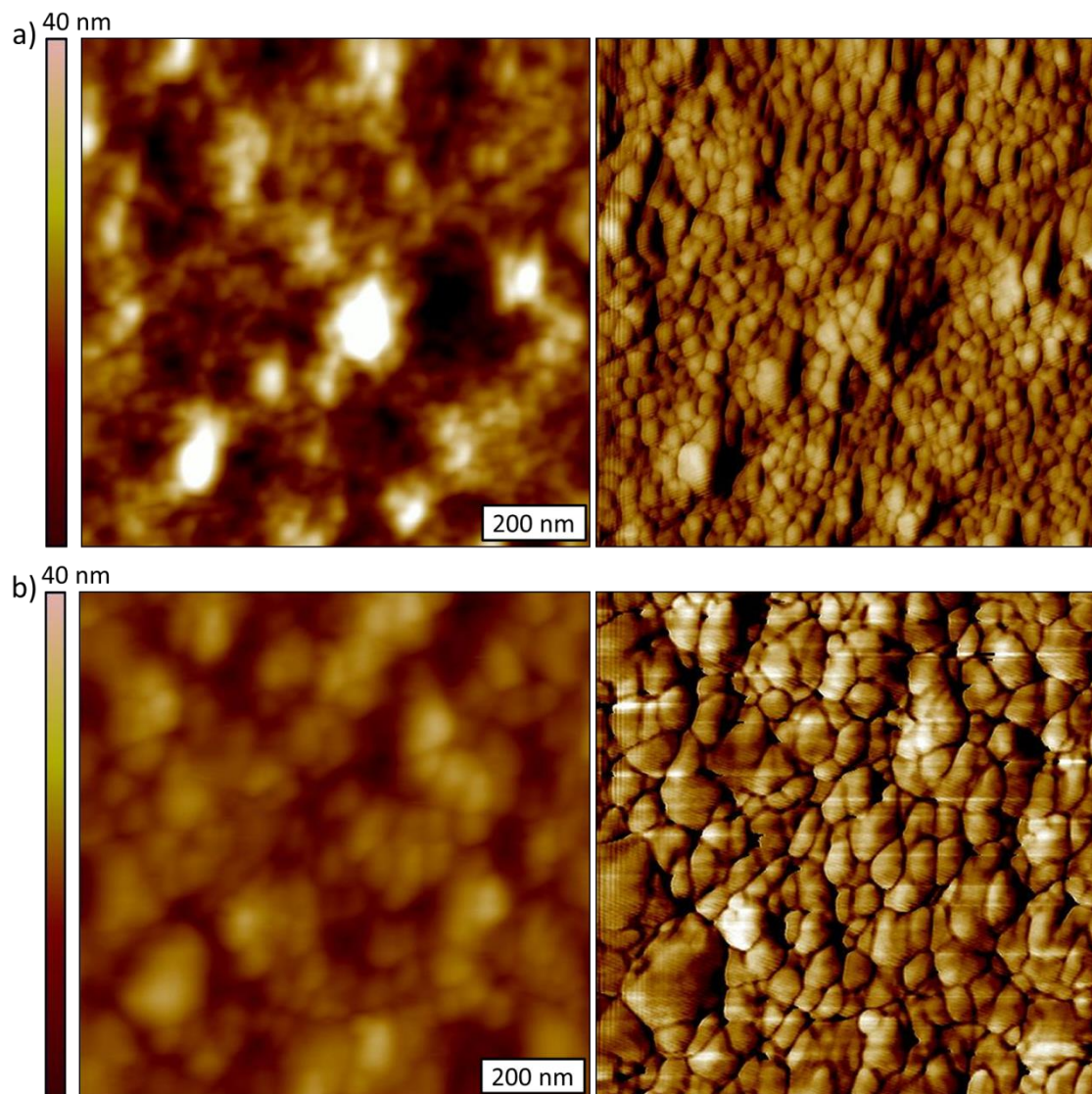


Figure 6–S8. AFM images (height: left, phase: right) of sample PDMTPD-*b*-PEt₃NH⁺SS 8c before (a) and after (b) thermal annealing at 193°C for 6 h.

Solvent annealed samples with lower magnification:

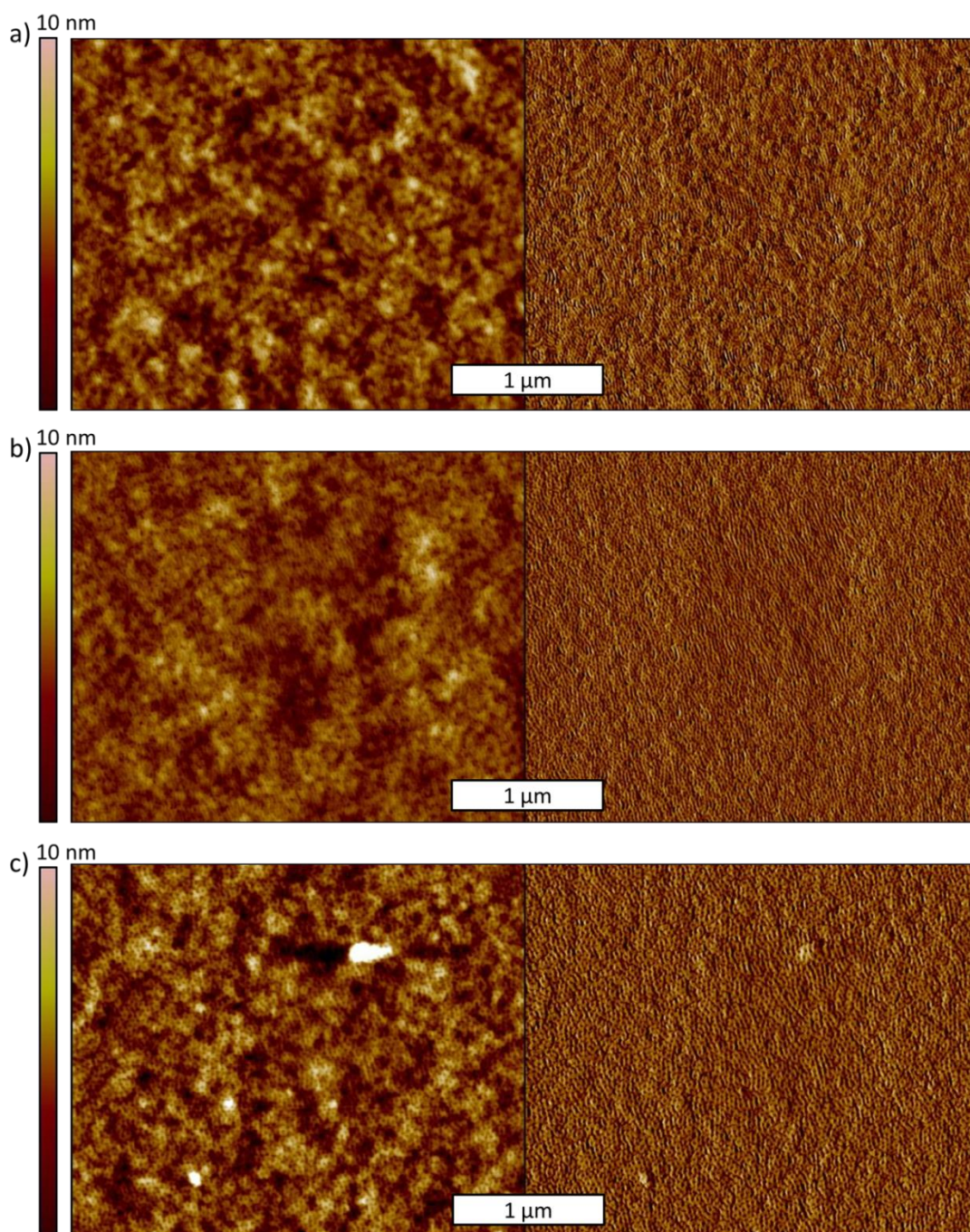


Figure 6-S9. AFM height (left) and phase (right) images of thin films made by spin coating a 10 wt% solution of PDMTPD-*b*-PEt₃NH⁺SS 8a (a), PDMTPD-*b*-PEt₃NH⁺SS 8b (b) and PDMTPD-*b*-PEt₃NH⁺SS 8c (c) in DMF. The films were annealed in saturated DMF vapor for 4 days.

References

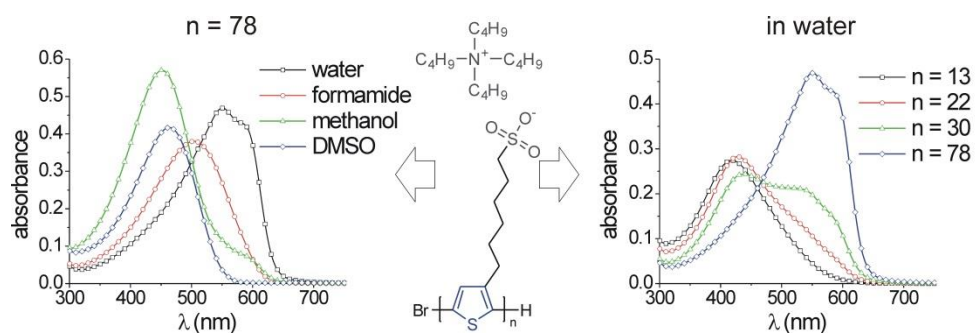
- (1) A. S. Lang, M. Thelakkat, *Polym. Chem.* **2011**, *2*, 2213-2221.
- (2) M. Sommer, S. M. Lindner, M. Thelakkat, *Adv. Funct. Mater.* **2007**, *17*, 1493-1500.

7. OPTICAL PROPERTIES OF WELL-DEFINED CONJUGATED POLYELECTROLYTES: INFLUENCE OF MOLECULAR WEIGHT, CONCENTRATION, SOLVENT AND ADDED SALT

Johannes C. Brendel, Martina Schmidt, Mukundan Thelakkat*

Applied Functional Polymers, Macromolecular Chemistry I, University of Bayreuth, 95440 Bayreuth, Germany

*E-mail of corresponding author: mukundan.thelakkat@uni-bayreuth.de



Prepared for submission.

ABSTRACT

Conjugated polyelectrolytes (CPE) attract considerable attention as sensor or interface materials in chemistry and biology and are subject matter of intensive studies concerning the conjugated backbone structure and the ionic groups. However, so far the influence of molecular weight of polyelectrolytes on their optical properties has not been studied as most CPEs are prepared *via* uncontrolled polycondensation reactions. Here, we present the synthesis and characterization of well-defined anionic conjugated polyelectrolytes comprising a polythiophene backbone and sulfonate side groups. Using the Kumada catalyst transfer polymerization we prepared four polymers with different molecular weights. Optimizing the subsequent substitution reaction we quantitatively converted the bromine side groups into anionic sulfonate groups giving the desired well-defined conjugated polyelectrolytes. The resulting polymers were studied in detail regarding their aggregation by monitoring the optical properties in solution. The CPEs aggregate in aqueous solutions. Further, a strong dependency of the polymer aggregation on the molecular weight was observed in aqueous solution. A concentration dependent aggregation was detected for medium chain lengths, while short chains remain unaffected. Long polymer chains are permanently aggregated in water. Further experiments revealed the dissolution of aggregates in organic solvents in contrast to water. This finding recommends that the hydrophobic character of the polymer backbone abets the aggregation in aqueous solution. Finally, we studied the influence of the salt concentration of the aqueous solution on the polymer properties and a continuous disintegration of the aggregates is observed with increasing ionic strengths of the solution. The screening effect of the ions reduces the coulomb repulsion between adjacent repeating units and induces an enhanced flexibility to the polymer chain. The corresponding increase in fluorescence intensity due to deagglomeration could be quantified both in organic solvents and in the presence of salt.

INTRODUCTION

Conjugated polyelectrolytes (CPEs) find widespread applications in photovoltaic devices, organic light emitting devices, photodetectors or chemical and biological sensors.^{1,2} A key issue for the development of functional CPEs for all these applications is certainly a detailed understanding of structure-property relationships. Especially the optical properties are considerably influenced by the backbone conformation and π - π interactions induced by aggregation. Several CPEs have already been studied concerning their optical properties and the influence of different backbone structures, ionic side groups and the surrounding media. Early reports focused on the synthesis, structure and optical properties of conjugated ionic poly(*p*-phenylene) (PPP) derivatives with either anionic or cationic side groups.³⁻⁷ Reynolds and Schanze *et al.* further paid particular attention to poly(*p*-phenylene ethynylene) (PPE) derivatives.⁸⁻¹⁰ The strong fluorescence of these polymers makes them promising materials for sensor applications.^{11,12} Further alternatives for the conjugated backbone are polyfluorenes (PF) and polythiophenes (PT).¹³⁻¹⁵ CPEs based on polythiophene were already prepared 1987 using electropolymerization of ionic monomers.¹⁶ While CPEs based on polyphenylene derivatives are mainly characterized by their stiff backbones, polythiophenes exhibit several backbone configurations inducing a considerable flexibility to the structure.¹⁷ These structural variations are related to the tilted bond angle between the repeating units and they have a major influence on the π -conjugation which

decides the optical and electronical properties of the polymers. Additionally, configuration changes in the backbone structure can be induced by external stimuli such as temperature.¹⁸ Many reports can be found on the application of polythiophenes as sensor materials for proteins and DNA, whereas the polymer undergoes a conformation change with addition and complexation of the analyte.¹⁹⁻²¹ In consequence, a shift of the absorption or a change in the fluorescence signal can be detected. A comprehensive study of solution structures and the respective optical properties of cationic polythiophenes was accomplished by Knaapila and Scherf *et al.*²²⁻²⁴ They found a complexation induced aggregation of the cationic polymers with addition of sodium dodecyl sulfate (SDS). In comparison, aggregation of anionic polythiophene carboxylates is prevented or broken up by bulky organic counter ions, while it is favored by adding bivalent counterions.^{25,26}

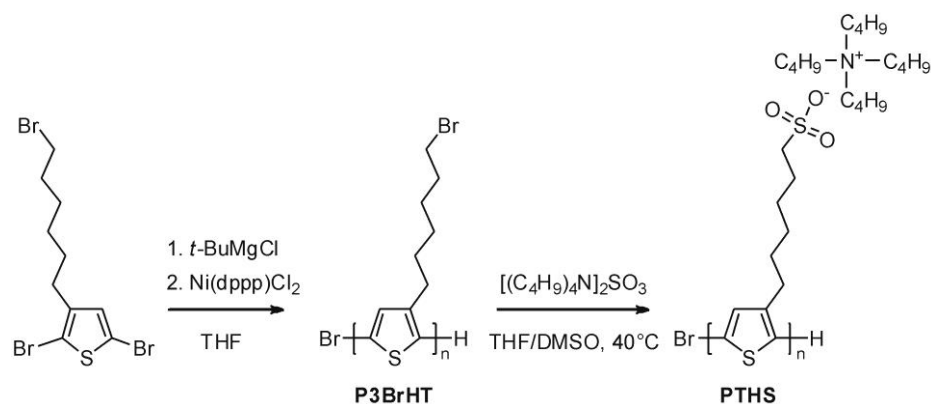
While the influence of polymer backbone, ionic group and solvent effects have been well described, no attention has so far been paid to the impact of molecular weight and its distribution on the conformation and aggregation of the polymers. This is probably due to the lack of control on the synthesis of CPEs as they are commonly prepared either *via* electropolymerization or polycondensation reactions.²⁷ Here, we present the controlled synthesis and characterization of a series of tailor-made anionic conjugated polyelectrolytes based on a polythiophene backbone. The Kumada catalyst transfer polymerization (KCTP, also called Grignard metathesis polymerization: GRIM) enables the preparation of well-defined precursor polymers carrying alkylbromide side-chains with definite molecular weights (MW) and narrow polydispersity (PDI).²⁸⁻³⁰ Accordingly, we prepared four different precursor polymers with different MWs, which were characterized by size exclusion chromatography (SEC) and matrix-assisted laser desorption/ionization – time of flight mass spectroscopy (MALDI-ToF-MS). In a subsequent polymer analogous reaction, we quantitatively substituted the bromine in the precursor polymers using tetrabutylammonium sulfite. Thus the final anionic CPEs, poly(6-(thiophen-3-yl)hexane-1-sulfonate) (PTHS) were obtained. The photophysical properties of PTHS in solution were examined in detail including the effect of MW, solvent and additionally added tetrabutylammonium salt. These characterizations lead to better understanding of structure-property relations in anionic CPEs based on polythiophene.

RESULTS AND DISCUSSION

Synthesis and characterization

The controlled chain growth mechanism of KCTP enables the preparation of conjugated polythiophenes, particularly poly(3-alkylthiophenes), with definite MWs, narrow PDI and defined end-groups.²⁸ Using this method, we synthesized four poly(3-(6-bromohexyl) thiophene)s (P3BrHT) with different degrees of polymerization. These precursor polymers were subsequently converted to the conjugated polyelectrolyte PTHS *via* polymer analogous substitution of the bromine group with a highly soluble tetrabutyl ammonium sulfite salt. An overview of the synthesis is presented in Scheme 7–1.

Scheme 7–1. Synthesis of Well-Defined Polyelectrolytes Using the Controlled Kumada Catalyst-Transfer Polymerization (KCTP) of 2,5-Dibromo-3-(6-bromohexyl)thiophene. The Ionic Groups were Subsequently Introduced *via* Polymer Analogous Substitution Reactions with Tetrabutylammonium Sulfite as Nucleophile



Since, the final polymers PTHS exhibits strong interactions of the charged side groups with column material or the matrices in SEC and MALDI-Tof-MS, respectively, the degree of polymerization n and the PDI were estimated for the respective precursor polymers P3BrHT 1-4. The SEC traces of these polymers are depicted in Figure 7–1.

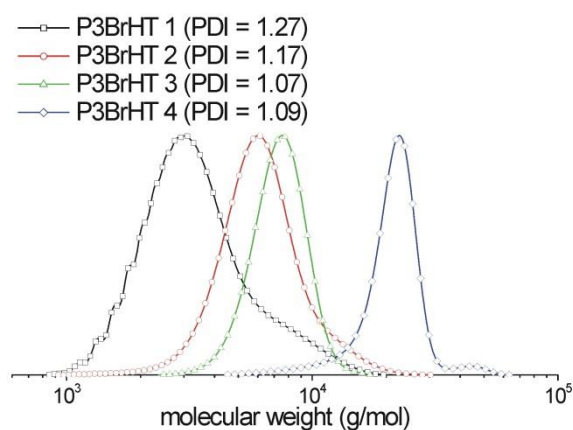


Figure 7–1. SEC traces of the precursor polymers P3BrHT 1 (black squares), P3BrHT 2 (red circles), P3BrHT 3 (green triangles) and P3BrHT 4 (blue diamonds). The determined PDI is given in parenthesis.

In all cases a narrow distribution was observed. Chain-chain coupling could not be fully avoided especially for the lower MW compounds, but the PDI always remains below 1.3, which proves the control of the synthesis. As the SEC is calibrated with polystyrene standards the molecular weights of the polymers may deviate from the estimated values. Therefore, an exact determination of the MW was accomplished by MALDI-Tof-MS measurements (Figure 7–2).

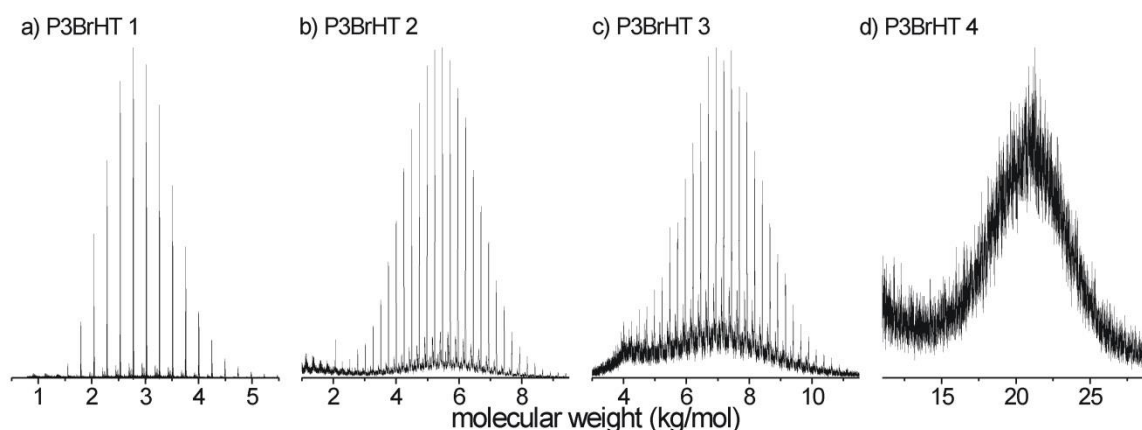


Figure 7–2. MALDI-Tof-MS spectra of the precursor polymers P3BrHT 1 (a), P3BrHT 2 (b), P3BrHT 3 (c) and P3BrHT 4 (d). P3BrHT 1-3 were measured in the reflection mode, while P3BrHT 4 was measured in the linear mode due to the high molecular weight. The minor peak series in (b) and (c) corresponds to H/H terminated chains and the major peak series in all polymers belong to H/Br chain ends.

From the absolute molecular weights obtained from MALDI-Tof-MS, the average number of repeating units were calculated to be 13, 22, 30, and 78 for the polymers P3BrHT 1-4, respectively. The high resolution measurements (reflection mode) for samples P3BrHT 1-3 reveal a major peak series, which is related to H/Br terminated polymers. For the samples P3BrHT 2 and 3 additionally a second peak minor series is observed, which belongs to the H/H terminated chains. However, in both cases the ratio of H/Br terminated chains is above 80%, which corroborate the control of the KCTP.

These well-defined P3BrHT polymers were finally converted to the polymers PTHS 1-4 *via* polymer analogous substitution of the bromine groups with tetrabutylammonium sulfite. The conversion of this reaction was monitored *via* ^1H NMR spectroscopy. Due to the strong difference in the polarity of the precursor polymers and the salt, the conditions had to be optimized to reach a quantitative conversion. Critical aspects in this context are the solubility of both the sulfite as well as the polymer and a sufficient polarity of the media to facilitate the substitution reaction. While the first was attained by the use of bulky organic tetrabutylammonium counter ions, the later required a systematically adjusted solvent composition to guarantee both the solubility of the polymer and a maximum polarity. A mixture of THF/DMSO (6/1 volume ratio) and a temperature of 40°C were found to give the ideal conditions for the reaction. For sample PTHS 4, a quantitative conversion of the bromine group to the corresponding sulfonate was already observed after 30 min as indicated by the NMR spectrum (Figure 7–3). The full spectra with all signals assigned are given in the supporting information (Figure 7–S1 and 7–S2).

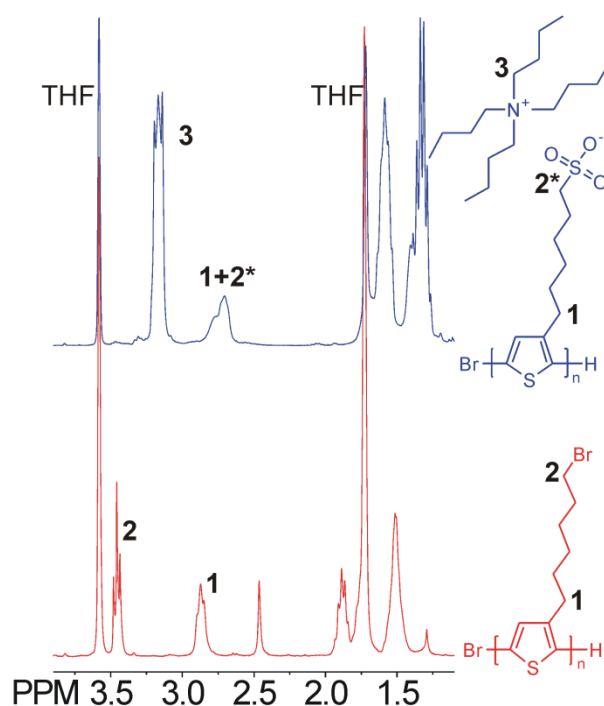


Figure 7–3. Comparison of the ^1H NMR spectra of the precursor polymer P3BrHT 4 (bottom, red) and the resulting CPE PTHS 4 (top, blue). The first was measured in $\text{THF-}d_8$ and the latter in a mixture of $\text{THF-}d_8/\text{D}_2\text{O}$ (4/1). In both cases the spectra were calibrated relative to the THF signals. The important signals are indicated by the assigned numbers.

The NMR depicts a complete disappearance of signal **2** ($-\text{CH}_2\text{-Br}$) and a new signal appears for **2*** ($-\text{CH}_2\text{-SO}_3^-$) which superimposes with signal **1** (thiophene- CH_2). Furthermore the new signal **3** at 3.17 ppm can be attributed to the tetrabutylammonium counterion. From the disappearance of signal **2** and the integrals of the new signals **2*** and **3** a quantitative conversion can be determined.

The final polyelectrolytes exhibit an excellent solubility in polar solvents such as methanol, DMSO, DMF, formamide and water. However, upon substitution of the bromine group with the sulfite they all become insoluble in less polar solvents such as chloroform, chlorobenzene, toluene and THF. The characteristic parameters of all synthesized precursor polymers and the respective CPEs are summarized in Table 7–1.

Table 7–1. Summary of the characteristic parameters M_n and PDI measured by SEC and M_n determined from the MALDI-Tof spectra for the precursor polymers P3BrHT 1, P3BrHT 2, P3BrHT 3 and P3BrHT 4.

precursor polymer	M_n (MALDI-Tof) kg/mol	M_n (SEC) (kg/mol) ^{a)}	PDI (SEC) ^{a)}	average n ^{b)}	CPE	MW (calc.) kg/mol ^{c)}
P3BrHT 1	3.1	2.9	1.27	13	PTHS 1	6.3
P3BrHT 2	5.5	5.6	1.17	22	PTHS 2	10.7
P3BrHT 3	7.3	7.0	1.07	30	PTHS 3	14.6
P3BrHT 4	19.1	19.4	1.09	78	PTHS 4	38.0

^{a)} The SEC was calibrated with polystyrene standards and the real MW may deviate from the given values.

^{b)} Calculated from the M_n from MALDI-Tof-MS analysis.

^{c)} Calculated from n and the MW of the repeating unit of PTHS.

Influence of molecular weight

On comparing aqueous solutions of the different polymers, on first sight, a clear difference in the optical properties is obvious. While the short polymer PTHS 1 appears yellow, the color changes gradually to orange, red and finally to purple with increasing MW (Figure 7–4).



Figure 7–4. Photographs of aqueous solutions (20 mg/L) of the polymers PTHS 1-4.

The respective UV-Vis absorption and fluorescence spectra are depicted in Figure 7–5.

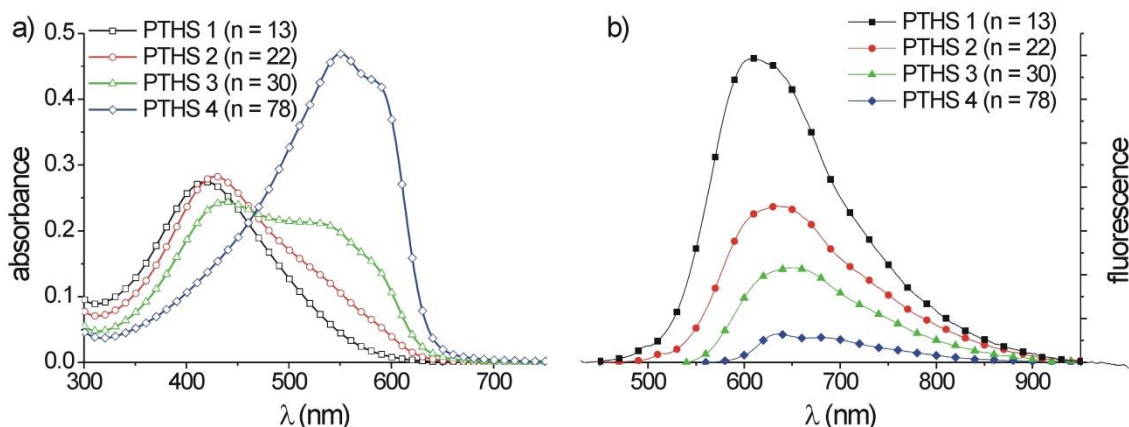


Figure 7–5. UV-Vis (a, empty symbols) and fluorescence (b, filled symbols) spectra of the different PTHS polymers in aqueous solution. PTHS 1 (black squares), PTHS 2 (red circles), PTHS 3 (green triangles) and PTHS 4 (blue diamonds). The concentration was set to 20 mg/l.

The shortest polymer PTHS 1 shows a broad absorption up to 600 nm but with a maximum at 420 nm. No additional signals are observed. PTHS 2 has a slightly red-shifted maximum at 430 nm, however it features one weak shoulder at approximately 510 nm. The latter signal increases further for PTHS 3 and a second shoulder appears at *ca.* 580 nm while the signal at 435 nm decreases. PTHS 4 exhibits a λ_{max} at 550 nm and a shoulder at 590 nm. Further, a drastic increase of the optical density was observed for the longest polymer PTHS 4 in the long wavelength range, although the concentration was equal to the other polymers (20 mg/L). In contrast to the previous polymers the absorption onset was considerably shifted up to 650 nm.

While the high energy absorption band at around 430 nm can be doubtless assigned to a non-aggregated, free polythiophene (as it is observed for amorphous polythiophenes and oligothiophenes), the additional signals at about 550 nm and 590 nm usually only arise for aggregated polythiophene chains.³¹⁻³³ Further evidence for the formation of aggregates is given by the photoluminescence spectra of the four samples. While for PTHS 1, a strong fluorescence is observed, the intensity drops for PTHS 2 and 3. For the sample PTHS 4 with high molecular weight the fluorescence is almost completely quenched indicating the presence of mainly aggregated chains. Further no dependence of aggregation on the concentration (for a broad concentration range from 1 mg/L to 2500 mg/L) for PTHS 4 is observed which is supported by the consistent absorption spectra (Figure 7-6).

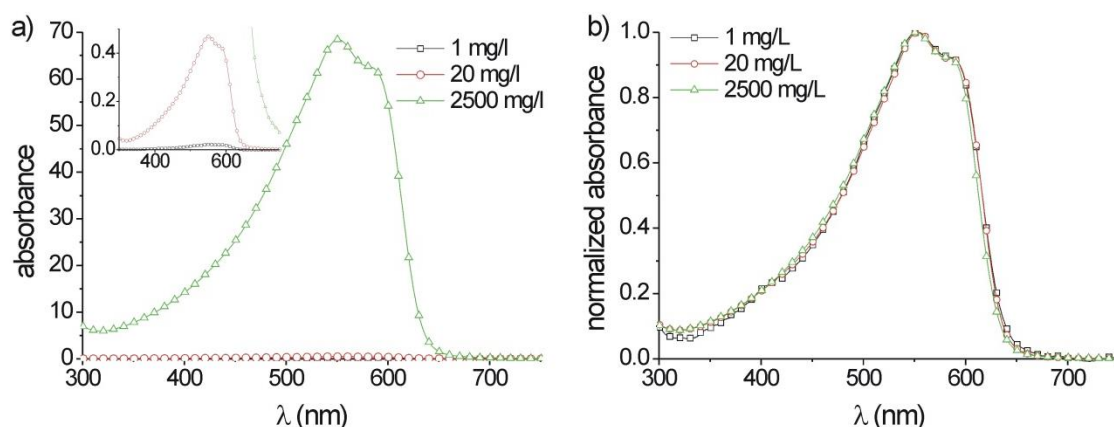


Figure 7-6. Absolute (a) and normalized (b) absorbance spectra of various concentrations of PTHS 4 ($n = 78$) in aqueous solution: 20 mg/l (black squares), 100 mg/l (red circles), 1000 mg/l (green triangles), 2500 mg/l (blue diamonds). The inset in (a) shows a magnification of the lower concentrations.

For PTHS 2 with an average of 22 repeating units, a clear dependence of aggregation on the concentration is observed as obvious by the absorption spectra (Figure 7-7).

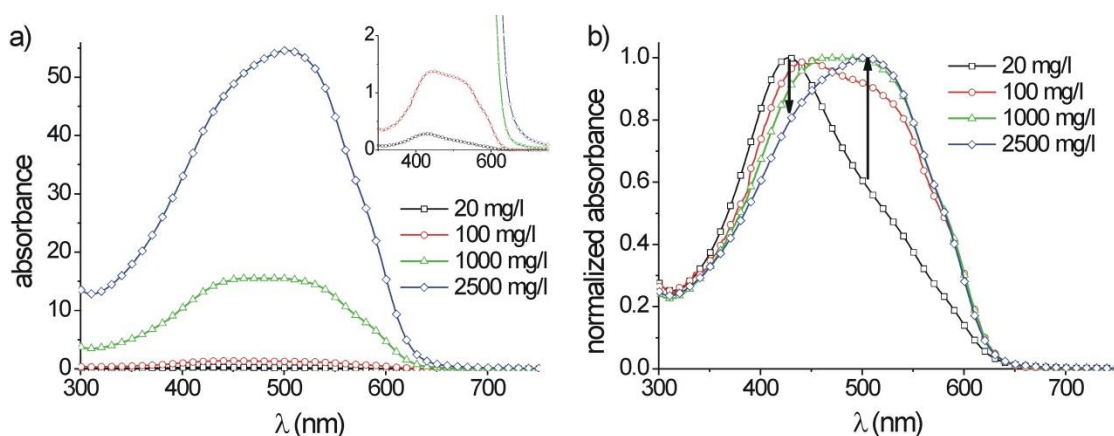


Figure 7-7. Absolute (a) and normalized (b) absorbance spectra of various concentrations of PTHS 2 ($n = 22$) in aqueous solution: 20 mg/l (black squares), 100 mg/l (red circles), 1000 mg/l (green triangles), 2500 mg/l (blue diamonds). The inset in (a) shows a magnification of the lower concentrations.

Starting from a low concentration of 20 mg/L, only a very weak shoulder at approximately 510 nm is visible. Increasing the concentration leads to a considerable enhancement of the

signal at 510 nm. This change of the absorption with variation of the concentration is a strong evidence for aggregation in the system. However, the pronounced shoulder at 590 nm as observed in PTHS 4 was not seen for PTHS 2 even at high concentrations.

In general, the aggregation of PTHS in aqueous solutions is not solely dependent on the concentration. It is further decided by the molecular weight of the polymer. This is evidenced by the fact that no aggregation occurs for short chains (PTHS 1) (Figure 7–S3), a concentration dependent aggregation is observed for the medium sized polymers (PTHS 2 and 3) (Figure 7–7 and 7–S4) and a permanent aggregated state was found for the high MW polymers (PTHS 4) (Figure 7–6). The aggregation in PTHS 4 was not affected by a change of the concentration. Such a strongly structured absorption as observed for PTHS 4 has so far only been reported for highly charged sulfonated polythiophenes.³⁴ While for carboxylated polythiophenes these signals are weaker, cationic polythiophene derivatives show no sign of aggregation unless complexing agents such as sodium dodecyl sulfate are added.^{22,35} For P3HT, it has been shown that chain folding starts at an M_n (SEC) of about 20 kg/mol.³⁶ In analogy to this, it can be expected that chain folding is a reasonable factor for the concentration independent aggregation of PTHS 4.

Effect of solvent

The conformation of polymer chains in general strongly depends on the interaction with the surrounding medium, *viz.* the solvent. In the special case of polyelectrolytes, the hydration effects of water are known to increase the counter ion dissociation. In consequence, the charge density on the polymer chain is increased, which causes repulsive coulomb forces and the stretching of the polymer chain.^{37,38} Other solvents usually do not lead to such strong ion dissociation and the polymer conformation may differ from the aqueous solution. In the case of CPEs, this conformational change influences the conjugation lengths and in consequence the optical properties of the polymer.

In addition to the aqueous solutions, we examined the optical properties of PTHS 1-4 in three different solvents: methanol, formamide and DMSO. Methanol is a polar protic solvent which has a comparable low dielectric constant (33) and a dipole moment of 1.70 D but it is able to form weak hydrogen bonds. In contrast, DMSO is a highly polar (dielectric constant: 46.7, dipole moment 3.96 D) aprotic solvent. Formamide was especially chosen, as it is considered to be most similar to water.^{39,40} It features a high dielectric constant of 109, a strong dipole moment of 3.37 D and is able to form hydrogen bonds similar to water. The UV-Vis absorption and fluorescence spectra for the polymer PTHS 4 in these solvents are shown in Figure 7–8. This high molecular weight sample shows the most distinct changes in the optical properties. The spectra of the other polymers are given in the SI (Figure 7–S5 – Figure 7–S7).

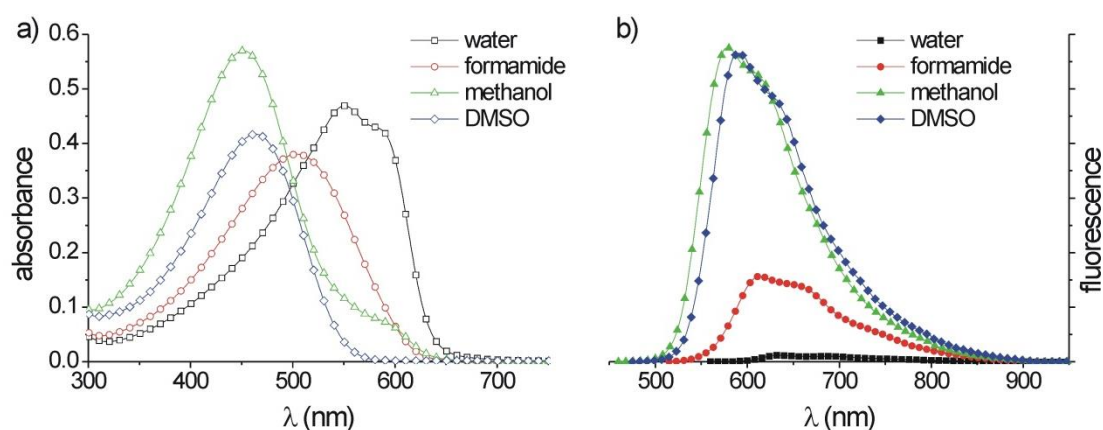


Figure 7–8. UV-Vis spectra (a, empty symbols) and fluorescence (b, filled symbols) of PTHS 4 in water (black squares), formamide (red circles), methanol (green triangles) and DMSO (blue diamonds). In all cases the concentration was set to 20 mg/l.

In comparison to the aqueous solution a clear blue-shift of the absorption maxima for all solvents was observed. The strongest shift ($\Delta\lambda_{\max} = 100$ nm) is observed for methanol ($\lambda_{\max} = 452$ nm). However, the spectrum in methanol still shows a shoulder at approximately 590 nm, which is related to the aggregated species. In contrast, the DMSO and formamide solutions feature only one main peak and no additional signals. DMSO as solvent gives an absorption similar to methanol with a maximum λ_{\max} at 464 nm but except the shoulder at 590 nm. This absorption profile is comparable to other well dissolved polythiophene derivatives such as poly(3-hexylthiophene) (P3HT) in chloroform and resembles the spectrum of a free polythiophene chain.³¹ In formamide a considerable red-shift of the maximum ($\lambda_{\max} = 504$ nm) is observed in comparison to methanol and DMSO, but no additional signals giving rise to aggregation can be found. The fluorescence of all solutions is enhanced in contrast to the aqueous solution. The DMSO and methanol solutions display similar spectra, while the spectrum of the formamide solution is red-shifted and the intensity is extenuated.

The observed differences in the optical properties with variation of the solvent substantiate the formation of aggregates in aqueous solution. Although formamide has properties comparable to water and the dissociation of counter ions may be similar in both cases, no sign of aggregation was observed in the formamide solution. In aqueous solution, the hydrophobic backbone and hexyl chains avoid an aqueous environment and favor the aggregation of chains. In contrast, the organic solvents including methanol, DMSO and formamide are able to interact with the polythiophene backbone and break up the aggregated chains. Nevertheless, the red-shift of λ_{\max} for the formamide solution in comparison to the methanol and DMSO solutions is most likely caused by a conformation change of the backbone, *viz.* a change in conjugation length, which is due to the good dissociation of counter ions in formamide.

To further elucidate the effect we examined various water/DMSO mixtures as solvent for polymer PTHS 4. For clarity, the UV-vis and fluorescence spectra of only some selected mixtures are depicted in Figure 7–9.

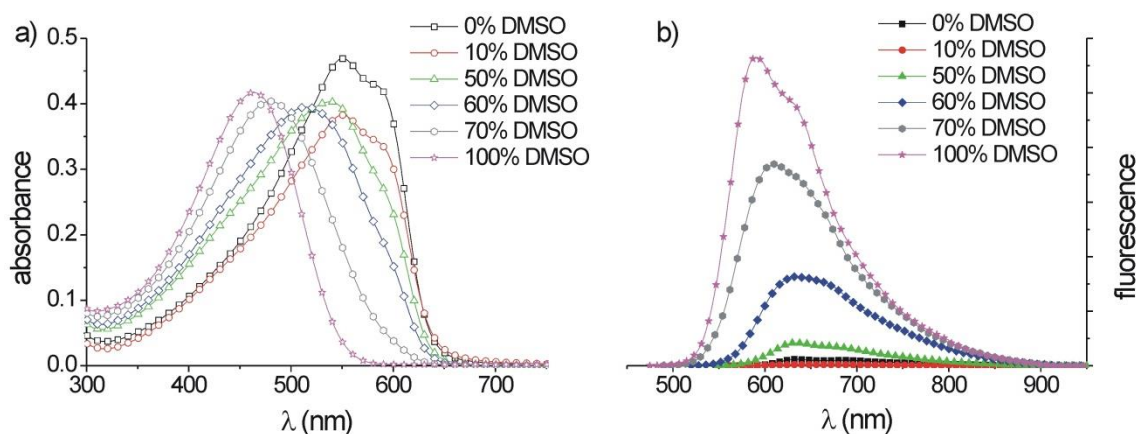


Figure 7-9. UV-Vis spectra (a, empty symbols) and fluorescence (b, filled symbols) of PTHS 4 in different solvent compositions of water/DMSO: 100% water (black squares), 90% water / 10% DMSO (red circles), 50% water / 50% DMSO (green triangles), 40% water / 60% DMSO (blue diamonds), 30% water / 70% DMSO (grey hexagons) and 100% DMSO (magenta stars). In all cases the concentration was set to 20 mg/l.

Starting from a pure aqueous solution the addition of only 10% DMSO leads to a drop of the absorption, but the structure of the spectrum is maintained. Interestingly, no significant change of the absorption is observed between samples having 10% and 50% addition of DMSO. In contrast, a considerable drop of the shoulder at 590 nm and a clear blue-shift of the absorption maximum occur with further addition of DMSO (50% - 70%). With higher DMSO content (>70%) the spectra feature only one main peak without any additional signals referring to aggregation. In accordance with this, the fluorescence spectra show a significant increase between 50% and 70% DMSO content, which can be related to the dissolution of the aggregated species which quenches the fluorescence. The high ratio of DMSO necessary to break the aggregation of the polymer chains underlines the hydrophobicity of the polythiophene backbone and suggests a strong inter-chain interaction in the aggregated species.

Variation of counter ion concentration

For aqueous solutions of non-conjugated polyelectrolytes, the addition of salt has a considerable influence on the chain conformation.⁴¹ At low ion concentrations a chain stretching is observed due to an enhanced counter ion dissociation which in consequence causes an amplified coulomb repulsion of the repeating units. On increasing the ion concentration, the ratio of dissociated ions decreases and the coulomb interactions are screened facilitating a coiled conformation of the polymer chains.⁴²

In general, conjugated polyelectrolytes possess stiffer polymer backbones in contrast to non-conjugated polymers. However, polythiophenes are still characterized by a coiled conformation in dilute solution due to the twisted bond angle between two repeating units.¹⁷ Considering the above mentioned facts the question arises whether the addition of salt has a similar effect on the polymer conformation of PTHS. Therefore, we dissolved PTHS 4 in aqueous solutions containing different amounts tetrabutylammonium chloride (0 M – 2 M). The tetrabutylammonium salt was chosen to avoid any additional effects due to counterion exchange. The absorption and fluorescence spectra for a series of salt concentrations are depicted in Figure 7–10. The spectra of all tested concentrations are given in the SI (Figure 7–S8)

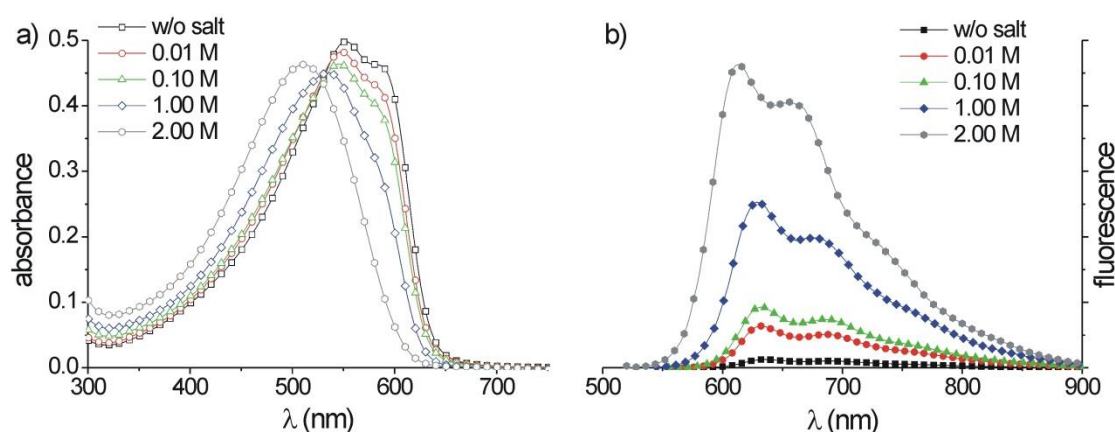


Figure 7–10. UV-Vis spectra (a, empty symbols) and fluorescence (a, filled symbols) of PTHS 4 in aqueous solutions with varying tetrabutylammonium chloride ($\text{N}(\text{Bu})_4\text{Cl}$) concentration: without salt (black squares), 0.01 M (red circles), 0.10 M (green triangles), 1.00 M (blue diamonds), 2.00 M (grey hexagons). The concentration of the polymer was set to 20 mg/l.

In the absorption spectra, a decrease of the signals at 550 nm (peak) and 590 nm (shoulder) and the appearance of a new signal at 510 nm with an isosbestic point at 529 nm are observed upon addition of the salt. The new signal at 510 nm corresponds to non-aggregated species in water, which could not be earlier observed in the absence of salt. Accordingly, the fluorescence signal of the solution steadily increases and slightly shifts towards shorter wavelengths. This change in both spectra certainly derives from the disintegration of the polymer aggregates in presence of salt. The break-up of the π - π interactions can be accompanied by a conformation change which is induced by the salt addition causing reduced coulomb repulsion between the monomer units. In contrast, this repulsion is enhanced in salt free water and favors a stretching of the polymer chains which abets the π - π interaction and aggregation.

CONCLUSIONS

In summary, we presented the controlled synthesis of anionic conjugated polyelectrolytes based on polythiophene. Using Kumada catalyst transfer polymerization we prepared polythiophene carrying bromohexyl side chains which were finally converted to the sulfonated CPE *via* polymer analogous reaction. The latter necessitated a careful optimization of the reaction conditions to obtain a quantitative conversion, which was monitored by ^1H NMR spectroscopy. Thus, we synthesized and characterized four polymers with different molecular weights but with narrow polydispersity index. The photophysical properties of these CPEs were studied in solution to elucidate the influence of molecular weight, concentration, the nature of solvent and the effect of salt. In aqueous solutions, we observed a correlation of aggregation with the degree of polymerization. While short chains (~ 13 repeating units) do not aggregate even at high concentrations, medium sized polymers (20–30 repeating units) show a concentration dependent aggregation behavior. For large macromolecules (> 70 repeating units) permanent aggregates are formed in aqueous solutions independent of the concentration. In contrast, in polar organic solvents no signals corresponding to aggregated species are observed. We attribute this divergence of the polymer aggregation to the strong hydrophobicity of the polymer backbone, which favors the chain-chain interaction in aqueous solutions. Organic

solvents instead are able to solvate the polymer backbone and interfere with the aggregation. This hydrophobic effect of the polymer backbone is preserved even for high solvent contents of 50% which emphasizes the strengths of the interchain aggregation. Another important parameter that we examined is the ionic strength of the solution. With addition of salt we observed a decrease of the aggregation signals in the UV-Vis spectra and a significant increase of the fluorescence. Increasing the ion concentration of aqueous solutions generally leads to an enhanced screening of coulomb forces and decrease the ratio of dissociated to non-dissociated ions of polyelectrolytes. Reducing the repulsive coulomb interaction between adjacent repeating units induces an extended flexibility to the polymer chains which finally lead to the dissolution of the aggregated chains. Overall, we conclude that the optical properties of conjugated polyelectrolytes are not only decided by the polymer backbone and the ionic groups, but also depend on the molecular weight, the polarity of the medium and the ionic strength. In consequence, the presented results give insight into a correlation of properties of CPEs based on well-defined polythiophenes.

EXPERIMENTAL SECTION

Materials and methods

The monomer 2,5-dibromo-3-(6-bromohexyl)thiophene was prepared according to procedures in literature.^{43,44} All reagents were purchased from commercial suppliers and used without further purification. The salt tetra-*n*-butyl ammonium sulfite was prepared *via* hydrolysis of dimethyl sulfite by 2 eq. of tetra-*n*-butyl ammonium hydroxide (40 wt% solution in methanol). ¹H NMR (300 MHz) spectra were recorded on a Bruker AC 300 spectrometer and calibrated relative to the respective solvent resonance signal. SEC measurements were carried out in THF with two Varian MIXED-C columns (300x7.5 mm) at room temperature and a flow rate of 0.5 mL/min using an UV detector (Waters model 486) with 254 nm detector wavelength and a refractive index detector (Waters model 410). Polystyrene in combination with *o*-DCB as an internal standard was used for calibration. Matrix assisted laser desorption ionizations spectroscopy with time of flight detection mass spectroscopy (MALDI-Tof) measurements were performed on a Bruker Reflex III using Dithranol as matrix and a mixture of 1000:1 (Matrix:Polymer). UV-Vis spectra were recorded on a Jasco V-670 spectrophotometer. The samples were either prepared in a 10 mm or in a 0.1 mm cuvette for high concentration guaranteeing an optical density between 0.1 and 1. The fluorescence was measured with a Jasco FP-8600 spectrofluorometer.

Polymer synthesis

A detailed procedure is given for the polymers P3BrHT 1 and PTHS 1. All other samples were prepared accordingly and only the varied amounts of reagents are listed.

Poly(3-(6-bromohexyl) thiophene) (P3BrHT) 1

2,5-Dibromo-3-(6-bromohexyl)thiophene (0.79 g, 1.95 mmol) was added to a dried 250 ml flask and the vessel was evacuated once again and flushed with nitrogen. With dry THF the concentration was set to 0.5 mmol/ml and *tert*-butylmagnesium chloride (1.25 M in THF, 1.50 ml, 1.88 mmol) was added dropwise. After 20 h of stirring the concentration was reduced to 0.1 mmol/ml. 1,3-Bis(diphenylphosphino)propan-nickel(II)chlorid (0.054 g, 0.10 mmol) (suspension in THF) was added to start the polymerization. After 1 h the polymerization was

quenched by adding 2 ml of 16% aqueous HCl. The mixture was concentrated and the polymer was precipitated in methanol. The polymer was purified by soxhlet extraction with methanol. SEC: $M_n = 2860$ g/mol, $M_w = 3630$ g/mol, PDI = 1.27; MALDI-Tof: $M_n = 3100$ g/mol; $^1\text{H NMR}$: δ_{H} (300 MHz; CDCl_3) 1.39-1.47 (4 H, m), 1.64-1.68 (2 H, m, $\beta\text{-CH}_2$), 1.78-1.85 (2 H, m, $-\text{CH}_2\text{-CH}_2\text{-Br}$), 2.73-2.78 (2 H, m, $\alpha\text{-CH}_2$), 3.36 (2 H, m, $\text{CH}_2\text{-Br}$), 6.91 (1 H, s, H_{arom}).

P3BrHT 2

2,5-Dibromo-3-(6-bromohexyl)thiophene (1.50 g, 3.70 mmol), and *tert*-Butylmagnesium chloride (1.25 M in THF, 2.90 ml, 3.63 mmol), 1,3-Bis(diphenylphosphino)propan-nickel(II)chlorid (0.051 g, 0.09 mmol). SEC: $M_n = 5560$ g/mol, $M_w = 6500$ g/mol, PDI = 1.17; MALDI-Tof: $M_n = 5500$ g/mol;

P3BrHT 3

2,5-Dibromo-3-(6-bromohexyl)thiophene (1.58 g, 3.90 mmol), and *tert*-Butylmagnesium chloride (1.25 M in THF, 3.00 ml, 3.75 mmol), 1,3-Bis(diphenylphosphino)propan-nickel(II)chlorid (0.036 g, 0.07 mmol). SEC: $M_n = 6960$ g/mol, $M_w = 7430$ g/mol, PDI = 1.07; MALDI-Tof: $M_n = 7300$ g/mol;

P3BrHT 4

2,5-Dibromo-3-(6-bromohexyl)thiophene (1.48 g, 3.65 mmol), and *tert*-Butylmagnesium chloride (1.25 M in THF, 2.80 ml, 3.50 mmol), 1,3-Bis(diphenylphosphino)propan-nickel(II)chlorid (0.020 g, 0.04 mmol). SEC: $M_n = 19360$ g/mol, $M_w = 21130$ g/mol, PDI = 1.09; MALDI-Tof: $M_n = 18900$ g/mol;

Poly(6-(thiophen-3-yl)hexane-1-sulfonate) (PTHS) 1

Poly(3-(6-bromohexyl)thiophene) (0.1 g, 0.032 mmol) was first dissolved in THF (27.0 ml) at 40°C and the mixture was degassed by a constant argon stream for 20 min. Tetra-*n*-butyl ammonium sulfite (1 M in DMSO, 4.50 ml, 4.50 mmol) was added and the mixture was kept at 40°C for 1 h. Water was added and the reaction mixture was dialyzed against ultrapure water (MilliQ) to purify the polymer. Finally the solution was freeze dried to get the polyelectrolyte powder. $^1\text{H NMR}$: δ_{H} (300 MHz; *d*-THF/ D_2O 2/1) 0.86-0.96 (12 H, m, $\text{N}^+(\text{-CH}_2\text{-CH}_2\text{-CH}_2\text{-CH}_3)_4$), 1.25-1.41 (8 H, m, $\text{N}^+(\text{-CH}_2\text{-CH}_2\text{-CH}_2\text{-CH}_3)_4$), 1.35-1.48 (4 H, m, $\beta\text{-CH}_2\text{-CH}_2\text{-CH}_2\text{-CH}_2\text{-CH}_2\text{-S}$), 1.52-1.67 (8 H, m, $\text{N}^+(\text{-CH}_2\text{-CH}_2\text{-CH}_2\text{-CH}_3)_4$), 1.67-1.80 (4 H, m, $\beta\text{-CH}_2\text{-CH}_2\text{-CH}_2\text{-CH}_2\text{-CH}_2\text{-S}$), 2.63-2.88 (4 H, m, $\alpha\text{-CH}_2\text{-CH}_2\text{-CH}_2\text{-CH}_2\text{-CH}_2\text{-S}$), 3.10-3.25 (8 H, m, $\text{N}^+(\text{-CH}_2\text{-CH}_2\text{-CH}_2\text{-CH}_3)_4$), 6.98-7.08 (1 H, s, H_{arom}).

PTHS 2

Poly(3-(6-bromohexyl)thiophene) (0.15 g, 0.027 mmol), Tetra-*n*-butyl ammonium sulfite (1 M in DMSO, 6.80 ml, 6.80 mmol).

PTHS 3

Poly(3-(6-bromohexyl)thiophene) (0.15 g, 0.021 mmol), Tetra-*n*-butyl ammonium sulfite (1 M in DMSO, 6.80 ml, 6.80 mmol).

PTHS 4

Poly(3-(6-bromohexyl)thiophene) (0.15 g, 0.0079 mmol), Tetra-*n*-butyl ammonium sulfite (1 M in DMSO, 6.80 ml, 6.80 mmol).

ASSOCIATED CONTENT

Supporting Information: Synthesis of the monomer, detailed ¹H NMR spectra of the polymers P3BrHT and PTHS, concentration dependent absorption spectra, UV-Vis and fluorescence spectra in various solvents and in aqueous solutions of various salt concentrations. This material is available free of charge *via* the Internet at <http://pubs.acs.org>.

ACKNOWLEDGMENT

We thank K. Neumann and M. Hufnagel for the SEC and MALDI-ToF measurements, respectively. Financial support from SFB 840, EU-India Largecells (GA. No. 261936) and the Elitenetzwerk Bayern (ENB), Macromolecular Science, are kindly acknowledged.

REFERENCES

- (1) A. Duarte, K.-Y. Pu, B. Liu, G. C. Bazan, *Chem. Mater.* **2010**, *23*, 501-515.
- (2) K. E. Achyuthan, T. S. Bergstedt, L. Chen, R. M. Jones, S. Kumaraswamy, S. A. Kushon, K. D. Ley, L. Lu, D. McBranch, H. Mukundan, F. Rininsland, X. Shi, W. Xia, D. G. Whitten, *J. Mater. Chem.* **2005**, *15*, 2648-2656.
- (3) T. I. Wallow, B. M. Novak, *J. Am. Chem. Soc.* **1991**, *113*, 7411-7412.
- (4) I. U. Rau, M. Rehahn, *Polymer* **1993**, *34*, 2889-2893.
- (5) R. Rulkens, M. Schulze, G. Wegner, *Macromol. Rapid Commun.* **1994**, *15*, 669-676.
- (6) G. Brodowski, A. Horvath, M. Ballauff, M. Rehahn, *Macromolecules* **1996**, *29*, 6962-6965.
- (7) S. Kim, J. Jackiw, E. Robinson, K. S. Schanze, J. R. Reynolds, J. Baur, M. F. Rubner, D. Boils, *Macromolecules* **1998**, *31*, 964-974.
- (8) C. Tan, M. R. Pinto, K. S. Schanze, *Chemical Communications Chem. Commun.* **2002**, 446-447.
- (9) C. Tan, E. Atas, J. G. Müller, M. R. Pinto, V. D. Kleiman, K. S. Schanze, *J. Am. Chem. Soc.* **2004**, *126*, 13685-13694.
- (10) X. Zhao, M. R. Pinto, L. M. Hardison, J. Mwaura, J. Müller, H. Jiang, D. Witker, V. D. Kleiman, J. R. Reynolds, K. S. Schanze, *Macromolecules* **2006**, *39*, 6355-6366.
- (11) S. W. Thomas, G. D. Joly, T. M. Swager, *Chem. Rev.* **2007**, *107*, 1339-1386.
- (12) Y. Liu, K. Ogawa, K. S. Schanze, *Journal of Photochemistry and Photobiology C: Photochemistry Reviews* **2009**, *10*, 173-190.
- (13) B. Liu, W.-L. Yu, Y.-H. Lai, W. Huang, *Macromolecules* **2002**, *35*, 4975-4982.
- (14) F. Huang, H. Wu, D. Wang, W. Yang, Y. Cao, *Chem. Mater.* **2004**, *16*, 708-716.
- (15) H. D. Burrows, V. M. M. Lobo, J. Pina, M. L. Ramos, J. Seixas de Melo, A. J. M. Valente, M. J. Tapia, S. Pradhan, U. Scherf, *Macromolecules* **2004**, *37*, 7425-7427.
- (16) A. O. Patil, Y. Ikenoue, F. Wudl, A. J. Heeger, *J. Am. Chem. Soc.* **1987**, *109*, 1858-1859.
- (17) B. McCulloch, V. Ho, M. Hoarfrost, C. Stanley, C. Do, W. T. Heller, R. A. Segalman, *Macromolecules* **2013**, *46*, 1899-1907.
- (18) M. Leclerc, *Adv. Mater.* **1999**, *11*, 1491-1498.
- (19) K. P. R. Nilsson, O. Inganäs, *Nat. Mater.* **2003**, *2*, 419-424.
- (20) K. P. R. Nilsson, A. Herland, P. Hammarström, O. Inganäs, *Biochemistry* **2005**, *44*, 3718-3724.

- (21) B. Liu, G. C. Bazan, *Chem. Mater.* **2004**, *16*, 4467-4476.
- (22) M. Knaapila, R. C. Evans, V. M. Garamus, L. s. Almásy, N. m. K. Székely, A. Gutacker, U. Scherf, H. D. Burrows, *Langmuir* **2010**, *26*, 15634-15643.
- (23) M. Knaapila, R. C. Evans, A. Gutacker, V. M. Garamus, N. K. Szekely, U. Scherf, H. D. Burrows, *Soft Matter* **2011**, *7*, 6863-6872.
- (24) A. Gutacker, S. Adamczyk, A. Helfer, L. E. Garner, R. C. Evans, S. M. Fonseca, M. Knaapila, G. C. Bazan, H. D. Burrows, U. Scherf, *J. Mater. Chem.* **2010**, *20*, 1423-1430.
- (25) R. D. McCullough, P. C. Ewbank, R. S. Loewe, *J. Am. Chem. Soc.* **1997**, *119*, 633-634.
- (26) R. D. McCullough, P. C. Ewbank, *Synth. Met.* **1997**, *84*, 311-312.
- (27) C. Zhu, L. Liu, Q. Yang, F. Lv, S. Wang, *Chem. Rev.* **2012**, *112*, 4687-4735.
- (28) R. H. Lohwasser, M. Thelakktat, *Macromolecules* **2011**, *44*, 3388-3397.
- (29) M. C. Stefan, A. E. Javier, I. Osaka, R. D. McCullough, *Macromolecules* **2008**, *42*, 30-32.
- (30) A. Kiriyy, V. Senkovskyy, M. Sommer, *Macromol. Rapid Commun.* **2011**, *32*, 1503-1517.
- (31) C. Scharsich, R. H. Lohwasser, M. Sommer, U. Asawapirom, U. Scherf, M. Thelakktat, D. Neher, A. Köhler, *J. Polym. Sci. B Polym. Phys.* **2012**, *50*, 442-453.
- (32) F. C. Spano, *J. Chem. Phys.* **2005**, *122*, 234701-234715.
- (33) H. Meier, U. Stalmach, H. Kolshorn, *Acta Polym.* **1997**, *48*, 379-384.
- (34) M. Chayer, K. Faïd, M. Leclerc, *Chem. Mater.* **1997**, *9*, 2902-2905.
- (35) A. Garcia, T.-Q. Nguyen, *J. Phys. Chem. C* **2008**, *112*, 7054-7061.
- (36) M. Brinkmann, P. Rannou, *Adv. Funct. Mater.* **2007**, *17*, 101-108.
- (37) A. V. Dobrynin, M. Rubinstein, *Prog. Polym. Sci.* **2005**, *30*, 1049-1118.
- (38) S. Förster, M. Schmidt, *Adv. Polym. Sci.* **1995**, *120*, 51-133.
- (39) H. Bipp, H. Kieczka, Formamides in *Ullmann's Encyclopedia of Industrial Chemistry*; Wiley-VCH Verlag GmbH & Co. KGaA: **2000**.
- (40) I. Bakó, T. Megyes, S. Bálint, V. Chihaia, M.-C. Bellissent-Funel, H. Krienke, A. Kopf, S.-H. Suh, *J. Chem. Phys.* **2010**, *132*, 014506-014507.
- (41) S. Förster, M. Schmidt, M. Antonietti, *Polymer* **1990**, *31*, 781-792.
- (42) T. Hofmann, R. G. Winkler, P. Reineker, *J. Chem. Phys.* **2003**, *119*, 2406-2413.
- (43) P. Bäuerle, F. Würthner, S. Heid, *Angew. Chem.* **1990**, *102*, 414-415.
- (44) S. Miyanishi, K. Tajima, K. Hashimoto, *Macromolecules* **2009**, *42*, 1610-1618.

SUPPORTING INFORMATION

NMR analysis of P3BrHT and PTHS

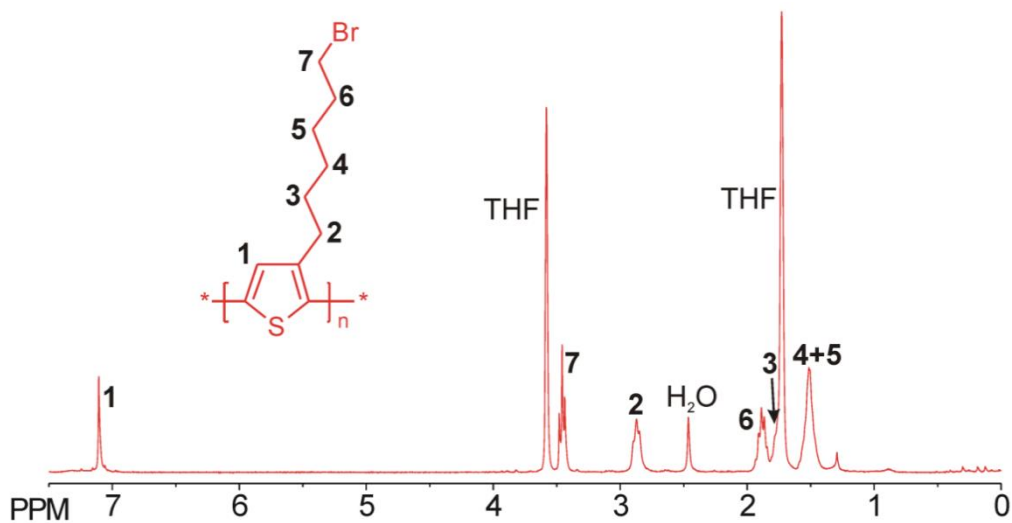


Figure 7-S1. NMR spectrum of poly(3-(6-bromohexyl) thiophene) (P3BrHT).

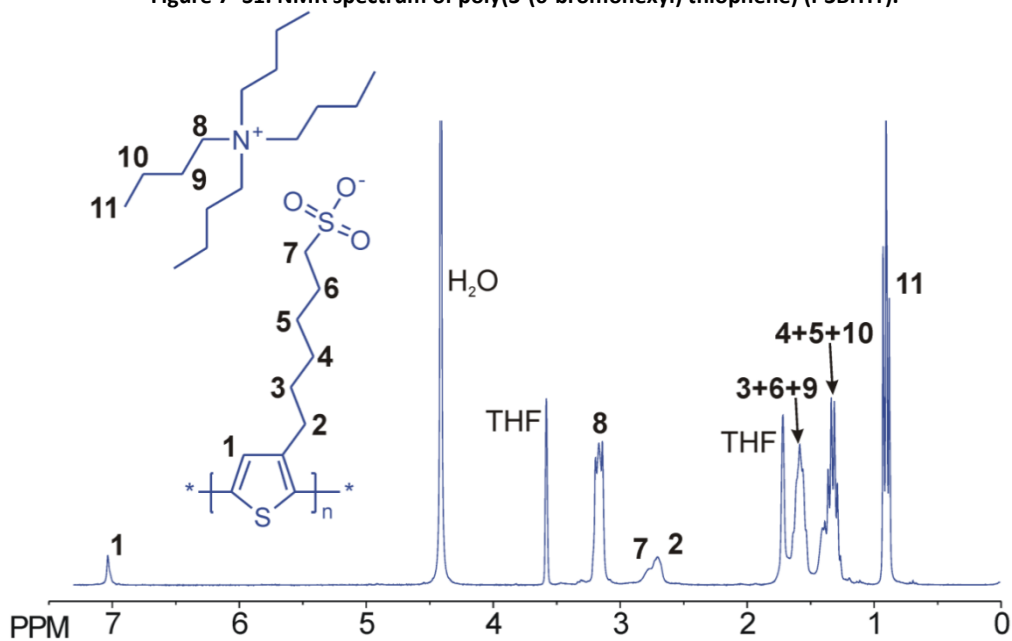


Figure 7-S2. NMR spectrum of tetrabutylammonium poly(6-(thiophen-3-yl)hexane-1-sulfonate) (PTHS).

Concentration dependent absorption spectra of PTHS 1 and 3

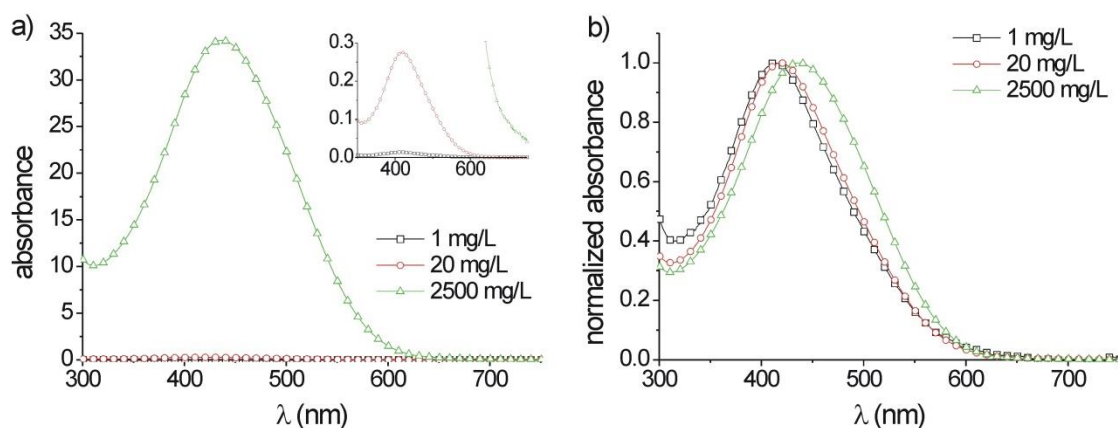


Figure 7-S3. Absolute (a) and normalized (b) absorbance spectra of different concentrations of PTHS 1 in aqueous solution. 1 mg/l (black squares), 20 mg/l (red circles) and 2500 mg/l (green triangles).

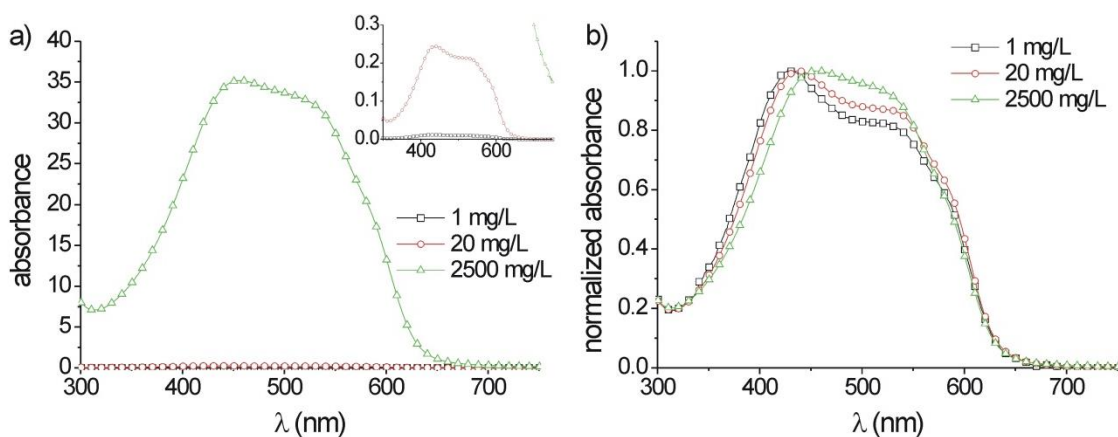


Figure 7-S4. Absolute (a) and normalized (b) absorbance spectra of different concentrations of PTHS 3 in aqueous solution. 1 mg/l (black squares), 20 mg/l (red circles) and 2500 mg/l (green triangles).

Absorption and fluorescence spectra of PTHS 1-3 for different solvents

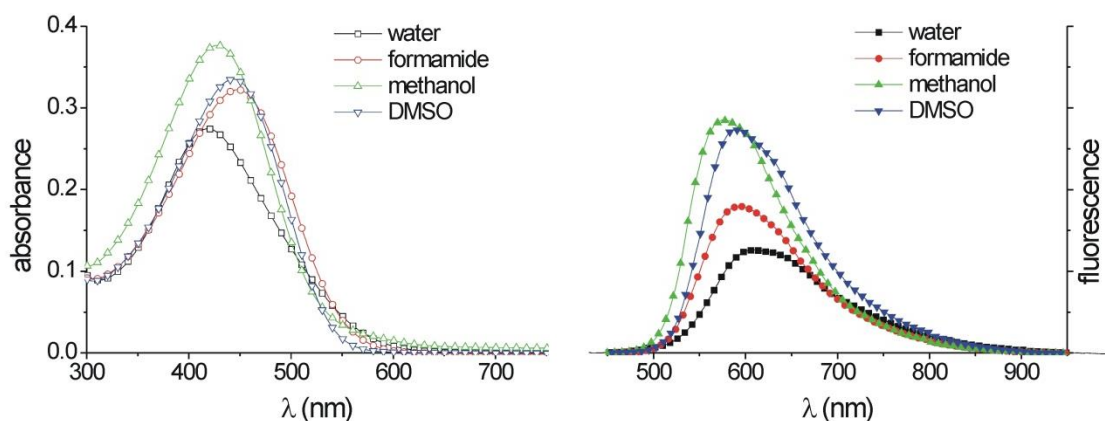


Figure 7-S6. UV-Vis spectra (left) and fluorescence (right) of PTHS 1 in water (black squares), formamide (red circles), methanol (green triangles) and DMSO (blue diamonds). In all cases the concentration was set to 2×10^{-5} g/ml.

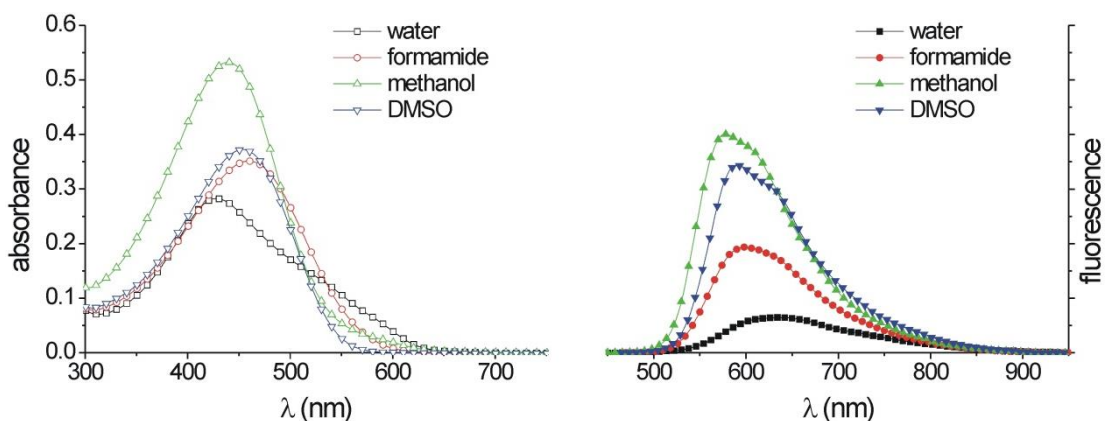


Figure 7-S7. UV-Vis spectra (left) and fluorescence (right) of PTHS 2 in water (black squares), formamide (red circles), methanol (green triangles) and DMSO (blue diamonds). In all cases the concentration was set to 2×10^{-5} g/ml.

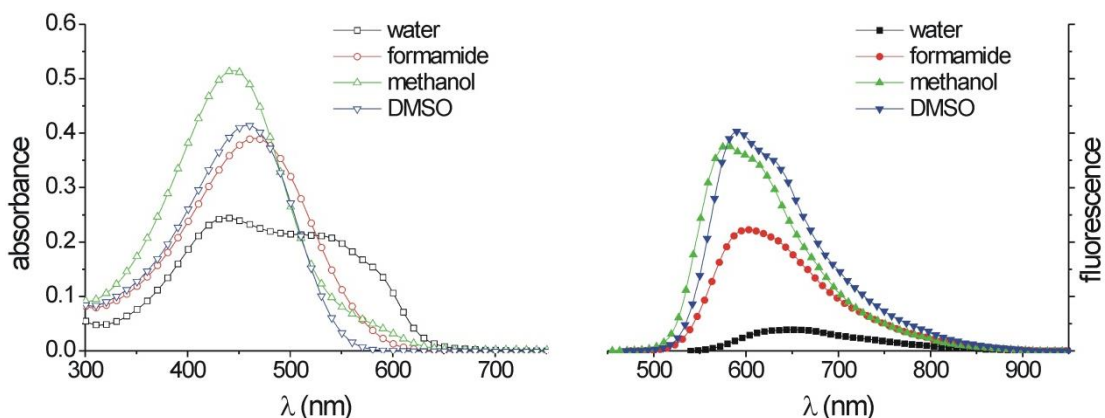


Figure 7-S8. UV-Vis spectra (left) and fluorescence (right) of PTHS 3 in water (black squares), formamide (red circles), methanol (green triangles) and DMSO (blue diamonds). In all cases the concentration was set to 2×10^{-5} g/ml.

Absorption and fluorescence for all examined tetrabutylammonium chloride (TBA Cl) salt concentrations

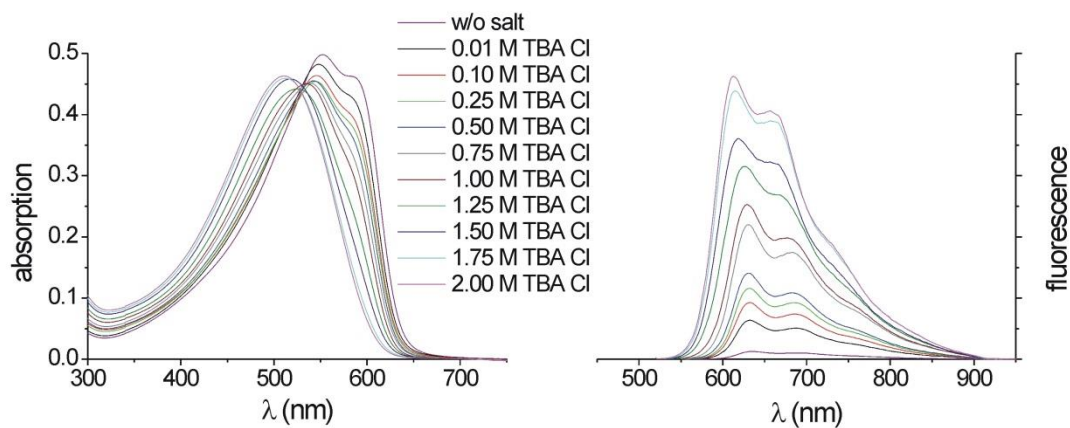


Figure 7–S9. UV-Vis spectra (left) and fluorescence (right) of PTHS 4 in aqueous solutions with varying tetrabutylammonium chloride ($N(Bu)_4Cl$) concentrations. The concentration of the polymer was set to 20 mg/l.

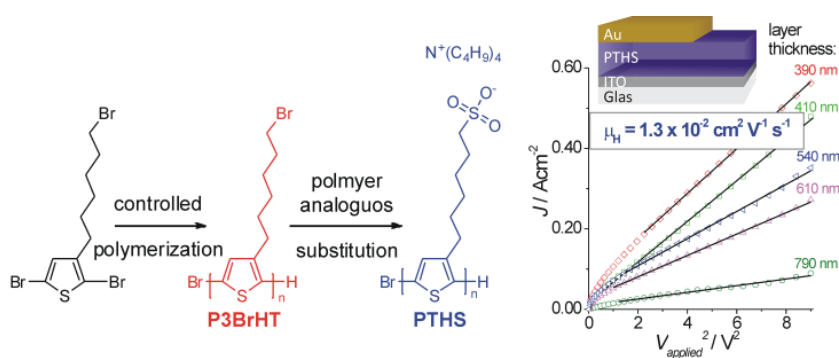
8. CONTROLLED SYNTHESIS OF A CONJUGATED POLYELECTROLYTE LEADING TO EXCELLENT HOLE TRANSPORT MOBILITY

Johannes C. Brendel,^a Gunter Hagen,^b Ralf Moos,^b Mukundan Thelakkat^{*,a}

^a Applied Functional Polymers, Macromolecular Chemistry I, University of Bayreuth, 95440 Bayreuth, Germany,

^b Department of Functional Materials, University of Bayreuth, 95440 Bayreuth, Germany.

*E-mail of corresponding author: mukundan.thelakkat@uni-bayreuth.de



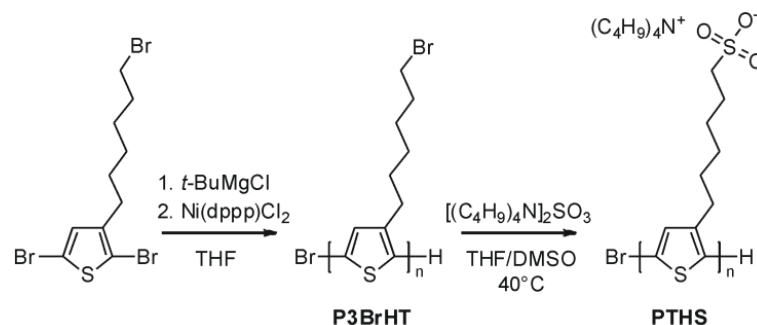
Submitted to *Chemistry of Materials*.

ARTICLE

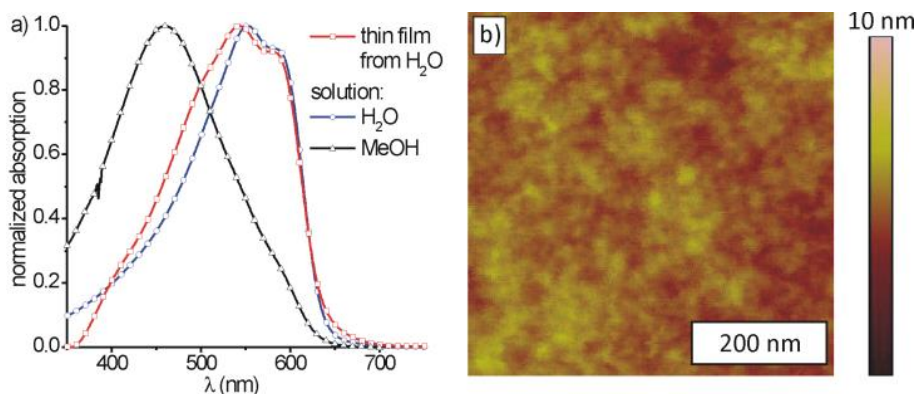
Conjugated polymers have been a key interest of scientific research since their development.^{1,2} Their applications range from light emitting diodes to sensors, actuators, transistors and solar cells.³⁻⁶ There is a strong demand for processible conjugated polymers from water or similar non-toxic polar solvents such as alcohols.^{7,8} A general pathway to increase the solubility of conjugated polymers in such solvents relies on the introduction of polar, particularly charged groups attached to the backbone of the polymers, which results in conjugated polyelectrolytes (CPE).^{9,10} The CPEs have mainly found applications as sensors in biochemistry or injection layers in polymer light emitting diodes (PLED), organic field effect transistors (OFET) and photovoltaic devices.¹¹⁻¹³ In general, the hole transport mobility of such materials have been low. The obtained mobilities of most CPEs vary from $1 \times 10^{-8} \text{ cm}^2 \text{ V}^{-1} \text{ s}^{-1}$ to $6 \times 10^{-6} \text{ cm}^2 \text{ V}^{-1} \text{ s}^{-1}$,¹⁴ which is three orders of magnitude lower than for the well-studied commercial poly(3-hexylthiophene) (P3HT).¹⁵ This lowering of mobility in CPEs is usually due to a loss of order in the polymer structure, *viz.* the conjugation length is decreased and the interchain aggregation is hindered.¹⁶ In particular, for applications involving charge transport, it may be very advantageous to have well-structured CPE systems, which in turn require well-controlled synthetic routes. Another issue is the reorientation of the ionic groups in an electric field resulting in an efficient screening of the applied bias. Friend *et al.* presented a detailed study based on experiments and model simulations that confirm this fact in a blend of poly(ethylene-oxide) (PEO) with lithium triflate and poly(*p*-phenylene-vinylene) (PPV).¹⁷ In consequence, the charge transport in the bulk becomes diffusion limited and is not affected by the applied bias.

Based on these facts, we synthesized in a well-controlled way a conjugated polyelectrolyte belonging to the polythiophene family carrying sulfonate side groups. Our intention was to improve the order using a controlled synthesis.¹⁸ Additionally, sterically demanding tetrabutylammonium cations were introduced to slow down the reorientation of the ions in an electric field.

Polythiophenes with permanently charged strong ionic side groups such as sulfonate were commonly synthesized in an uncontrolled way by electrochemical polymerization of thiophene monomers, already carrying the sulfonate substituent.¹⁹ This method does not lead to high regioregularity or well-defined polymers. To overcome this, we adapted a new synthetic route involving the polymer analogous conversion of a bromine side group to sulfonate. The polymer poly(3-(6-bromohexyl)thiophene) (P3BrHT) was obtained with high regioregularity (> 98%) and narrow polydispersity index (PDI: 1.12) using Kumada catalyst transfer polymerization (Scheme 8-1).^{20,21} The SEC number average molecular weight M_n is 20020 g mol^{-1} . We converted the alkyl-bromide substituent quantitatively to tetrabutylammonium poly(6-(thiophen-3-yl)hexane-1-sulfonate) (PTHS). The detailed synthesis procedure and characterization including MALDI-Tof MS (Figure 8-S1) are given in the supporting information.

Scheme 8–1. Synthesis Route Toward Regioregular and Narrowly Distributed Tetrabutylammonium Poly(6-(thiophen-3-yl)hexane-1-sulfonate) (PTHS)


The final polymer PTHS is highly soluble in water (up to 20 wt%), methanol, etc., but insoluble in pure chloroform or THF. In methanol and DMSO PTHS does not aggregate and therefore exhibit blue-shifted absorption spectra. In aqueous solutions the absorption spectrum is red-shifted and shows distinct vibrational bands similar to those of aggregated crystalline P3HT (Figure 8–1a).²² The absorption peak in water is at 543 nm and a strong shoulder appears at 580 nm. Comparable features were observed for other polythiophene based CPEs.²³ The absorption spectrum of a PTHS thin film resembles the spectrum in aqueous solution with a negligible broadening of the high energy region (Figure 8–1a).


Figure 8–1. a) Normalized absorption spectrum of PTHS in water, methanol and as dried thin film; b) Topographic AFM image of a PTHS thin film.

There is no significant difference between the thin-film spectra obtained from methanol or water except that the spectra of thin film from aqueous solution show more pronounced shoulder at 580 nm. In P3HT the crystallization of the chains leading to lamellar crystals are visible in topographic AFM images of thin films.²⁴ However, AFM micrographs of a PTHS thin film (Figure 8–1b) show a homogeneous surface with no indication of periodically ordered structures on the surface.

In general, electronic mobilities of CPEs have been estimated from the space-charge-limited-current (SCLC) applying a short pulsed bias to suppress ion motion.²⁵ Otherwise the applied bias will not only affect the charge transport but also cause the reorganization of the ions, leading to a diffusion limited transport. To examine this, PTHS was tested in a diode geometry, *i.e.* PTHS was coated onto a ITO substrate in different thicknesses and Au was evaporated on top as

counter electrode. The current density versus voltage square (J - V^2) characteristics for various film thicknesses for these hole-only device structures are depicted in Figure 8–2a.

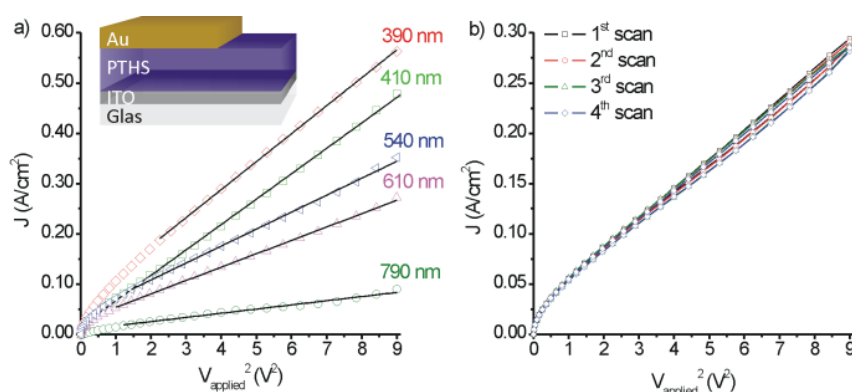


Figure 8–2. a) J - V^2 characteristics for various layer thicknesses. The straight lines represent the fits used for the calculation of the mobility and the inset shows a scheme of the device geometry; b) J - V^2 plots for four scan cycles of the diode with a 610 nm layer of PTHS.

Surprisingly, no hysteresis was observed for the measurements, although a constant bias was applied instead of a pulsed voltage sweep. This is in strong contrast to reported CPEs in literature, where ion motion and redistribution leads to a strong hysteresis between forward and reverse scans.^{25,26} To confirm the reproducibility, we conducted several scan cycles, of which the scans 1-4 are representatively shown in Figure 8–2b. The results obviously confirm the consistency of the measurements, as no significant changes of the current-voltage characteristics were observed. The charge carrier mobility was calculated from the slope of the J - V^2 -plot according to Mott-Gurneys law for space charge limited current.²⁷ An average hole mobility of $(1.3 \pm 0.5) \times 10^{-2} \text{ cm}^2 \text{ V}^{-1} \text{ s}^{-1}$ was determined and confirmed for various thicknesses ranging from 390 nm to 790 nm (the individual values are summarized in the supporting information). The hole mobility is almost four orders of magnitude higher than those for previously reported CPEs based on polythiophenes.¹⁴ The SCLC bulk mobility reported here is even better than for highly crystalline P3HT and it is one of the highest reported values for conjugated systems.^{15,25,28-30}

To further study the influence of any possible ion motion on the charge carrier mobility, we examined the temporal response of the current density for different voltages. CPEs generally show a slow increase of current after turning on voltage to reach a constant value for a particular voltage. This response time is usually in the order of several seconds due to a slow reorganization of ions.³¹ In the case of PTHS, a constant current flow was observed within less than 200 ms after the respective voltage was applied. The response curves for a series of voltages are given in Figure 8–3a. The current values remain constant over a period of at least 300 s, at which time the measurement was not further continued (Figure 8–S2). It is noteworthy to mention that the observed current values matches well with the previously shown diode characteristics.

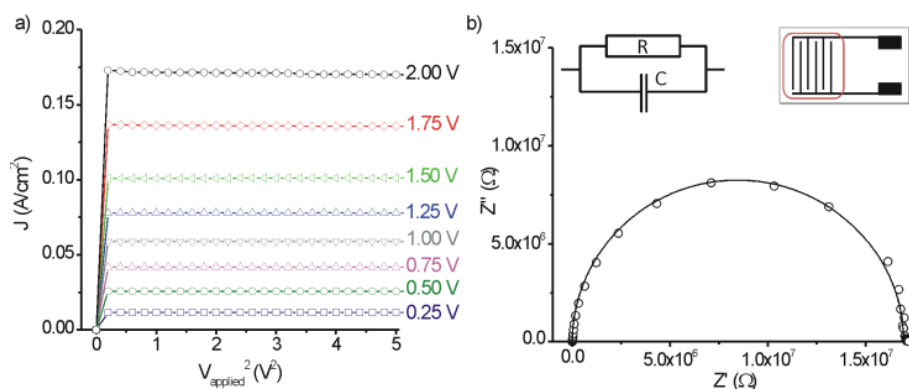


Figure 8–3. a) The temporal response of the current density for voltages ranging from 0.25 V to 2.0 V of a thin film with a thickness of 540 nm; b) Nyquist plot of impedance spectroscopy data conducted on the polymer PTHS and the respective fit using a parallel combination of a resistor and a capacitor (left inset); the geometrical structure of the electrodes is shown in the right inset.

Additional impedance spectroscopy measurements should provide a comprehensive insight into the basic charge transport mechanism in thin films of PTHS.³² Impedance data were taken for frequencies ranging from 10 MHz down to 0.1 Hz and were plotted in a Nyquist-representation in the complex impedance plane as shown in Figure 8–3b. The measurement resulted in only one semicircle, which can be attributed to an equivalent circuit with a resistor parallel to a capacitor. The extrapolation of the respective fit to the real axis (Z') gives the resistance of the material and we estimated a specific material conductivity of $(1.4 \pm 0.3) \times 10^{-6} \text{ S cm}^{-1}$ (details of calculation are given in SI). For comparison, regioregular P3HT exhibits a specific conductivity in the range of 10^{-6} - $10^{-9} \text{ S cm}^{-1}$.^{33,34} The electronic configuration of a parallel capacitor and resistor is characteristic for semiconductor materials.³² In contrast, ion conducting materials or mixed conductors give rise to a capacitive tail at low frequencies or additional semicircles, respectively.³⁵ Recent studies on PEDOT:PSS with variable amounts of poly(styrene sulfonate) (PSS) depict characteristic results for electronic or ion conductive materials depending on the PSS content.³⁶ The temporal response of the current density and the impedance spectroscopy unambiguously substantiate the pure semiconducting characteristics of PTHS and exclude any ion motion or reorganization.

In conclusion, we developed for the first time a well-defined conjugated polyelectrolyte comprising a highly regioregular and narrowly dispersed polythiophene backbone carrying permanently charged strong anionic sulfonate groups. The low PDI could be guaranteed using the Kumada catalyst transfer polymerization. The final polymer PTHS was obtained by a quantitative conversion of the bromine side group to tetrabutylammonium sulfonate. The UV-vis absorption spectra of the final polymer PTHS in aqueous solution and thin film indicate aggregated species. The material exhibits a remarkably high hole carrier mobility of $(1.3 \pm 0.5) \times 10^{-2} \text{ cm}^2 \text{ V}^{-1} \text{ s}^{-1}$ as determined from the space charge limited current method. In contrast to CPEs reported in literature, no ion motion was detectable in PTHS upon applying a bias or in impedance spectroscopy measurements. The sterically demanding tetrabutylammonium counter ions contribute towards this restricted ion mobility. This unique combination of a series of synergic parameters finally results in an excellent hole transporting conjugated polyelectrolyte.

ASSOCIATED CONTENT

Supporting Information

Detailed experimental procedure, characterization of polymers, details on the J-V measurements and impedance spectroscopy. This material is available free of charge *via* the Internet at <http://pubs.acs.org>.

ACKNOWLEDGMENT

We thank Mathis Muth, Katharina Neumann and Martin Hufnagel for the help with the mobility calculations, SEC analysis and MALDI-ToF measurements, respectively. Financial support from SFB 840, EU-India Largecells (GA. No. 261936) and the Elitenetzwerk Bayern (ENB), Macromolecular Science, are kindly acknowledged.

REFERENCES

REFERENCES

- (1) A. Facchetti, *Chem. Mater.* **2010**, *23*, 733-758.
- (2) Y. Li, Y. Zou, *Adv. Mater.* **2008**, *20*, 2952-2958.
- (3) D. T. McQuade, A. E. Pullen, T. M. Swager, *Chem. Rev.* **2000**, *100*, 2537-2574.
- (4) C. D. Dimitrakopoulos, P. R. L. Malenfant, *Adv. Mater.* **2002**, *14*, 99-117.
- (5) E. W. H. Jager, E. Smela, O. Inganäs, *Science* **2000**, *290*, 1540-1545.
- (6) S. Günes, H. Neugebauer, N. S. Sariciftci, *Chem. Rev.* **2007**, *107*, 1324-1338.
- (7) R. Sondergaard, M. Helgesen, M. Jorgensen, F. C. Krebs, *Adv. Energy Mater.* **2011**, *1*, 68-71.
- (8) C. Zhu, L. Liu, Q. Yang, F. Lv, S. Wang, *Chem. Rev.* **2012**, *112*, 4687-4735.
- (9) C. Zhong, C. Duan, F. Huang, H. Wu, Y. Cao, *Chem. Mater.* **2010**, *23*, 326-340.
- (10) H. Jiang, P. Taranekar, J. R. Reynolds, K. S. Schanze, *Angew. Chem., Int. Ed.* **2009**, *48*, 4300-4316.
- (11) K. P. R. Nilsson, O. Inganäs, *Nat. Mater.* **2003**, *2*, 419-424.
- (12) A. Herland, K. P. R. Nilsson, J. D. M. Olsson, P. Hammarström, P. Konradsson, O. Inganäs, *J. Am. Chem. Soc.* **2005**, *127*, 2317-2323.
- (13) A. Duarte, K.-Y. Pu, B. Liu, G. C. Bazan, *Chem. Mater.* **2010**, *23*, 501-515.
- (14) G. K. V. V. Thalluri, J.-C. Bolsée, A. Gadisa, M. Parchine, T. Boonen, J. D'Haen, A. E. Boyukbayram, J. Vandenberg, T. J. Cleij, L. Lutsen, D. Vanderzande, J. Manca, *Sol. Energy Mater.* **2011**, *95*, 3262-3268.
- (15) C. Goh, R. J. Kline, M. D. McGehee, E. N. Kadnikova, J. M. J. Frechet, *Appl. Phys. Lett.* **2005**, *86*, 122110-122113.
- (16) A. Garcia, R. Yang, Y. Jin, B. Walker, T.-Q. Nguyen, *Appl. Phys. Lett.* **2007**, *91*, 153502-153503.
- (17) J. C. deMello, N. Tessler, S. C. Graham, R. H. Friend, *Phys. Rev. B: Condens. Matter Mater. Phys.* **1998**, *57*, 12951-12963.
- (18) C. Scharsich, R. H. Lohwasser, M. Sommer, U. Asawapirom, U. Scherf, M. Thelakkat, D. Neher, A. Köhler, *J. Polym. Sci. B Polym. Phys.* **2012**, *50*, 442-453.
- (19) R. H. Karlsson, A. Herland, M. Hamedi, J. A. Wigenius, A. Åslund, X. Liu, M. Fahlman, O. Inganäs, P. Konradsson, *Chem. Mater.* **2009**, *21*, 1815-1821.
- (20) L. Zhai, R. L. Pilston, K. L. Zaiger, K. K. Stokes, R. D. McCullough, *Macromolecules* **2002**, *36*, 61-64.
- (21) R. H. Lohwasser, M. Thelakkat, *Macromolecules* **2011**, *44*, 3388-3397.
- (22) J. Clark, C. Silva, R. H. Friend, F. C. Spano, *Phys. Rev. Lett.* **2007**, *98*, 206406.

- (23) M. Chayer, K. Faïd, M. Leclerc, *Chem. Mater.* **1997**, *9*, 2902-2905.
- (24) Z. Wu, A. Petzold, T. Henze, T. Thurn-Albrecht, R. H. Lohwasser, M. Sommer, M. Thelakkat, *Macromolecules* **2010**, *43*, 4646-4653.
- (25) A. Garcia, T.-Q. Nguyen, *J. Phys. Chem. C* **2008**, *112*, 7054-7061.
- (26) J. Park, C. V. Hoven, R. Yang, N. Cho, H. Wu, T.-Q. Nguyen, G. C. Bazan, *J. Mater. Chem.* **2009**, *19*, 211-214.
- (27) M. Giulianini, E. R. Waclawik, J. M. Bell, N. Motta, *Appl. Phys. Lett.* **2009**, *94*, 083302-083303.
- (28) Y. Liang, D. Feng, Y. Wu, S.-T. Tsai, G. Li, C. Ray, L. Yu, *J. Am. Chem. Soc.* **2009**, *131*, 7792-7799.
- (29) C. Hunziker, X. Zhan, P. A. Losio, H. Figi, O. P. Kwon, S. Barlow, P. Gunter, S. R. Marder, *J. Mater. Chem.* **2007**, *17*, 4972-4979.
- (30) D. S. Chung, D. H. Lee, C. Yang, K. Hong, C. E. Park, J. W. Park, S.-K. Kwon, *Appl. Phys. Lett.* **2008**, *93*, 033303-033303.
- (31) A. Garcia, R. C. Bakus li, P. Zalar, C. V. Hoven, J. Z. Brzezinski, T.-Q. Nguyen, *J. Am. Chem. Soc.* **2011**, *133*, 2492-2498.
- (32) E. Barsoukov, J. R. Macdonald *Impedance Spectroscopy*; Wiley-Interscience: Hoboken, N.J., **2005**.
- (33) T.-A. Chen, X. Wu, R. D. Rieke, *J. Am. Chem. Soc.* **1995**, *117*, 233-244.
- (34) J. Obrzut, K. A. Page, *Phys. Rev. B: Condens. Matter Mater. Phys.* **2009**, *80*, 195211.
- (35) S. N. Patel, A. E. Javier, G. M. Stone, S. A. Mullin, N. P. Balsara, *ACS Nano* **2012**, *6*, 1589-1600.
- (36) T. Stöcker, A. Köhler, R. Moos, *J. Polym. Sci. B Polym. Phys.* **2012**, *50*, 976-983.

SUPPORTING INFORMATION

Experimental section:

Materials and characterization:

Unless otherwise stated, all chemicals were used as received from commercial suppliers. 2,5-Dibromo-3-(6-bromohexyl)thiophene and the catalyst 1,3-bis(diphenylphosphino)propanenickel(II) chloride ($\text{Ni}(\text{dppp})\text{Cl}_2$) were prepared according to known procedures.¹⁻³ The salt tetra-*n*-butyl ammonium sulfite was prepared *via* hydrolysis of dimethyl sulfite by 2 eq. of tetra-*n*-butyl ammonium hydroxide (40 wt% solution in methanol)

¹H-NMR spectra were recorded on a Bruker Avance 250 spectrometer at 300 MHz. The spectra were calibrated according to the respective solvent signal. Size exclusion chromatography (SEC) measurements were performed utilizing a Waters 515-HPLC pump with stabilized THF as the eluent at a flow rate of 0.5 mL/min. A 20 μL volume of a solution with a concentration of approximately 1 mg/mL was injected into a column setup, which consists of a guard column (Varian, 50 \times 0.75 cm, ResiPore, particle size 3 μm) and two separation columns (Varian, 300 \times 0.75 cm, ResiPore, particle size 3 μm). The compounds were monitored with a Waters UV detector at 254 nm. Polystyrene was used as external standard and 1,2-dichlorobenzene as an internal standard for calibration. Matrix assisted laser desorption ionizations spectroscopy with time of flight detection mass spectroscopy (MALDI-ToF MS) measurements were performed on a Bruker Reflex III using Dithranol as matrix and a mixture of 1000:1 (Matrix:Polymer).

Synthesis of the precursor polymer poly(3-(6-bromohexyl)thiophene) (P3BrHT):

2,5-Dibromo-3-(6-bromohexyl)thiophene (3 g, 7.41 mmol) was added to a dried 250 ml flask and the vessel was evacuated once again and flushed with nitrogen. With dry THF (15 ml) the concentration was set to 0.5 mmol/ml and tert-Butylmagnesium chloride (1.25 M in THF, 5.93 ml, 7.41 mmol) was added dropwise. After 20 h of stirring the concentration was reduced to 0.1 mmol/ml. 1,3-Bis(diphenylphosphino)propan-nickel(II)chlorid (0.040 g, 0.074 mmol) (suspension in THF) was added to start the polymerization. After 1 h the polymerization was quenched by adding 2 ml of 16% aqueous HCl. The mixture was concentrated and the polymer was precipitated in Methanol. The polymer was purified by soxhlet extraction with methanol.

GPC: $M_n = 20020$ g/mol, $M_w = 21860$ g/mol, PDI = 1.09; MALDI-tof: $M_n = 20700$ g/mol, $M_w = 21100$ g/mol, PDI = 1.02; NMR: δ_{H} (300 MHz; CDCl_3) 1.39-1.47 (4 H, m), 1.64-1.68 (2 H, q, $\beta\text{-CH}_2$), 1.78-1.85 (2 H, q, $-\text{CH}_2\text{-CH}_2\text{-Br}$), 2.73-2.78 (2 H, t, $\alpha\text{-CH}_2$), 3.36 (2 H, $\text{CH}_2\text{-Br}$), 6.91(1 H,s, $H_{\text{arom.}}$).

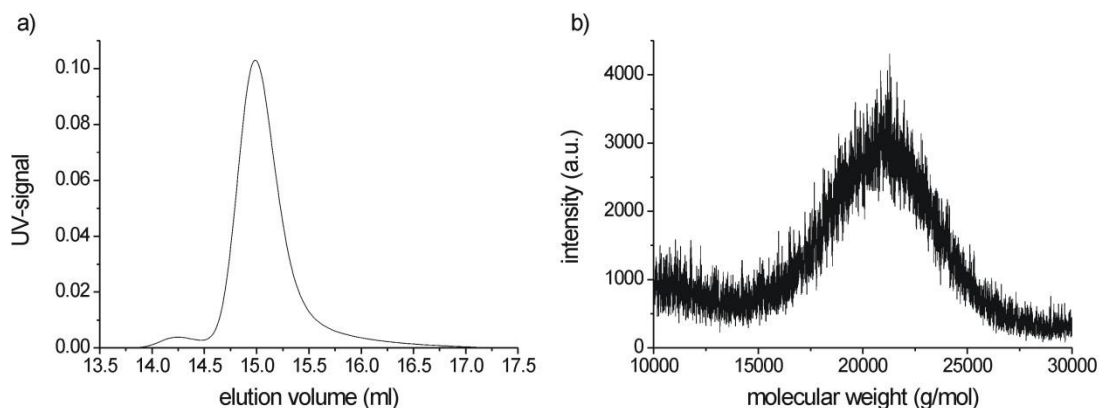


Figure 8-S1. SEC trace (a) and MALDI-ToF spectrum (b) of the precursor polymer poly(3-(6-bromohexyl)thiophene) (P3BrHT).

Synthesis of poly(6-(thiophen-3-yl)hexane-1-sulfonate) (PTHS):

Poly(3-(6-bromohexyl)thiophene) (0.1 g, 0.41 mmol) was first dissolved in THF (27.0 ml) at 40°C and the mixture was degassed by a constant argon stream for 20 min. Tetra-*n*-butyl ammonium sulfite (1 M in DMSO, 4.05 ml, 4.05 mmol) was added and the mixture was kept at 40°C for 24 h. Water was added and the reaction mixture was dialyzed against ultrapure water (MilliQ) to purify the polymer. Finally the solution was freeze dried to get the polyelectrolyte powder.

NMR: δ_{H} (300 MHz; *d*-THF/D₂O 2/1) 0.86-0.96 (12 H, t, N⁺(-CH₂-CH₂-CH₂-CH₃)₄), 1.25-1.41 (8 H, dt, N⁺(-CH₂-CH₂-CH₂-CH₃)₄), 1.35-1.48 (4 H, m, β -CH₂-CH₂-CH₂-CH₂-CH₂-S), 1.52-1.67 (8 H, m, N⁺(-CH₂-CH₂-CH₂-CH₃)₄), 1.67-1.80 (4 H, m, β -CH₂-CH₂-CH₂-CH₂-CH₂-S), 2.63-2.88 (4 H, m, α -CH₂-CH₂-CH₂-CH₂-CH₂-S), 3.10-3.25 (8 H, m, N⁺(-CH₂-CH₂-CH₂-CH₃)₄), 6.98-7.08 (1 H, s, *H*_{arom.}).

J-V measurements:

The hole mobility was estimated in a diode geometry from the space charge limited current (SCLC) regime.⁴ As substrate we used ITO coated glass (Merck, 10 Ω/□). On top an active layer of PTHS was knife coated from a 5 wt% solution in water varying the gap thicknesses. PEDOT/PSS was abandon due to the similar solubility, as it may swell or even form intermixed layers with PTHS. The thickness of the active layer was determined with a profilometer (Bruker, Veeco, DekTak 150). As counterelectrode gold was thermally evaporated on top using an Edwards Auto 306 vapor depositor. The J-V curves were recorded with a Keithley 2420 sourcemeter and a connected PC at room temperature in the dark. Long-term temporal response curves of the current density for voltages ranging from 0.25 V to 2.0 V of a thin film with a thickness of 540 nm are shown in Figure 8–S2. The individual hole mobilities of the samples with varying layer thicknesses are summarized in Table 8–S1. The mobilities were calculated according to Mott-Gurneys law for space charge limited current:⁴

$$J = \frac{9}{8} \epsilon_r \epsilon_0 \mu \frac{V^2}{L^3}$$

In this equation J is the current density, ϵ_r is the relative dielectric constant of the film, ϵ_0 is the vacuum permittivity, μ is the mobility at a specified electrical field, V is the applied voltage and L is the thickness of the active layer.

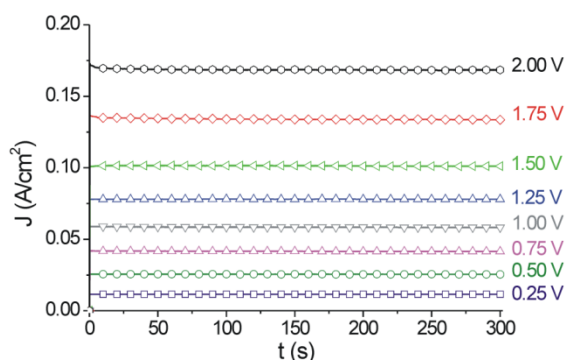


Figure 8–S2. Long-term temporal response of the current density for voltages ranging from 0.25 V to 2.0 V of a thin film with a thickness of 540 nm.

Table 8–S1. Overview of hole transport mobilities μ_h determined for the individual samples with different layer thickness d .

layer thickness (d)	hole transport mobility (μ_h)
390 nm	$9.5 \times 10^{-3} \text{ cm}^2/\text{Vs}$
410 nm	$1.0 \times 10^{-2} \text{ cm}^2/\text{Vs}$
540 nm	$1.5 \times 10^{-2} \text{ cm}^2/\text{Vs}$
610 nm	$1.7 \times 10^{-2} \text{ cm}^2/\text{Vs}$
790 nm	$1.2 \times 10^{-2} \text{ cm}^2/\text{Vs}$

Impedance measurements:

The test material was coated as a thin layer (300 nm) on top of planar micro-patterned Au electrodes. The electrode structure (Figure 8–S2) consists of interdigital electrodes (IDE) with a line width and spacing of 100 μm . The length of one finger electrode is 4.7 mm. The IDE structure represents a parallel arrangement of 29 single resistors, *i.e.* test material within one spacing between each two electrode fingers. A Novocontrol Alpha-Analyzer was used as DC source and recorder. The data was fitted according to the following equation:

$$\underline{Z} = \frac{R}{1 + (i\omega CR)}$$

In this equation \underline{Z} is the complex impedance, R is the resistivity, C is the capacitance and ω is the applied frequency. As the structure is a combination of single resistors the resistivity of the individual resistor R_{single} is related to the total resistivity R by

$$\frac{1}{R} = \frac{N}{R_{single}}$$

where N is the number of resistors, which was 29 in our case.

Taking the electrode structure into account and assuming a homogeneous electrical field distribution inside the test material, we calculated the specific conductivity σ of PTHS. With

$$R_{single} = \rho \cdot \frac{s}{l \cdot d}$$

the specific electrical resistance ρ of the material was calculated according to

$$\rho = N \cdot R \cdot \frac{l \cdot d}{s}$$

with the length of the electrodes l , the thickness of the material d and the spacing between the electrodes s . These values are further shown in Figure 8–S2. The specific conductivity σ of PTHS was obtained as the reciprocal value of ρ .

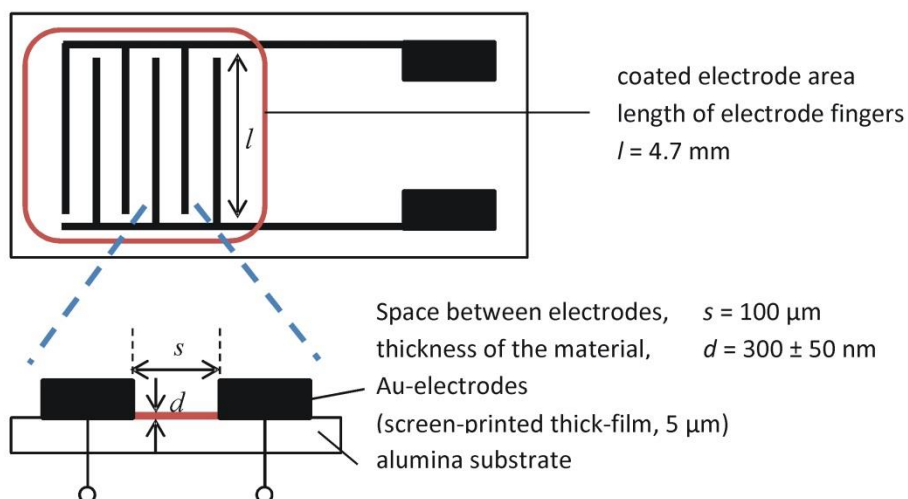


Figure 8–S3. Geometrical scheme of the electrodes used for the impedance measurements.

References:

- (1) Bäuerle, P.; Würthner, F.; Heid, S. *Angew. Chem.* **1990**, *102*, 414.
- (2) Miyanishi, S.; Tajima, K.; Hashimoto, K. *Macromolecules* **2009**, *42*, 1610.
- (3) Van Hecke, G. R.; Horrocks, W. D. *Inorg. Chem.* **1966**, *5*, 1968.
- (4) Mott, N. F.; Gurney, R. W. *Electronic processes in ionic crystals*; 2. ed.; Dover Publ.: New York, 1964.

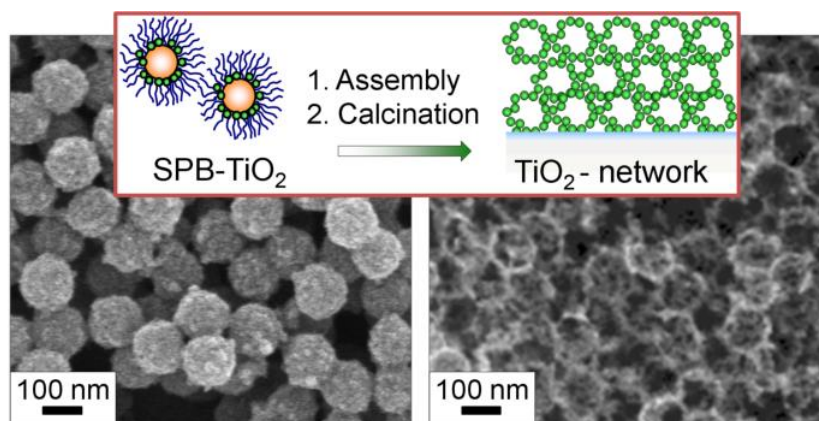
9. APPENDIX: POLYMER TEMPLATED NANOCRYSTALLINE TITANIA NETWORK FOR SOLID STATE DYE SENSITIZED SOLAR CELLS

Johannes C. Brendel,^a Yan Lu,^b Mukundan Thelakkat^{*,a}

^a Applied Functional Polymers, Macromolecular Chemistry I, University of Bayreuth, 95440 Bayreuth, Germany,

^b Physikalische Chemie I, University of Bayreuth, 95440 Bayreuth, Germany.

*E-mail of corresponding author: mukundan.thelakkat@uni-bayreuth.de



Published in *Journal of Materials Chemistry* **2012**, 20, 7255-7265.

ABSTRACT

We report a novel preparation method for nanocrystalline TiO₂ networks with controlled pore sizes using spherical polyelectrolyte brushes (SPB) as templates. The SPB consists of a solid polystyrene core from which anionic polyelectrolytes are densely grafted. The SPB templates are synthesized *via* conventional photoemulsion polymerization with efficient control of core size and brush length. Subsequently, the TiO₂ precursor is hydrolyzed at room temperature within the anionic brush to obtain anatase nanocrystals of 12–20 nm size. These stable and form-persistent composite particles of SPB decorated with anatase nanocrystals are then assembled on a conductive substrate. The subsequent calcination of this composite layer leads to a robust nanocrystalline TiO₂ network, in which the pores and the wall thickness are directly correlated to the polystyrene core size and the amount of TiO₂ hydrolyzed within the brush respectively. In this study, we optimized different thin-film preparation methods and characterized the resulting nanocrystalline TiO₂ networks using SEM and XRD. Moreover, the applicability of these nanocrystalline networks as electron transport layers are tested in solid-state dye-sensitized solar cells (SDSCs). The first test devices exhibited efficiencies up to 0.8%. The precise and individual control of parameters such as porosity, thickness and crystallinity makes this concept highly attractive for the realization of efficient solid-state hybrid devices.

INTRODUCTION

Low cost photovoltaic devices based on porous titanium dioxide electrodes have been in the focus of scientific research within the last decades. The advantages of high chemical stability, low toxicity and good availability turn this material into the most attractive inorganic broad-band electron transport material.¹ Several methods are established for the preparation of mesoporous nanocrystalline TiO₂, which includes hydrothermal methods,² chemical vapor deposition,³ liquid phase deposition⁴ and sol–gel processes.⁵ The latter is most commonly used in combination with polyethylene glycol additives to form stabilized mesoporous layers.⁶ Grätzel *et al.* obtained high power conversion efficiencies of above 10% on the basis of a mesoporous TiO₂ layer sensitized with dye in combination with a I⁻/I₃⁻ redox electrolyte as hole transport material.⁷ However, to guarantee an adequate long-term stability for photovoltaic devices attempts have been undertaken to replace this liquid hole conductor using solid-state materials. Organic low molecular weight materials as well as semiconductor polymers are promising alternatives.^{8,9} Using low molecular weight spiro-OMeTAD efficiencies in the range of 5% have been already reported.¹⁰ On the other hand the use of polymer sensitizers and/or hole conductors lead to insufficient pore filling and decreased device performance.^{11–14} In general for solid-state devices, the thickness of the porous layer must be reduced to 1–2 mm from the original 10–20 mm in electrolyte cells to guarantee an efficient pore filling and charge transport through the solid organic hole conductor. Since the infiltration of porous TiO₂ with solid-state hole conductors depends largely on the pore size and the pore continuity of the TiO₂ network, an exact control of the morphology in terms of porosity is required.¹⁵ Additionally a high electron diffusion length, almost 2–3 times the thickness of the porous TiO₂ layer is essential to transport and collect all separated charges.^{16–18} Therefore a better individual control of the pore size, morphology and thickness of the porous titania layer is desired for solid state devices. Several approaches have been attempted to gain control over the resulting TiO₂ structures. One of these

methods deals with the use of amphiphilic block copolymers as additives in sol–gel to control the resulting mesoscale structure of the titania network.^{19,20} This control is based both on the microphase separation and the diverse colloid structures of the block copolymer used. During this self-organization process several factors such as the polymer concentration, the nature of the colloid structures such as micelles or vesicles or the precursor content influence the resulting metal oxide network morphology. In consequence, much effort has to be spent in this concept to guarantee the control and reproducibility of the resulting titania networks. Another concept that is already successfully applied in solid-state dye-sensitized solar cells is based on vertically aligned TiO₂ nanostructures as nanotubes or rods prepared by anodic oxidation.^{21,22} Further initiatives utilize replica of titania prepared from blockcopolymer templates carrying sacrificial blocks^{23,24} or well-ordered scaffolds of polystyrene latex particles as templates to gain control over the pore size as well as periodicity of the TiO₂ network.²⁵

We present a new convenient templated preparation of porous nanocrystalline metal oxide networks with control of the morphology. Spherical polyelectrolyte brushes (SPB) were used as templates to crystallize titania within these brushes and these SPB-TiO₂ composite particles were assembled on a conducting surface. In a final step these hybrid layers were calcinated to remove the organic templates resulting in a nanocrystalline titania network with well-defined pore sizes. These porous titania layers were characterized using SEM and XRD. Further they were applied as electrodes in solid-state solar cells.

EXPERIMENTAL

Materials

Tetraethylorthotitanate (TEOT, 97%), glycerin (99%), 4-tertbutyl pyridine (99%), titanium(IV)bis(acetoacetonato)-di(isopropanoxyate) (TAA, 75 wt% solution in isopropanol) and N-lithiofluoromethane sulfonamide (LiN(SO₂CF₃)₂, 99%) were purchased from Sigma-Aldrich and used as received. The solvents ethanol (VWR p.a.), DMF (Fluka, puriss. absolute over molecular sieve) and chlorobenzene (Fluka, puriss. absolute over molecular sieve) were also purchased and used as received. The Solid hole conductor, 2,2',7,7'-tetrakis-(*N,N*-di-4-methoxyphenyl amino)-9,9'-spiro-bifluorene (spiro-OMeTAD) was purchased from Merck, Germany. Glass substrates (Tec 15) covered with a 0.5 mm thick fluorine-doped tin oxide (FTO) layer having a sheet resistance of 15 Ohm per square were purchased from Hartford Glass Co. Inc., Indiana, USA. The dye *cis*-di(isothiocyanato)-(2,2'-bipyridyl-4,4'-dicarboxylic acid)-(2,2'-bipyridyl-4,4'-bis[4-(diphenylamino)styryl]-ruthenium(II) (RuNCS-TPA) was previously synthesized in our workgroup. Characterization methods Optical studies were made using a Zeiss Axio Imager A1m optical microscope. All images were recorded with an attached AxioCam MRc5 digital camera and transferred to the connected computer. All SEM images were recorded on a Zeiss 1530 field emission scanning electron microscope (FESEM). The applied voltage was always between 1 and 3 kV. To increase the contrast and to improve the uniformity of the images, in some cases a thin layer of carbon (10–15 nm) was sputtered on the samples with a Bal-tec MED 010 machine under vacuum. TEM images were recorded on a Zeiss CEM902 transmission electron microscope. The samples were prepared by drying a drop of a highly diluted dispersion of SPB-TiO₂ composite particles on a carbon coated Cu grid (200 mesh).

Preparation of the SPB-TiO₂ composite particles

For the preparation of the SPB-TiO₂ composite particles we used PS-NaSS (polystyrene sodium sulfonate) brush particles with a core radius of 74 nm (measured by dynamic light scattering) and a brush length of approximately 200 nm prepared by photoemulsion polymerization.^{26,27} For the synthesis of TiO₂ nanocomposite particles only a batch process has been used. The reaction conditions are listed in Table 9–1.

Table 9–1. Reagent Contents of the Respective Samples SPB-TiO₂-1, SPB-TiO₂-2 and SPB-TiO₂-3

sample	SPB [g]	TEOT [ml]	water [ml]	ethanol [ml]
SPB-TiO ₂ -1	0.10	0.40	0.40	100
SPB-TiO ₂ -2	0.20	0.80	3.60	200
SPB-TiO ₂ -3	0.20	1.20	3.60	200

For a typical run, PS-NaSS brush particles were dispersed in ethanol. Water was then added while stirring to enable the hydrolysis of the TiO₂ precursor. The reaction was initiated by adding a solution of 0.15 ml tetraethylorthotitanate (TEOT) dissolved in 8 ml ethanol. For a semi-batch process, the TEOT solution was added drop wise at a feeding rate of 0.08 ml/min. The reaction mixture was stirred vigorously for two more hours after the complete addition of TEOT solution at room temperature. The TiO₂ alcosols were then washed with ethanol and water by repeated centrifugation 3 times and redispersed into water after cleaning. For the exchange of solvent the aqueous dispersion was washed with ethanol *via* ultra filtration columns over a filter with 100 nm pore size until the water was removed completely. The glycerin dispersions were prepared by the addition of glycerin at a weight ratio of 9 : 1 against SPB-TiO₂ composite and a subsequent evaporation of the ethanol.

TiO₂ network preparation

To assemble the SPB-TiO₂ composite particles on conductive substrates, 100 ml of a 5 wt% dispersion of SPB-TiO₂ particles for example in ethanol were spread over an active area of 2.5 cm to 1 cm, leading to a film thickness of approximately 2 mm after drying. The alternative 10 wt% dispersions in glycerin were applied using a 30 mm doctor blade, to receive a comparable film thickness after evaporation of the solvent. All samples, their respective preparation conditions and the resulting dry film thicknesses are summarized in Table 9–2.

Table 9–2. Preparation Conditions and Resulting Film Thicknesses

sample	preparation technique / dispersion composition / drying temperatur	dry film thickness
SPB-TiO ₂ -1a	Drop coating / 1 wt% (water) / 25°C	1.4 μm
SPB-TiO ₂ -1b	Drop coating / 5 wt% (ethanol) / 25°C	1.9 μm
SPB-TiO ₂ -1c	Drop coating / 5 wt% (ethanol) / 2°C	1.9 μm
SPB-TiO ₂ -1d	Blade gap 30μm / 10 wt% (glycerin) / 120°C	2.1 μm
SPB-TiO ₂ -2	Blade gap 30μm / 10 wt% (glycerin) / 120°C	2.0 μm
SPB-TiO ₂ -3	Blade gap 30μm / 10 wt% (glycerin) / 120°C	1.9 μm

To avoid direct contact of FTO and hole conductor, the substrates were previously covered with a compact layer of TiO₂ by spray pyrolysis of a 0.2 M titanium(IV)bis(acetoacetonato)-di(isopropanoxylate) solution in ethanol as reported elsewhere.²⁸

The direct calcination in air was carried out on a thermally controlled hot plate according to the following program: heating to 250°C at a ramp of 5 K/min, keeping at 250°C for 6 h, further heating to 500°C at a ramp of 5 K/min, keeping at 500°C for 1 h and cooling to room temperature at a ramp of 20 K/min. In the two-step calcination process a robust carbon composite was obtained after 2 h at 250°C and 5 h at 500°C in a quartz glass tube thoroughly flushed with argon. The removal of this composite was achieved by heating the substrates for additional 30 min at 500°C under air.

Solar cell preparation and characterization

After the calcination, the samples were washed with demineralized water to remove residual salt contents (see supporting information) and we immersed the substrates in a 0.5 mM solution of Ru-NCS-TPA for sensitization.²⁹ For the preparation of the organic hole conductor layer, 70 ml solution of 0.14 mol/l 2,2',7,7'-tetrakis-(*N,N*-di-4-methoxyphenyl amino)-9,9'-spirobifluorene, 0.02 mol/l Li[(CF₃SO₂)₂N] and 0.12 mol/l 4-*tert*-butyl pyridine (*t*-bp) in chlorobenzene were spin coated at 2000 rpm for 40 s. Au was finally applied by sublimation in an AUTO 306 vacuum chamber from Edwards. The photovoltaic current–voltage measurements were carried out by a Keithley 6517 Source-Measure unit under AM 1.5 G conditions (xenon arc lamp, Air Mass filters from Oriel). The intensity of light was calibrated with a standard Si-reference cell from the Fraunhofer Institut für Solarenergie (ISE), Freiburg as 100 mW/cm². For preparation of mesoporous TiO₂ as reference, a commercial paste (Dyesol TiO₂ Paste DSL 18NR-T) was diluted with terpineol to give a 2 mm thick layer after calcination, using a 90T screen printing mesh.

TiO₂ content and dye load determination

All tested substrates with FTO and a compact TiO₂ blocking layer were first weighted by a micro balance. After film preparation and calcination the weight of the substrates was again determined. Out of these values the weight of the dry film and the calcinated network was calculated. The TiO₂ content is given as the fraction of the TiO₂ network mass against the dry film mass.

For dye load measurements the substrates were laid into a glass basin of 20 ml volume without touching any side walls. For dye coating the substrates were covered with exactly 400 ml of an 0.5 mM solution of Ru-TPA-NCS in DMF and kept in the closed glass basins for 16 h. Afterwards, the substrates were carefully taken off the solution using a pair of tweezers. Kept above the basin the coated samples were washed with exactly 10 ml of DMF. For exact determination all solution must be collected in the glass basin. The concentrations of the washing solutions were estimated from UV-Vis absorption measurements. The exact dye amount in the solutions was calculated according to Lambert-Beer using the known absorption coefficients.³⁰ As reference a bare substrate with blocking layer was treated equally and the dye amount in the washing solution was also calculated. Finally the exact dye quantity on the TiO₂ network was determined as the difference of the residual dye amount in the reference cell solution and the respective sample solutions.

RESULTS AND DISCUSSION

The SPB template system consists of a solid polystyrene (PS) core, from which anionic polyelectrolyte chains are densely grafted by covalent bonds.²⁶ Similar to simple latex particles, the polystyrene core is easily synthesized in an emulsion polymerization with good control of the polydispersity and size. Subsequently polyelectrolyte brushes are grown from the photoinitiator immobilized surface of the PS-core *via* photopolymerization of sodium styrene sulfonate (NaSS) monomer. These SPB particles allow the growth of nanocrystals of titania within the brush by the hydrolysis of any TiO₂ precursor at room temperature. However these SPB particles – in contrast to common PS-beads – enable the control of the TiO₂ wall thickness, by their adjustable brush length. Thus we combine the advantages of both the rigidity of the latex template process and the flexibility of the block copolymer templated sol–gel approach. Recently, we have reported the catalytic activity of similarly prepared SPB-TiO₂ composites.²⁷ Additionally, the possibility of obtaining porous TiO₂ network from SPB-TiO₂ nanocomposites were also demonstrated. However it is a challenge to prepare porous TiO₂ electrodes from these composite particles on conducting substrates suitable for device application.

Here we report the successful preparation, optimization and application of porous TiO₂ electrodes from SPB-TiO₂ nanocomposites. In general, we used an aqueous dispersion of PSNaSS brush particles with a core radius of 74 nm (measured by dynamic light scattering) and a brush length of approximately 200 nm prepared by photo-emulsion polymerization. By reducing the feed rate of tetraethylorthotitanate (TEOT), the hydrolysis of the precursor can be controlled and nanocrystalline TiO₂ particles are formed within the brush at room temperature. After washing the as synthesized particles, we obtained stable SPB-TiO₂ composite particles dispersed in water. The solvent was finally exchanged *via* ultrafiltration to improve the wetting characteristics of the dispersions. In this way, diverse dispersions in solvents such as ethanol and glycerin with different contents of SPB-TiO₂ particle were prepared. For obtaining electrodes suitable for solid-state dye-sensitized solar cells (SDSCs) we focused on a continuous assembly of composite particles on transparent conductive substrates (fluorinated tin-oxide: FTO). The dispersions were applied on conductive substrates using doctor blade or drop cast techniques and dried. The final removal of the polymer brush templates by calcination leads to a macroporous scaffold of anatase nanoparticles. A general scheme of the preparation of a porous network on a conductive substrate is shown in Figure 9–1.

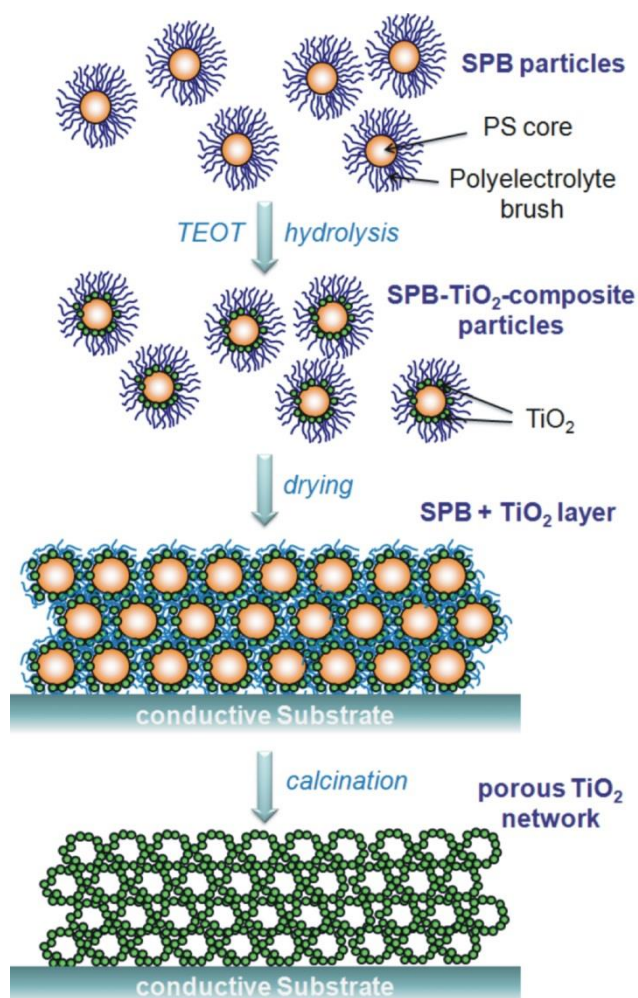


Figure 9–1. General scheme for the preparation of a porous TiO_2 network with controllable crystalline structures and morphology on a FTO substrate using spherical polyelectrolyte brush (SPB) particles as template. The precursor tetraethylorthotitanate (TEOT) is hydrolyzed within the brush to form the SPB- TiO_2 composite particles that are applied to a conductive substrate and calcinated to get a highly crystalline TiO_2 network.

Independent of the nature of the substrate the resulting nanocrystalline TiO_2 networks exhibit a large surface area in the range of 60 to 70 m^2/g (from BET analysis) after calcination in air. Figure 9–2 presents SEM images of SPB- TiO_2 nanocomposite particles on conductive substrate (a) and the resulting TiO_2 network after calcination (b). Obviously the removal of the PS core leaves macropores of approximately 100 nm and robust TiO_2 network walls of few nanometers thickness on FTO substrate.

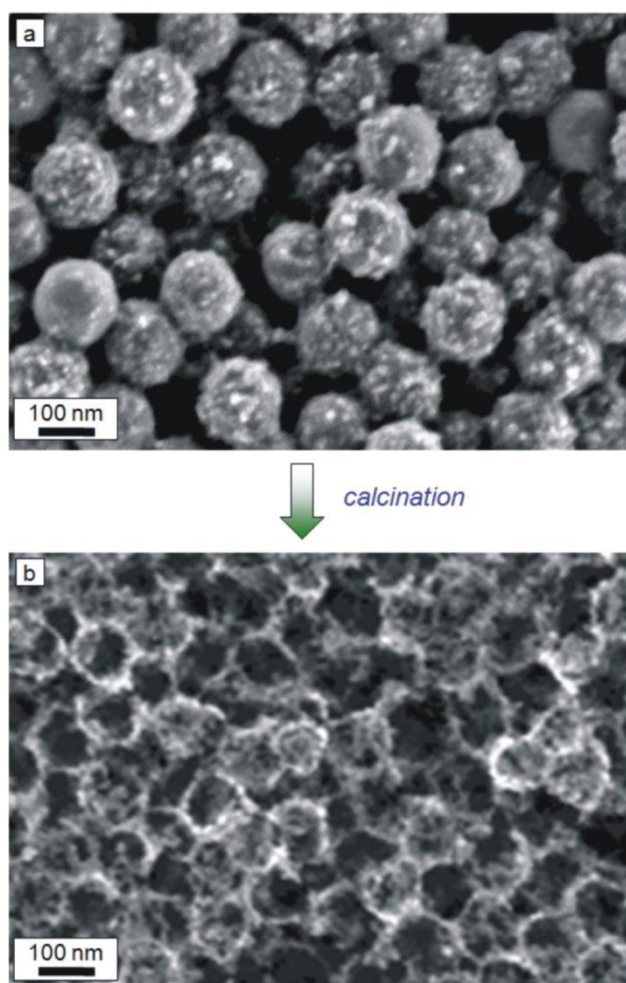


Figure 9–2. a) SEM image of SPB-TiO₂ composite particles applied to a conductive substrate before (a) and the resulting network after calcination (b). The pore size in the network responds to the PS core size.

Further XRD measurements of the SPB-TiO₂ composite particles obtained at room temperature and the resulting scaffold after calcination in air were carried out (Figure 9–3). Usually sol–gel approaches lead to amorphous TiO₂ structures which can be transformed into anatase or rutile crystallites *via* heat and pressure treatment. In our case the XRD measurements of the composite particles indicate, that a pure anatase phase of the nanocrystals is formed at room temperature (Figure 9–3a taken from ref. 27). After calcination on FTO substrate the pure anatase phase of titania is maintained in the porous titania network (Figure 9–3b). All the characteristic reflection peaks of anatase phase could be observed in both samples.

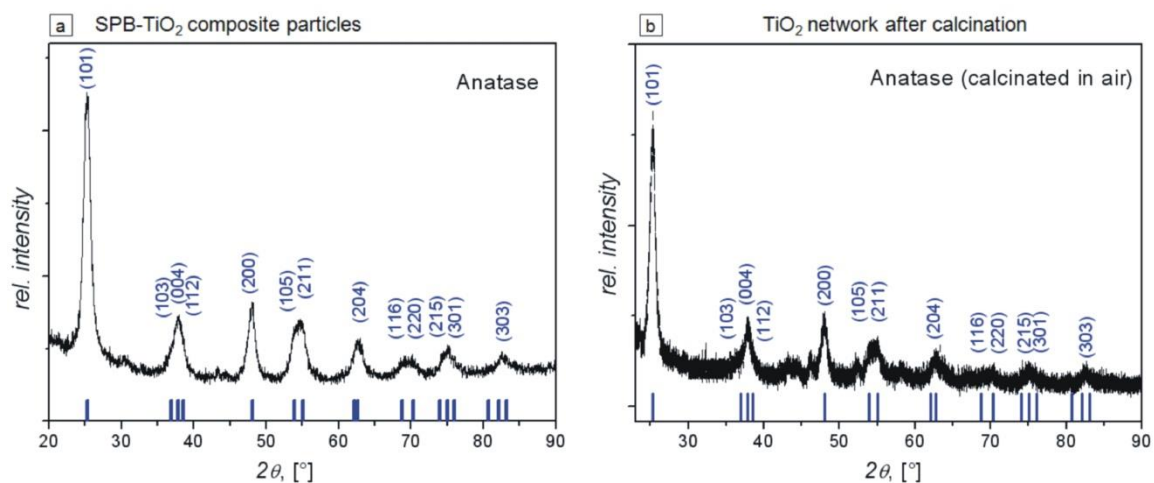


Figure 9–3. a) XRD measurements of the SPB-TiO₂ composite particles (a) taken from ref. 27 and the resulting TiO₂ network after calcination on FTO substrate in air (b).

A key requirement for highly efficient electrodes for solid-state dye-sensitized solar cells (SDSC) is a homogeneous and uniform porous layer of nanocrystalline TiO₂.⁹ Any formation of cracks during the assembly/drying or calcination process of the dispersions has to be avoided. In this context the surface polarity and roughness have a significant influence on avoiding cracks and the formation of smooth films. Secondly, several other factors such as temperature, humidity, nature of solvent (polarity, surface tension and boiling point) and colloidal concentration affect the assembly process of the SPB-TiO₂ composite particles. For the preparation of homogeneous thin films with thickness of about 2 μm, we tested different solvents such as water, ethanol and glycerin as dispersion mediums, different drying temperatures and concentrations of SPB-TiO₂ composite particles. Here we report the following four different preparation techniques SPB-TiO₂-1a-d for the assembly and drying of composite particles. All these SPB-TiO₂ composite particles were obtained by the hydrolysis of TEOT under the conditions of SPB : TEOT : water = 1 : 4 : 4 (weight ratio). The concentration of the SPB-TiO₂ composite particles in dispersion was also varied from 1 to 10 wt%: Sample SPB-TiO₂-1a: drop coating from 1 wt% water dispersion, dried at 25°C, Sample SPB-TiO₂-1b: drop coating from 5 wt% ethanol dispersion, dried at 25°C, Sample SPB-TiO₂-1c: drop coating from 5 wt% ethanol dispersion, dried at 2°C, Sample SPB-TiO₂-1d: doctor blading from 10 wt% glycerin dispersion, dried at 120°C.

The resulting composite films on FTO obtained from the above four different preparation methods were characterized using optical as well as scanning electron microscopy (SEM). The films obtained from water (SPB-TiO₂-1a) and ethanol at 25°C (SPB-TiO₂-1b) exhibited macroscopic cracks which could be observed in an optical microscope and therefore were not further considered for application. On the other hand the films from ethanol at 2°C (SPB-TiO₂-1c) and glycerin (SPB-TiO₂-1d) showed almost uniform crack-free films under the optical microscope. Therefore these two samples were further characterized and the SEM images are given in Figure 9–4.

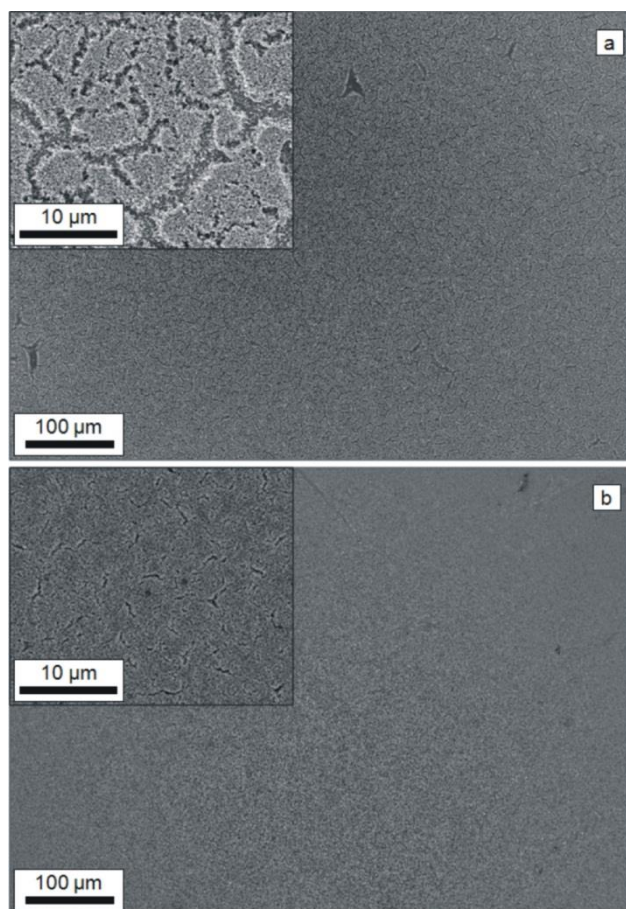


Figure 9–4. SEM images of samples on an FTO substrate: a) Sample SPBTiO₂-1c (drop casted from 5 wt% ethanol dispersion, dried at 2°C), b) Sample SPB-TiO₂-1d (doctor bladed from 10 wt% glycerin dispersion, dried at 120°C).

The samples assembled from water led to an uncontrolled aggregation of the particles and a non-uniform surface. Also the fast evaporation of ethanol as solvent at 20°C resulted in cracks. In order to reduce the evaporation speed, we additionally dried the dispersion on the substrates at low temperature of 2°C. This approach results in an almost homogeneous and uniform layer (Figure 9–4a), but at larger magnification still small cracks are visible. In spite of the relatively good film properties the preparation using ethanol as solvent also appeared to be very sensitive to the environmental conditions such as humidity. An exchange of the solvent from ethanol to glycerin resulted in dense dispersions suitable for doctor blade coating method. The high viscosity of this medium led to stable and homogenous wet films after coating. Due to the high boiling point of glycerin, we were also able to raise the temperature for the drying process to 120°C inhibiting all humidity effects. This combination provided the best conditions for the reproducible formation of highly homogeneous films (Figure 9–4b), which was not affected by any changes in environmental conditions.

The two latter assembly methods (sample SPB-TiO₂-1c and sample SPB-TiO₂-1d) were selected for the calcination step in which the SPB is burnt away and a TiO₂ nanocrystalline network is generated. The surface SEM images of these two samples after calcinations in air are shown in Figure 9–5.

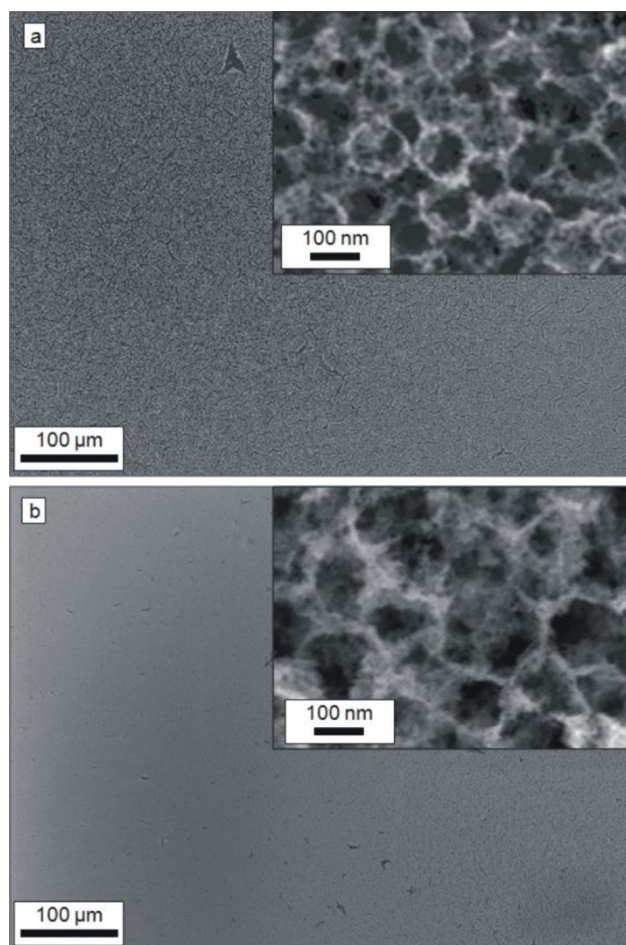


Figure 9–5. Surface SEM images under different magnification of porous TiO₂ films obtained from different samples on FTO substrates after calcination: a) Sample SPB-TiO₂-1c (drop casted from 5 wt% ethanol dispersion, dried at 2°C), b) Sample SPB-TiO₂-1d (doctor bladed from 10 wt% glycerin dispersion, dried at 120°C).

The smooth surfaces as expected from the assembled films are maintained after the calcination step, but the porosity is increased considerably. Furthermore, as visible from the insets in Figure 9–5, the pore size correlates well with the SPB particle size of 100 nm. Comparing the preparation techniques, the sample SPB-TiO₂-1d exhibits better smoothness than the sample SPB-TiO₂-1c. It has been shown in our earlier work that a two-step calcination procedure, first under argon followed by air, suppresses the tendency of the network to collapse. Moreover, contaminations of the titania network could also be minimized.²⁷ Therefore we applied a two-step calcination process for preparing electrodes (see methods section).

An additional question here was whether the TiO₂ wall thickness/content can be varied by changing the added TEOT precursor concentration. In this regard, we varied the precursor and water content during the hydrolysis reaction from the standard SPB-TiO₂-1 (SPB/TEOT/water ratio of 1/4/4 wt/wt) used for the assembly and thin film preparation described above to get additional SPB-TiO₂-2 and SPB-TiO₂-3 samples as summarized in Table 9–3.

Table 9–3. Ratio of Different Components (SPB, TEOT and Water) Used for the Preparation of SBP-TiO₂ Composite

sample	SPB	TEOT	water
SPB-TiO ₂ -1	1	4	4
SPB-TiO ₂ -2	1	4	18
SPB-TiO ₂ -3	1	6	18

In SPB-TiO₂-2 the water content was increased by a factor of about 4 keeping the TEOT amount constant, whereas in SPB-TiO₂-3, the TEOT amount was also increased. The resulting SPB-TiO₂ composite particles were examined by transmission electron microscopy. The TEM images of the respective samples are shown in Figure 9–6.

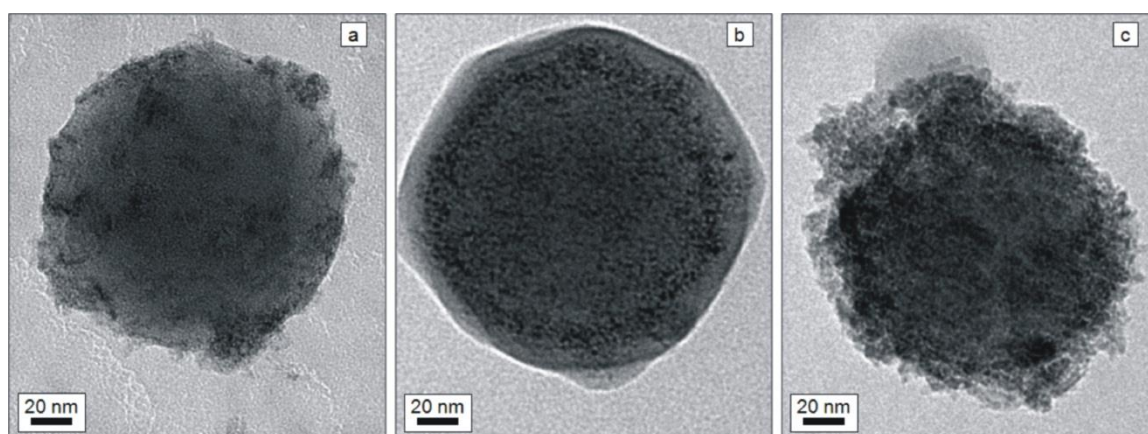


Figure 9–6. Comparison of different SPB-TiO₂ composite particles prepared according to the following reaction conditions: a) TEM image of SPB-TiO₂-1 obtained from SPB/TEOT/water wt/wt ratio of 1/4/4, b) SPB-TiO₂-2 prepared from SPB/TEOT/water wt/wt ratio of 1/4/18 and c) SPB-TiO₂-3 from SPB/TEOT/water wt/wt ratio of 1/6/18.

By increasing the water content from the sample SPB-TiO₂-1 to sample SPB-TiO₂-2, a dense layer of titania was formed covering the whole PS-core. A possible explanation is the presence of a dense layer of water soaked up in the polyelectrolyte corona at high water content, which hydrolyzes TEOT uniformly. In consequence at low water content (in SPB-TiO₂-1) the precursor can only be hydrolyzed in the water covered parts of the SPB particle. On the other hand, the increase of the precursor content from sample SPB-TiO₂-2 to SPB-TiO₂-3 resulted in densely packed titania nanocrystals on SPB surface. Thus there is an enormous influence of precursor/water content on the resulting TiO₂ nanocrystal morphology. For the assembly and calcination on conducting surface, SPB-TiO₂-2 and SPB-TiO₂-3 samples were treated under the same conditions as those for SPB-TiO₂-1d (assembled from 10 wt% glycerin dispersion and dried at 120°C) and calcinated in a two-step procedure as described above.

Finally, we prepared solid-state dye-sensitized solar cells (SSSCs) in order to study the suitability of these differently prepared TiO₂ networks as porous electrodes in devices. The details of the different preparation steps are given in the methods section. The FTO substrates used were previously covered with a compact layer of titania to avoid contact of the hole conductor with the FTO electrode as described earlier.²⁸ Subsequent to calcination of different titania samples on such substrates, we immersed the substrates in a solution of cis-Di(isothiocyanato)-(2,2'-bipyridyl-4,4'-dicarboxy)-(2,2'-bipyridyl-4,4'-bis[4-(diphenylamino)styryl]-ruthenium(II) (Ru-TPA-NCS) for sensitization.²⁹ As organic hole conductor we used 2,2',7,7'-Tetrakis-(N,N-di-4-

methoxyphenylamino)-9,9'-spiro-bifluorene (Spiro-OMeTAD), doped with *N*-lithiofluoromethane sulfonamide ($\text{Li}[(\text{CF}_3\text{SO}_2)_2\text{N}]$) and *tert*-butyl pyridine (*t*-bp). This combination of dye and hole conductor materials is well tested in solid-state dye-sensitized solar cells.⁹

The SEM cross sectional images of the various stages such as assembled SPB-TiO₂ composite layer, calcinated TiO₂ network and the complete solar cell from sample SPB-TiO₂-1d as a typical example is shown in Figure 9–7. The pore size in Figure 9–7b corresponds to the composite particle size in Figure 9–7a and a complete infiltration of the pores by the solid hole conductor is obvious in Figure 9–7c.

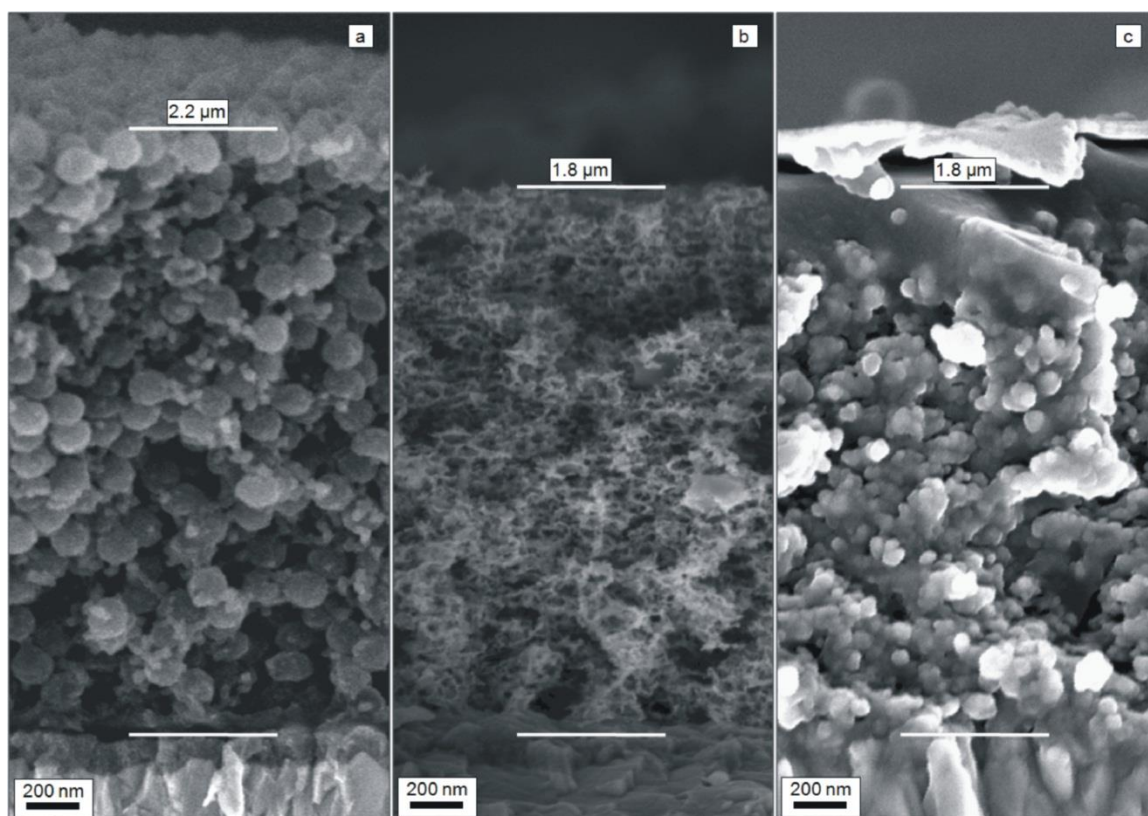


Figure 9–7. SEM cross sectional images of sample SPB-TiO₂-1d as a representative example for all samples at different stages of preparation: a) SPB-TiO₂ composite particles assembled on conductive substrate, b) calcinated porous TiO₂ network, c) SDSC sensitized with dye and filled with organic hole conductor.

The thickness variation between Figure 9–7a and 7b is due to a partial shrinkage of the structure during the calcination process and was visible in all samples. The solar cell performance from the samples SPB-TiO₂-1c (under two different calcinations conditions) and SPB-TiO₂-1d in a two-step calcination method are first compared in Figure 9–8. Also a schematic presentation of the cross section of such a solar cell is given.

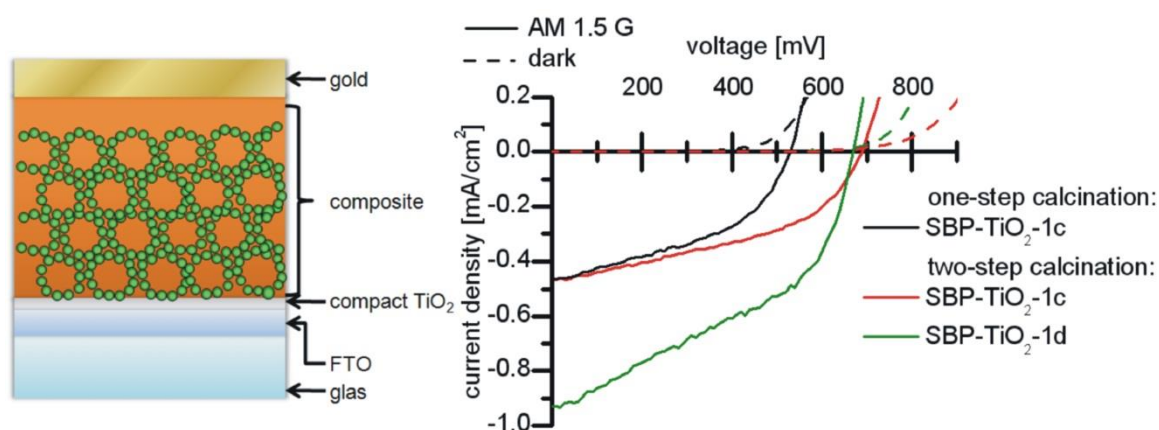


Figure 9–8. General scheme of the resulting solid-state dye-sensitized solar cells and the I - V characteristics (dotted lines: dark current and solid lines: photocurrent) of the devices prepared from samples SPB-TiO₂-1c and SPB-TiO₂-1d under different procedures summarized in Table 9–4.

For the sample SPB-TiO₂-1c (one-step calcination in air), a low photocurrent and a photovoltage of 525 mV was observed. By changing the calcination process from one-step calcinations in air to the two-step procedure an increase of 160 mV was obtained for this sample. The lower open circuit voltages of sample SPB-TiO₂-1c calcinated in one-step could be attributed to surface defects and impurity enclosures caused by the fast agglomeration of the particles while sintering under air.

The impurities enclosed affect the electron transport in the TiO₂ network and the energy level of its conduction band. In contrast, the two-step calcination leading to a robust carbon composite stabilizes the structure and leaves the surface unaffected. The final removal of the amorphous carbon occurs very fast and releases the solidified TiO₂ structure so that no impurities are enclosed. Thus the solar cells prepared from titania obtained in a two-step calcinations process deliver a remarkable open circuit voltage of 685 mV, which is close to reported values for devices prepared with highly optimized commercial nanocrystalline TiO₂ pastes. Additionally, a two-fold improvement in short circuit was achieved from 0.5 mA/cm² (for the ethanol route) in SPB-TiO₂-1c to 0.9 mA/cm² in SPB-TiO₂-1d using glycerin as medium for the assembly of the particles. The high V_{oc} (> 650 mV) could be maintained in the sample SPB-TiO₂-1d. This can be attributed to the improved smoothness and crack-free titania layers obtained in this sample (compare Figure 9–5).

Additionally SPB-TiO₂-2 and SPB-TiO₂-3 were used for the preparation of the mesoporous TiO₂ electrode and tested SDSC. For comparison an optimized commercial TiO₂ paste (sample: com. TiO₂) was used to prepare devices with similar thickness under same conditions. Table 9–4 summarizes all the TiO₂ samples used for solar cell studies.

Table 9–4. Summary of All Samples Tested in Solar Cell Devices and the Respective Preparation Conditions

sample	concentration/ solvent	application/drying temperature	calcination
SPB-TiO ₂ -1c	5 wt % / ethanol	drop casting / 2 °C	one-step (air)
SPB-TiO ₂ -1c	5 wt % / ethanol	drop casting / 2 °C	two-step (argon+air)
SPB-TiO ₂ -1d	10 wt % / glycerin	30 µm doctor blade / 120 °C	two-step (argon+air)
SPB-TiO ₂ -2	10 wt % / glycerin	30 µm doctor blade / 120 °C	two-step (argon+air)
SPB-TiO ₂ -3	10 wt % / glycerin	30 µm doctor blade / 120 °C	two-step (argon+air)
com. TiO ₂	~10 wt % / terpineol	Screen printing	optimized procedure ^a

^a see methods section

The *I*–*V*-characteristics of solar cells obtained from samples SPB-TiO₂-1d, SPB-TiO₂-2, SPB-TiO₂-3 and com. TiO₂ under dark as well as under AM 1.5 G conditions at 1 sun light intensity are shown in Figure 9–9. All solar cell parameters are summarized in Table 9–5.

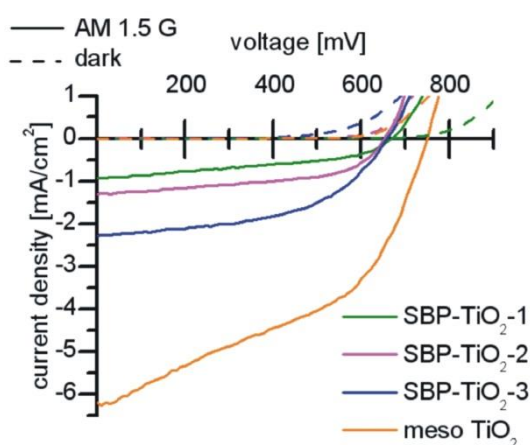


Figure 9–9. *I*–*V* characteristics (dotted lines: dark current and solid lines: photocurrent) of the devices prepared with different SPB-TiO₂ electrodes and an optimized commercial TiO₂ paste (com. TiO₂) for comparison.

Table 9–5. Summary of Results of the Solar Cells with Differently Prepared TiO₂ Networks. All Measurements were Carried Under AM 1.5 G Spectral Conditions at 100 mW/cm² Light Intensity

sample	V _{oc} [mV]	J _{sc} [mA/cm ²]	FF [%]	η [%]
SPB-TiO ₂ -1c (one-step)	525	0.47	44.9	0.11
SPB-TiO ₂ -1c (two-step)	685	0.47	45.2	0.14
SPB-TiO ₂ -1d	665	0.92	43.3	0.26
SPB-TiO ₂ -2	655	1.30	53.0	0.45
SPB-TiO ₂ -3	655	2.29	51.3	0.77
com. TiO ₂	755	6.20	44.2	2.07

Drastic improvements in photocurrent as well as fill factor were observed by varying the preparation conditions of the SPB composite particles. Thus an J_{sc} to 1.3 mA/cm² was obtained by increasing the water content during the hydrolysis of TiO₂ in sample SPB-TiO₂-2. A further increase in J_{sc} was observed to 2.3 mA/cm² by a higher TEOT content in SPB-TiO₂-3. For both samples SPB-TiO₂-2 and SPB-TiO₂-3 higher fill factor values above 50% were obtained. To

understand the factors contributing towards improvement in the performance of TiO₂ electrodes, the following studies with respect to the amount of TiO₂ on FTO substrates as well as dye uptake and morphology were carried out. Table 9–6 shows a summary of these results.

Table 9–6. Comparison of TiO₂ Content, Absolute Mass of TiO₂ on the Substrate, Dye Load and J_{sc} of Different SBP-TiO₂ Samples and an Optimized Commercial TiO₂ Paste (com. TiO₂).

Sample	TiO ₂ content in SPB-TiO ₂ composite ^a [%]	absolute mass of TiO ₂ on substrate [mg]	Amount of dye adsorbed [10 ⁻⁸ mol]	Amount of dye / mg TiO ₂ [10 ⁻⁸ mol/mg]	J _{sc} [mA/cm ²]
SPB-TiO ₂ -1d	34.95	0.264	3.14	11.89	0.92
SPB-TiO ₂ -2	13.81	0.101	0.79	7.79	1.30
SPB-TiO ₂ -3	51.49	0.336	3.54	10.54	2.29
com. TiO ₂	-	0.928	7.40	7.98	6.20

^a measured on calcinated samples

First the exact amount of TiO₂ in the composite film as well as TiO₂ network was determined using gravimetric analysis. For this purpose, the exact weight of the bare substrate, the dry film and the calcinated network was determined using a micro balance and the TiO₂ content was calculated. The TGA measurements of the dried bulk material confirm the gravimetric measurements performed on substrates (see supporting informations). The TiO₂ content varies drastically from sample SPB-TiO₂-1d to SPB-TiO₂-2 and SPB-TiO₂-3. It is obvious from Table 9–6 that with addition of more water during the hydrolysis, the TiO₂ content in composite decreases drastically in sample SPB-TiO₂-2, despite an equal precursor content in both samples. This can be explained as due to an enhanced hydrolysis of the TEOT outside the brushes, which is washed off during the purification. Moreover, an increased TiO₂ content was observed in sample SPB-TiO₂-3 with increasing precursor content. Thus sample SPB-TiO₂-3 exhibits the highest TiO₂ content after calcination.

In a second experiment the exact dye uptake for different titania electrodes was measured by UV-Vis spectroscopy. As the dye Ru—TPA—NCS shows only limited solubility in basic methanol or acetonitrile solutions, it was not possible to desorb the dye from the TiO₂ surface completely. In consequence, we calculated the adsorbed dye amount from the residual dye solution left after chemisorbtion. The detailed procedure is given in the methods section. In short, the substrates were covered with exactly 400 ml of an 0.5 mM solution of Ru-TPA-NCS in DMF for coating over night (16 h) and after removing the substrates the residual dye solution was diluted and analyzed. As control experiment a bare substrate without a porous TiO₂ layer was treated in a similar fashion and the amount of dye uptake for all substrates was corrected using this data. The dye uptake results were compared to the TiO₂ contents as well as the obtained short circuit current for the solar cells using the respective samples (Table 9–6).

The absolute amount of dye adsorbed, which is a measure for the available active area on the TiO₂ network for dye anchoring, is directly correlated to the TiO₂ amount on the substrates as well as the porosity for all the samples. Thus SPB-TiO₂-3 having highest TiO₂ content absorbs also the highest amount of dye (3.45 10⁻⁸ mol per 0.336 mg of TiO₂). Interestingly, SPB-TiO₂-3 also delivers the highest J_{sc} in solar cells (2.3 mA/cm²). We also calculated the amount of dye adsorbed/mg TiO₂ for all the samples. This gives a clear picture regarding the available surface area and compactness of the different films. Thus sample SPB-TiO₂-1d with an appreciable amount of titania exhibits the highest amount of dye/mg TiO₂, which means that the TiO₂

network is very fine, favoring high dye uptake, but detrimental for electron transport in network. In sample SPB-TiO₂-2 the absolute amount of TiO₂ is the lowest corresponding to a less amount absorbed dye. It also corresponds to the lowest value of dye/mg TiO₂, which can be explained as due to the presence of a more compact network structure, which favors better charge transport. Even though the absolute amount of dye adsorbed in sample SPB-TiO₂-3 is the highest, the amount of dye/mg TiO₂ increases. Therefore an expected 3fold increase in J_{sc} could not be observed on comparison with SPB-TiO₂-2. On the other hand the commercial sample has very high amount of TiO₂ with large available active area for dye adsorption. It also has an optimum of amount of dye/mg TiO₂ ($7.98 \cdot 10^{-8}$ mol/mg) indicating dense TiO₂ network, which favors efficient electron transport.

The above facts are fully supported by high resolution SEM images of the resulting morphology of the respective samples, shown in Figure 9–10. While sample SPB-TiO₂-1d mainly leads to the formation of a very thin network, sample SPB-TiO₂-2 forms dense, even closed spherical TiO₂ wall structures. These observations can be directly correlated to the TEM images of the composite particles (Figure 9–6). The sample SPB-TiO₂-3 possesses a similar dense structure as sample SPB-TiO₂-2, but showing a increased roughness of the TiO₂ structures. Thus this SPB template method allows the tuning of the network density, the absolute amount of TiO₂ and morphology of the resulting porous electrode. Also the differences in solar cell performance could be well correlated with the network properties and dye uptake. It is also worthy to note that in first results, the electrode obtained from sample SPB-TiO₂-3 exhibits an appreciable power conversion efficiency of 0.8% in a solid-state device.

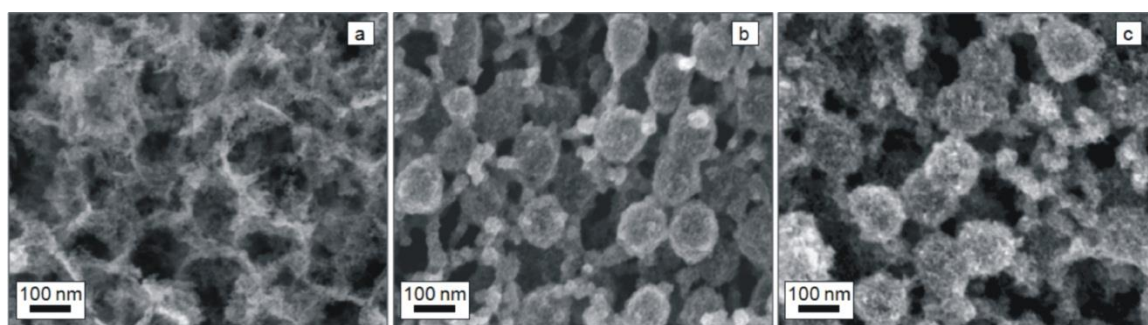


Figure 9–10. High resolution SEM images of the TiO₂ network morphologies. The samples a) SPB-TiO₂-1d, b) SPB-TiO₂-2 and c) SPB-TiO₂-3 were prepared according to the same procedures used for the device preparation (Table 9–4).

CONCLUSIONS

In conclusion, we successfully introduced a new template system using spherical polyelectrolyte brush particles for the controlled preparation of a nanocrystalline TiO₂ network on conducting substrates. We examined different preparation methods and studied the titania structures as photoelectrodes in solid-state dye-sensitized solar cells. The dispersant as well as the drying conditions had a major influence on the resulting structure and in consequence on the device performance. One of the key advantages of this method is that the pore size in the final TiO₂ network is well correlated to the SPB core size, which can allow the tuning of pore size by varying the SPB size. Additionally the size of the TiO₂ nanocrystals as well as the wall thickness of

the resulting TiO₂ network can be regulated by varying the precursor/water content. The first results in solar cells emphasize the importance of a homogeneous film and a stable and pure TiO₂ structure. Furthermore, by varying the morphology of the TiO₂ network, dense and well connected TiO₂ walls were found to be key parameters for efficient dye uptake and charge transport. Finally, the best device reached a power conversion efficiency of 0.8% under AM 1.5 G conditions. The advantages of controlling the different criteria like surface effects, pore size and wall thickness in an effortless and fast system offer this concept the potential to solve numerous issues concerning solid-state dyesensitized solar cells. The final aim should be directed towards high TiO₂ content with maximum active area for dye adsorption and optimum dense network morphology as in highly optimized commercial TiO₂ pastes.

ACKNOWLEDGMENT

Financial support from DFG (SFB 840), ESF (EUROCORES: SOHYD) and fruitful discussions within the ENB Macromolecular Science are kindly acknowledged.

REFERENCES

- (1) X. Chen, S. S. Mao, *Chem. Rev.* **2007**, *107*, 2891-2959.
- (2) J. Yang, S. Mei, J. M. F. Ferreira, *J. Colloid Interface Sci.* **2003**, *260*, 82-88.
- (3) J.-J. Wu, C.-C. Yu, *J. Phys. Chem. B* **2004**, *108*, 3377-3379.
- (4) H. Strohm, P. Lobmann, *J. Mater. Chem.* **2004**, *14*, 2667-2673.
- (5) A. Chemseddine, Thomas Moritz, *Eur. J. Inorg. Chem.* **1999**, *2*, 235-245.
- (6) B. Smarsly, D. Grosso, T. Brezesinski, N. Pinna, C. Boissiere, M. Antonietti, C. Sanchez, *Chem. Mater.* **2004**, *16*, 2948-2952.
- (7) B. O'Regan, M. Grätzel, *Nature* **1991**, *353*, 737-740.
- (8) U. Bach, D. Lupo, P. Comte, J. E. Moser, F. Weissortel, J. Salbeck, H. Spreitzer, M. Grätzel, *Nature* **1998**, *395*, 583-585.
- (9) C. S. Karthikeyan, M. Thelakkat, *Inorg. Chim. Acta* **2008**, *361*, 635-655.
- (10) H. J. Snaith, A. J. Moule, C. Klein, K. Meerholz, R. H. Friend, M. Grätzel, *Nano Lett.* **2007**, *7*, 3372-3376.
- (11) E. M. J. Johansson, A. Sandell, H. Siegbahn, H. Rensmo, B. Mahrov, G. Boschloo, E. Figgemeier, A. Hagfeldt, S. K. M. Jönsson, M. Fahlman, *Synth. Met.* **2005**, *149*, 157-167.
- (12) Y. Saito, N. Fukuri, R. Senadeera, T. Kitamura, Y. Wada, S. Yanagida, *Electrochem. Commun.* **2004**, *6*, 71-74.
- (13) D. Gebeyehu, C. J. Brabec, N. S. Sariciftci, D. Vangeneugden, R. Kiebooms, D. Vanderzande, F. Kienberger, H. Schindler, *Synth. Met.* **2001**, *125*, 279-287.
- (14) K. R. Haridas, J. Ostrauskaite, M. Thelakkat, M. Heim, R. Bilke, D. Haarer, *Synth. Met.* **2001**, *121*, 1573-1574.
- (15) L. Schmidt-Mende, M. Grätzel, *Thin Solid Films* **2006**, *500*, 296-301.
- (16) J. Bisquert, *J. Phys. Chem. B* **2002**, *106*, 325-333.
- (17) J. Krüger, R. Plass, M. Grätzel, P. J. Cameron, L. M. Peter, *J. Phys. Chem. B* **2003**, *107*, 7536-7539.
- (18) H. K. Dunn, L. M. Peter, *J. Phys. Chem. C* **2009**, *113*, 4726-4731.
- (19) J. Perlich, M. Memesa, A. Diethert, E. Metwalli, W. Wang, S. V. Roth, A. Timmann, J. S. Gutmann, P. Müller-Buschbaum, *ChemPhysChem* **2009**, *10*, 799-805.
- (20) G. J. d. A. Soler-Illia, C. Sanchez, B. Lebeau, J. Patarin, *Chem. Rev.* **2002**, *102*, 4093-4138.
- (21) M. Paulose, K. Shankar, O. K. Varghese, G. K. Mor, B. Hardin, C. A. Grimes, *Nanotechnology* **2006**, 1446.

- (22) G. K. Mor, O. K. Varghese, R. H. T. Wilke, S. Sharma, K. Shankar, T. J. Latempa, K.-S. Choi, C. A. Grimes, *Nano Lett.* **2008**, *8*, 1906-1911.
- (23) K. M. Coakley, Y. Liu, M. D. McGehee, K. L. Frindell, G. D. Stucky, *Adv. Funct. Mater.* **2003**, *13*, 301-306.
- (24) E. J. W. Crossland, M. Kamperman, M. Nedelcu, C. Ducati, U. Wiesner, D.-M. Smilgies, G. E. S. Toombes, M. A. Hillmyer, S. Ludwigs, U. Steiner, H. J. Snaith, *Nano Lett.* **2009**, *9*, 2807-2812.
- (25) S. Nishimura, N. Abrams, B. A. Lewis, L. I. Halaoui, T. E. Mallouk, K. D. Benkstein, J. van de Lagemaat, A. J. Frank, *J. Am. Chem. Soc.* **2003**, *125*, 6306-6310.
- (26) M. Ballauff, *Prog. Polym. Sci.* **2007**, *32*, 1135-1151.
- (27) Y. Lu, M. Hoffmann, R. S. Yelamanchili, A. Terrenoire, M. Schrunner, M. Drechsler, M. W. Möller, J. Breu, M. Ballauff, *Macromol. Chem. Phys.* **2009**, *210*, 377-386.
- (28) B. Peng, G. Jungmann, C. Jäger, D. Haarer, H.-W. Schmidt, M. Thelakkat, *Coord. Chem. Rev.* **2004**, *248*, 1479-1489.
- (29) C. S. Karthikeyan, H. Wietasch, M. Thelakkat, *Adv. Mater.* **2007**, *19*, 1091-1095.
- (30) K. Willinger, K. Fischer, R. Kisselev, M. Thelakkat, *J. Mater. Chem.* **2009**, *19*, 5364-5376.

SUPPORTING INFORMATION

High resolution transmission electron microscopy

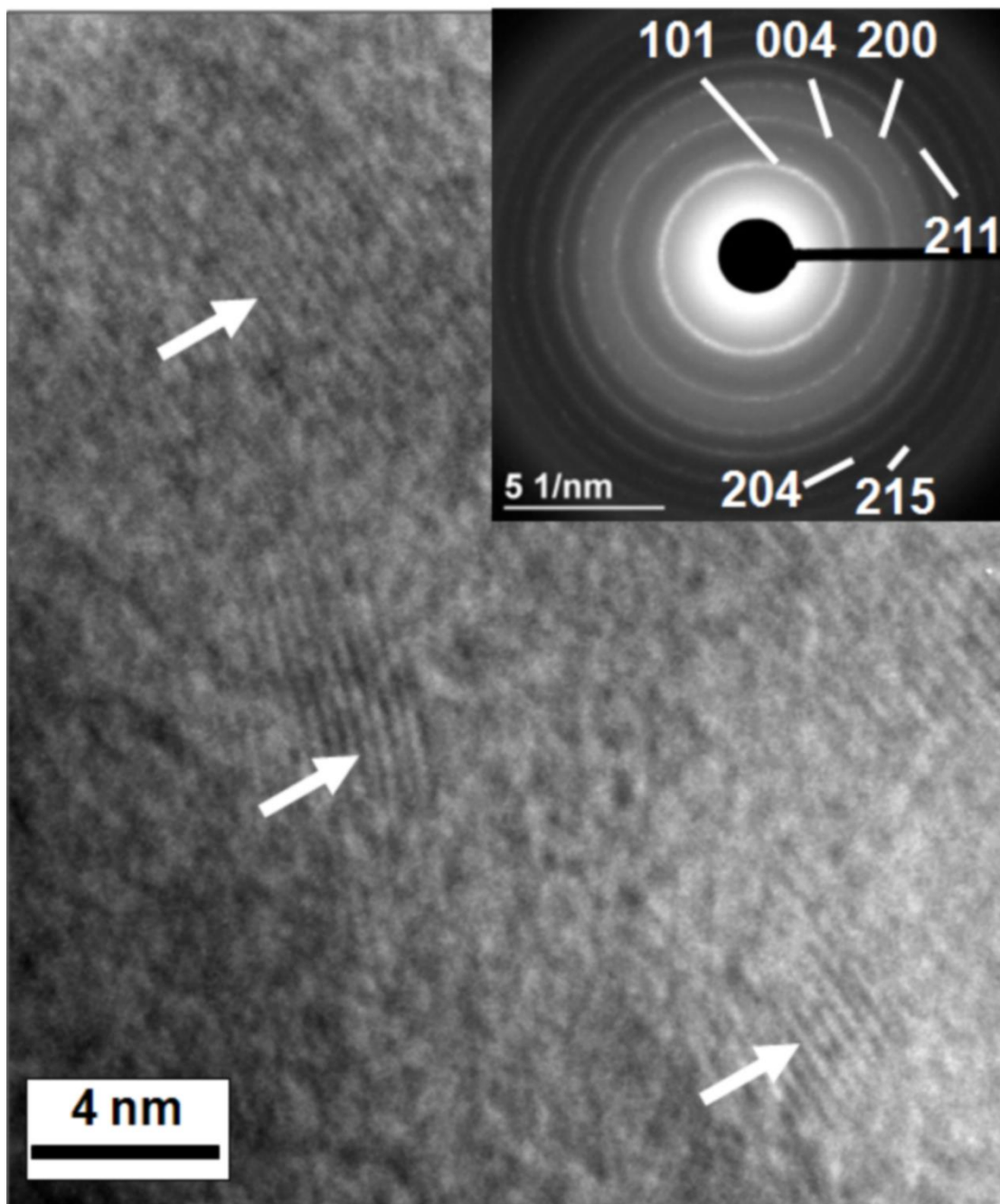


Figure 9–S1. HR-TEM image of sample SPB-TiO₂-1 (SPB/TEOT/water ratio of 1/4/4) and the selected area electron diffraction (SAED) patterns of a single crystal immobilized within the brush. The diffraction rings consist with the anatase phase of TiO₂.

EDX spectra of calcinated samples

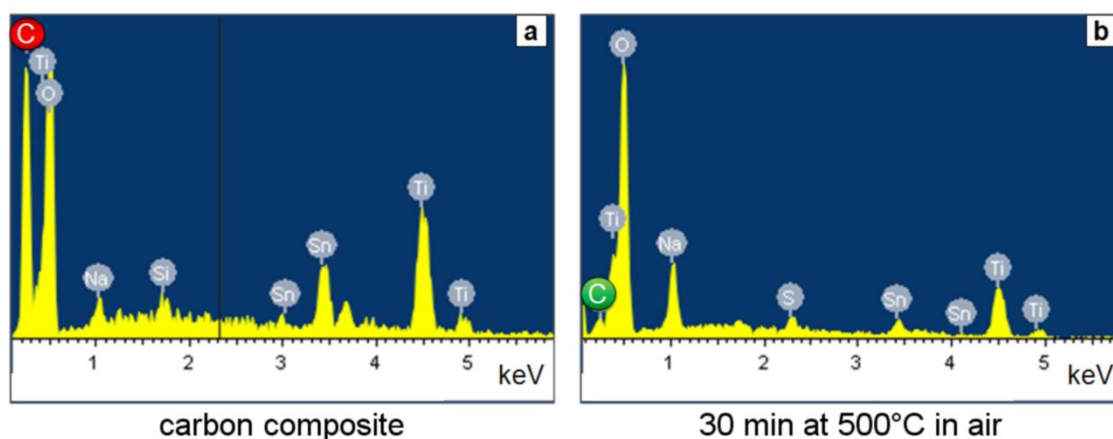


Figure 9-S2. EDX spectra of the SPB-TiO₂ films were recorded after calcination under argon and after the final removal of the carbon composite in air. A high carbon peak at 0.2 keV was obtained after heating under Argon for 5 h at 500 °C (left). The right spectrum indicates the complete removal of the carbon after 30 min at 500 °C under air.

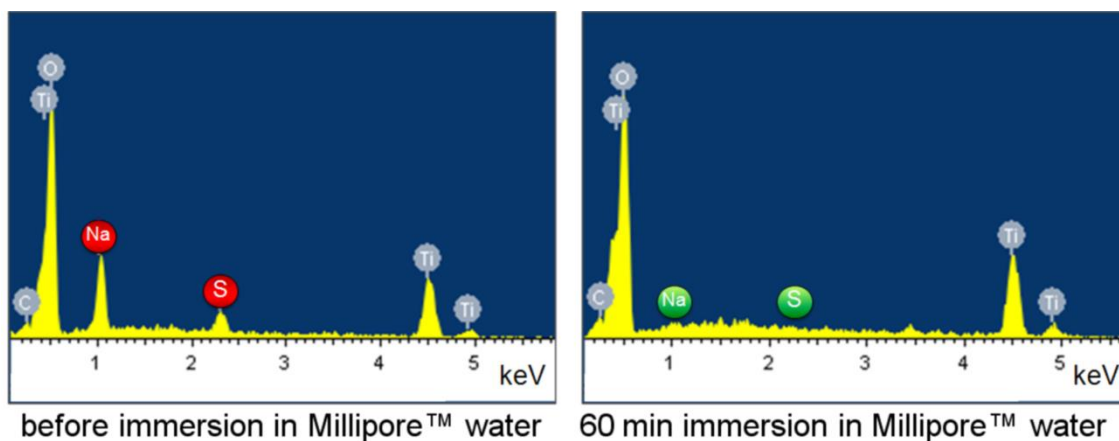


Figure 9-S3. Further inorganic impurities as sodium and sulphur were detected *via* EDX analysis. These rests of the sulfonate groups were removed by immersing the samples in Millipore® water for 1 h. The respective EDX spectra display the complete removal of those impurities.

TGA measurements

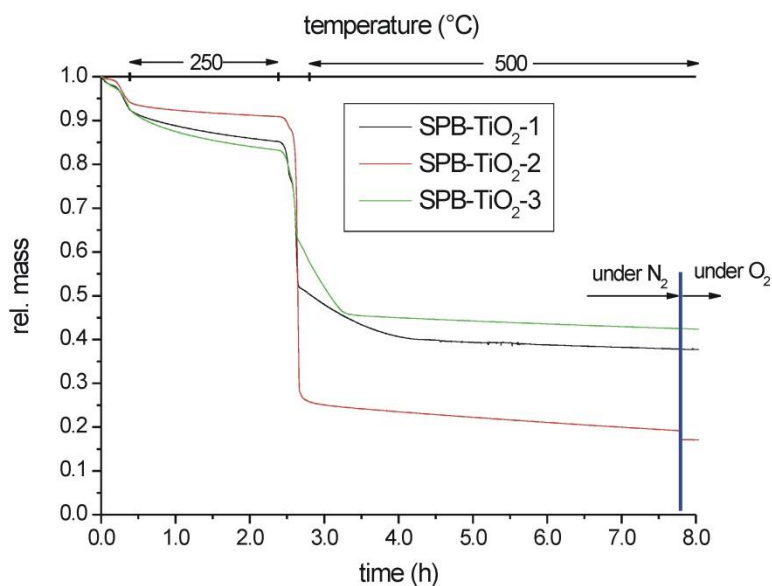


Figure 9–S4. TGA measurements of the samples SPB-TiO₂-1, SPB-TiO₂-2 and SPB-TiO₂-3. The program for the TGA measurement was adjusted to the two-step calcination program (under N₂: heating to 250 °C at a ramp of 10 K/min, keeping at 250 °C for 2 h, further heating to 500 °C at a ramp of 10 K/min, keeping at 500 °C for 5 h, flush with O₂ and keep for another 30 min at 500 °C). The residual relative masses of the individual samples are summarized in Table 9–S1.

Table 9–S1. Relative Residual Masses Determined by TGA Measurements

Sample	TiO ₂ content in SPB-TiO ₂ composite
SPB-TiO ₂ -1d	37.68%
SPB-TiO ₂ -2	17.01%
SPB-TiO ₂ -3	42.23%

LIST OF PUBLICATIONS

1. **Johannes C. Brendel**, Yan Lu and Mukundan Thelakkat:
Polymer templated nanocrystalline titania network for solid state dye sensitized solar cells,
J. Mater. Chem. **2010**, *20*, 7255-7265.
2. Safacan Kolemen, Yusuf Cakmak, Sule Erten-Ela, Yigit Altay, **Johannes C. Brendel**, Mukundan Thelakkat and Engin U. Akkaya:
Solid-State Dye-Sensitized Solar Cells Using Red and Near-IR Absorbing Bodipy Sensitizers,
Org. Lett. **2010**, *12*, 3812-3815.
3. Sule Erten-Ela, **Johannes C. Brendel** and Mukundan Thelakkat:
Solid-state dye-sensitized solar cells fabricated with nanoporous TiO₂ and TPD dyes: Analysis of penetration behavior and I–V characteristics,
Chem. Phys. Lett. **2011**, *510*, 93-98.
4. **Johannes C. Brendel**, Hubertus Burchardt and Mukundan Thelakkat:
Semiconductor amphiphilic block copolymers for hybrid donor-acceptor nanocomposites,
J. Mater. Chem. **2012**, *22*, 24386-24393.
5. **Johannes C. Brendel**, Feng Liu, Andreas S. Lang, Thomas P. Russell and Mukundan Thelakkat:
Vertical alignment of microdomains in semiconductor amphiphilic block copolymers thin films,
ACS Nano **2013**, in print, DOI: 10.1021/nn401877g.
6. **Johannes C. Brendel**, Gunter Hagen, Ralf Moos and Mukundan Thelakkat:
Controlled Synthesis of a Conjugated Polyelectrolyte Leading to Excellent Hole Transport Mobility,
Chemistry of Materials, submitted.

DANKSAGUNG

An dieser Stelle möchte ich mich schließlich herzlich bei allen bedanken, die direkt oder indirekt zum Gelingen dieser Arbeit beigetragen haben.

Mein erster Dank gilt hierbei meinem Betreuer Prof. Mukundan Thelakkat für das interessante und abwechslungsreiche Thema und die immerwährende Bereitschaft zu hilfreichen Diskussionen. Die vielen Möglichkeiten an internationalen Konferenzen teilzunehmen und den Kontakt zu zahlreichen Kooperationspartnern, die er mir geboten hat, sind nicht selbstverständlich und haben mir einen tiefen Einblick in die aktuellen Themen in Wissenschaft und Forschung gegeben. Deine kritische Betrachtungsweise und Entwicklung immer neuer und spannender Fragestellungen waren schließlich wegweisend für meine zukünftige Karriereplanung. Aber auch deine offene und herzliche Art außerhalb der Universität weiß ich sehr zu schätzen. Ich hoffe wir bleiben auch weiterhin in gutem Kontakt. Herzlichen Dank!

Für eine umfangreiche finanzielle Unterstützung möchte ich mich auch bei der Universität Bayern e.V. bedanken. Neben einem Graduiertenstipendium wurden die Kosten sowohl für verschiedene Tagungen und als auch für meinen Forschungsaufenthalt in Amherst, USA übernommen.

In Folge möchte ich mich hier auch besonders bei meinen Kooperationspartnern im In- und Ausland bedanken. Prof. Dr. Sule Erten-Ela hat mit ihren Arbeiten an den verschiedenen organischen Farbstoffen einen großen Beitrag zu dieser Arbeit geleistet. Einen weiteren großen Anteil am Gelingen dieser Arbeit hatten die Zusammenarbeit mit der Arbeitsgruppe von Prof. Russell und mein Forschungsaufenthalt in Amherst, USA. Bei allen Beteiligten in Amherst möchte ich mich im Folgenden gerne auf Englisch bedanken:

First I would like to thank Prof. Russell for the chance to spend two month in his group at the University of Massachusetts, Amherst. The excellent working atmosphere and the fruitful discussions helped a lot to improve this work. I gained a lot of experience during that stay. Many, many thanks I would like to give to Bugra Toga who was the best roommate in that office I could ever expect. I am very glad to find a friend like you there. But I also would like to thank Hsin-Wei and Takeko who always helped me, if I had any problems. A special thank I would like to give to Feng Liu. He always was a helpful partner and a good part of this work would not have been possible without his support. Furthermore, I thank all the other people at the Conte Research Center which all made it a very pleasant stay and I will keep fond memories of it. Thank you all very much!

Eine sehr große Hilfe für das Gelingen dieser Arbeit war mir auch Prof. Moos und Gunter Hagen am Lehrstuhl für Funktionsmaterialien. Die genaue elektrische Charakterisierung der Polyelektrolyte wäre ohne ihr Zutun nicht möglich gewesen. Herzlichen Dank!

Mein Dank gilt auch den vielen anderen Kooperationspartnern mit denen ich während meiner Dissertation zusammenarbeiten durfte: Jens Balko für die vielen Messungen zu den Polyelektrolyten und die daraus resultierenden Diskussionen; Prof. Matthias Karg für die vielen Ideen und Anregungen zur Strukturaufklärung und natürlich für die Neutronenstreuemessungen;

Subila für die Synthese und vielen Erkenntnissen von anorganischen Nanopartikeln; Abey Issac, Richard Hildner und Christina Scharsich für die Hilfe bei der Charakterisierung optischer Eigenschaften; Christian Schwarz für die Hilfe beim Bau von Solarzellen.

Sehr bedanken möchte ich mich auch bei den vielen Studenten, die mich während ihrer Praktika, HiWis oder Bachelorarbeiten unterstützt haben: Sebastian Gödrich, Samuel Shehata, Bianca Fischer, Jonas Schubert, Cathrin Müller, Alessia Weiß, Paul Reichstein und Stephanie Schindler. Besonders möchte ich mich hierbei bei Hubertus Burchardt und Martina Schmidt bedanken, die mit ihren Bachelorarbeiten, den HiWis und den vielen Praktika entscheidend an dieser Arbeit mitgewirkt haben.

Ein besonderer Dank gilt allen Mitarbeitern des Lehrstuhls Makromolekulare Chemie I. Die Hilfsbereitschaft und die Offenheit an diesem Lehrstuhl haben mir die Arbeit doch sehr erleichtert und eine sehr angenehme Atmosphäre geschaffen an die ich sicher immer gerne zurückdenken werde. In labortechnischer Hinsicht möchte ich mich auch bei allen Gerätebetreuern und Technikern, auch der MC 2, bedanken für die viele Hilfe bei allen Messungen und Untersuchungen, sowie der Bereitstellung der Lösungsmittel. Besonders Helga gilt hier mein Dank, die nicht nur die technischen bzw. chemischen Arbeiten sehr erleichtert hat, sondern mit ihrer lockeren Art auch immer wieder für Erheiterung gesorgt hat.

Vor allem möchte ich mich hierbei auch bei allen anderen Kollegen und Freunden in unserer AFuPo-Arbeitsgruppe bedanken, sei es in der B6 oder im NW II. Ihr habt es immer geschafft mir wieder Motivation zu geben oder Hilfestellung bei allen Arten von Problemen geleistet. Katja möchte ich dabei ganz besonders danken, die mir über mehrere Jahre immer mit Rat und Tat als Labor- und Bürokollegin zur Seite stand. Auch außerhalb der Uni hatte ich immer wieder sehr viel Spaß mit euch allen, sei es bei Ausflügen oder gemeinsamen Abenden gewesen. Vielen Dank für die schöne Zeit!

Nicht zuletzt möchte ich mich aller herzlichst bei allen Freunden bedanken, die ich noch nicht erwähnt habe. Thomas, Katja, Andreas, Sebastian, Sascha, Alex und Denise, ihr wart mir in allen Bereichen, sei es fachlich oder auch außerhalb der Uni, immer eine große Stütze und habt mir auch immer geholfen neue Kraft und Mut zu schöpfen für die anstehenden Arbeiten. Ihr habt mein Leben während der gesamten Studienzeit bereichert und ich hoffe wir bleiben auch nachdem sich unsere Wege wahrscheinlich trennen in gutem Kontakt. Danke euch allen!

Ein ganz großer Dank gilt auch Barbara, die mich sehr lange während dieser Arbeit begleitet hat. Auch wenn sich unsere Wege trennten, so hast du doch einen ganz besonderen Anteil an dem Gelingen dieser Arbeit gehabt, indem du mich immer unterstützt und auch in schwierigen Zeiten wieder aufgebaut hast. Ich hoffe wir bleiben auch in Zukunft noch gute Freunde.

Zuletzt gilt mein größter Dank meiner Familie, meiner Mutter Monika, meinem Vater Heinrich, meinen Schwestern Sabine und Susanne, ihren Kindern David, Lukas, Margarete, Jacob, Rebecca, Sophia, Leo und Franzi, meinem Bruder Philipp, sowie ihren Ehepartnern Georg, Harald und Monika. Ihr wart es, die mir den Mut gegeben haben dieses Studium auf mich zu nehmen und mir immer neue Energie geschenkt haben weiter zu machen, auch in schweren Zeiten. Unser familiärer Zusammenhalt bot mir immer einen starken Rückhalt und einen Rückzugsort in dem ich mich geborgen fühlen konnte. Ohne euch wäre all dies nicht möglich gewesen und wäre nicht da, wo ich heute bin.

ERKLÄRUNG

Hiermit erkläre ich, dass ich die vorliegende Arbeit selbstständig verfasst und keine anderen als die von mir angegebenen Quellen und Hilfsmittel verwendet habe.

Ferner erkläre ich, dass ich weder anderweitig mit oder ohne Erfolg versucht habe, diese Dissertation einzureichen, noch eine gleichartige Doktorprüfung an einer anderen Hochschule endgültig nicht bestanden habe.

Bayreuth, den 06.11.2013

Johannes Brendel